The Journal of Gemmology

Volume 37 / No. 1 / 2020

Late 14th-Century Royal Crown of Blanche of Lancaster

Black Spinel from Thailand

Camera-Drone Gem Exploration

SSEF
SCHWEIZERISCHES GEMMOLOGISCHES INSTITUT
SWISS GEMMOLOGICAL INSTITUTE
INSTITUT SUISSE DE GEMMOLOGIE

Gem-A
THE GEMMOLOGICAL ASSOCIATION OF GREAT BRITAIN

SSEF

SCHWEIZERISCHES GEMMOLOGISCHES INSTITUT
SWISS GEMMOLOGICAL INSTITUTE
INSTITUT SUISSE DE GEMMOLOGIE

ORIGIN DETERMINATION · TREATMENT DETECTION

DIAMOND GRADING · PEARL TESTING

EDUCATION · RESEARCH

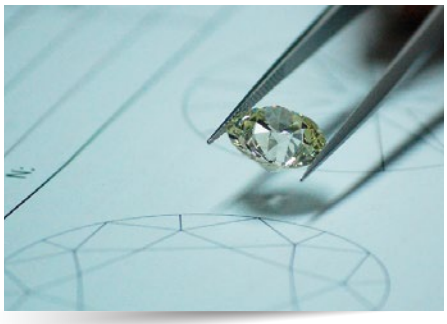

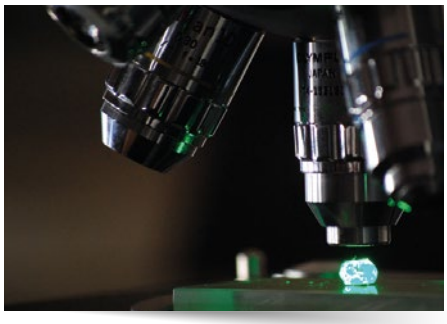

THE SCIENCE OF GEMSTONE TESTING™

Aeschengraben 26, 4051 Basel, Switzerland Tel. +41 61 262 06 40 Fax + 41 61 262 06 41 admin@ssef.ch www.ssef.ch

The Journal of Gemmology

Volume 37 / No. 1 / 2020

Cover photo: *The royal crown of Blanche of Lancaster (14.5 cm tall) is preserved in the Treasury of the Munich Residence (Munich, Germany), and is one few extant examples of Late Middle Ages royal regalia. An article on pp. 26–64 of this issue describes its history and the gems it contains. The various polishing/cutting styles demonstrate the transition in gemstone fashioning as the Late Middle Ages gave way to the Renaissance. Photo by K. Schmetzer, with permission from Bayerische Schlösserverwaltung, Munich.*

COLUMNS

ARTICLES

Photo by L. Nasdala

Photo by M. Wildner

Photo by M. Bainbridge

The Journal is published by Gem-A in collaboration with SSEF and with the support of AGL.

Gem-A THE GEMMOLOGICAL ASSOCIATION OF GREAT BRITAIN

SSEF SCHWEIZERISCHES GEMMOLOGISCHES INSTITUT SWISS GEMMOLOGICAL INSTITUTE INSTITUT SUISSE DE GEMMOLOGIE

AGL AMERICAN GEMOLOGICAL LABORATORIES

The Journal of Gemmology

COVERED BY THE FOLLOWING ABSTRACTING AND INDEXING SERVICES:

Clarivate Analytics' (formerly Thomson Reuters/ISI) Science Citation Index Expanded (in the Web of Science), *Journal Citation Reports (Science Edition)* and *Current Contents (Physical, Chemical and Earth Sciences)*; Elsevier's Scopus; Australian Research Council's Excellence in Research for Australia (ERA) Journal List; China National Knowledge Infrastructure (CNKI Scholar); EBSCO's Academic Search Ultimate; ProQuest (Cambridge Scientific Abstracts); GeoRef; CrossRef; Chemical Abstracts (CA Plus); Mineralogical Abstracts; Index Copernicus ICI Journals Master List; Gale Academic OneFile; British Library Document Supply Service; and Copyright Clearance Center's RightFind application.

Science Citation Index Expanded
Web of Science Clarivate Analytics

CONTENT SUBMISSION

The Editor-in-Chief is glad to consider original articles, news items, conference reports, announcements and calendar entries on subjects of gemmological interest for publication in *The Journal of Gemmology*. A guide to the various sections and the preparation of manuscripts is given at https://gem-a.com/index.php/news-publications/journal-of-gemmology/submissions, or contact the Editor-in-Chief.

SUBSCRIPTIONS

Gem-A members receive *The Journal* as part of their membership package, full details of which are given at https://gem-a.com/membership. Laboratories, libraries, museums and similar institutions may become direct subscribers to *The Journal*; download the form from *The Journal*'s home page.

ADVERTISING

Enquiries about advertising in *The Journal* should be directed to advertising@gem-a.com.
For more information, see https://gem-a.com/news-publications/media-pack-2020.

DESIGN & PRODUCTION

Zest Design, London. www.zest-uk.com

PRINTER

DG3 Group (Holdings) Ltd, London. www.dg3.com

Mixed Sources
Product group from well-managed forests and other controlled sources
www.fsc.org Cert no. TT-COC-002454
© 1996 Forest Stewardship Council
FSC

ISSN 1355-4565 (Print), ISSN 2632-1718 (Online)

Gem-A
THE GEMMOLOGICAL ASSOCIATION OF GREAT BRITAIN

21 Ely Place
London EC1N 6TD
UK
t: +44 (0)20 7404 3334
f: +44 (0)20 7404 8843
e: information@gem-a.com
w: https://gem-a.com

Registered Charity No. 1109555
A company limited by guarantee and registered in England No. 1945780
Registered office: Palladium House, 1–4 Argyll Street, London W1F 7LD

What's New

INSTRUMENTATION

GemLightbox Photography System

Released in July 2019 by Picup Media, GemLightbox is a lighting-and-environment system for the jewellery industry that enables the user to take 'studio quality' images using a smartphone or other camera. The basic GemLightbox comes with a lightbox, white backdrop, necklace-and-earring stand and smartphone holder. A free app is available for the Android operating system on Google Play, but the lightbox can also be used with an iPhone. Available accessories include turntable and aerial attachments that also enable video capture. Visit https://picupmedia.com/shop-page.

SmartPro Aura

In late 2019, Thailand-based SmartPro Instruments released the Aura Synthetic Diamond Scanner. The unit is designed to test both mounted jewellery and loose gems to separate natural diamond, synthetic diamond (CVD or HPHT grown) and cubic zirconia. It accommodates samples weighing 0.002+ ct, in the colour range D–K. It has a built-in smartphone with Android operating system and can automatically generate reports with test results. For details, including a user manual, visit www.smartproinstrument.com/products/aura.

Universal Smartphone Microscope Adapter

Gem-A Instruments is offering a microscope attachment that enables the user to take high-quality photomicrographs with a smartphone. It fits binocular, monocular and trinocular microscopes with 21–44 mm eyepieces, as well as most smartphones (56–85 mm wide). Cushioned surfaces protect both the microscope and smartphone, while the latter remains steady to prevent image blur. The adapter also works with telescopes and binoculars. Visit https://shop.gem-a.com/gemmological-instruments/microscopes/universal-smart-phone-microscope-adapter.

NEWS AND PUBLICATIONS

AGTA GemFair Tucson 2020 Seminars

The American Gem Trade Association's 38th GemFair was held 4–9 February 2020 in Tucson, Arizona, USA. The event offered nearly three dozen educational lectures and presentations that covered gem identification, appraisals, marketing strategies, industry trends and much more (visit https://agta.org/agta-gem-fair-tucson/seminars/all-seminars for a full list). Audio recordings and slides from most of these seminars are available on a flash drive for USD50.00 (non-AGTA-member price). To order flash drives from 2020 and previous years, visit https://agta.org/resources.

Blockchain in the Mining Industry: Implications for Sustainable Development in Africa

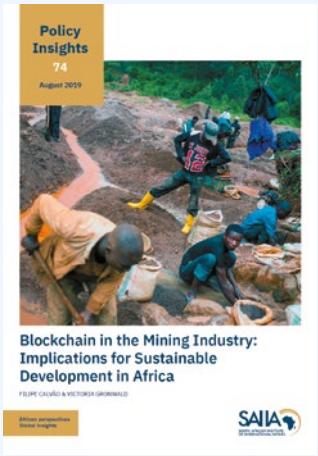

The South African Institute of International Affairs (SAIIA) released this report in August 2019 as part of its SAIIA Policy Insights series. The 13-page report features research by Filipe Calvão (Graduate Institute, Geneva, Switzerland) and Victoria Gronwald (Levin Sources, Cambridge). They describe 'distributed ledger technologies' whereby blockchains can securely record and publish transactions. The report uses the diamond industry as an example of how such blockchain technology can benefit local communities in Africa. Download the PDF at https://saiia.org.za/research/blockchain-in-the-mining-industry-implications-for-sustainable-development-in-africa.

Colourless CVD Diamonds Under the Loupe from HRD Antwerp

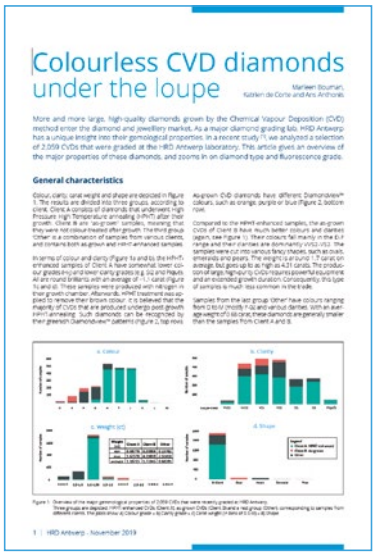
Colourless CVD diamonds under the loupe

Marleen Bouman, Katleen de Corte and Ans Anthonis

More and more large, high-quality diamonds grown by the Chemical Vapour Deposition (CVD) method enter the diamond and jewellery market. As a major diamond grading lab, HRD Antwerp has a unique insight into their gemological properties. In a recent study, [1] we analysed a selection of 2,059 CVDs that were graded at the HRD Antwerp laboratory. This article gives an overview of the major properties of these diamonds, and zooms in on diamond type and fluorescence grade.

General characteristics

More chemical vapour deposition (CVD) synthetic diamonds of larger size and higher quality are entering the market and, thus, passing through grading laboratories. HRD Antwerp released this two-page report in November 2019 with data from 2,059 CVD samples (mostly from two clients) that were recently seen in their laboratory. The majority of the samples were type IIa, 1.0–1.5 ct, H–J colour, VVS_2–SI_2 clarity and almost entirely brilliant cut. The data also suggest that all were HPHT annealed to remove the as-grown brown colour. Download the report at www.hrdantwerp.com/en/news/colourless-cvd-diamonds-under-the-loupe.

Dallas Mineral Collecting Symposium Presentations

The Dallas Mineral Collecting Symposium is held annually in August in Dallas, Texas, USA, and attracts mineral and gem enthusiasts from around the world. Presentations from the 2019 Symposium are now available online and include topics such as gem pocket formation in pegmatites, jewels created by Paula Crevoshay, and gems from Brazil, Colombia and elsewhere. Visit www.dallassymposium.org/videos.

DALLAS MINERAL COLLECTING SYMPOSIUM

De Beers Diamond Insight Report 2019

Released in October 2019, this annual De Beers report reviews 2018 global market data for diamonds. Consumer demand increased 2% worldwide for both polished diamonds and jewellery, with the strongest growth in the USA and China, followed by Japan. India and the Gulf region saw slight declines, while the rest of the world rose less than 1%. Much of the report focuses on the value of marketing diamonds as a symbol of love, including engagement and commitment rings, and 'milestone' gifts of diamond jewellery after marriage. Same-sex couples represent a rising market in both the USA and China. Download the report at www.debeersgroup.com/~/media/Files/D/De-Beers-Group/documents/reports/insights/the-diamond-insight-report-2019.pdf.

Global Diamond Industry Report 2019

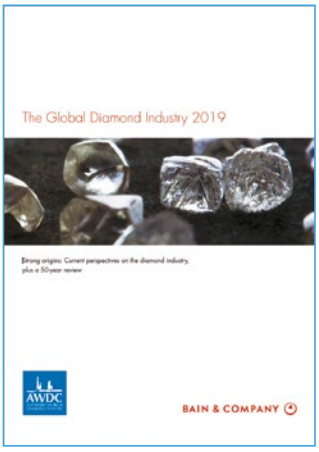

The ninth annual report from the Antwerp World Diamond Centre and Bain & Co. was released in December 2019. The report covers 2018 and the first half of 2019, reviews the diamond industry's performance over the past 50 years and examines key trends affecting the industry. The long-term forecast (through 2030) has been updated to reflect recent information on mining operations, production plans, lab-grown diamonds and economic developments, both global and regional. In general, data for 2019 showed declines in diamond jewellery retail sales, polished diamond demand and rough sales, despite stable production. Visit www.bain.com/insights/global-diamond-industry-report-2019 to read a summary online or download the full report.

Gold Demand Trends 2019

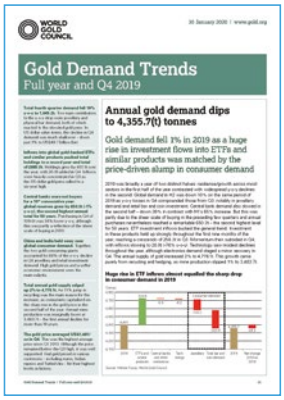

The World Gold Council released a combined report in January 2020 that covers all of 2019 and its fourth quarter. Overall demand for gold during the first half of 2019 was higher but dropped in the second half compared to 2018. In the fourth quarter, the demand for gold jewellery by volume sank to its lowest level since 2011, especially in India and China. However, demand for gold jewellery by value rose to its highest level in five years, in part due to the elevated price of gold in some currencies. Gold supply for the year rose slightly to 4,776.1 t. To read the full report online or download it (the latter requires log-in), go to www.gold.org/goldhub/research/gold-demand-trends/gold-demand-trends-full-year-2019.

ID of Green Gems with Portable Instruments

Released in February 2020, this booklet offers information on identifying various green gem materials that is oriented towards travelling gemmologists or those equipped with minimal instrumentation. It provides a catalogue of typical visible features, fluorescence, CPF (crossed-polarised features) and visible spectra for 64 natural, treated and synthetic green gem materials, arranged alphabetically. The authors explain how to identify green gem materials using basic gemmological knowledge in conjunction with a 10× loupe, long- and short-wave UV lamp, portable polariscope and hand spectroscope. Order the booklet at www.brankogems.com/shop/product-category/books.

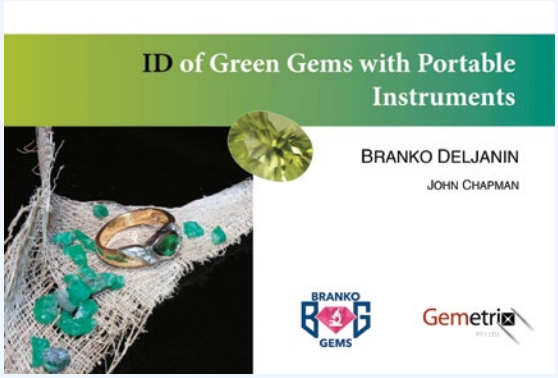

The Journal's Cumulative Index and Bibliography Lists Updated

The Journal of Gemmology's cumulative index has been updated to cover all issues through 2019. The index is provided in electronic (PDF) format, so it can be searched for specific first-authors as well as topics. In addition, the subject bibliographies covering articles and notes published in *The Journal* have been updated through 2019, and include various topics and gem materials: asterism and chatoyancy, biogenic gems, chrysoberyl and alexandrite, colour-change gems, diamond, emerald and other beryls, feldspar, ruby and sapphire, garnet, jade, opal, pearl, quartz, spinel and tourmaline. Download the index and bibliographies at https://gem-a.com/news-publications/journal-of-gemmology.

New Journal: *Gemmae—An International Journal on Glyptic Studies*

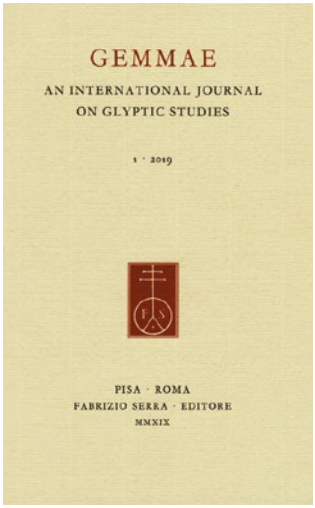

Volume 1 of this new annual journal was released in late 2019. From Italian publisher Fabrizio Serra, the focus is on the 'fascinating field of glyptics' (the art of engraving or carving gem materials). Peer-reviewed articles cover methodology, art history, iconography and technical issues, as well as the identification of copies and forgeries, the study of gems in museums and the description of items from well-documented excavations. English abstracts are provided for all articles, and some articles are written entirely in English. For more information or to subscribe, visit www.libraweb.net/riviste.php?chiave=142&h=430&w=300. To view abstracts or purchase PDFs of individual articles from Volume 1, go to www.libraweb.net/articoli.php?chiave=201914201&rivista=142.

MISCELLANEOUS

Maine Mineral & Gem Museum Opens

A museum dedicated to minerals, meteorites and gem materials officially opened in December 2019 in Bethel, Maine, USA. The 15,000-square-foot Maine Mineral & Gem Museum is situated on a land trust that includes the historic Bumpus mine, where several giant beryls were unearthed in the 1920s. The museum's collection includes numerous specimens of quartz, tourmaline and beryl, along with other minerals from Maine and elsewhere, as well as The Stifler Collection of Meteorites. Visit https://mainemineralmuseum.org.

What's New provides announcements of new instruments/technology, publications, online resources and more. Inclusion in What's New does not imply recommendation or endorsement by Gem-A. Entries were prepared by Carol M. Stockton unless otherwise noted.

The Fire Within

"For in them you shall see the living fire of the ruby, the glorious purple of the amethyst, the sea-green of the emerald, all glittering together in an incredible mixture of light."

– Roman Elder Pliny, 1st Century AD

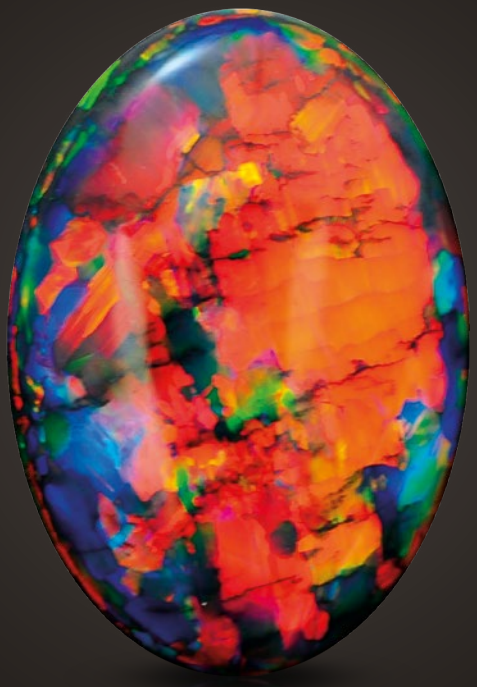

Black Opal 15.7 Carats

Suppliers of Australia's finest opals to the world's gem trade.

CODY OPAL

Level 1 - 119 Swanston Street Melbourne Australia

T. +61 3 9654 5533 E. info@codyopal.com

www.codyopal.com

ICA International Colored Gemstone Association Member

JOG

Gem Notes

COLOURED STONES

Hessonite from Kunar Province, Afghanistan

The hessonite variety of grossular has been known from eastern Afghanistan for many years and reportedly has been produced from two localities there: Munjagal in Kunar Province and Kantiwa (or Kantiwow) in Nuristan Province (Laurs & Quinn 2004). In November 2018, gem dealer Dudley Blauwet (Dudley Blauwet Gems, Louisville, Colorado, USA) obtained some additional hessonite—reportedly from Kunar Province—that turned out to have some properties which were significantly different from those reported by Laurs & Quinn (2004). He obtained seven pieces of rough totalling 36.7 g from a trusted dealer while on a buying trip to Peshawar, Pakistan, and cutting of this material yielded a total of 75.29 carats consisting of three faceted stones and four cabochons.

The faceted samples were loaned to these authors for examination, and consisted of two medium 'golden' orange stones weighing 3.85 and 6.41 ct, and a deep reddish orange gem that was 10.49 ct (Figure 1). Their RIs were 1.744 (6.41 ct) and 1.752 (10.49 ct); the 3.85 ct stone did not yield a clear RI reading. These values are higher than those recorded by Laurs & Quinn (2004; i.e. 1.739 and 1.740). Hydrostatic SG values were 3.60 for the 3.85 ct hessonite, 3.85 for the 6.41 ct stone and 3.64 for the 10.49 ct sample; the two lighter measurements are comparable to the 3.63 and 3.64 SG values reported by Laurs & Quinn (2004).

Between crossed polarisers, the 10.49 ct stone exhibited a fine, light-appearing cross-hatched pattern and a weaker anomalous double refraction that appeared similar to a birefringence blink and occurred four times upon a 360° rotation of the stone. The 3.85 and 6.41 ct samples remained light when rotated between crossed polarisers. All of the samples exhibited the classic 'whisky and water' or treacle optic effect (e.g. Figure 2a), which has been ascribed to a polycrystalline structure in hessonite (Hänni 2019). This is in contrast to the Afghan samples characterised by Laurs & Quinn (2004), which did not show a roiled appearance.

The 3.85 ct hessonite contained several colourless, prismatic crystalline inclusions, as well as a few reflective whitish features with a granular appearance (Figure 2b) that may be related to structural interruptions (i.e. fissures) formed along a series of polycrystalline grain boundaries. The 6.41 ct sample contained thinly dispersed colourless crystalline inclusions (again, see Figure 2a), together with some planar whitish areas similar to those described above; turbidity prevented careful observation of deeper inclusions. The 10.49 ct stone exhibited strong turbidity, and microscopic examination revealed fissures and what appeared to be irregular hollow growth tubes. Unidentified whitish clusters were also observed.

The GemmoRaman-532SG spectrometer confirmed that all three stones were grossular. Energy-dispersive X-ray fluorescence (EDXRF) chemical analysis using an Amptek X123-SDD instrument revealed the expected

Figure 1: The Afghan hessonites examined for this report consist of (**a**) two medium orange gems weighing 6.41 and 3.85 ct, and (**b**) a deep reddish orange 10.49 ct oval. Photos by (a) B. Williams and (b) Dean Brennan, Stone Group Laboratories.

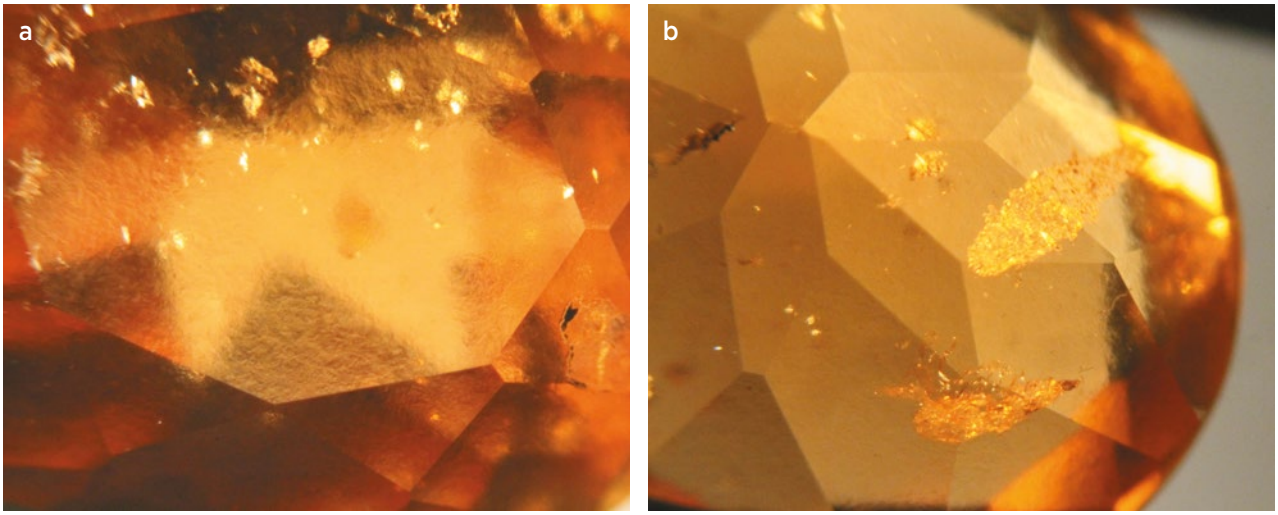

Figure 2: Internal features in the hessonites included (**a**) a treacle optic effect with colourless crystalline inclusions and (**b**) reflective whitish features. Photomicrographs by B. Williams; magnified about 20× (a) and 15× (b).

high level of Ca, but interestingly also recorded enriched Fe, together with minor Mn and Ti. While some of the Fe may be present in a minor andradite component (consistent with the RI and SG values), there was little to no evidence for the presence of andradite (or other garnet species) in the Raman spectra. We suspect that Fe, Mn and Ti impurities may be present along the polycrystalline grain boundaries of the garnet structure, although more research would be needed to confirm this.

Cara Williams FGA and Bear Williams FGA
(info@stonegrouplabs.com)
Stone Group Laboratories
Jefferson City, Missouri, USA

References

Hänni, H.A. 2019. Gemstones of the garnet group – About mixed crystals and solid solution. *Journal of the Gemmological Association of Hong Kong*, **40**, 36–42.

Laurs, B.M. & Quinn, E.P. 2004. Gem News International: Hessonite from Afghanistan. *Gems & Gemology*, **40**(3), 258–259.

Olshanskyite from Japan, Offered as Parasibirskite

During the December 2019 Minéral Expo Paris show, at the booth of Emmanuel Thoreux (White River Gems, Alsace region, France), the author noticed a few cabochons of opaque white material offered as parasibirskite, a rare mineral from Japan. This material was also available at the 2019 Denver gem and mineral shows in Colorado, USA.

Parasibirskite ($Ca_2B_2O_5 \bullet H_2O$) is a borate known only from the Fuka mine, a marble quarry in Bicchu-cho near Takahashi, Okayama Prefecture, Japan (Kusachi *et al.* 1998). It is a polymorph of sibirskite, and both minerals occur at the Fuka mine in veins along the boundary between spurrite-bearing skarn and limestone. Additional borates present within the veins include olshanskyite ($Ca_2[B_3O_3(OH)_6](OH) \bullet 3H_2O$; Kusachi & Henmi 1994), frolovite ($Ca[B(OH)_4]_2$; Kusachi *et al.* 1995), takedaite, nifontovite, pentahydroborite and henmilite (Kusachi *et al.* 1999).

Thoreux loaned a 2.74 ct cabochon (Figure 3) to the

Figure 3: This 2.74 ct cabochon (13 × 8 × 4.5 mm) from the Fuka mine in Japan was offered as parasibirskite but actually consists of another borate mineral, olshanskyite. Photo by T. Cathelineau.

author for examination, and it showed the following properties: colour—white; lustre—dull; diaphaneity—opaque with slightly translucent veins; RI—about 1.56–1.58 (difficult to read even after repolishing the cabochon's underside); birefringence—about 0.02; optic character and sign—undetermined because of the approximate RI reading; hydrostatic SG—2.14; and fluorescence—inert to long- and short-wave UV radiation.

The RI, birefringence and SG values are all lower than those reported for parasibirskite (Kusachi *et al.* 1998), and are more consistent with those of olshanskyite (Kusachi & Henmi 1994) and frolovite (Kusachi *et al.* 1995) than with other borates from the same location, even if the sample's SG was slightly lower. A search of the Mindat and Webmineral online databases showed that only a few borates have such a low SG, but those also have higher RIs than recorded from the present sample. Olshanskyite and frolovite are therefore the best possibilities according to the sample's gemmological properties, but conclusive identification required additional testing.

Infrared (IR) reflectance spectra were collected from several spots on the cabochon, at various orientations to look for anisotropy, and all yielded the same pattern without any significant difference (Figure 4). The overall pattern was consistent with that of a borate mineral. Borates comprise various radical anions (e.g. BO_3, B_2O_5, $B_2(OH)_5$, etc.) that produce a large variety of IR features. The spectrum collected from the study specimen did not show any analogous features with those of parasibirskite in transmittance mode (cf. Kusachi *et al.* 1998), especially in the 1500–1200 cm^{-1} range, which is related to vibrations of the B_2O_5 radical. This confirmed the results indicated by the sample's gemmological properties.

There is a lack of available IR spectra for borates in reflectance mode; almost all of the published spectra (for samples from both Japan and Russia) are in transmittance mode. A visual comparison of the reflectance spectrum from the present cabochon to the absorption spectrum of olshanskyite from Russia (Bogomolov *et al.* 1969) and to the transformed log(1/T) spectrum of olshanskyite from the Fuka mine in Japan (Kusachi & Henmi 1994) showed correlative features, and identified the cabochon as olshanskyite.

Raman spectroscopy with 514 nm laser excitation showed an almost perfect match with reference spectra for olshanskyite, which have distinctive bands at 636 and 717 cm^{-1} (Figure 5). An additional band of unknown origin was also present at 465 cm^{-1}.

A visible-near infrared spectrum was collected from a thin, translucent area of the cabochon. The resulting spectrum showed an absorption edge below 410 nm accompanied by an asymptotic 'tail' that extended into the NIR, together with three superimposed absorption bands at approximately 675 nm (weak and very broad),

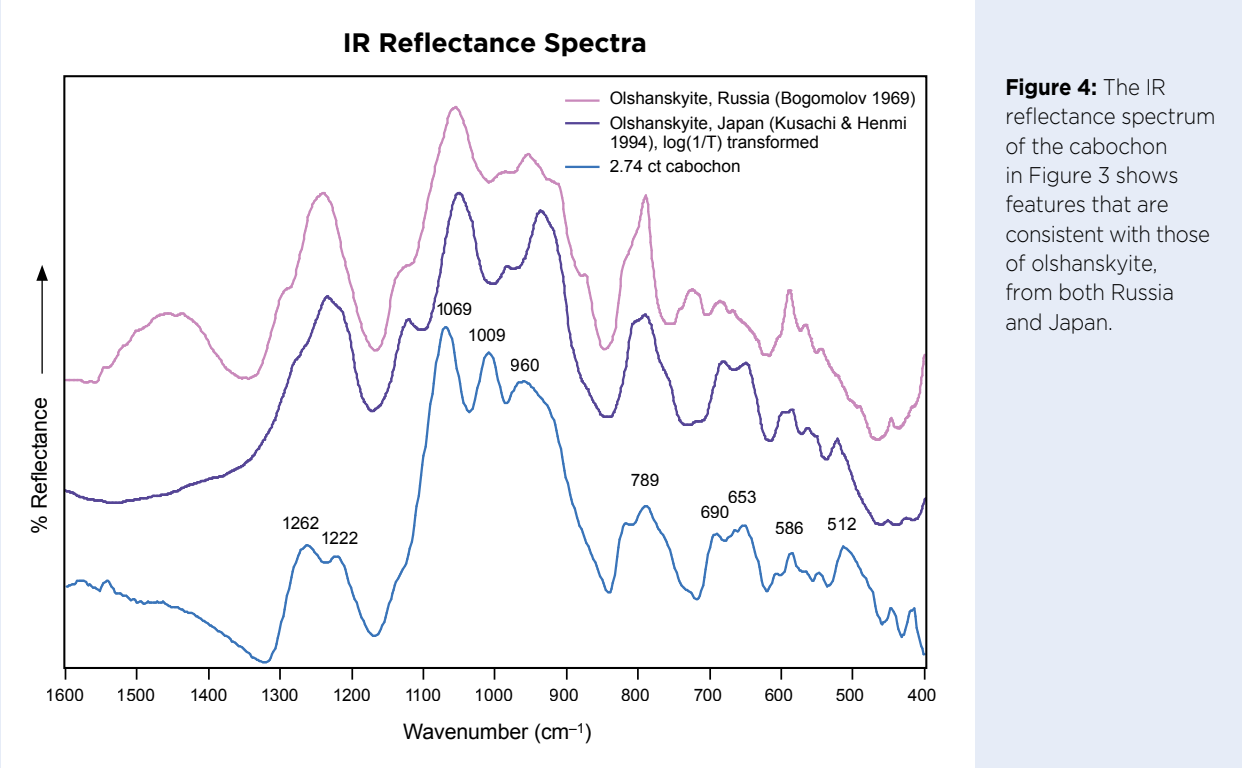

Figure 4: The IR reflectance spectrum of the cabochon in Figure 3 shows features that are consistent with those of olshanskyite, from both Russia and Japan.

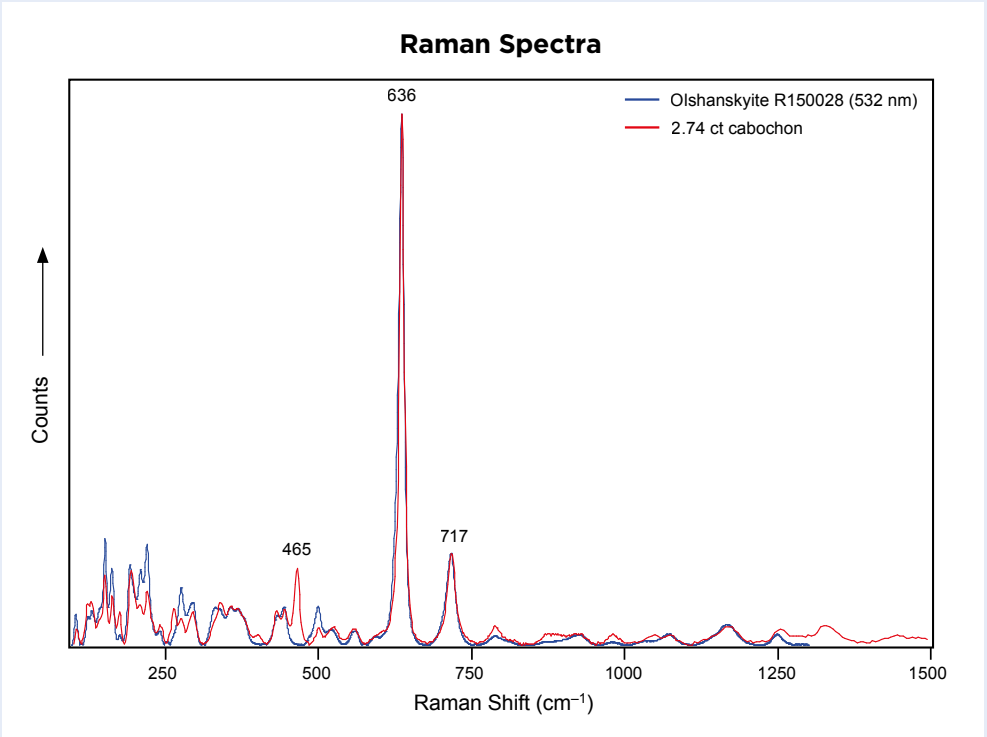

Figure 5: The Raman spectrum of the stone in Figure 3 shows a good match with a reference spectrum for olshanskyite (here, from the Shijiangshan mine, China: RRUFF R150028, collected with 532 nm laser excitation).

770 nm (weak) and 990 nm (moderate). All of these are unexplained except for the 990 nm band, which the author interprets as being related to OH overtones and combinations, in accordance with the hydrous character of the material.

The stone's photoluminescence (PL) spectrum was studied using several excitation sources: 254, 280, 375, 405 and 532 nm, but only those of 375 and 405 nm gave results, yielding bluish white luminescence (visible to the unaided eye only with the 405 nm laser). The PL spectra obtained from the two excitations differed only in their intensity, and consisted of a broad asymmetric emission from 400 to 700 nm. Such luminescence is known for olshanskyite and has been attributed to organic fluorophors (Gorobets & Rogojine 2002, pp. 269 and 272).

Standard gemmological testing showed that the cabochon was not parasibirskite, and suggested olshanskyite or frolovite as possibilities. Both IR and Raman spectroscopy conclusively identified the cabochon as olshanskyite despite the relative rareness of reference spectra for such uncommon borate minerals.

Acknowledgement: The author thanks Aurélien Delaunay (Laboratoire Français de Gemmologie, Paris, France) for performing Raman spectroscopy.

Thierry Cathelineau
(thierry.cathelineau@spec4gem.info)
Paris, France

References

Bogomolov, M.A., Nikitina, I.B. & Pertsev, N.N. 1969. Olshanskyite, a new calcium borate. *Doklady Akademii Nauk SSSR*, **184**(6), 1398–1401 (in Russian).

Gorobets, B.S. & Rogojine, A.A. 2002. *Luminescent Spectra of Minerals*. RPC VIMS, Moscow, Russia, 300 pp.

Kusachi, I. & Henmi, C. 1994. Nifontovite and olshanskyite from Fuka, Okayama Prefecture, Japan. *Mineralogical Magazine*, **58**(391), 279–284, https://doi.org/10.1180/minmag.1994.058.391.10.

Kusachi, I., Henmi, C. & Kobayashi, S. 1995. Frolovite from Fuka, Okayama Prefecture, Japan, *Mineralogical Journal*, **17**(7), 330–337, https://doi.org/10.2465/minerj.17.330.

Kusachi, I., Takechi, Y., Henmi, C. & Kobayashi, S. 1998. Parasibirskite, a new mineral from Fuka, Okayama Prefecture, Japan, *Mineralogical Magazine*, **62**(4), 521–525, https://doi.org/10.1180/002646198547891.

Kusachi, I., Kobayashi, S., Henmi, C. & Takechi, Y. 1999. Calcium borate minerals in the CaO-B_2O_3-H_2O system at Fuka, Okayama Prefecture, Japan. *Journal of Physics of the Earth*, **28**(2), 41–46, https://doi.org/10.2465/gkk1952.28.41 (in Japanese).

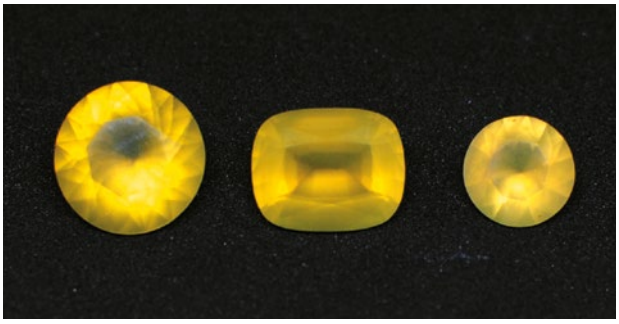

Figure 6: These faceted yellow opals, weighing (from left to right) 5.69, 5.08 and 2.24 ct, are reportedly from the Kasula District in western Tanzania. Photo by J. Štubňa.

Figure 7: Tanzanian yellow opal has also been polished into translucent cabochons (here, 8.32 and 6.83 ct). Photo by J. Štubňa.

Yellow Opal from Tanzania

Opal ($SiO_2 \bullet nH_2O$) is amorphous (opal-A) or poorly crystalline (opal-CT) hydrated silica with a water content that usually varies from 4% to 10% (Gaillou 2015). It is appreciated for its wide range of body colours and, in some cases, for its play-of-colour. Gem-quality yellow 'common' opal (without play-of-colour) has been described from Mexico (Gaillou *et al.* 2008), West Africa (Moe 2012) and Brazil (Laurs & Renfro 2018).

At the June 2014 Sainte-Marie-aux-Mines Mineral & Gem show in France, the present authors obtained some rough yellow opal samples reportedly from the Kasula District in the Kigoma region of western Tanzania, which is bordered on the north-west by Burundi. The seller had several tens of kilograms of rough material for sale. For this study, we selected 500 g of rough that was not cracked and ranged from transparent to semi-transparent. We stored the material in our laboratory for a few years to see if it was resistant to crazing but it has shown no signs of instability.

Some of the more-transparent rough material was faceted into round- and cushion-shaped mixed cuts that ranged from 10 to 13 mm in maximum dimension (2.24–5.69 ct; Figure 6). In addition, two cabochons with dimensions of 17 × 12 mm (6.83 and 8.32 ct; Figure 7) were polished from translucent material. The stones had RIs of 1.436–1.450 and hydrostatic SG values of 1.98–2.07. They were inert to long- and short-wave UV radiation. The samples were placed in water for 60 minutes to check for hydrophane character, but no improvement in their transparency was seen. Microscopic observations revealed a transparent flow structure with an oily appearance in each sample, as well as whitish clouds (Figure 8a). Small whitish globules were also observed in all stones (Figure 8b).

Powder X-ray diffraction analysis indicated that the stones were structurally opal-CT with the presence of cristobalite, tridymite and quartz. Chemical analysis by electron microprobe yielded 91.72 wt.% SiO_2, 0.40 wt.%

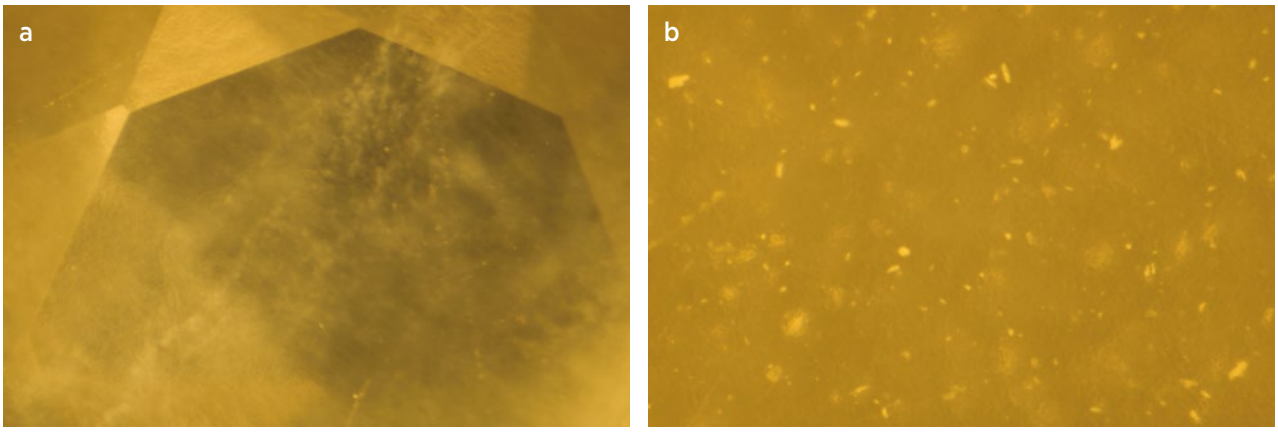

Figure 8: Whitish clouds (**a**) and small whitish globules (**b**) are present in the Tanzanian yellow opals. Photomicrographs by J. Štubňa; magnified 20× (a) and 30× (b).

FeO, 0.13 wt.% MgO and 0.12 wt.% CaO. The traces of Fe are consistent with the yellow colouration of this opal (cf. Gaillou *et al*. 2008). The characteristics of our Tanzanian samples overlap with those of the yellow opals documented from Mexico, West Africa and Brazil, which all consist of opal-CT.

Dr Ján Štubňa (janstubna@gmail.com)
Gemmological Laboratory, Constantine the Philosopher University, Nitra, Slovakia

Dr Radek Hanus
Gemological Laboratory of e-gems.cz
Prague, Czech Republic

References

Gaillou, E. 2015. Overview of gem opals: From the geology to color and microstructure. *In*: Overlin, S. (ed) *Thirteenth Annual Sinkankas Symposium—Opal*. Pala International, Fallbrook, California, USA, 10–19.

Gaillou, E., Delaunay, A., Rondeau, B., Bouhnik-le-Coz, M., Fritsch, E., Cornen, G. & Monnier, C. 2008. The geochemistry of gem opals as evidence of their origin. *Ore Geology Reviews*, **34**(1–2), 113–126, https://doi.org/10.1016/j.oregeorev.2007.07.004.

Laurs, B.M. & Renfro, N.D. 2018. Gem Notes: Yellowish green to yellow opal from Brazil. *Journal of Gemmology*, **36**(3), 188–189.

Moe, K.S. 2012. Gem News International: Yellow opal from West Africa. *Gems & Gemology*, **48**(3), 226–227.

Titanite (Sphene) Inclusions in Ruby Identified by Infrared Spectroscopy

Figure 9: This 7.79 ct unheated ruby proved to contain an unusual mid-infrared absorption band, which correlated to its unusual inclusions. Photo by Alex Mercado, AGL.

More than 20 years ago, one of these authors demonstrated how mid-infrared spectroscopy could be used to identify mineral inclusions in gem corundum (Smith 1995). Since that time, author CPS has catalogued a number of mineral inclusions found in ruby and sapphire using this method. These include aluminium hydroxides (both diaspore and boehmite), calcite and weathering minerals (e.g. kaolinite and goethite), as well as various micas and other minerals.

Recently, a 7.79 ct ruby was submitted to the American Gemological Laboratories (AGL) for analysis (Figure 9). In addition to concentrations of rutile silk and a few partially healed fissures, this unheated natural ruby also possessed a large number of small, transparent, light yellow crystals (Figure 10). Raman analysis of several of these crystals identified them as titanite (sphene).

Interestingly, the mid-infrared spectrum of this ruby revealed an unusual absorption band centred at approximately 3482 cm^{-1}. Experience indicated to the authors that this band was not intrinsically related to corundum, so we compared it to the spectrum of titanite, which also shows a dominant absorption band in this region. To confirm that the 3482 cm^{-1} band recorded in the ruby was related to the dominant absorption present in titanite, the two spectra were overlaid (Figure 11).

Most minerals reveal characteristic identifying absorption features in the 7000–1000 cm^{-1} region (e.g. Hainschwang & Notari 2008). Because corundum (Al_2O_3)

Figure 10: The ruby in Figure 9 contains an unusually high concentration of titanite (sphene) inclusions. Photomicrograph by C. P. Smith; magnified 42×.

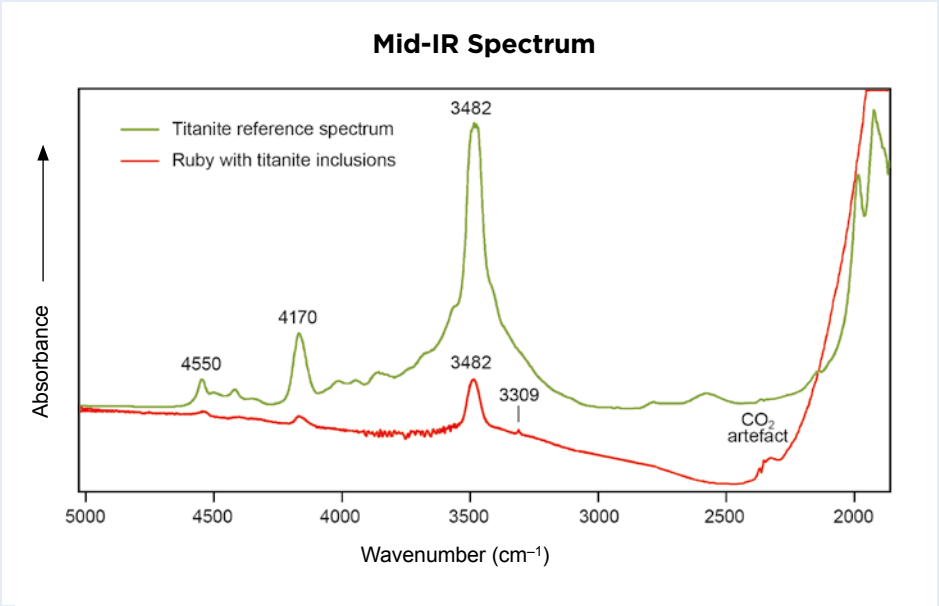

Figure 11: The mid-IR spectrum of the ruby reveals an unusual absorption band at approximately 3482 cm^{-1}. The mid-IR region of titanite possesses a dominant absorption band in the same position. The presence and shape of this band in the corundum spectrum further demonstrates the usefulness of IR spectroscopy to identify the presence of titanite inclusions.

is an anhydrous mineral, the mid-infrared region of the spectrum between 5000 and 1800 cm^{-1} can be useful for the identification of mineral inclusions, as well as the heated or unheated condition of a ruby or sapphire.

Christopher P. Smith FGA
(chsmith@aglgemlab.com),
Adrian Hartley and Dr Riadh Zellagui
American Gemological Laboratories
New York, New York, USA

References

Hainschwang, T. & Notari, F. 2008. Specular reflectance infrared spectroscopy—A review and update of a little exploited method for gem identification. *Journal of Gemmology*, **31**(1), 23–29, http://doi.org/10.15506/jog.2008.31.1.23.

Smith, C.P. 1995. A contribution to understanding the infrared spectra of rubies from Mong Hsu, Myanmar. *Journal of Gemmology*, **24**(5), 321–335, http://doi.org/10.15506/JoG.1995.24.5.321.

Sphalerite from Slovakia

Sphalerite is a zinc ore mineral (ZnS) that is usually opaque black due to the presence of Fe impurities. Gem-quality material has relatively lower Fe and forms transparent crystals that are yellow to orange, brown or green. One of the most notable characteristics of sphalerite is its high dispersion (0.156), which is nearly four times greater than that of diamond.

The Banská Štiavnica precious- and base-metal ore district is one of the largest in the Carpathian arc of central Europe (Lexa *et al.* 1999). It is situated in the central zone of a large andesite stratovolcano, including the caldera, resurgent dome and an extensive subvolcanic intrusive complex (Lexa *et al.* 1999). The deposit is one of the most studied in Europe and has been well known since the 8th century, particularly for its gold and silver deposits, as well as its lead, zinc and copper ores (Lexa *et al.* 1999; Prokofiev *et al.* 1999). Base-metal production increased gradually during the 19th century from deeper veins, and attained a maximum during the 20th century, before ceasing in 1992 (Lexa *et al.* 1999).

Transparent sphalerite crystals up to 1 cm in dimension showing yellow-orange, brown and sometimes green colouration are quite common in the Banská Štiavnica ore district. However, the sphalerite has received relatively little attention as a gem material since the miners were mainly focused on the recovery of precious and base metals.

For this study, we examined 100 g of rough (1–7 mm in maximum dimension) and two relatively large (for Slovakia) representative samples of faceted sphalerite from Banská Štiavnica. The cut stones weighed around 1 ct each (Figure 12); they consisted of a brown, round, mixed cut with dimensions of 6.17 × 6.19 × 3.51 mm (1.16 ct) and a yellow-orange octagon that measured 5.62 × 5.60 × 3.41 mm (1.00 ct). The RIs of each cut stone were 2.179–2.255 (measured with a Presidium Refractive Index Meter II)

Figure 12: These faceted sphalerites from Banská Štiavnica, Slovakia, weigh 1.16 (left) and 1.00 ct (right). Photo by J. Štubňa.

and hydrostatic SG ranged from 4.09 to 4.14. Their identity as sphalerite was confirmed by Raman spectroscopy, which showed bands at 220, 278, 300, 350, 377, 393, 400, 408, 420, 609, 614, 635, 669 and 696 cm^{-1}. EDXRF spectroscopy detected Zn as a major element, along with some minor Fe, Cd, Pb and Ga. Ultraviolet-visible-near infrared (UV-Vis-NIR) spectroscopy revealed absorption bands at 460 nm (in the yellow-orange stone), 492 nm (in the brown stone), and at 668, 700 and 725 nm (in both samples; Figure 13). Overall, both the yellow-orange and brown gems showed strong absorption in the blue and violet regions and lesser absorption in the red part of the spectrum (cf. Anderson & Payne 1956).

Local collectors still obtain sphalerite from the old mine dumps in the Banská Štiavnica ore district, and rough material of various qualities and sizes is commonly available at local gem and mineral shows (where it is typically sold as mineralogical samples). A neighbouring mine in Hodruša-Hámre, Slovakia, has the potential to produce additional sphalerite. It is currently the only active underground gold mine in central Europe, and transparent sphalerite occurs there as an accompanying mineral.

Dr Jana Fridrichová and Dr Peter Bačík
Comenius University, Bratislava, Slovakia

Dr Ján Štubňa (janstubna@gmail.com) and
Dr Ľudmila Illášová
Gemmological Laboratory, Constantine the Philosopher University, Nitra, Slovakia

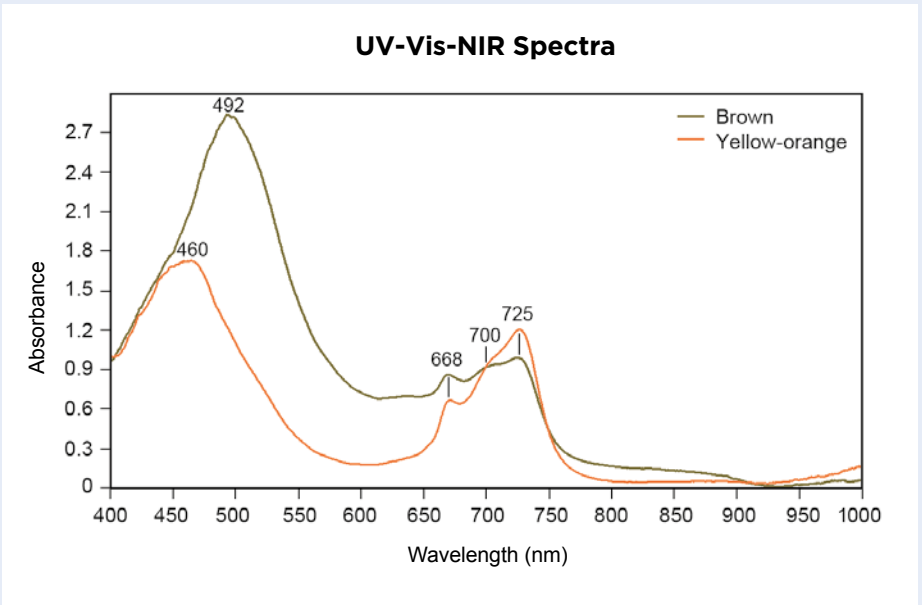

Figure 13: The UV-Vis-NIR spectra of the two faceted sphalerite samples show absorption bands at 460 (yellow-orange sample), 492 (brown sample), and at 668, 700 and 725 nm (both gems).

References

Anderson, B.W. & Payne, C.J. 1956. The spectroscope and its applications to gemmology. Part 36: Notes on miscellaneous spectra. *The Gemmologist*, **25**(301), 143–144.

Lexa, J., Štohl, J. & Konečný, V. 1999. The Banská Štiavnica ore district: Relationship between metallogenetic processes and the geological evolution of a stratovolcano. *Mineralium Deposita*, **34**(5–6), 639–654, https://doi.org/10.1007/s001260050225.

Prokofiev, V., Kamenetsky, V.S., Kovalenker, V., Bodon, S.B. & Jelen, S. 1999. Evolution of magmatic fluids at the Banska Stiavnica precious and base metal deposit, Slovakia; evidence from melt and fluid inclusions. *Economic Geology*, **94**(6), 949–955, https://doi.org/10.2113/gsecongeo.94.6.949.

DIAMONDS

Kimberley Diamond Acquired by the Smithsonian Institution, and Its Fluorescence and Phosphorescence Characteristics Revealed

The remarkable 55.08 ct Kimberley diamond was recently donated to the Smithsonian Institution's National Gem Collection by Bruce Stuart. It was unveiled to the public in the Museum of Natural History's National Gem Collection Gallery in October 2019. The Fancy yellow Kimberley diamond is noted for its distinctive emerald cut and classically elegant Baumgold Brothers necklace setting (Figure 14a). The diamond is named for its place of origin—the famous Kimberley mining region of South Africa.

Investigations into the history of the Kimberley diamond, via the Internet and classic books on famous diamonds, typically reveal some variations on a story that begins with a rough diamond of about 490 ct, sometimes described as elongated and flat, that was found in the 1870s or 1880s (or, in one case, between 1869 and 1871) at the Kimberley mine. Some sources then suggest, without references or other evidence, that the diamond became part of the Russian Crown Jewels.

It supposedly reached Europe during the upheavals of the 1917 Bolshevik revolution, and in 1921 was purchased by an anonymous buyer who had the large flat stone cut (or recut) into a 70 ct modern-shaped flawless gem. But later, as the story goes, in 1958 the stone was again recut by its new owners, Baumgold Brothers Inc. (New York, New York, USA), to improve its proportions and increase its brilliance. They then sold it to an undisclosed collector in 1971. Various newspaper accounts during the 1960s described the diamond as weighing 55 or 70 ct.

Our research has revealed that some of the early history of the Kimberley diamond is inaccurate. It was, in fact, cut around 1940 by the Baumgold Brothers to the 55.08 ct elongated emerald-cut gem we know today from a 490 ct diamond found in the Kimberley mining region of South Africa. In *Notable Diamonds of the World* (Diamond Information Center 1971), the rough diamond is referred to as the Baumgold II. This Fancy yellow diamond was then set into the current platinum necklace and accented with 80 baguette-cut diamonds that weighed an additional 20 ct. The first-known reference to the faceted diamond mounted in the current necklace is a jewellery store advertisement in the 10 March 1940 issue of *Miami News* (p. 9).

It travelled to many jewellery stores and other venues throughout the United States in the 1940s to the 1960s, often being featured in local newspapers and other media. The necklace appeared on the television shows *It Takes a Thief* and *Ironside* in 1968. (The Smithsonian's Victoria-Transvaal Diamond, which was also cut and set into a necklace by the Baumgold Brothers, appeared with the Kimberley diamond necklace on several occasions, including the episode of *Ironside*.)

The Kimberley diamond necklace was sold to an undisclosed collector in 1971. In April 1977, chemist Dr Herchel Smith acquired the necklace at a Sotheby Parke-Bernet auction in New York. Dr Smith's estate consigned the necklace to Christie's auction house in October 2002,

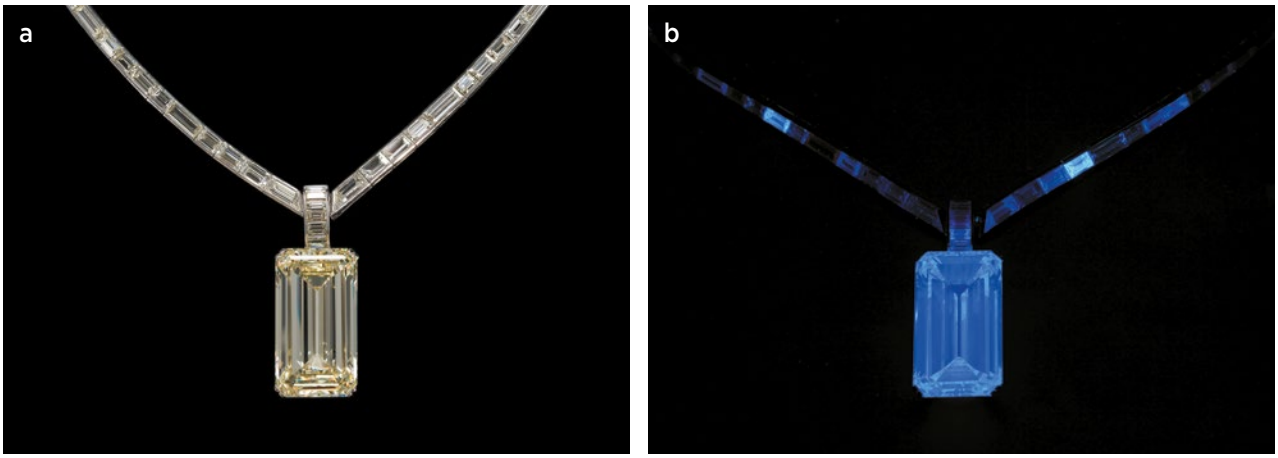

Figure 14: (**a**) The 55.08 ct Kimberley diamond was cut and mounted in a necklace by Baumgold Brothers around 1940. (**b**) The diamond fluoresces moderately strong blue under a 370 nm (long-wave) Convoy UV lamp. Photos courtesy of Smithsonian Images.

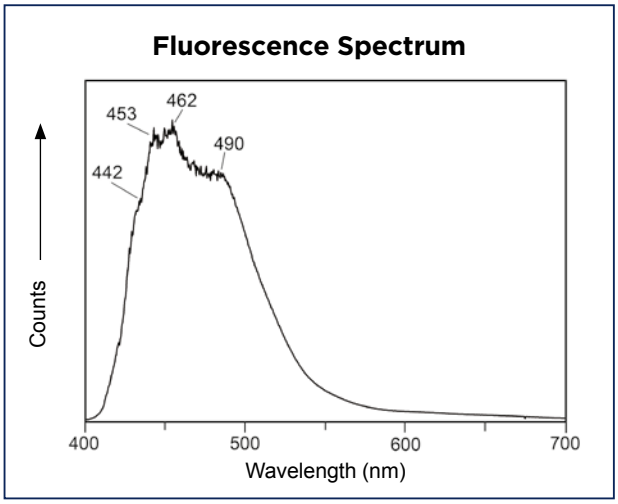

Figure 15: The fluorescence spectrum of the Kimberley diamond shows that the main emission is between 440 and 500 nm.

where it was acquired by Bruce Stuart. The diamond was on exhibit at the American Museum of Natural History in New York from July 2013 to June 2014. In July 2019, Bruce Stuart generously donated the Kimberley diamond necklace to the Smithsonian Institution.

The Gemological Institute of America issued a grading report for the Kimberley diamond in June 2002, which described it as natural Fancy yellow with VS_1 clarity (with the plot showing a chip, pinpoint, 'natural' and extra facet) having dimensions of 31.69 × 17.46 × 9.64 mm and a weight of 55.08 ct. The report also noted a faint fluorescence. We observed moderately strong blue fluorescence under long-wave UV radiation (Figure 14b), followed by a short-lived but noticeable orange phosphorescence. Several of the baguette diamonds in the necklace also exhibited weak to strong fluorescence, in various colours, under long-wave UV radiation.

We further examined the spectral characteristics of the UV-excited fluorescence and phosphorescence emissions with the spectrometer previously used to study the Hope and other coloured diamonds (Eaton-Magaña *et al.* 2007, 2008). In the present experiments, the UV source employed was a Convoy LED lamp (370 nm). Figure 15 displays the fluorescence spectral emission between 400 and 700 nm (approximately 10 nm resolution), and Figure 16 shows the phosphorescence emission as a function of time after turning off the UV source. The phosphorescence peak is centred at about 590 nm, consistent with the observed orange colour.

The fluorescence spectrum is similar to the one we measured from a small fragment of the Foxfire diamond, also donated to the Smithsonian's collection. The phosphorescence spectra are likewise similar (Butler *et al.* 2017), although the emission from the Kimberley diamond is considerably weaker than that measured for the Foxfire.

Dr Jeffrey E. Post (postj@si.edu), Russell Feather, and Dr James E. Butler
Department of Mineral Sciences
Smithsonian Institution, Washington DC, USA

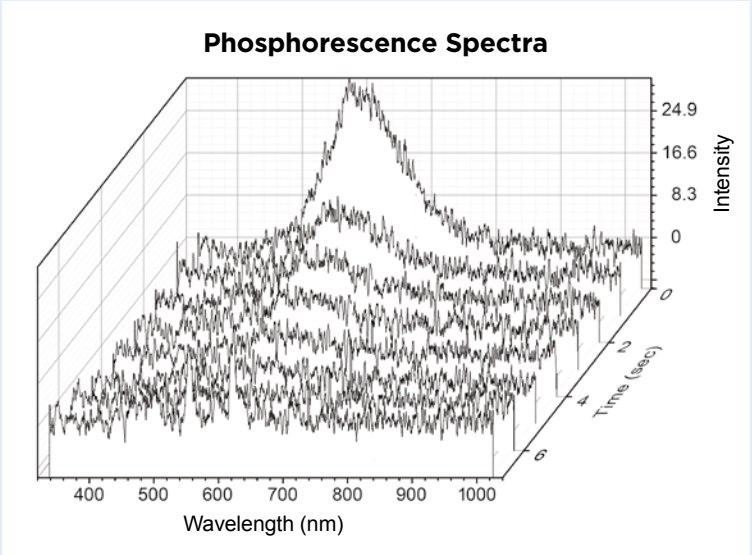

Figure 16: This series of phosphorescence spectra reveals the time of decay of emission after exposure to a 370 nm Convoy UV lamp. The spectra were collected at intervals of 1.5 seconds, with integration times of 1.5 seconds per spectrum.

References

Butler, J.E., Post, J.E. & Wang, W. 2017. Gem News International: The Foxfire diamond, revisited. *Gems & Gemology*, **53**(4), 79–81.

Diamond Information Center 1971. *Notable Diamonds of the World*. N.W. Ayer & Son, New York, New York, USA, 56 pp.

Eaton-Magaña, S., Post, J.E., Heaney, P.J., Walters, R.A., Breeding, C.M. & Butler, J.E. 2007. Fluorescence spectra of colored diamonds using a rapid, mobile spectrometer. *Gems & Gemology*, **43**(4), 332–351, https://doi.org/10.5741/gems.43.4.332.

Eaton-Magaña, S., Post, J.E., Heaney, P.J., Freitas, J., Klein, P., Walters, R. & Butler, J.E. 2008. Using phosphorescence as a fingerprint for the Hope and other blue diamonds. *Geology*, **36**(1), 83–86, https://doi.org/10.1130/g24170a.1.

SYNTHETICS AND SIMULANTS

CVD Synthetic Diamonds Identified in a Parcel of Light Brown Melee

Figure 17: These six 2.5-mm-diameter CVD synthetic diamonds were found in a parcel of more than 1,000 light brown diamonds. Photo by T. Hainschwang.

The Liechtenstein branch of GGTL Laboratories received a parcel of more than 1,000 melee-sized (1.2–3 mm diameter) light brown diamonds for authenticity and treatment identification (part of the lab's fancy-colour diamond screening services). Their depth of colour was below that required to be called 'Fancy'.

As per the lab's common procedure, the parcel was tested with the prototype of GGTL's Mega-DFI fluorescence microscopy and spectroscopy system. The vast majority of the samples showed the expected luminescence reactions, with the exception of seven diamonds (2.5 mm diameter) that showed distinct orange fluorescence. The PL spectra of these samples, which the DFI system records simultaneously during visual observation, revealed that six of the seven were synthetic diamonds grown by chemical vapour deposition (CVD; Figure 17). Between crossed polarisers the synthetics showed obvious brush-like extinction (e.g. Figure 18), which is characteristic for CVD products but sometimes resembles the extinction patterns seen in natural type IIa brown diamonds.

The room-temperature UV-excited PL spectra recorded with the DFI system for all seven samples revealed the presence of the NV^0 centre, which is characterised by a zero-phonon line at 575 nm and vibronic sidebands extending into the red part of the spectrum, which causes orange to reddish orange fluorescence (Figure 19a). Such UV-excited PL dominated by the NV^0 centre is very rare in natural brown diamonds since it is only found in type Ib samples. Brown does occur in type Ib diamonds, although it is the rarest colour for this type (Hainschwang *et al.* 2013).

Using the seven different fluorescence excitations of the DFI system for visual and spectral analysis, we confirmed that the six samples were as-grown CVD synthetic diamonds and the one additional diamond was a natural type Ib stone. The fluorescence pattern of the synthetics revealed the characteristic CVD layer-by-layer growth and associated dislocations, while the natural diamond exhibited deformation-related green PL from the H3 centre together with the orange NV^0 luminescence.

When excited by the 405 nm laser, the luminescence of all seven samples was a distinct green (e.g. Figure 19b), a phenomenon known in both natural type Ib and CVD synthetic diamonds. In natural diamonds the 405 nm laser excites the H3 centre more strongly than the NV^0 centre, while in as-grown CVD synthetics the laser excites the 467.6 nm centre more strongly than the NV^0 centre; both the H3 and the 467.6 nm centres result in green fluorescence. The room-temperature PL spectra recorded for the seven diamonds confirmed these respective centres were responsible for the green luminescence.

Infrared spectroscopy identified the six CVD synthetic diamonds as type IIa and the natural diamond as pure type Ib. The latter displayed a very distinct 'amber centre' absorption at 4110 cm^{-1}. The IR spectra of the other samples exhibited several features characteristic for CVD synthetic diamonds, such as lines at 7362, 6856, 6424, 5566 and 3123 cm^{-1}.

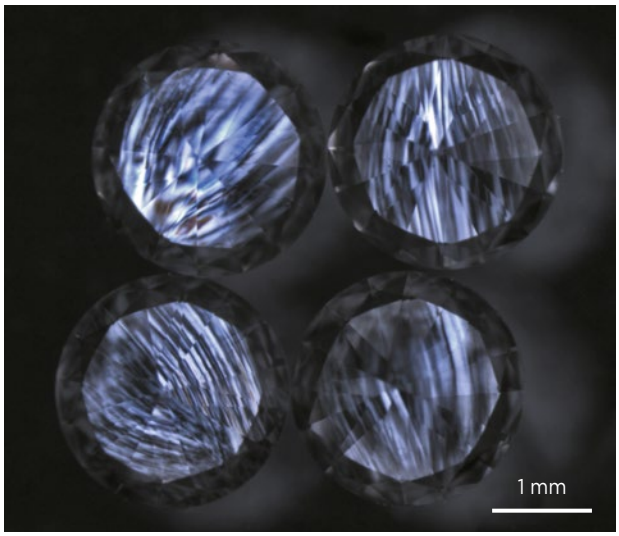

Figure 18: Some of the CVD synthetics are shown here between crossed polarising filters (and immersed in alcohol) to reveal their distinct brush-like extinction patterns. Photo by T. Hainschwang.

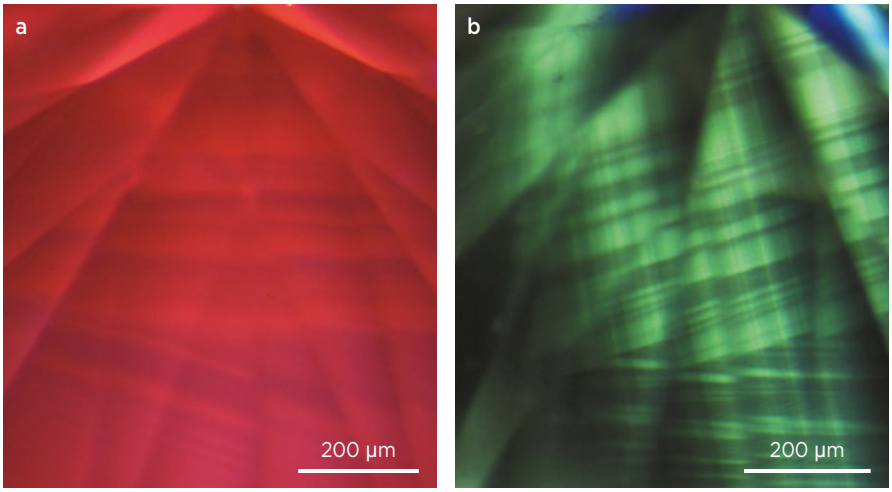

Figure 19: (**a**) Under all of the UV excitations of GGTL's DFI system, the CVD synthetic diamonds generally fluoresce a distinct orange due to the presence of the NV^0 centre, while also revealing their growth layers under some specific excitations of shorter wavelength. (**b**) Under 405 nm (in the visible range) laser excitation, the CVD synthetic diamonds fluoresce green from the 467.6 nm centre and show even more distinct growth layers. Both images were taken from the same sample. Photomicrographs by T. Hainschwang.

High-resolution, low-temperature PL spectroscopy using 360, 402, 473 and 532 nm laser excitations on a GGTL Photoluminator research PL system confirmed the findings made by DFI testing. The CVD samples all exhibited very similar spectra, with a series of defects characteristic for CVD synthetic diamonds, such as the 388.8 nm, 467.6 nm, NV^0 and Si-V^- centres. In addition to these, numerous sharp PL peaks were measured, particularly in the spectra recorded using the 360 nm laser (Figure 20). The vast majority of those are, in the author's experience, unique to CVD synthetic diamond, even though their causes are generally unknown.

The evaluation of melee-sized fancy-colour diamonds for their authenticity and colour origin is a specialised task that requires a combination of extensive diamond-testing experience and instrumentation created specifically for this type of screening. Until now, the mixing of synthetics (and colour-treated diamonds) into melee-sized parcels has almost exclusively been restricted to yellow to orange diamonds. However, the present case confirms rumours that untreated brownish CVD synthetics are now being mixed into parcels of natural brown diamonds, thereby eliminating the need for HPHT treatment of as-grown CVD material to render it near-colourless to colourless.

After preparing the first draft of this article, we received several parcels of brown and pinkish brown diamonds from various sources totalling more than 20,000 pieces,

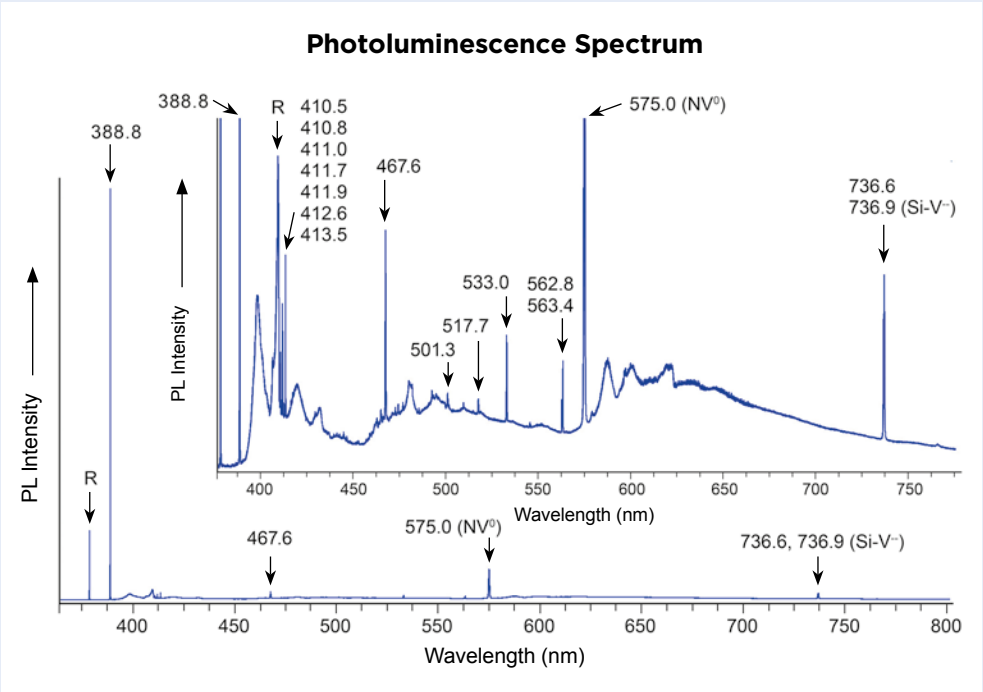

Figure 20: This PL spectrum, recorded for one of the CVD samples using 360 nm laser excitation, shows characteristic features for as-grown (that is, untreated) CVD synthetic diamond. The spectrum displays numerous very sharp peaks, and the most intense ones include the 388.8 nm, 467.6 nm, NV^0 and Si-V^- centres. The inset includes all spectral details, while the general spectral view shows the dominance of the very narrow 388.8 nm peak compared to the other PL emissions. R = Raman line.

and in these we detected more than 200 CVD synthetic diamonds, all with properties very similar to the ones described here. This provides further evidence that the contamination of brown melee parcels with CVD synthetics seems to have become a significant problem.

Dr Thomas Hainschwang FGA
(thomas.hainschwang@ggtl-lab.org)
GGTL Laboratories, Balzers, Liechtenstein

Reference

Hainschwang, T., Fritsch, E., Notari, F., Rondeau, B. & Katrusha, A. 2013. The origin of color in natural C center bearing diamonds. *Diamond and Related Materials*, **39**, 27–40, https://doi.org/10.1016/j.diamond.2013.07.007.

Multicoloured Synthetic Corundum and Multicoloured Glass Doublets in the Thai Gem Market

Gem-quality synthetic corundum can be grown in virtually all colours by means of the flame-fusion (Verneuil) technique (Nassau 1980). Even color-zoned samples have occasionally been observed (Kiefert 2004; Choudhary 2009). Recently, some high-quality synthetic corundum showing multiple colours has appeared in the Thai gem market. The gems are cut from colour-zoned Verneuil boules (Figure 21) that are grown by changing the composition of trace elements during synthesis (including Cr for red; Ti and Fe for blue; Cr, Ti and Fe for purple; Ni for yellow; etc.). The multicoloured rough material is produced by Thai Tech Sapphire Co. Ltd (Sathon, Bangkok, Thailand), which operates its own corundum-growth factory in Rayong Province, Thailand. Although the company only mentions monochrome synthetic sapphire on its website, it does offer production of custom-coloured boules.

We performed a basic gemmological and Raman spectroscopic investigation on six half-boules of the new multicoloured synthetic corundum (five of them are shown in Figure 21), and the experimental procedures corresponded to those described in Zeug *et al.* (2018). The material showed properties typical of synthetic corundum, including RIs of 1.753–1.760 and SG values (here reported as mass density) of 3.98–4.01 g/cm^3. The nature of this material as a synthetic flame-fusion product could be recognised by occasional curved striae visible under white-light illumination and/or UV radiation (Figure 22a; cf. Anderson 1967), as well as the presence of small, round-to-elongated gas bubbles (Figure 22b). When exposed to UV radiation, the luminescence colour and intensity depended mainly on Cr concentration and body colour. Most of the colour zones showed various intensities of red (and occasionally orange) luminescence, which was particularly strong under long-wave UV radiation. Only under short-wave UV radiation did amethyst-coloured zones (see left boule in Figure 21) show pale whitish luminescence.

Figure 21: A 24.45 ct faceted synthetic corundum and five Verneuil half-boules (21.7–33.1 g) are representative of material now being produced by Thai Tech Sapphire Co. Ltd. Photo by L. Nasdala.

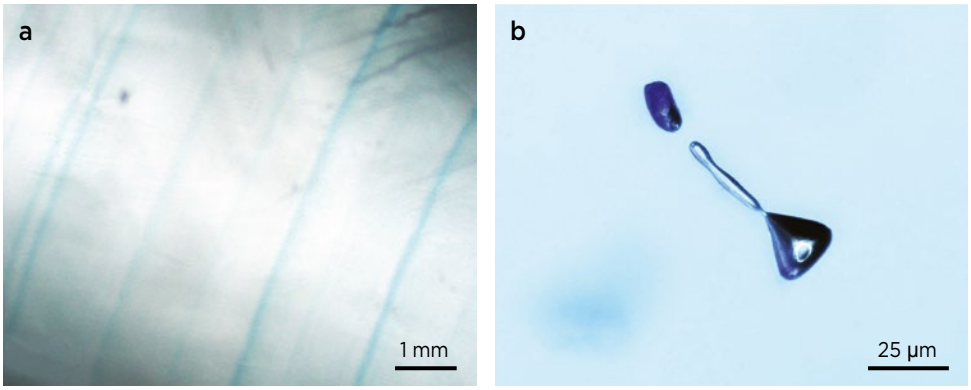

Figure 22: (**a**) Coloured curved striae visible in some samples of the multicoloured synthetic corundum are typical of Verneuil products. (**b**) This elongated gas inclusion (53 µm in length) is also characteristic of this material. Photomicrographs by L. Nasdala (a) and Michael Korntner (b).

Interestingly, the recent appearance of the multicoloured synthetic corundum in the Thai gem market seems to be accompanied by a vast increase in the supply of cheap multicoloured doublets (Figure 23a). Six of these samples (four of them are shown in Figure 23) were investigated. In contrast to the high-quality doublets described by Hänni and Henn (2015) with crown and pavilion pieces made of quartz, topaz, beryl or tourmaline, these new products simply consist of colourless soda-lime glass (identified by Raman spectroscopy; see Figure 24 and Deschamps *et al.* 2011 for a reference spectrum). A coloured resin layer (25–50 µm in thickness) is used to impart colouration and cement the two glass layers together. In some samples a single resin layer is present, whereas others contain two resin layers (i.e. coloured and colourless; Figure 24). The resins consist of acrylic polymers that are soluble in acetone, and Raman spectroscopy of the coloured ones showed a polystyrenic component (cf. Serafim *et al*. 2014) in polymethylmethacrylate (cf. Thomas *et al*. 2008). The colourless resin mainly consists of polybutylmethacrylate (cf. Kang *et al.* 2006).

These doublets are easily recognised. Viewed from the side, the colourless nature of the material could be seen through the girdle facets (Figure 23b); colour was evident when observed at angles to the central resin membrane. Insufficient contact between resin and glass may cause the appearance of colourless spots that were also visible at angles to the resin layer (Figure 23b), a quality problem that we saw in about one-third of the doublets we observed on the market. Under long-wave UV radiation, the samples (especially yellow and pink zones) showed intense 'lemon'-yellow to whitish luminescence that originated from the resin

Figure 23: (**a**) Four faceted glass doublets (6.4–14.9 ct) represent another multicoloured material that has recently appeared on the Thai gem market. (**b**) Even without immersion it can be seen that the pavilion and crown of this 6.7 ct doublet are colourless; the apparent colouration is caused by the central resin layer. The small colourless spot in the upper right of this sample (only visible from the side) is caused by insufficient contact between the pavilion and the resin layer. Photos by L. Nasdala.

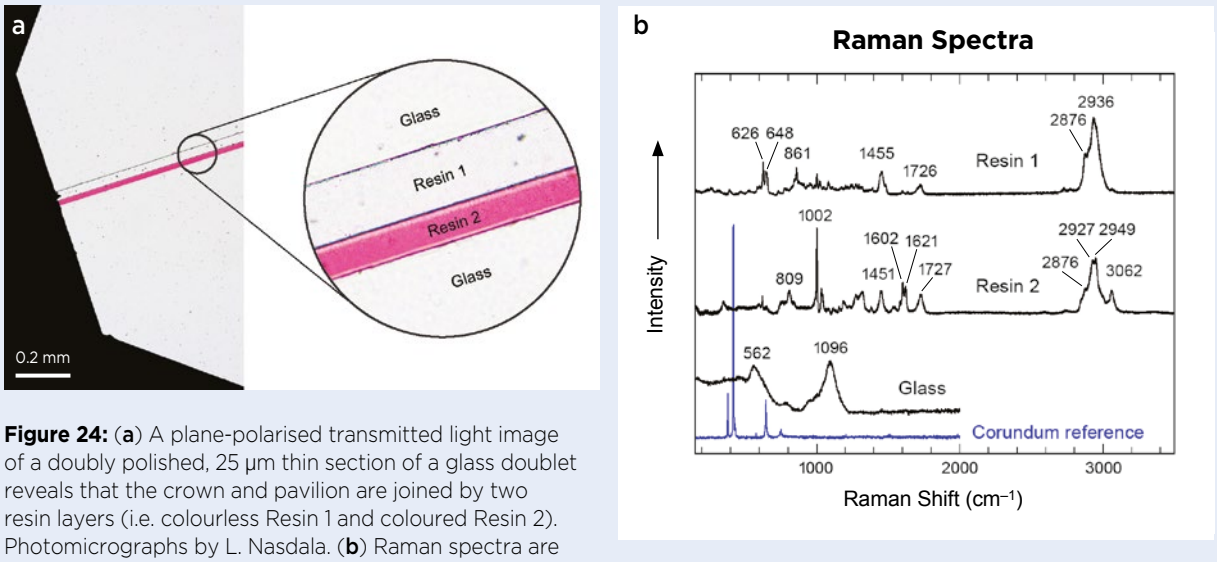

Figure 24: (**a**) A plane-polarised transmitted light image of a doubly polished, 25 µm thin section of a glass doublet reveals that the crown and pavilion are joined by two resin layers (i.e. colourless Resin 1 and coloured Resin 2). Photomicrographs by L. Nasdala. (**b**) Raman spectra are shown for both resin layers and for the glass composing the doublet. Comparison with a reference spectrum for corundum (obtained from the faceted sample shown in Figure 22) clearly shows that no corundum is present in these doublets.

membrane; only mild luminescence was seen in the green and dark blue zones. The doublets had low SG values (corresponding to a mass density of 2.48–2.50 g/cm^3) and a relatively low, glassy lustre (RI ranged from 1.510 to 1.515).

Acknowledgements: We thank Narongsak Putthapornmongkol for providing most of the boules and Kongpapat Leeniticharoenkit (both of Thai Tech Sapphire Co. Ltd) for comments. We also thank Andreas Wagner (University of Vienna) for sample preparation and Michael Korntner (Keyence International [Belgium] NV/SA) for the photo of the gas inclusion in Figure 22b.

Prof. Dr Lutz Nasdala (lutz.nasdala@univie.ac.at),
Dr Chutimun Chanmuang N. and
Prof. Dr Gerald Giester
University of Vienna, Austria

Dr Bhuwadol Wanthanachaisaeng
Srinakharinwirot University, Bangkok, Thailand

References

Anderson, B.W. 1967. Notes and News: Curved striae under short-wave ultra-violet light. *Journal of Gemmology*, **10**(6), 199, https://doi.org/10.15506/JoG.1967.10.6.198.

Choudhary, G. 2009. Synthetic sapphires with 'natural-like' sheen. *Gems&Jewellery*, **18**(3), 6–9.

Deschamps, T., Martinet, C., Bruneel, J.L. & Champagnon, B. 2011. Soda-lime silicate glass under hydrostatic pressure and indentation: A micro-Raman study. *Journal of Physics: Condensed Matter*, **23**(3), article 035402 (8 pp.), https://doi.org/10.1088/0953-8984/23/3/035402.

Hänni, H.A. & Henn, U. 2015. Gem Notes: Modern doublets, manufactured in Germany and India. *Journal of Gemmology*, **34**(6), 478–482.

Kang, E., Wang, H., Kwon, I.K., Robinson, J., Park, K. & Cheng, J.-X. 2006. In situ visualization of paclitaxel distribution and release by coherent anti-stokes Raman scattering microscopy. *Analytical Chemistry*, **78**(23), 8036–8043, https://doi.org/10.1021/ac061218s.

Kiefert, L., Hänni, H.A. & Schmetzer, K. 2004. Gem News International: Synthetic Verneuil corundum with unusual color zoning. *Gems & Gemology*, **40**(4), 354–355.

Nassau, K. 1980. *Gems Made by Man*. Chilton Book Co., Radnor, Pennsylvania, USA, 364 pp.

Serafim, A., Mallet, R., Pascaretti-Grizon, F., Stancu, I.-C. & Chappard, D. 2014. Osteoblast-like cell behavior on porous scaffolds based on poly(styrene) fibers. *BioMed Research International*, **2014**, article 609319 (6 pp.), https://doi.org/10.1155/2014/609319.

Thomas, K.J., Sheeba, M., Nampoori, V.P.N., Vallabhan, C.P.G. & Radhakrishnan, P. 2008. Raman spectra of polymethyl methacrylate optical fibres excited by a 532 nm diode pumped solid state laser. *Journal of Optics A: Pure and Applied Optics*, **10**(5), article 055303 (5 pp.), https://doi.org/10.1088/1464-4258/10/5/055303.

Zeug, M., Nasdala, L., Wanthanachaisaeng, B., Balmer, W.A., Corfu, F. & Wildner, M. 2018. Blue zircon from Ratanakiri, Cambodia. *Journal of Gemmology*, **36**(2), 112–132, https://doi.org/10.15506/JoG.2018.36.2.112.

Imitations of Trapiche Ruby and Emerald

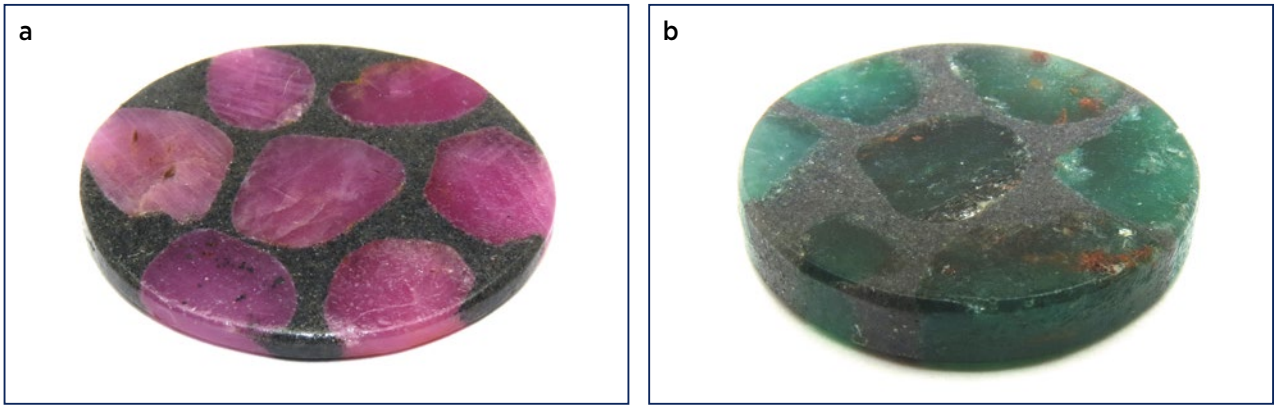

Figure 25: The two samples reported here were originally identified as (**a**) 'natural trapiche ruby' (about 27 mm wide) and (**b**) 'natural trapiche emerald' (about 24 mm wide). Photos by Dirk van der Marel.

In October 2019, a concerned customer came to the Netherlands Gemmological Laboratory with several stones, each accompanied by a report from the Authentic Gem Security Laboratory. This name did not sound familiar, but according to the lab reports this organisation is based in Delhi, India. The customer asked us to check whether the issued reports were accurate. Testing of some initial samples reported as 'natural star sapphire, heated, from Madagascar', 'natural sapphire, heated, from Sri Lanka' (in pink, purple and blue) and 'natural ruby, heated, from Mogok' showed that they were synthetic corundum.

We also selected a 'natural trapiche ruby from Mogok (Burma)' and a 'natural trapiche emerald from Colombia' for further study. Both of them had translucent areas (pink to purplish red and bluish green, respectively) together with opaque dark grey 'matrix' material. The 'ruby' specimen consisted of an oval slab measuring 26.97 × 22.93 × 2.56 mm and weighing 3.56 g (Figure 25a), and the 'emerald' specimen was a round slab measuring 24.05–24.51 × 4.29 mm and weighing 5.02 g (Figure 25b).

The pink to purplish red areas of the first specimen yielded a Cr spectrum and strong red fluorescence to long-wave UV radiation, both typical of ruby. They had rounded or hexagonal shapes and were heavily included. Lamellar twinning showed comparatively random orientations between the various areas, indicating they were actually different pieces rather than part of a single crystal. Raman analysis of these fragments with a Thermo Scientific DXR Raman microscope using 532 nm laser excitation focused slightly underneath the surface revealed Raman and PL spectra typical of ruby. Small, orangey brown inclusions were identified as rutile, confirming these ruby fragments to be of natural origin.

The dark 'matrix' areas fluoresced strong whitish blue to long-wave UV radiation (Figure 26). Magnification revealed that they were not entirely opaque, but contained abundant granular, dark angular fragments and gas bubbles within a translucent to transparent material (Figure 27).

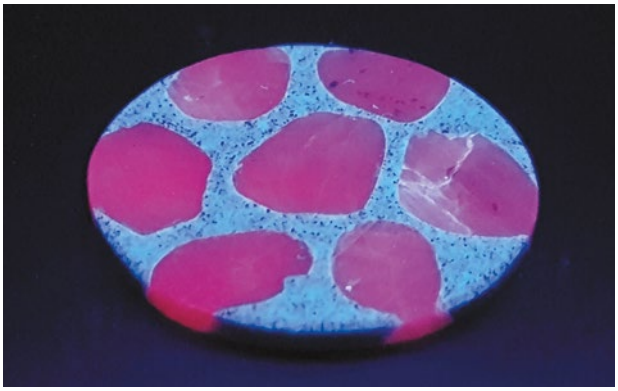

Figure 26: Exposure of the supposed 'trapiche ruby' to long-wave UV radiation produces strong red fluorescence in areas corresponding to ruby and whitish blue luminescence from the interstitial material. Photo by J. C. Zwaan.

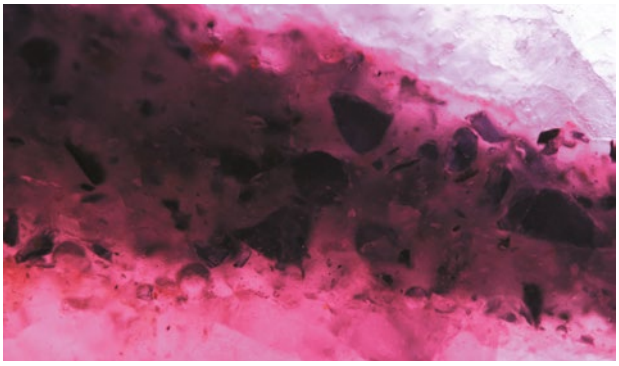

Figure 27: Microscopic examination of the 'matrix' material of the ruby-bearing sample shows abundant small, dark angular fragments and gas bubbles within a translucent to transparent material. Photomicrograph by J. C. Zwaan, brightfield illumination; image width 1.4 mm.

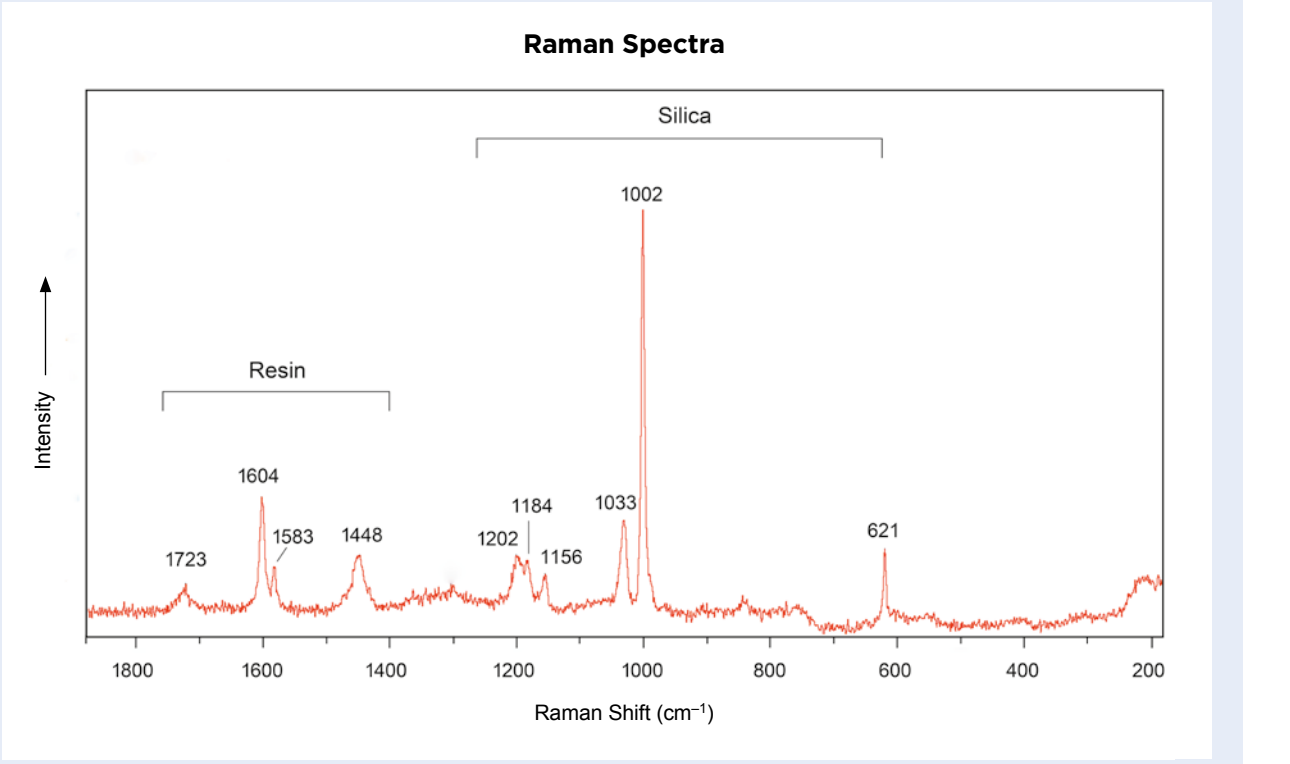

Figure 28: Raman spectroscopy of the 'matrix' material (here, from the ruby-bearing specimen) showed bands typical for a resin and silica mixture, confirming their manufactured nature.

EDXRF spectroscopy with an EDAX Orbis Micro-XRF Analyzer, using a spot size of 300 µm, revealed that the dark areas contained mainly Zr, Y and Si. At the surface of the ruby areas, a high concentration of Si was measured. Raman analysis of the small angular fragments confirmed the presence of cubic zirconia in a matrix that produced Raman bands characteristic of a mixture of resin and silica (Figure 28), as seen in some imitation or 'synthetic' opals. These same Raman bands were observed at the surface of the ruby fragments. We concluded that this imitation of trapiche ruby was an assemblage consisting of seven ruby fragments embedded in a resin-and-silica 'matrix' containing cubic zirconia grains.

The round slab with the green material was essentially the same type of product—an assembled imitation of a trapiche gem—although no emerald was detected. Raman analysis of the green areas identified them as muscovite, and EDXRF spectroscopy showed the expected presence of major Al, Si and K, along with minor Cr and Fe. An absorption spectrum viewed with a prism spectroscope revealed a band at about 565–610 nm and a sharp line at about 630 nm, which are consistent with the optical spectrum associated with Cr^{3+} in fuchsite, a Cr-bearing muscovite (cf. Reddy *et al.* 2003 and http://minerals.gps.caltech.edu//FILES/Visible/Mica/Index.html).

Dr J. C. (Hanco) Zwaan FGA
(hanco.zwaan@naturalis.nl)
Netherlands Gemmological Laboratory
National Museum of Natural History 'Naturalis'
Leiden, The Netherlands

Reference

Reddy, S.L., Reddy, R.R.S., Reddy, G.S., Rao, P.S. & Reddy, B.J. 2003. Optical absorption and EPR spectra of fuchsite. *Spectrochimica Acta Part A: Molecular and Biomolecular Spectroscopy*, **59**(11), 2603–2609, https://doi.org/10.1016/s1386-1425(03)00019-2.

TREATMENTS

Blue Sapphire with Partial Red Surface Diffusion

A 1.94 ct cushion-cut stone was recently submitted for confirmation of treatment. The stone was identified as corundum using a GemmoRaman-532SG spectrometer. It exhibited what at first appeared to be unusual dichroism in pale violetish blue and pink (Figure 29). Closer examination showed that the stone's body colour was pale violetish blue, while a deep reddish pink surface-related colouration was limited to the table and a small area along the pavilion (seen more easily with immersion; Figure 30a). Microscopic observation revealed several 'fingerprint' inclusions that confirmed a natural (not synthetic) origin of the sapphire. RI readings could not be obtained from the table facet.

Due to the proliferation of new coating treatments, it was initially presumed this the stone had undergone a coating process on selected surfaces. However, careful microscopic observation showed that the pink-coloured areas diffused slightly below the surface of the stone (Figure 30b), and EDXRF spectroscopy with an Amptek X123-SDD instrument indicated significant Cr. Also, the pink areas showed red fluorescence to long-wave UV excitation, whereas red-coated stones previously seen by the authors were inert. These characteristics are consistent with Cr-diffused corundum (e.g. McClure *et al.* 1993; Smith 2015). Moreover, infrared spectral features recorded with a GemmoFtir spectrometer confirmed the stone had been heat treated, so a red surface diffusion is presumed, most of which was polished off at some point.

Figure 29: This 1.94 ct sapphire exhibits an unusual colour appearance. Photo by Jeff Scovil.

It remains puzzling why the diffusion treatment was retained on some surface areas when the resulting overall appearance is so unnatural. Perhaps the intention was to create something different and unusual. With pale colours currently being in greater demand, it would not be surprising to see older treated stones

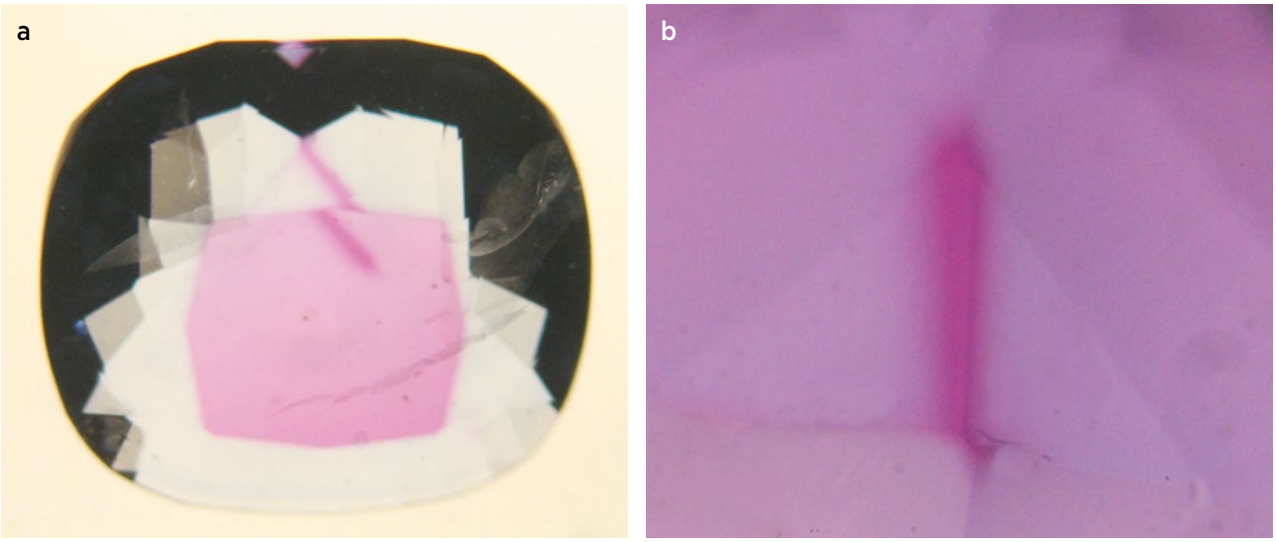

Figure 30: (**a**) Closer examination of the sapphire (immersed in water) shows pink colouration restricted to the table and along one portion of the pavilion. (**b**) At higher magnification (here, 22×), the deep pink area on the pavilion can be seen to penetrate slightly below the surface of the stone, as expected for Cr diffusion treatment. Photomicrographs by B. Williams.

being 'rejuvenated' by polishing off near-surface treatments, and such material may be more commonly encountered in the future.

Bear Williams FGA and Cara Williams FGA

Charles I. Carmona
Guild Laboratories Inc.
Los Angeles, California, USA

References

McClure, S.F., Kammerling, R.C. & Fritsch, E., 1993. Update on diffusion-treated corundum: Red and other colors. *Gems & Gemology*, **29**(1), 16–28, http://doi.org/10.5741/gems.29.1.16.

Smith, C.P. 2015. Gem Notes: Chromium-diffused corundum. *Journal of Gemmology*, **34**(6), 486–488.

Glass-filled White Sapphire

In January 2020, a client submitted for treatment verification a 62.59 ct translucent white cabochon, stated to be white sapphire (Figure 31). The stone's vitreous lustre matched what is expected for corundum, and its internal features consisted of lamellar twinning, parting planes and fractures (e.g. Figure 32), typical of cabochon-grade material. There were no dark inclusions present in the stone. The RI was measured by the spot method at approximately 1.77 and the hydrostatic SG was 3.99, identifying it as corundum. Overall the stone was inert to long-wave UV excitation, although some flat areas within fissures exhibited a whitish fluorescence that might be expected for polishing residues. There were also several areas that fluoresced a weak red that appeared to correspond with internal fissures and voids; this reaction could be consistent with the presence of some type of clarity enhancement.

Raman analysis of the stone with an Enwave spectrometer equipped with 785 nm laser excitation confirmed it as corundum, and an additional PL peak centred around 1321 cm^{-1} was present in the range expected for a glass. EDXRF spectroscopy with an Amptek X123-SDD instrument showed the presence of significant amounts of Pb, indicating that the cabochon was filled with a lead glass (Figure 33). While we have encountered many colours of corundum with lead-glass filling, this was the first white sapphire submitted to our laboratory treated in this manner.

It is interesting to note that none of the usual visual indicators of lead-glass filling were visible with magnification (such as gas bubbles or blue and orange flash effects; see, e.g., McClure *et al.* 2006 and Milisenda *et al.* 2006). Also, the sapphire's surface did not have the variable lustre that is sometimes seen on such treated

Figure 31: This 62.59 ct white sapphire proved to be filled with lead glass. Photo by B. Williams.

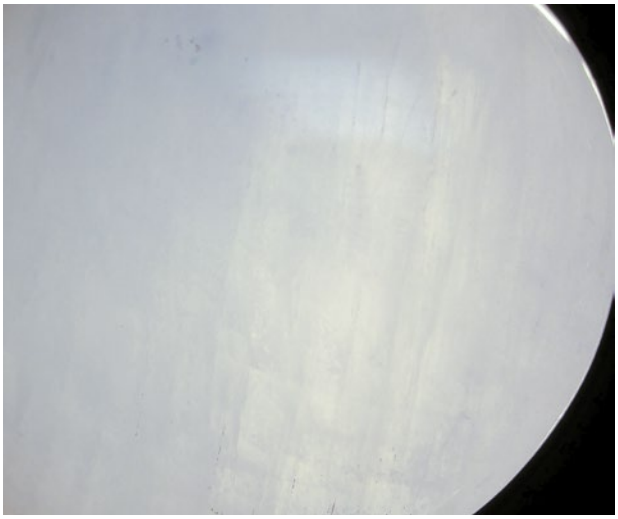

Figure 32: The low transparency of the white sapphire is due to numerous parting planes and fractures, which are typical of low-quality gem corundum. Photomicrograph by Dean Brennan, Stone Group Laboratories; magnified 20×.

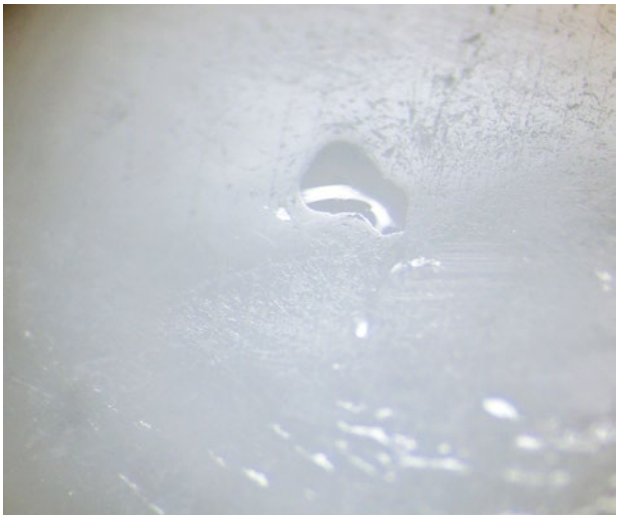

Figure 34: Depressions on the surface of the filled sapphire exhibit a glassy appearance. Photomicrograph by Dean Brennan, Stone Group Laboratories; magnified 30×.

stones, although there were at least two depressions that exhibited a glassy appearance (e.g. Figure 34). Although EDXRF spectroscopy showed the presence of significant Pb, the SG was not elevated and was in fact slightly below the 4.00 value that is typical of corundum. The lack of any dark inclusions may be due to the acid treatment that is an initial stage of this treatment process.

While identifying a treatment such as this does not pose a challenge to a well-equipped gemmological laboratory, the lack of common visual features associated with lead-glass filling could be problematic for the unsuspecting gemmologist.

Cara Williams FGA and Bear Williams FGA

Figure 33: EDXRF spectroscopy of the white sapphire shows significant amounts of Pb associated with the lead-glass filling.

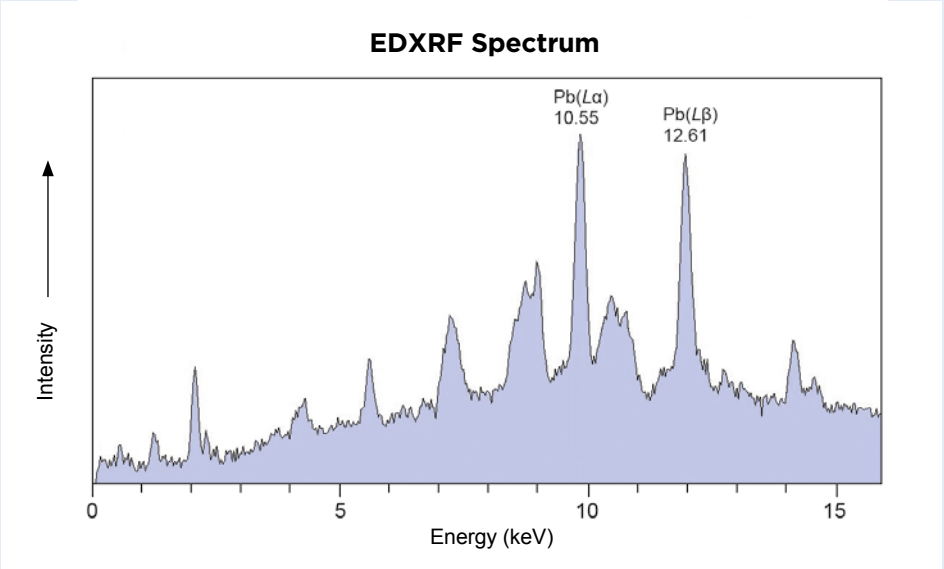

References

McClure, S.F., Smith, C.P., Wang, W. & Hall, M. 2006. Identification and durability of lead glass-filled rubies. *Gems & Gemology*, **42**(1), 22–36, http://doi.org/10.5741/gems.42.1.22.

Milisenda, C.C., Horikawa, Y., Manaka, Y. & Henn, U. 2006. Rubies with lead glass fracture fillings. *Journal of Gemmology,* **30**(1–2), 37–42, http://doi.org/10.15506/jog.2006.30.1.37.

The Late 14th-Century Royal Crown of Blanche of Lancaster—History and Gem Materials

Karl Schmetzer and H. Albert Gilg

ABSTRACT: The richly bejewelled crown preserved in the Treasury of the Munich Residence offers a window into both European dynastic history and contemporaneous decorative practices and gem use. The crown's history can be traced from the late 14th-century court of Richard II and his wife Anne of Bohemia in London; through its role as part of the dowry in 1402 of Blanche of Lancaster, bride of future Elector Palatine Louis III in Germany; to its later decades in Heidelberg, Mannheim and finally Munich by the late 18th century. In this study, all gem materials currently decorating the piece—one of few extant examples of Late Middle Ages royal regalia—were identified by a combination of microscopy, EDXRF analysis and Raman spectroscopy, using mobile instruments on site at the museum. The gems included blue and pink sapphires, pink spinels, garnets, emeralds, diamond octahedra and pearls. Various imitations were also present, including black-coated gold pyramids (substituting for diamonds) and green and pink lead glass. The forms of the gems reflect a progression from use of merely irregularly shaped polished pebbles, to rudimentary shaping or preforming without sharp edges, to sharply faceted regular shapes, thereby demonstrating the transition in gemstone fashioning as the Late Middle Ages gave way to the Renaissance.

The Journal of Gemmology, **37**(1), 2020, pp. 26–64, http://doi.org/10.15506/JoG.2020.37.1.26

Regalia owned and worn by royalty for both political and symbolic purposes have long been a source of fascination for scholars and the general population alike. The construction and materials used, modifications over time, and transitions between owners as a result of marriages, alliances and wars have all drawn interest.

A number of opulent crowns from the High Middle Ages (circa 1000–1250) are well documented (Schramm 1956) and preserved in museum collections. By contrast, the more-refined and less-massive crowns from the Late Middle Ages (circa 1250–1500) have received less attention and tend to be known largely from short descriptions in royal inventories or from depictions in artwork of the era (e.g. Figures 1 and 2). Such inventories reflect that, in general, English and French monarchs typically owned multiple crowns during the 14th century, with artistic design varying widely (Holmes 1937). An English inventory from 1324, for example, listed as many as 10 crowns, with the number of fleurons ranging from eight to 22 (Twining 1960). (*Fleurons* in this context refers to the elongated ornaments that attach to the circlet and decorate the top of a crown.) A French inventory from 1380 also enumerated 10 crowns, which contained from four to 16 fleurons (Labarte 1879).

Likewise apparent from systematic study of 14th- and 15th-century inventories is that the royal and ducal crowns were characteristically adorned with jewels, but only a limited selection of mineral gem varieties (along with pearls) was used: diamonds, blue sapphires, emeralds and three different types of pink to red gems. The latter included rubies, *balases* (or *balays*, *baleis*,

Figure 1: The *Liber Regalis*, a manuscript dated to the 1390s, depicts the coronation ceremony of an English king and queen. The monarchs shown are thought to be Richard II and Anne of Bohemia, for whom the crown in this study was most likely created. Reproduced by permission of Westminster Abbey, London.

pallas and related variants)[1] and rarely garnets (Holmes 1934). Occasionally, descriptors such as *rubis d'Alexandrie* or *saphirs d'orient* were employed, indicating that the gems found their way from the East to Europe within the stream of merchandise passing through major Mediterranean trade centres such as Alexandria, Aleppo or Constantinople. At the same time, royal regalia also contained various imitations of rubies, sapphires and emeralds (e.g. designated as *esmeraudes contrefeites*) such as glass simulants and doublets.

The scarcity of regalia that survive from the Late Middle Ages, however, has meant that modern mineralogical examinations of such items are rare. A notable exception is a detailed study undertaken to identify the gems decorating the Crown of Saint Wenceslaus (Hyršl & Neumanova 1999). That work, in turn, brought to

[1] Before it was recognised through modern mineralogy that the historical term *balas* encompassed two mineral species–corundum and spinel–European inventories in the Middle Ages frequently employed *balases*, *balays*, *baleis*, *pallas* or similar terms to indicate light red or purplish red to pink or purplish pink gems. Such stones were often described in 19th- or 20th-century mineralogical and gemmological literature as rubies or *balas rubies*, although it had been recognised that some particularly large and more famous gems such as the Black Prince's Ruby were pink to red spinels. Insofar as gemmological textbooks ('lapidaries') from the Middle Ages or the Renaissance era used *balas* to reference a light-coloured variety of the group of red gems, it is logical to assume that if texts or inventories from the Middle Ages spoke of rubies, these were darker, more intense red or purplish red gems. The methods applied in Europe in the late 14th or early 15th century did not permit separation between pink sapphires and spinels because classification was based primarily on colour.

Figure 2: A historical drawing shows Louis III, Elector Palatine from the House of Wittelsbach (centre), together with his first wife Blanche of Lancaster (right of centre), wearing a crown, and his second wife Mechthild of Savoy (far right). Likewise shown are Louis's father Rupert III, Elector Palatine and King of the Romans (King of Germany; far left) and his wife Elisabeth of Hohenzollern-Nuremberg (left of centre). This 1772 illustration is one of a series by Anna Maria Johanna Wisger, after a line of portraits from the Amberg residence depicting members of the Palatine branch of the House of Wittelsbach (see von Wiltmaister 1783). The 18th-century series was copied from an older series at Heidelberg Castle, painted circa 1500, which has been lost. Reproduced by permission of the Bayerisches Nationalmuseum, Munich.

light that descriptions offered in the crown's inventories, despite being repeated over the course of centuries, were not necessarily accurate. In particular, several of the larger red gems frequently characterised in the written record as rubies were identified as spinels and one red tourmaline, with the only rubies being small gems incorporated in the crown's arches. Other components included sapphires, emeralds and an aquamarine, while the presence of foil-backed gems offered another cautionary caveat to the inventories' claims.

An additional Late Middle Ages piece is preserved in the collection of the Treasury at the Munich Residence (Residenz München, Schatzkammer, Bayerische Verwaltung der staatlichen Schlösser, Gärten und Seen in Munich, Germany) and is referred to as the 'crown of an English queen' or the 'crown of Princess Blanche' (Figure 3 and cover of this issue). It is one of two surviving English crowns from the Late Middle Ages and is dated circa 1380. Although further appellations such as the 'Bohemian crown' or the 'Palatine crown' have been used, they have been called into question based on European chronology, amongst other factors, insofar as might concern any implications regarding origin.

The other remaining English crown from the Late Middle

Figure 3: The crown of Blanche of Lancaster, daughter of King Henry IV of England, was part of her dowry in 1402 when she married Louis, son of the King of the Romans (King of Germany) and Elector Palatine Rupert III. The piece consists of 12 segments, with six larger fleurons (18 cm tall) and six smaller fleurons (14.5 cm tall). It is richly decorated with blue and pink sapphires, pink spinels, garnets, emeralds, diamonds and pearls. Photo by K. Schmetzer, with permission from Bayerische Schlösserverwaltung, Munich.

Figure 4: The crown of Margaret of York, Duchess of Burgundy and wife of Charles the Bold, dated circa 1461, is the only other remaining English crown from the Late Middle Ages, now in the collection of the Aachen Cathedral Treasury, Aachen, Germany. Photo by P. Siebigs, reproduced by permission.

Ages (Figure 4), dated to 1461, served as the wedding coronet of Margaret of York, sister of Kings Edward IV and Richard III of England, upon her marriage to Charles the Bold, Duke of Burgundy, in 1468 (Hammond 1984). A similar crown, attributed to Margaret of Bavaria, consort of John the Fearless, Duke of Burgundy, is dated circa 1385 (Twining 1967). Both of these pieces, however, differ substantially in style and decoration from the one in the Munich Residence. Conversely, two crowns referenced in the 1380 inventory of King Charles V of France have descriptions suggesting that they could have been more analogous in style. Yet these crowns are not extant for study, nor do any drawings exist for comparison (Labarte 1879; Eikelmann 1984). Only the Crown of Saint Wenceslaus mentioned above, originally made for the coronation of Charles IV as King of Bohemia in 1347, would seem to offer any meaningful comparatives in an extant jewel, albeit a less elaborate example. The scarcity of available parallels thus heightens the academic value of the crown in the Munich Residence.

Overall Form and Characteristics

The studied crown is composed of a circlet of 12 numbered segments (designated I–XII) that serve as bases supporting 12 fleurons (again, see Figure 3). The diameter of the circlet—about 18 cm—is consistent with the size represented in the literature as usual for a woman's crown. Additional textile components, such as a fillet and barbette arrangement, would have been required to secure the piece to the head, serving as another indication that the crown was intended for a female.

No rigid metallic ring is used in the framework of the crown, resulting in a relatively flexible circular construction. The flexibility is further enhanced by elongated hinges connecting the 12 base segments (Figure 5). Each base segment consists of gold latticework displaying a stylised hexagon in the centre of a circle, from which rises a detachable fleuron composed of a gold stem topped by a lily or *fleur-de-lis* motif. The stems are fixed by prongs to vertical bars attached to the backs of the hexagons. The fleurons alternate in size, with six larger ones measuring approximately 18 cm tall (from the tip to the lowest point of the base segment) and six smaller ones measuring approximately 14.5 cm tall. The 12 base segments are each flanked by small panels containing enamelled patterns (e.g. white flowers; see Figure 5a). Both the segments and fleurons are heavily jewelled and decorated with coloured stones, diamonds and pearls. The hinge pivot between segments X and XI is easily removable, thereby allowing the segmented crown to be opened and laid flat.

While historical aspects of this crown have been studied in detail from the perspectives of both politics and art (Deibel 1927, 1928; Eikelmann 1980), a thorough examination of the numerous gem materials decorating

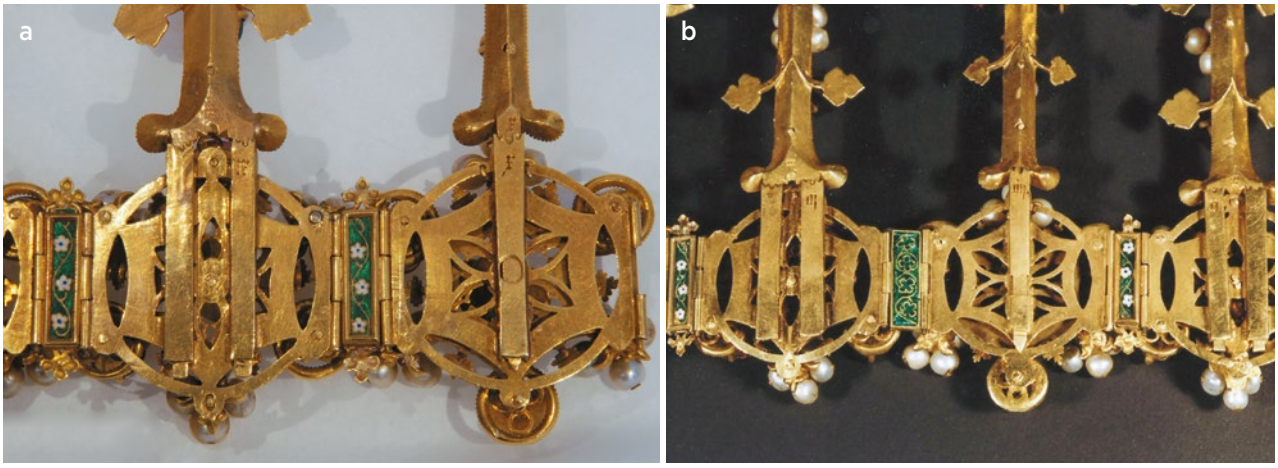

Figure 5: (**a**) The underlying gold structural framework of the crown of Blanche of Lancaster is revealed by this interior view. The base segments are flexibly connected by elongated hinges, and each segment consists of a latticework displaying a stylised hexagon in the centre of a circle. Each hexagon is backed by a vertical bar attached by prongs to its corresponding fleuron. (**b**) Another interior view of the crown shows how a base segment that was added in 1402 (centre, numbered 'iiii', but referenced as IV for purposes of this study) contrasts with the other segments in terms of its enamel decoration (left side) and goldsmith's work (see the right side of Figure 5a for comparison). Photos courtesy of Bayerische Schlösserverwaltung, Munich.

the piece has not yet been documented. Most descriptions, even in gemmological journals or textbooks (Gray 1989; Gübelin 1990), have relied only upon visual inspection and have been limited to characterising the gems primarily on the basis of their colour as sapphires, rubies, spinels (or *balas rubies* or *balases*), emeralds and diamonds. Thus, the principal aim of the present study is to offer a more thorough description of the crown's constituent gems, while taking into account its historical background.

HISTORICAL CONTEXT

Late 14th- and Early 15th-Century History and Descriptions

Documentation in early sources can offer insights into the crown's past, albeit with caveats. A general summary of the various members of the English, French, German and Bohemian royal families involved in its history in the late 14th and early 15th centuries is presented in Figure 6. In reviewing the history of this period, it is useful to recall that during the Late Middle Ages, the Holy Roman Empire (primarily equated with present-day Germany) also included Bohemia and part of Italy.

Scholars of history and art generally concur that two royal inventories, both dated 1398–1399, include catalogue entries for the Munich crown. As such, they represent the only known late 14th-century written evidence and the earliest references. The first, an inventory of the jewels and plate of Richard II (1367–1400) of England penned after January 1398 and before March 1399, was rediscovered in the 1990s (Stratford 2012). The inventory contained 1,206 entries covering nearly 2,300 treasury items accumulated by Richard II. Dispersed within was the personal jewellery of his queens, Anne of Bohemia (1366–1394, married 1382) and Isabella of Valois (1389–1409, married 1396). The list opened with 11 crowns, of which only the subject of this article (no. 7) is extant today.

The description of the crown, written in late 14th-century Norman French, was recounted by Stratford (2012)[2], and a modern translation (www.history.ac.uk/richardII/crowns.html) provides:

> Item, a crown of eleven plaques, set with eleven sapphires, thirty-three balas rubies[3], a hundred and thirty-two pearls, thirty-three diamonds, eight of them imitation gems. Item, six fleurons each with a balas ruby, five sapphires, and nine pearls, seven pearls in all being missing. Item, six smaller fleurons, each with a sapphire, four small balas rubies, an emerald

[2] *Item, j coronne de xj overages, garniz de xj saphirs, xxxiij balays et Cxxxij perles, xxxiij diamantz, dont viij contrefaitz. Item, vj florons chescun d'un balays, v saphirs chescun de ix perles, dont defaut en tout vij perles. Item, vj meyndres florons, chescun d'un saphirs, iiij petitz balays, j emeraud', dont defaut j emeraud' et ij petitz perles en chescun, pois' v marcz vij unc', et vaut outre CC li., dont la somme, CCxlvj li. xiijs. iiijd.*

[3] Notably, this modern translation, as quoted, uses the expression *balas rubies*, whereas the original text referred only to *balays*; see also footnote 1.

(one emerald being missing) and two little pearls in each, weighing 5 marks 7 oz., additional value £200, total, £246 13s. 4d.

The values given placed this crown amongst the lower-priced objects in the inventory. Noteworthy is the fact that the crown at that time was incomplete and unwearable because only 11 of the 12 base segments existed.

The second 14th-century documentation was an inventory of jewels and plate transferred from the royal treasury to Richard II's successor, Henry IV, and dates to November 1399. The inventory, comprising 340 entries, was first published in the 19th century with an introductory preamble (Palgrave 1836). The preamble indicates that the various items belonged to Edward III, Richard II, Queen Anne, the Duchess of York, the Duke of Gloucester and Sir John Golafre. The description of an item presented as entry no. 175 is nearly identical to that of crown no. 7 of the earlier inventory (including having 11 base segments).

Several theories as to how the crown came to be so included in these lists have been offered in the literature (see, e.g., Alexander 1987; Cherry 1988):

1. The crown was made and used before Anne of Bohemia came to England in December 1381 and married Richard II in January 1382.
2. The crown was part of Anne's dowry and was brought to London at the end of 1381.
3. The crown was made for and used by Anne after 1382 and before she died in 1394.
4. The crown was part of the rich dowry of Isabella of Valois, the second wife of Richard II, whom he married in 1396.

As to the first possibility, the lack of earlier references or other indications of a similar piece available in the relevant time frame renders the idea highly speculative at best. Evaluation of the remaining three theories requires considering how the crown might have fit into what was happening in Europe during the late 14th century (again, see Figure 6).

The end of the 1370s brought a number of changes in the prominent European dynasties. In 1377, Edward III, King of England, died and was succeeded to the English throne by his grandson as Richard II. In 1378, Charles IV (Holy Roman Emperor and King of Bohemia) died and

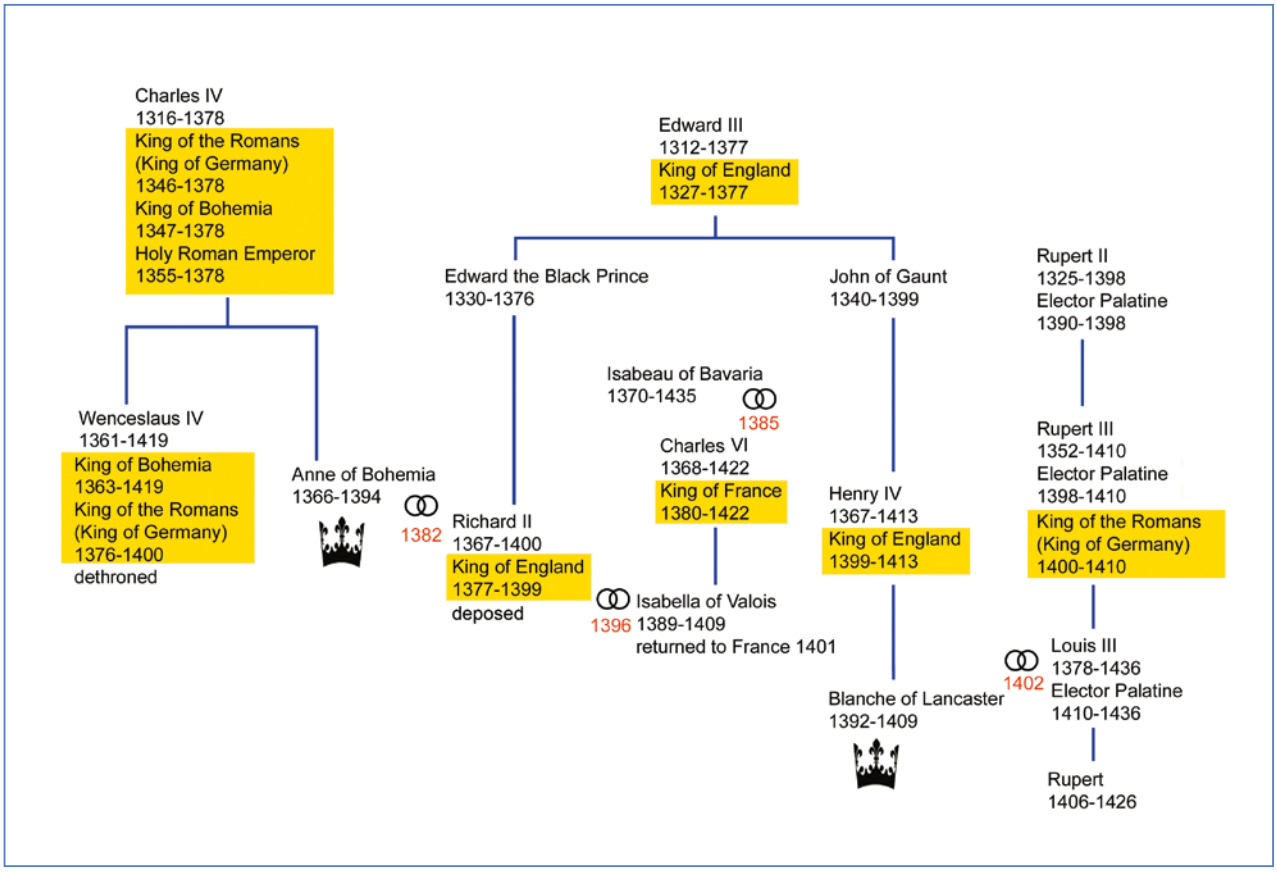

Figure 6: Relationships between royal dynasties in England, France, Germany and Bohemia in the second half of the 14th century and the first decades of the 15th century played a key role in the crown's history. The interlocking circles indicate marriages (with the year shown in red) and the crown symbols show the two inferred owners of the crown, as discussed in this article.

his son Wenceslaus IV began to rule by succession as King of Bohemia (after having been so crowned in 1363 at the age of two). Wenceslaus IV had also been elected King of the Romans (King of Germany) in 1376 through his father's influence. When Charles V, King of France, died in 1380, he was succeeded by his son Charles VI. As the new rulers sought to consolidate their power, an exigency further exacerbated by rivalries in the ongoing Hundred Years' War (1337–1453), both England and France were led to seek alliances with German dynasties (Emerson 1910).

Although Charles IV (Figure 7) had initially broached the idea of a marriage between his daughter Anne of Bohemia and Richard II in 1377, serious negotiations by envoys travelling between London and Prague began only in 1380 at the initiative of Pope Urban VI. In 1381, an agreement was signed setting forth details for a marriage between Richard II and Anne, the half-sister of Wenceslaus IV (Figure 7). However, despite promises from Wenceslaus to give his half-sister a dowry consistent with her high noble status, specifics were never fixed by contract. Instead, records indicate that Wenceslaus was not in a position to compile a lavish endowment

Figure 7: Charles IV (left), King of Bohemia from 1347 to 1378 and Holy Roman Emperor from 1355 to 1378, was succeeded by his son Wenceslaus IV (right), King of Bohemia from 1363 to 1419 and King of the Romans (King of Germany) from 1376 to 1400. This engraving is part of the reliquary cross of Pope Urban V, St Vitus Cathedral, Prague, dated to the 1370s. From Podlaha & Sittler (1903).

and even began to conflate the marriage negotiations with requests for substantial 'loans' or 'grants' from England to fund his government (20,000 and 80,000 guilders, at least a portion of which was paid). Anne ultimately left Prague in the autumn of 1381 without a dowry. She arrived in London in December 1381 and married Richard II in January 1382, followed by a coronation ceremony in London a few days later (Pelzel 1788; Strickland 1849; Heeren 1910; Saul 1997; Reitemeier 1999; Tuck 1999; Stratford 2012).

The foregoing circumstances, in particular the dire financial straits coupled with the absence of any formal written contract to supply a dowry, would thus seem to eliminate the second-listed concept—that the crown was part of Anne's dowry—and to make unlikely any similar variation in which such an ornate crown could have been manufactured in Prague and brought to London by Anne or someone else with other gifts from Bohemia (Campbell 1997).

Conversely, much about the style and decoration of the crown lends support to the third theory of procurement by Richard II for Anne between 1382 and 1394. First, regarding the crown's general style, evidence reflects that an arrangement of larger and smaller fleurons was one favoured by Richard. For example, in preparation for his marriage, Richard sent a communication directing the return of a crown with five large and five small fleurons from the City of London, where it was being held with other jewels as a pledge (Riley 1868; Stratford 2012). Such communication was described by Riley (1868): 'there is a Letter (in French) of King Richard, dated 1st of January…(A.D. 1382), requesting that the Mayor and Commonalty will lend him back the above jewels, as he requires them for his intended marriage'. It is unknown whether Richard II planned to wear this crown himself or whether he retrieved it for his future queen.

In a similar vein, a portrait of Richard II and Anne in the Shrewsbury Charter of 1389 shows both wearing crowns with larger and smaller fleurons (Whittingham 1971; Figure 8). It has also been speculated (Binski 1997) that the image of a coronation ceremony of a king and queen wearing analogous crowns in the *Liber Regalis*, a manuscript most likely dated to the 1390s, depicts Richard II and Anne (Figure 1), and at least the physiognomy of Richard is close to that in the Shrewsbury Charter. The portrait of Richard II from the 1390s in Westminster Abbey, however, reflects a different-style crown with fleurons of the same length (Scharf 1867; Holmes 1937; Campbell 1997).

Richard II was additionally known to be prolific in

Figure 8: King Richard II of England and Anne of Bohemia are depicted in the Shrewsbury Charter of 1389, a document in which Richard confirmed rights given to the people of Shrewsbury. Reproduced by permission from the Shropshire Archives, Shrewsbury.

procuring new pieces, and the crown's decoration is consistent with his purchasing habits. While orders from London goldsmiths were predominant, Richard II also turned to international suppliers. He bought costly objects, including new gold crowns from Italian and French goldsmiths or merchants (Campbell 1997), but to date no document related directly to the purchase or order of the subject crown has come to light. The artwork employed on the piece, especially the enamel embellishment, points towards one of the great courts and economic centres in France, Flanders or Burgundy. Numerous enamelled pieces of jewellery of exceptional quality with such provenance, using a technique characterised as *émail en ronde bosse* (enamelling on rounded or irregular surfaces), are known from the late 14th or early 15th century (Eikelmann 1984). Conversely, although enamel was applied to adorn the work of goldsmiths in England as well, the number of pieces comparable to the lavish examples from what is today France, Belgium and the Netherlands is small or non-existent (R. Eikelmann, pers. comm. 2018).

Moreover, further details of the decoration support a link to Anne herself. As recounted briefly above, the base segments are festooned with enamelled flowers. These flowers may be representative of daisies, an image considered symbolic of Anne of Bohemia, to the extent that she was referred to as the 'daisy queen', and the flower was used to represent her in poetry at the time (see Lawrance 1840; Morley 1873; Percival 1998; Bowers 2001; Thomas 2007; Hilton 2008; Van Dussen 2009). While a more comprehensive evaluation of such associations in late 14th-century poetry is beyond the scope of this study, one notable example should be highlighted: the English poet Geoffrey Chaucer (circa 1343–1400) was closely intertwined with the Ricardian court, and since the 19th century it has been assumed that the 'daisy queen' in Chaucer's poem *The Legend of Good Women* represented and honoured Anne of Bohemia. In addition, certain other jewellery belonging to Queen Anne was enamelled with small white flowers such as marguerites or daisies.

The fourth and last theory listed above for the origin of the crown finds little foundation in the historical record. After Anne died childless in 1394, Richard II married Isabella of Valois, daughter of King Charles VI of France and Isabeau of Bavaria, in 1396. The concomitant written agreement provided for an extended 28-year armistice in an effort to bring the Hundred Years' War to a close (Reitemeier 1999). Isabella brought a rich dowry to England, and two crowns with eight fleurons each were incorporated therein. After Richard II's death, however, Isabella returned to France in 1401, together with a substantial portion of the jewellery from her dowry, including the two crowns (Stratford 2012).

Thus, considering and evaluating the facts available at present, the most probable explanation for the crown's origin is found in the third theory: that it was made in the 1380s for Anne of Bohemia, after her marriage to Richard II.

The turn of the century saw a period of renewed turmoil amongst the ruling families in England and the Holy Roman Empire (including Germany and Bohemia). In London, Richard II's dictatorial policies had aroused the ire of powerful aristocrats, and he was deposed in a military campaign and forced to abdicate in 1399. His cousin succeeded him to the throne as Henry IV. Richard II is thought to have died in captivity the following year, although questions remain about the exact circumstances.

In Germany, Wenceslaus IV was dethroned as King of the Romans in 1400 by a vote of the four electors from the Rhineland region: Rupert III of the Palatinate (Elector Palatine) and the Archbishops of Mainz, Cologne and Trier. The deposition of Wenceslaus IV was premised on an apparent complete ineptitude in management over matters of both church and state, not to mention a widespread reputation for ruthlessness, drunkenness and a general lack of dignity. Rupert III (Figure 9a) was elected King of Germany by the same four votes, including his own, within days. He was

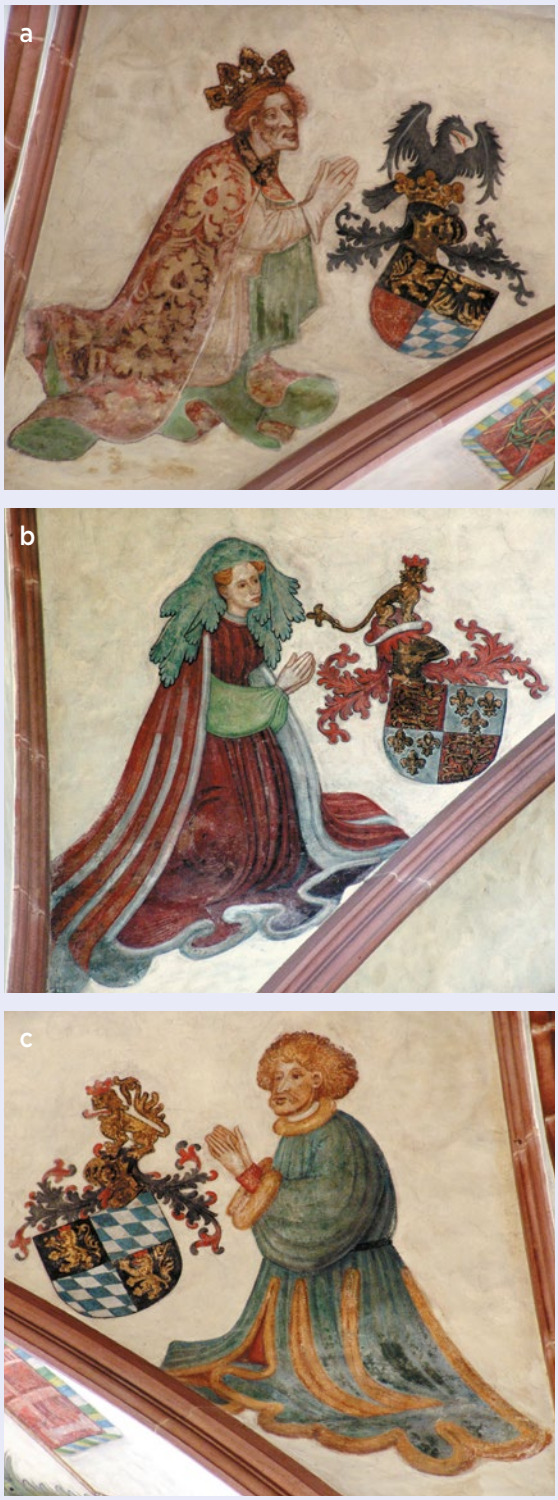

Figure 9: Portraits of (**a**) Rupert III, King of the Romans (King of Germany), (**b**) Blanche of Lancaster and (**c**) her husband Louis III, Elector Palatine, decorate the Stiftskirche church in Neustadt an der Weinstraße, Germany, where Blanche is buried. The paintings were created between 1410 and 1417 on Louis III's initiative (see Keddigkeit *et al.* 2015) and comprise Blanche's most contemporary depiction. Photos by R. Schädler, reproduced by permission.

crowned by Archbishop Frederick III in Cologne in January 1401, and a second short coronation ceremony was performed in Aachen several years later, in November 1407 (Höfler 1861; Weizsäcker 1882, 1885; Oberndorff 1912; Dürschner 2003; Auge 2005). Wenceslaus IV continued to rule as King of Bohemia and never acquiesced in his deposition as King of Germany at any time prior to Rupert's death in May 1410 (Lindner 1896; Reitemeier 1999; Dürschner 2003). In such fraught circumstances, both Henry IV and Rupert III looked again to the device of a prestigious marriage between the families as a way to elevate their status and create beneficial foreign alliances.

Serious negotiations began in 1401 concerning a marriage between Henry IV's daughter Blanche of Lancaster (1392–1409)[4]—also known as Blanche, Blanca or Blanka of England—and Rupert III's son Louis (1378–1436). Written agreements providing for an extremely rich dowry, including a monetary component of 40,000 nobles, were signed in 1401 and 1402. Taking into account the gold content and weight of the coin in the relevant time frame, the value of 1 noble is estimated to be equivalent to approximately 2.2 guilders. Communications between Rupert III and Louis, however, equated the 40,000 nobles with an estimated 100,000 guilders (see Oberndorff 1912).

Between March and April 1402, the crown was repaired by London goldsmith Thomas Lamport, who constructed a replacement base segment (labelled 'iiii' [see Figure 5b], but hereinafter numbered IV) and also added one missing emerald and nine missing pearls to existing components of the crown (Stratford 2012). Blanche (Figure 9b) and her entourage left England in June 1402 and arrived in Cologne in July, where she married the future Louis III (Figure 9c) before being guided to Heidelberg, carrying much of her dowry with her (Stratford 2012). Heidelberg served at that time as the capital of the Palatinate branch of the House of Wittelsbach and was the site of the principal castle. Records from July 1402 confirm that the crown, now complete and wearable, was formally received as part of the dowry, as was a fillet of the type that might have been used to affix a crown to a woman's head (Rall 1965). The financial component was paid by instalments, commencing in 1402 and continuing in the ensuing years (Devon 1837; Green 1857; Weizsäcker 1885; Oberndorff 1912; Holtzmann 1930; Reitemeier

[4] Not to be confused with Henry IV's mother Blanche (1342–1368), likewise called Blanche of Lancaster.

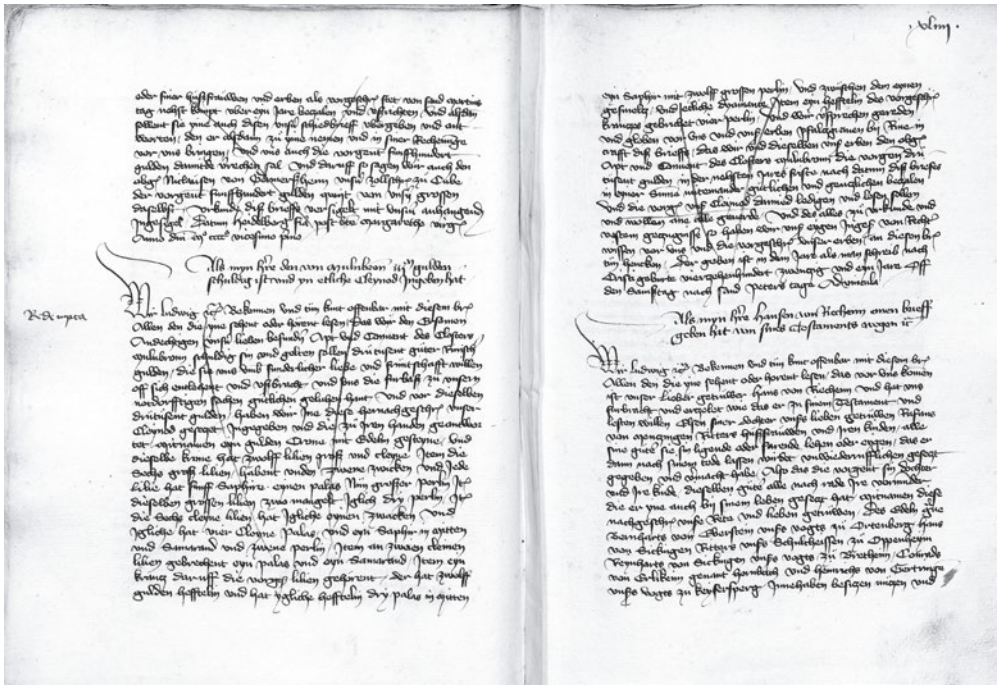

Figure 10: The crown of Blanche of Lancaster was pawned in 1421 to the monastery of Maulbronn, Germany, for 3,000 guilders. The transaction is memorialised in a volume of Elector Louis III's administrative records that set forth a detailed description of the crown's embellishment and the gems missing at that date (Generallandesarchiv Karlsruhe, Kopialbuch 67/810, Blatt 43v–44r, reproduced by permission).

1999). A portion of the sum remained outstanding as of 1444 and was sought by Louis IV, the son of Louis III and his second wife, Mechthild of Savoy (Brandenstein 1983).

In 1406, Blanche gave birth to a son, Rupert, named after his grandfather, but she died from a serious illness only three years later in 1409. Both Louis and Rupert III wrote personal letters to Blanche's father in London, expressing deep grief and mourning, and thereby suggesting a close, affectionate relationship between the spouses (Schreibmüller 1959). Blanche's widower became Elector Palatine as Louis III in 1410 upon the death of his father. Louis III was remarried in 1417 to Mechthild (or Mathilde or Matilda) of Savoy. Blanche's son Rupert, nicknamed 'the English', died in 1426, before his father.

The crown meanwhile was pawned by Louis III in 1421 to the monastery of Maulbronn, located south-east of Heidelberg, in return for 3,000 guilders. A description prepared in connection with the transaction (Figure 10), written in 15th-century German, reflects that by that point several gems were missing, including three *perlin* (pearls) from two of the larger fleurons, one *palas* (*balas*) and one *samarand* (emerald) from two of the smaller fleurons, and four *perlin* from one of the base segments. Annotations on the original administrative document indicate that the loan was subsequently repaid, and the piece was returned to Louis III from Maulbronn at an unknown date (Deibel 1927, 1928; Brandenstein 1983).

Later History and Descriptions

Later eras, from the 16th to the 20th centuries, saw the crown being kept at three primary locations in Germany—Heidelberg, Mannheim and Munich—with intermittent removals for safekeeping during times of war. Throughout the 16th and 17th centuries, the crown remained within the treasury of the Elector Palatine at the capital in Heidelberg, the ownership passing with succession. The treasury of the Elector Palatine also continued to be tracked through various inventories.

Two 16th-century inventories detailed the crown's constituent gems. One from 1544 characterised the 12 base segments as each having three *baleis*, one sapphire and 12 pearls; the six larger fleurons as each having five sapphires, one *baleis*, one small emerald and nine pearls; four of the smaller fleurons as each having one emerald, one sapphire, four *baleis* and two pearls; and two of the smaller fleurons as each having one emerald, five *baleis* and two pearls (Eikelmann 1980). The other inventory, from 1568, delineated the segments and fleurons together. The larger fleurons and attached segments were described as being decorated with six sapphires, four *rubin pallas*, 21 pearls, three diamonds and one small emerald. The smaller fleurons and attached segments contained two sapphires, seven *rubin pallas*, 14 pearls, three diamonds and one emerald (Sillib 1903).

In general, and somewhat inexplicably, the inventories from the 16th century typically denoted the crown as that of Rupert III of the Palatinate, Louis III's father

and Blanche's father-in-law. Written evidence from the 17th century is limited to various brief references, which tended to repeat the attribution to Rupert III (see, e.g., Sandrart 1679; and Huffschmid 1910, publishing a French travelogue from 1664). Such assignment, however, is contravened not only by the documented journey of Blanche's crown as recounted above but also by what has been revealed about Rupert's own crown and the fate of his valuables. Specifically, Rupert's crown was described as having 14 fleurons decorated with gems and pearls, and it was pawned at least twice, in 1401 and 1403, with the latter transaction involving just 150 guilders. Thus, neither the number of fleurons nor the apparent low value seem consistent with Blanche's crown. Moreover, Rupert's will, written two days before his death in May 1410, directed that his crown and other valuables should be sold to liquidate outstanding debt. While further details are unknown, Rupert's crown is not believed to have survived (Weizsäcker 1882, 1885; Rödel 2000; Moraw 2001; Schneidmüller 2011).

The year 1720 witnessed relocation of the capital of the Palatinate, as well as the residence and treasury of the Elector Palatine, from Heidelberg to Mannheim. Following the transfer, the crown continued to be cited in various inventories from 1729 and thereafter. Such 18th-century sources, as well as others penned in the 19th century, often attributed the crown erroneously to Frederik V, who reigned as Elector Palatine from 1610 to 1623 and as King of Bohemia from 1619 to 1620 (Deibel 1927, 1928; Brunner 1968, 1971; Eikelmann 1980). Instances in which the piece was referred to as the 'Bohemian crown' also appeared (see, e.g., Deibel 1927, 1928). The questionable nature of such attributions and appellations regarding the crown's origin was already being raised by the late 19th century (von Schauss 1879), and they were entirely discredited by the early 1900s (Sillib 1903; Weiß 1911). With respect to the condition of the crown, sporadic information included mention in a 1745 inventory that two pearls were missing and that one sapphire had been replaced by an amethyst (Brunner 1971).

Throughout the centuries following the treaty of Pavia in 1329, separate branches of the House of Wittelsbach had ruled over the Electorate of the Palatinate and the Electorate of Bavaria, which were independent hereditary estates within the Holy Roman Empire. In 1777, the last in the Bavarian line of succession died, and Charles Theodore of the Palatine branch of the House of Wittelsbach and Elector Palatine, residing in Mannheim, became Elector of Bavaria by succession. The electorates were united and combined, and Charles Theodore relocated in 1778 from Mannheim to Munich. The treasury was transferred to Munich over the course of multiple journeys and was thereafter characterised as that of the Elector of Bavaria, with the crown in particular being listed in a 1783 inventory (Eickelmann 1980).

During 1805 and 1806, in conjunction with the abolishment of the Holy Roman Empire by Napoleon, what had formerly been known as the Electorate of Bavaria became the Kingdom of Bavaria, and the ruling Elector of Bavaria became the King of Bavaria. Per the constitution enacted in 1818, the treasury was deemed to belong to the state, rather than being the private property of the royal family. The kingdom ended in 1918, giving way to a secular state. The crown is now owned by the Wittelsbacher Landesstiftung (WL) and is on display in the collection of the Treasury at the Munich Residence (inventory no. 16 WL), a museum which opened to the public in the early 1930s.

Sources dating from the late 18th century through the early 20th century incorporate details about the crown's condition as follows (Eikelmann 1980):

- 1783: Amongst the sapphires was one imitation.
- 1818/1820: Two gems (rubies?) and two pearls were missing. Amongst the sapphires was one glass piece.
- 1833: Amongst the sapphires was one glass piece.
- 1868 and 1872: Four sapphires, one ruby, two emeralds and six pearls were missing, but three of the sapphires were still available as loose gems.
- 1880: One sapphire, two rubies, one emerald and five pearls were missing.
- Undated (between 1880 and 1905): Five sapphires, one ruby, two emeralds and one pearl were missing, but three of the sapphires were still available as loose gems.

In 1925 all missing gems and pearls were replaced by Munich goldsmith Max Heiden (Deibel 1927, 1928). When the crown was examined in 1980, the numbers of only seven of the base segments corresponded with the numbers of the attached fleurons (Eikelmann 1980).

As the early 20th century progressed, it was increasingly apparent that what had been referred to as the 'Palatine crown', the 'Bohemian crown' and the crown of Blanche of Lancaster were one and the same (Sillib 1903; Weiß 1911). Finally, scholars in 1927 reached the now-accepted conclusion that the crown in Munich had come from Blanche's dowry and is identical to the crown which Louis III had pawned in 1421 (Deibel 1927, 1928).

MATERIALS AND METHODS

The crown was examined by the authors at the Munich Residence in October 2018 and January 2019. During each visit to the museum, initial evaluation took place with the crown in its fully assembled circular state (Figure 11). During the latter visit, the removable hinge pin mechanism was used to open the crown and allow the 12 pivoted segments to be laid flat for further inspection (Figure 12).

Microscopy, energy-dispersive X-ray fluorescence (EDXRF) analysis and Raman spectroscopy were employed on site. Microscopic examination utilised an Olympus X binocular stereo microscope with 6.3×–40× objectives and fibre-optic illumination (Figure 13).

Identification of the individual gems and imitations decorating the crown was achieved through EDXRF analysis (light and heavy elements) alone or in combination with Raman spectroscopy. In general, all samples were measured twice by one or both methods. The initial focus was on Raman analysis to identify the gems, but it was later established that EDXRF was sufficient to separate the rubies and pink sapphires from spinels because the Mg peak of the spinels was clearly detectable. Furthermore, Raman spectroscopy was not performed on the garnets, for which the chemical data were sufficient to determine the species or variety present. (Gemmological examination of the pearls, being an organic gem material, was not within the scope of this study. Thus, the pearls are mentioned henceforth only where relevant to explain the overall pattern of the decoration.)

The EDXRF measurements were performed using a handheld Bruker Tracer III-SD EDXRF analyser (Figure 11) equipped with a rhodium anode, a silicon drift detector with a resolution of 147 eV at 10,000 cps, and a portable vacuum pump. The size of the beam directed at the gem was about 2 × 3 mm, which in some instances, especially for smaller samples, yielded chemical signals from both

Figure 13: The flattened geometry of the opened crown facilitated microscopic examination of the 12 base segments and fleurons and allowed the individual gem materials to be more easily targeted by the EDXRF spectrometer (not shown here). Photo by K. Schmetzer, with permission to photograph and reproduce from Bayerische Schlösserverwaltung, Munich.

Figure 11: A portable EDXRF spectrometer was used to analyse constituents of the crown on site at the museum, initially with the piece in its circular state. Photo by K. Schmetzer, with permission to photograph and reproduce from Bayerische Schlösserverwaltung, Munich.

Figure 12: Once the crown was opened by means of a removable pin in one of the connecting hinges, the 12 base segments supporting the 12 fleurons could be laid flat in a band measuring approximately 60 cm in length. Photo by K. Schmetzer, with permission to photograph and reproduce from Bayerische Schlösserverwaltung, Munich.

the gem and the mounting. Light elements (Mg to K) were analysed with an accelerating voltage of 15 kV and beam current of 25 µA in a vacuum; heavier elements (K to U) were measured with 40 kV and 30 µA, employing a yellow filter (0.001 mil Ti, 0.012 mil Al). The Artax 7.4.8.2 software package (provided by Bruker Nano Analytics) and various mineral standards were used for quantification. For example, quantitative chemical analyses for garnets were measured by means of using standard samples with known compositions (as determined by electron microprobe) for comparison.

The Raman measurements utilised a portable Enwave EZRaman-N-785-B spectrometer. The instrument was equipped with a 785 nm IR laser with a maximum power of 300 mW, a glass fibre-optic probe with a 7 mm working distance, and an f/1.6 CCD spectrograph with a spectral range from 3300 to 100 cm^{-1} (resolution of 6 cm^{-1}). Spectra were plotted using CrystalSleuth software.

RESULTS

The Framework of the Crown

Previous work had indicated that the crown was constructed of 18-carat gold (Deibel 1927, 1928). EDXRF measurements revealed strong signals for gold as well as silver and copper, which is not unusual for gold from the 14th century. Quantitative analyses of several components of the framework (including the replaced segment IV), using seven calibrated gold-silver-copper standards for comparison, resulted in a composition of 81.0–82.3 wt.% Au, 7.8–8.4 wt.% Ag and 9.8–10.6 wt.% Cu (which calculates to 19.4–19.8-carat gold).

The non-original nature of segment IV was evident from differences visible on the back in both the goldsmith's work and the enamel embellishment (Figure 5b).

The Decoration – Overview

A schematic diagram depicting the arrangement of gem materials decorating the crown is provided in Figure 14. The gems are drawn to scale to show approximate size relationships between them. Table I summarises the main features of the gems, including their varieties, shapes and fashioning.

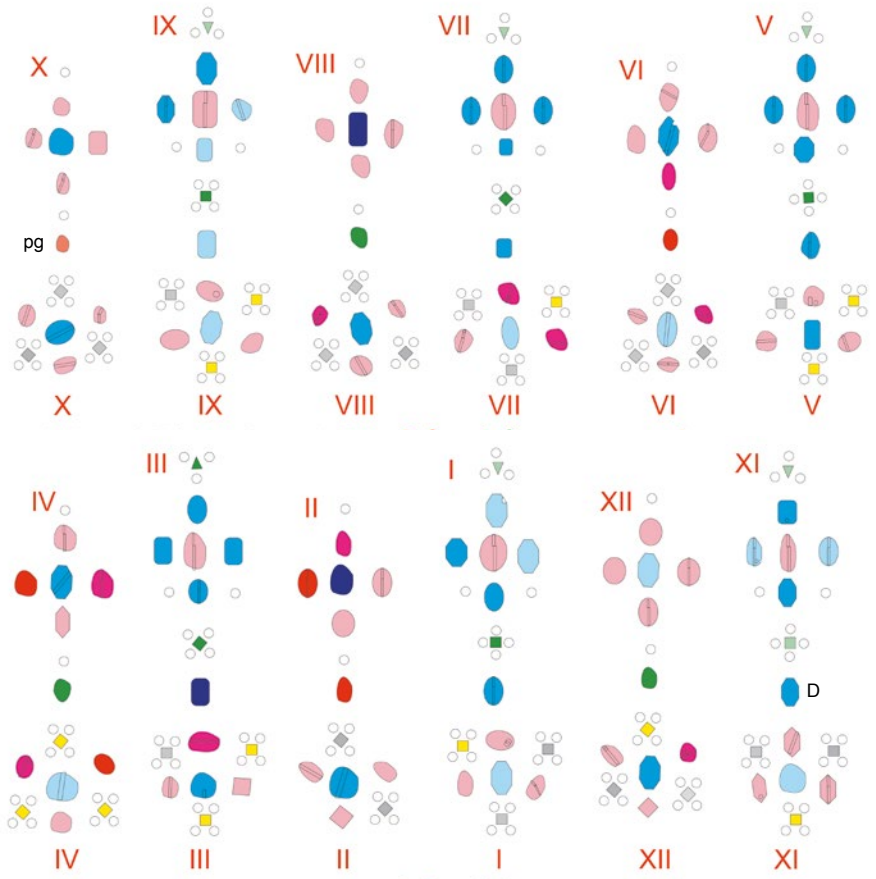

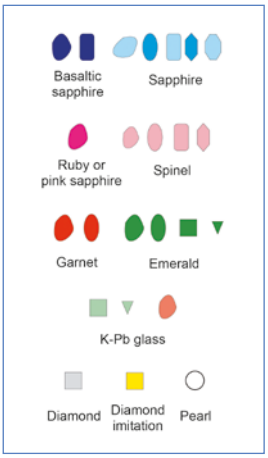

Figure 14: This schematic diagram depicts the arrangement of the gem materials decorating the crown. The general shapes and relative sizes for the gems are indicated, as are drill holes. The labels of the individual base segments/fleurons (red Roman numerals) correspond with those in Figure 12. Abbreviations: D = doublet and pg = pink glass. Drawings by H. A. Gilg.

Table I: General survey of gem materials in the late 14th-century crown of Blanche of Lancaster.

Outline/ shape as mounted	Form and cut [a]	Sapphire (dark blue, translucent)	Sapphire (light to intense blue, transparent)	Sapphire doublet (intense blue)	Pink sapphire to ruby	Pink spinel	Garnet	Emerald	Green K-Pb glass	Pink K-Pb glass	Diamond	Diamond imitation
Irregular/ pebble-like	Irregularly shaped with generally curved upper surface	1	11	—	8	41	2 + 2[b]	2	—	1	—	—
	Irregularly shaped with curved upper surface topped by shaped or preformed table	—	1	—	2	4	—	—	—	—	—	—
Oval or near oval	Curved dome	—	9[c]	—	—	1	—	1	—	—	—	—
	Dome topped with planar table	—	2	—	—		1					
Rectangle	Shaped or preformed table and one row of inclined surfaces, with rounded edges	2	4	—	—	1	—	—	—	—	—	—
	Planar table and one row of inclined crown facets, with sharp edges	—	2	—	—	2	—	—	—	—	—	—
Hexagon	Shaped or preformed table and one row of inclined surfaces, with rounded edges	—	—	—	—	1	—	—	—	—	—	—
	Planar table and one row of inclined crown facets, with sharp edges	—	1	—	—	3	—	—	—	—	—	—
Octagon	Shaped or preformed table and one row of inclined preformed surfaces, with rounded edges	—	5[d]	—	—	—	—	—	—	—	—	—
	Planar table and one row of inclined crown facets, with sharp edges	—	5[e]	—	—	—	—	—	—	—	—	—
	Planar table and one row of inclined crown facets, scissor cut, with sharp edges	—	1	—	—	—	—	—	—	—	—	—
	Planar table and one row of inclined crown facets, as well as one row which is nearly perpendicular to the table, with sharp edges	—	3	—	—	—	—	—	—	—	—	—
	Planar table and two rows of weakly inclined crown facets, with sharp edges	—	—	1	—	—	—	—	—	—	—	—
Square	Curved upper surface	—	—	—	—	—	—	5	1	—	—	—
Triangle	Curved upper surface	—	—	—	—	—	—	1	5	—	—	—
Square	Four-sided pyramid, natural octahedron	—	—	—	—	—	—	—	—	—	22	13
Sum[f]		3	44 (21)	1	10 (8)	53 (36)	5 (1)	9	6	1	22	13

[a] Green text indicates gems that appear to have only been polished without prior fashioning or were used in their natural state; red indicates shaping or preforming and polishing; blue indicates preforming, faceting and polishing.

[b] Numbers in red represent gems that were most likely replaced after 1700.

[c] Includes three asteriated sapphires.

[d] One stone with pavilion facets.

[e] One stone with crown and pavilion facets.

[f] Number of samples (from the total amount given) with drill holes is shown in parentheses.

Gems—Colour, Identity, Shape and Size. The inorganic gem materials and imitations thereof can be divided into four broad groups based on colour: blue, pink to red, green, and colourless (including black imitations, which were fashioned to simulate diamond crystals). The different varieties identified across these groups were blue sapphires; rubies, pink sapphires, pink spinels, garnets and pink glass; emeralds and green glass; and diamonds and diamond imitations. Insofar as the majority of the pink-to-red corundum would be classified as pink sapphire in the trade today, and because no precise boundary between ruby and pink sapphire exists, for simplicity only the term *pink sapphire* will be used hereinafter for this range.

The basic shapes of the gems (seen as mounted) spanned from irregular waterworn (pebble-like) or fragmented forms to more regular oval, rectangular, hexagonal, octagonal, square and triangular outlines. The larger gems—which tended to be rectangular, hexagonal and octagonal sapphires and pink spinels—measured approximately 14 × 10 mm in size. The smallest gems, which were primarily diamonds, diamond imitations and emeralds, were all approximately 4.3 mm (including the bezel setting). The remaining samples fell between these two groups (e.g. the piece of pink glass in fleuron X was 7.1 × 6.8 mm; see again Figures 12 and 14). These sizes also provide an approximation of the scale in photographs of the gems that are shown below.

Arrangement. The base segments supporting the larger fleurons incorporated a stylised hexagonal motif bordered in red enamel with small dots that appear to represent flowers (Figure 15a). Each of these segments also includes a central blue stone (sapphire) surrounded by three pink sapphires or spinels and three diamonds or diamond imitations, the latter of which, in turn, are each surrounded by four pearls. Each of the attached larger fleurons is embellished, from top to bottom, with a tiny emerald or piece of green glass surrounded by three pearls; a pink spinel surrounded by four blue sapphires,

Figure 15: Each base segment is decorated by a central blue sapphire surrounded by three pink to red stones (pink sapphires or spinels) and three diamonds or diamond imitations, with each diamond or imitation in turn being surrounded by four pearls. As further embellishment, (**a**) the base segments underlying the larger fleurons incorporate stylised hexagonal lattices that are bordered in red enamel and decorated with small white flowers, while (**b**) the segments supporting smaller fleurons have blue enamel backgrounds for the white flowers. The lowest stones on the fleurons, also visible in these images, were identified as (a) a sapphire and (b) an emerald. Photos by K. Schmetzer, with permission to photograph and reproduce from Bayerische Schlösserverwaltung, Munich.

with a pearl to the right and left of the lowest of the four sapphires; another emerald or piece of green glass surrounded by four pearls; and another blue sapphire just above the base (Figure 16a).

The base segments supporting the smaller fleurons resemble those of the larger fleurons, with the primary differences being a blue enamel border underlying the dotted pattern (Figure 15b) and a slightly broader selection of choices for the surrounding pink to red stones (sapphire, spinel or garnet). In segment II, a portion of the gold framework that would have held one diamond and the surrounding four pearls is missing. The smaller fleurons are each decorated with a pearl; a blue sapphire surrounded by four pink sapphires, spinels, or garnets; another pearl; and just above the base an emerald (in three fleurons, see Figure 16b) or a garnet or piece of pink glass (in three fleurons; not shown).

Gem Fashioning and Enhancements. The degree and style of fashioning exhibited extreme variation across the gems, from minimal processing to extensive work. The diamonds all appeared to have been left as natural crystals. For the coloured stones, a generally ascending scale of complexity could be characterised according to three basic levels, with one, two or three main steps, respectively:

1. Irregular, pebble-like shapes, with only surface polishing, achieved either naturally through erosion and alluvial transport or through deliberate polishing.
2. Materials shaped or preformed without sharp edges and then polished, ranging from cabochon or other curved forms, to curved forms with a planar table, to more polygonal forms with potentially several inclined planar surfaces.
3. Materials preformed, faceted with sharp edges and polished.

Drill holes were often visible within the gems, most commonly in those with irregular, pebble-like shapes

Figure 16: (**a**) The larger fleurons are ornamented, from top to bottom, with a tiny emerald or piece of green glass surrounded by three pearls; a pink spinel surrounded by four blue sapphires, with one pearl each to the right and left of the lowest of the four sapphires; an emerald or piece of green glass surrounded by four pearls; and another blue sapphire just above the base. (**b**) The smaller fleurons are decorated with a pearl; a blue sapphire surrounded by four pink sapphires, spinels or garnets; another pearl; and an emerald in three of the fleurons (shown here) or a garnet or piece of pink glass (not shown) just above the base. Photos by K. Schmetzer, with permission to photograph and reproduce from Bayerische Schlösserverwaltung, Munich.

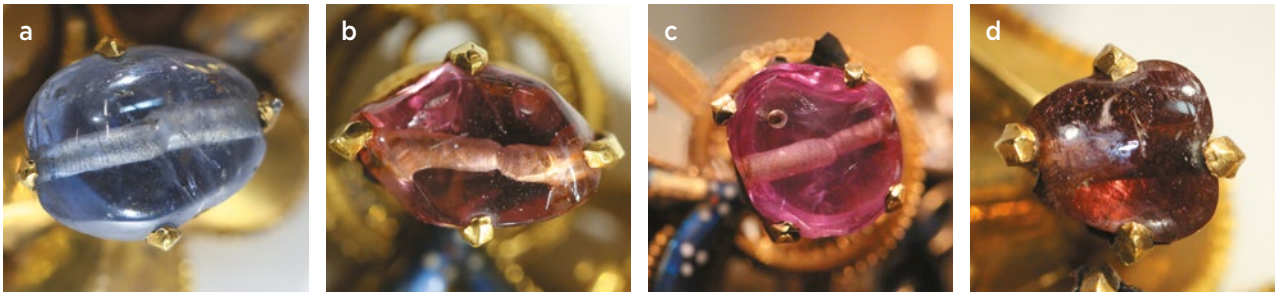

Figure 17: Drill holes are present in (**a**) a blue sapphire, (**b**) a pink spinel, (**c**) a pink sapphire and (**d**) a garnet. The holes were drilled from the opposite sides of each gem, meeting approximately in the middle. The gems may also exhibit a second drill hole at a right angle to the first, as shown in the upper left of (c). Photos by H. A. Gilg.

(Figures 17–19), but also occasionally in more polygonal gems with or without sharp facet edges (e.g. Figure 19a). The holes had been made from opposite sides of the samples, meeting approximately in the centres. Several of the gems displayed two separate drill holes oriented at right angles to each other (Figure 17c, 18b and 19d). Rarely, one complete and one incomplete drill hole could be found in the same specimen, with the incomplete hole terminating abruptly within the sample, suggesting that a problem had been encountered in the drilling operation. Some of the drill holes appeared visually empty (Figures 18a, 18b, 19a and 19b), while others exhibited darker and/or lighter material, potentially indicative of a foreign filler (Figures 18c–f and 19c–f). In general, the presence of drill holes implied previous use of the gems in other jewellery pieces or ornaments.

Evidence of a dark layer or foil behind the samples was regularly seen (Figures 17c, 18c, 18d, 19d and 19e). Also present were concave indentations or grooves on otherwise planar or convex surfaces of some gems (Figure 20). Such techniques to remove flaws by eliminating inclusions, fissures and other impurities were described in medieval Arabic and Persian texts (e.g. by Al-Beruni dated to the 10th century), and are said to have been used in India and Sri Lanka (Ceylon) even several centuries before (Said 1989; Ogden 2013, 2014; J. Ogden, pers. comm. 2019).

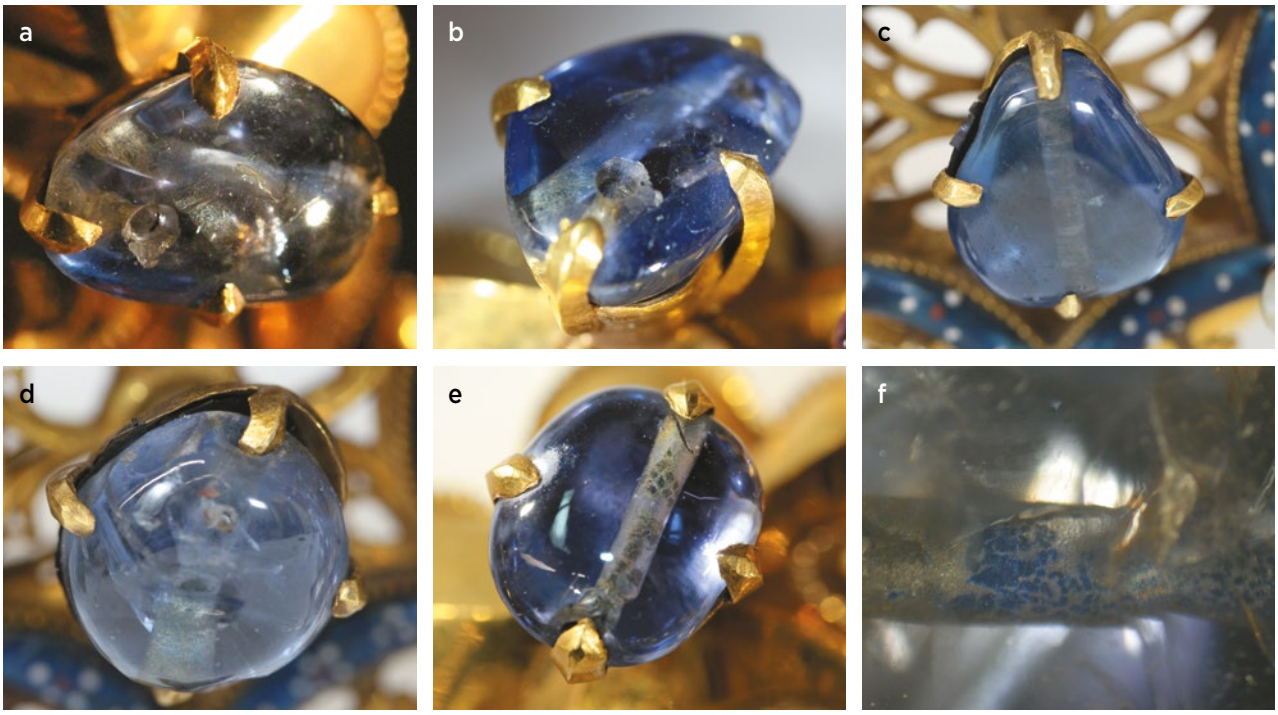

Figure 18: (**a**, **b**) In some of the blue sapphires, drill holes are exposed at the surface and appear empty, thus showing no colour improvement. (**c**–**f**) Other drill holes are filled, at least partially, with a blue material that exhibits a mosaic-like pattern at higher magnification. Particularly in instances where the setting is larger than the gem, some sapphires reveal a dark layer or foil between the gem and the gold mounting, sometimes even protruding from the setting, as visible in (c) and (d). Photos by H. A. Gilg; field of view in photomicrograph (f) is 5.80 × 4.35 mm.

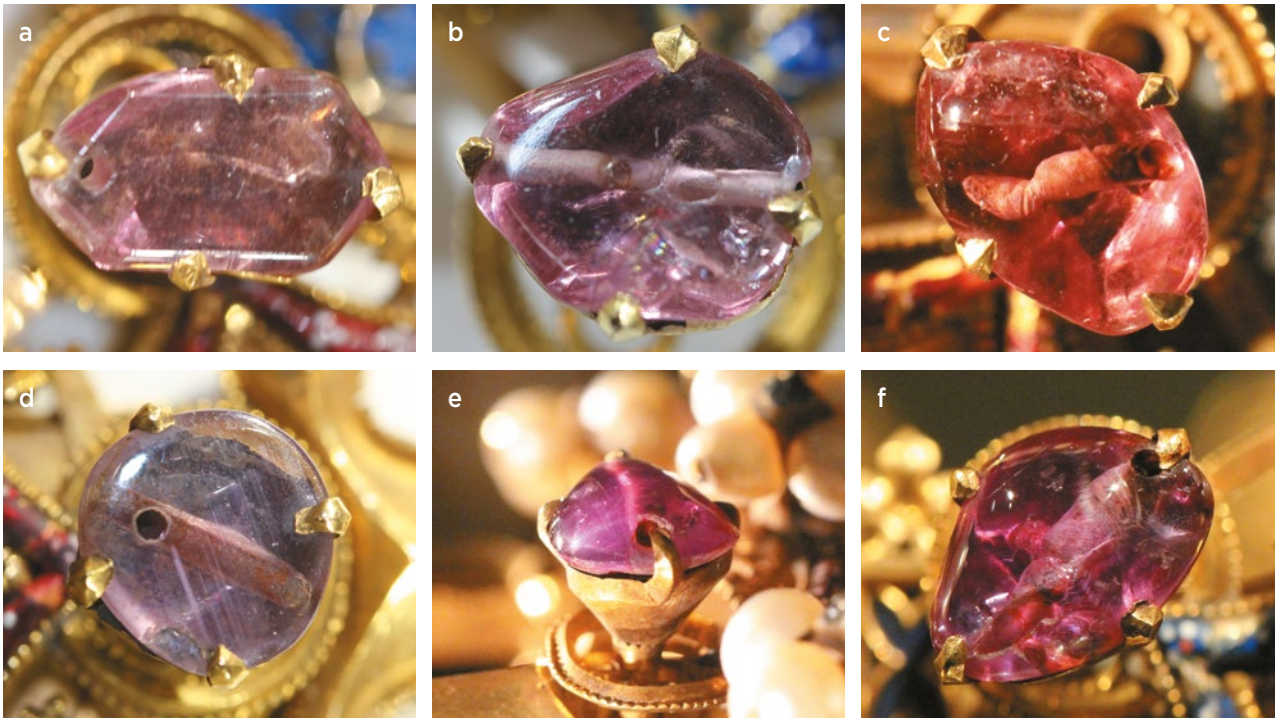

Figure 19: Several of the pink spinels (**a**–**c**) and pink sapphires (**d**–**f**) have drill holes. In some (**a**, **b**), the holes are exposed at the surface and appear empty, affording no colour improvement. Other drill holes (c–f) are filled, at least partially, with a reddish brown material that in some cases seems to be attached only to the walls of the drill holes. Some pink gems, particularly those for which the setting is larger than the gem or the gem is broken, have a dark reddish brown layer or foil between the sample and the gold mounting, sometimes even protruding from the setting, as in (e). A similar layer may also be visible through drill holes and/or if the foil does not back the entire stone, as in (d), where the unenhanced sapphire is almost colourless. Photos by H. A. Gilg.

Blue Gem Materials in Detail

The blue gems in the crown were all identified as sapphires. Two distinct subcategories were present, consisting of translucent dark blue sapphires and transparent pale-to-intense blue sapphires.

Dark Blue Sapphires. Three dark blue sapphires were used, all only translucent at best and without drill holes (Figure 21). Two had been shaped or preformed and then polished to show a rectangular outline, a large table and a single row of inclined, rounded surfaces framing the table, without sharp demarcations (Figure 21a). The third dark blue sapphire was an irregularly broken fragment surrounded, and apparently affixed within the setting, by a blue wax-like mass (Figure 21b). The Fe content measured in the three dark blue sapphires by EDXRF analysis was higher than that found in the larger group of lighter blue sapphires.

Pale-to-Intense Blue Sapphires. The 44 transparent pale-to-intense blue sapphires (plus one doublet) displayed the greatest variability in shape and amount of processing. Outlines ranged from irregular or pebble-like to oval, rectangular, hexagonal and octagonal. Processing spanned through all three categories listed above, with polishing, shaping or preforming, and faceting all present

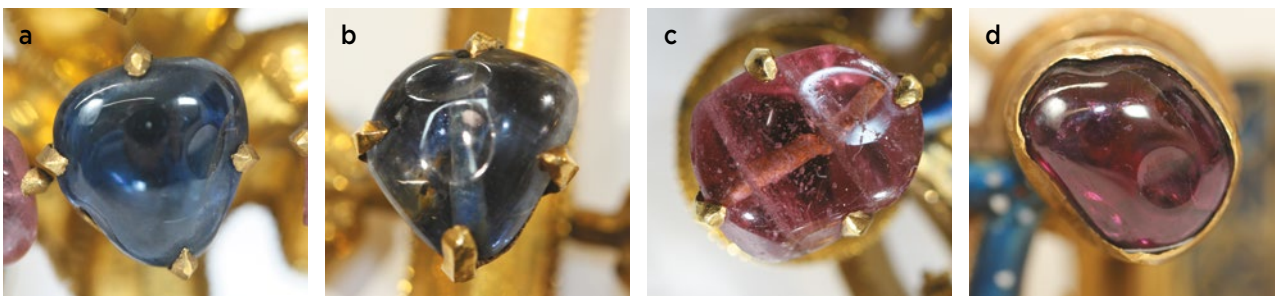

Figure 20: Surface indentations in the form of shallow cavities, presumably from attempts to remove impure areas or inclusions through polishing, are seen on sapphire (**a**, **b**), spinel (**c**) and garnet (**d**). Photos by H. A. Gilg.

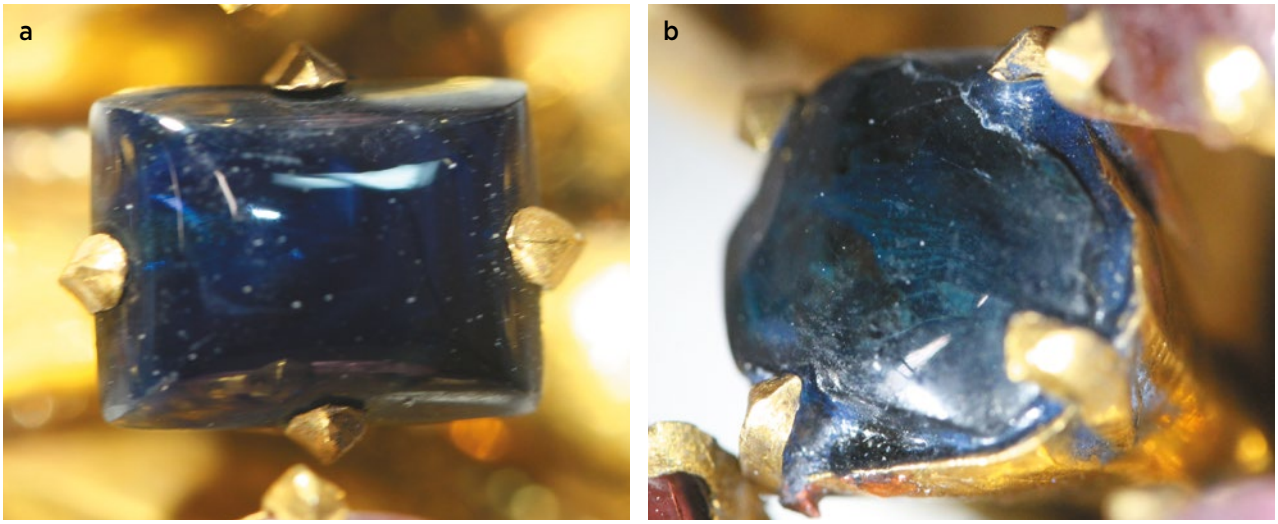

Figure 21: Three translucent dark blue sapphires are mounted in the crown. Two are rectangular without sharp edges, as shown here in one example (**a**), while the third consists of an irregular fragment surrounded by a dark blue wax-like substance (**b**). Photos by H. A. Gilg.

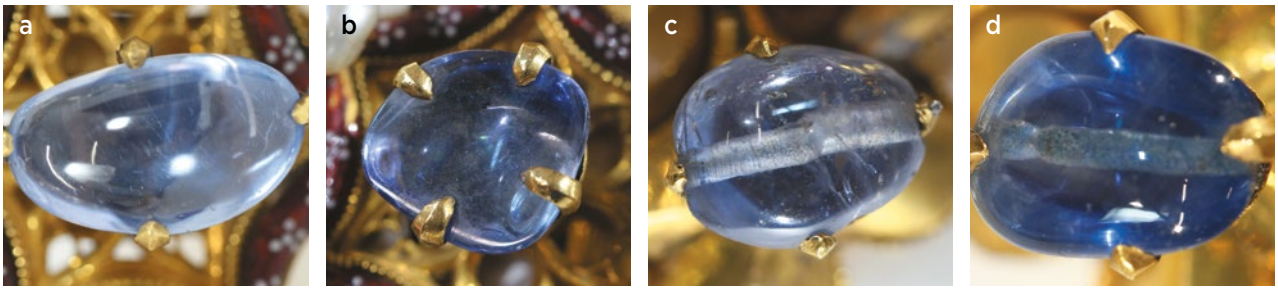

Figure 22: Many of the pale-to-intense blue sapphires are irregularly shaped (**a**), and some are topped with a planar or near-planar table face (**b**). Others are more regular ovals with curved domes (i.e. cabochons; **c**), but occasionally some of these also have a planar top surface truncating the dome (**d**). Photos by H. A. Gilg.

in different combinations and arrangements. For some of the more irregular shapes, it was difficult to ascertain if the form and surface polish were achieved naturally or via deliberate polishing. At the opposite end of the spectrum were the stones that had been preformed, faceted and polished, with sharp edges. Several different facet arrangements were present.

Among those with irregular, near-oval and oval outlines, some were topped with a curved upper surface or dome (Figure 22a, c), while others showed the addition of a planar or near-planar table (Figure 22b, d). Three of the oval cabochons displayed asterism (e.g. Figure 23).

The more polygonal shapes included six rectangles, one hexagon and 14 octagons. The six rectangles each showed a central table surrounded by one row of four inclined surfaces; this pattern was seen in four samples with indistinct curves and two with sharp-edged crown

Figure 23: A few of the blue sapphire cabochons show six-rayed asterism. Photo by K. Schmetzer, fibre-optic illumination.

facets (Figures 24f and 25f). The sole hexagon was sharply faceted with a planar table and six crown facets (Figures 24e and 25d).

The octagons demonstrated particular diversity in fashioning, with all having a near-planar or planar table, as well as:

- In five stones, one row of eight inclined curved surfaces surrounding the table (Figure 25a), with one gem having been oriented in the setting such that the eight inclined surfaces appeared akin to pavilion facets
- In six stones, one row of sharp crown facets (Figure 24a), with one of those gems also including pavilion facets (Figure 25b) and another having the eight crown facets further subdivided with a scissor-cut pattern (Figure 24d)
- In three stones, two rows of circumscribing sharp facets, the first being weakly inclined to the table and the second nearly perpendicular to the table, suggestive of girdle facets (Figures 24b and 25c)

A final octagon, which did not fit exactly in the setting, proved to be a doublet, with a table and two rows of weakly inclined crown facets (Figures 24c and 26a). The upper part of the sample was determined to be sapphire, and the separation plane was partly decomposed, revealing bubble-like structures (Figure 26b).

Drill holes were frequently seen in the blue sapphires (Figures 17a, 18, 22c, 22d and 25d), and also relatively common were surface indentations (Figure 20a). Several drill holes exposed at the surface appeared open and empty (Figure 18a, b), while a number of others seemed to display a mosaic-like appearance, consisting of irregular dark blue areas separated by granular whitish material (Figure 18e, f). This visual impression strongly indicated the presence of a foreign material, but coverage of the drill holes by the settings prevented confirmation (Figure 18c, e). Dark layers behind some of the sapphires and evidence of foil-backing (Figure 18c, d) were observed as well.

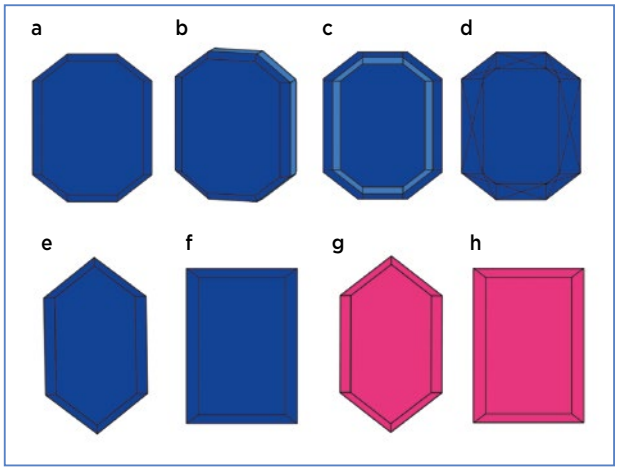

Figure 24: The sharply faceted blue sapphires and pink spinels display a multiplicity of cut layouts, including octagonal, hexagonal and rectangular outlines with flat tables, and either crown facets (**a** and **c**–**h**) or a combination of crown and girdle facets (**b**). Drawings by K. Schmetzer.

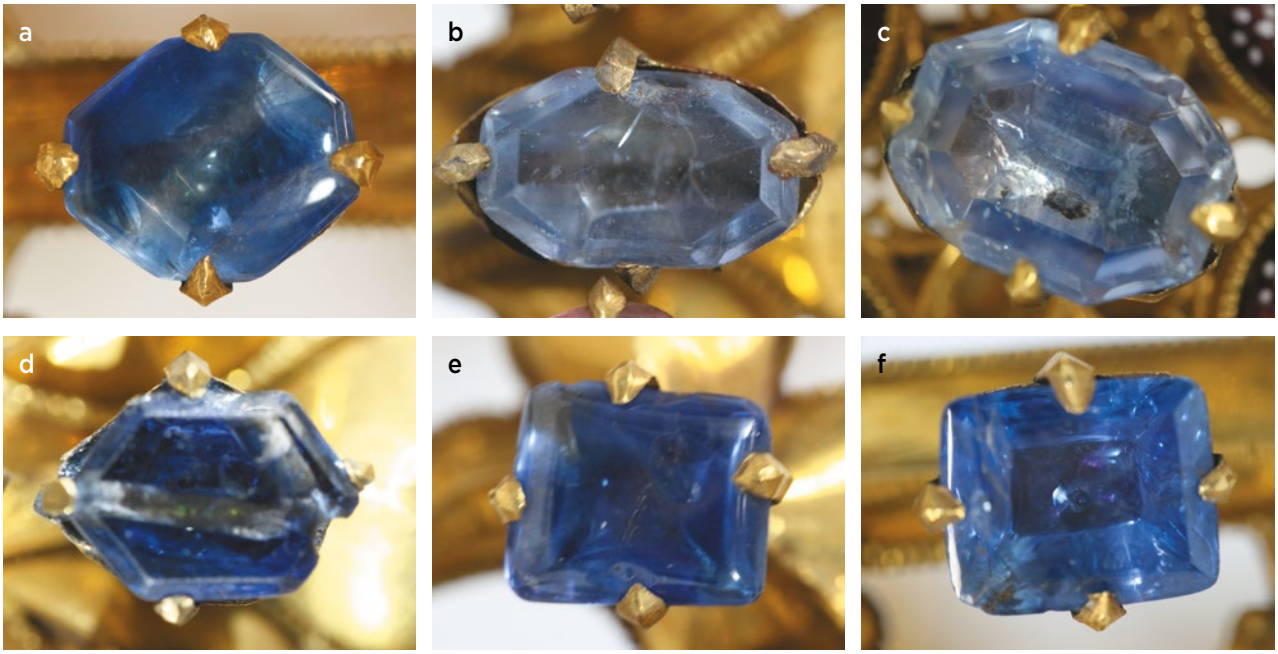

Figure 25: Blue sapphires in the crown exhibit octagonal (**a**–**c**), hexagonal (**d**) and rectangular (**e** and **f**) forms, either without sharp edges (a, e) or with sharp planar facets. Among the sharply faceted sapphires are those with one row of crown facets (d and f), crown and pavilion facets (b), crown and girdle facets (c), and even a more complex scissor cut. Photos by H. A. Gilg.

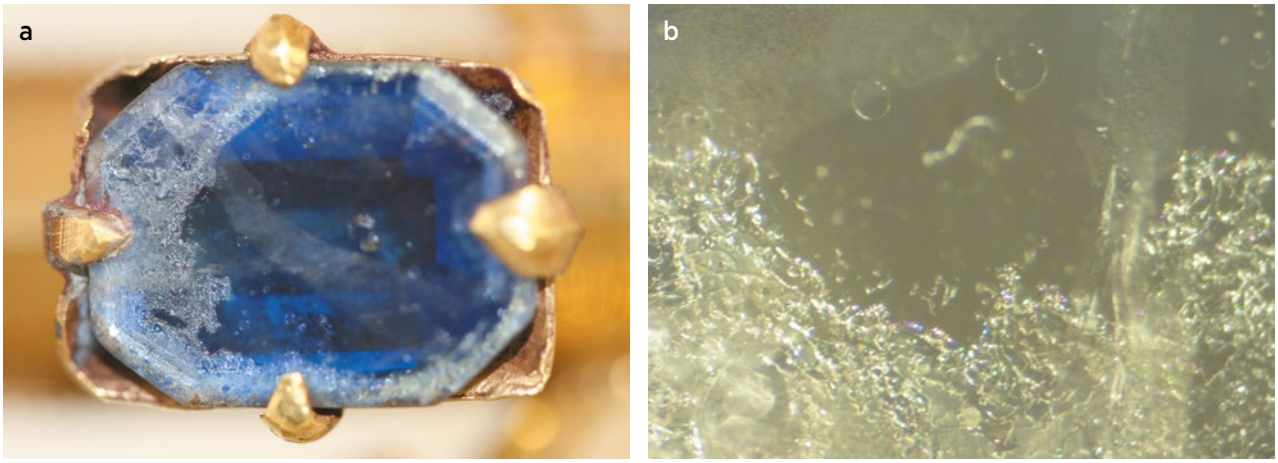

Figure 26: One sapphire doublet was found in the crown. It is mounted in a setting that is too large for it (**a**) and shows a partially decomposed separation plane with bubble-like structures (**b**). Photos by H. A. Gilg, field of view in (b) is 3.7 × 2.8 mm.

Pink to Red Gem Materials in Detail

The pink to red group comprised the greatest number of gem varieties but exhibited substantially less variation in fashioning than the blue group.

Pink Sapphires. The 10 pink sapphires were all irregular or pebble-like, with a few approaching oval in outline (Figure 27). Each exhibited a surface polish. The upper surface of most was curved (Figure 27a, c), but for two stones the curve or dome had been topped by a planar table (Figure 27b, d). As with the blue sapphires, the contribution to the shape and polish by nature or human intervention was not always discernible.

Drill holes were common (Figures 17c, 19d–f and 27), and potential enhancement by reddish brown fillers (Figures 19e, 19f and 27b) and underlying layers (analogous to those detailed below for the pink spinels) was likewise detected. If both backing and fillers were present, their respective contributions to the colouration could be challenging to separate (Figure 19f).

Pink Spinels. These were used in the crown's decoration more than any other inorganic gem variety, with 53 identified. A substantial majority (45) were irregularly shaped and primarily curved (Figure 28a), with four also incorporating a planar table (e.g. Figure 28b). More-regular shapes included one oval, three rectangles and four hexagons. The oval was a domed cabochon, while the rectangles and hexagons included both those having a table surrounded by a row of inclined curved surfaces (Figure 28c, e) and those having sharp-edged crown facets circumscribing the table (Figures 24g, 24h, 28d and 28f).

Drill holes were quite pervasive among the spinels (Figures 17b, 19a–c, 28a–d). Some, as with the blue sapphires, appeared empty (Figure 19a, b). In other instances, the holes were filled with an unknown reddish brown substance, either adhering to the walls or partially blocking the holes (Figures 19c, 28a, 28b and 28d). The likely intent was to hide the drill holes and/or intensify the gem's colour. Additional enhancement was suggested by the presence of a reddish brown layer or foil, particularly visible when a sample was broken or a drill hole was perpendicular to the table (Figure 19a). In one spinel, the incomplete nature of the backing showed its effect on colour (Figure 19c). Surface indentations were also common on the spinels (Figure 20c).

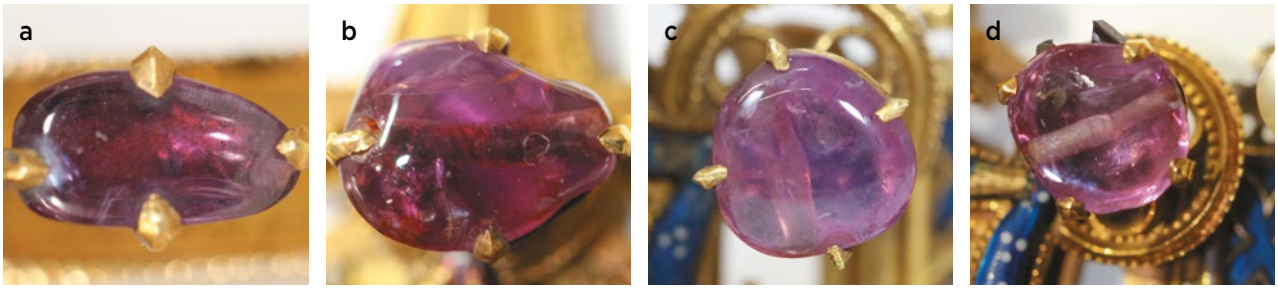

Figure 27: Most of the pink sapphires are irregularly shaped (**a**) and sometimes topped with a planar or near-planar face (**b**). A few are almost oval, with curved domes (**c**) or occasionally with a planar top surface truncating the dome (**d**). Photos by H. A. Gilg.

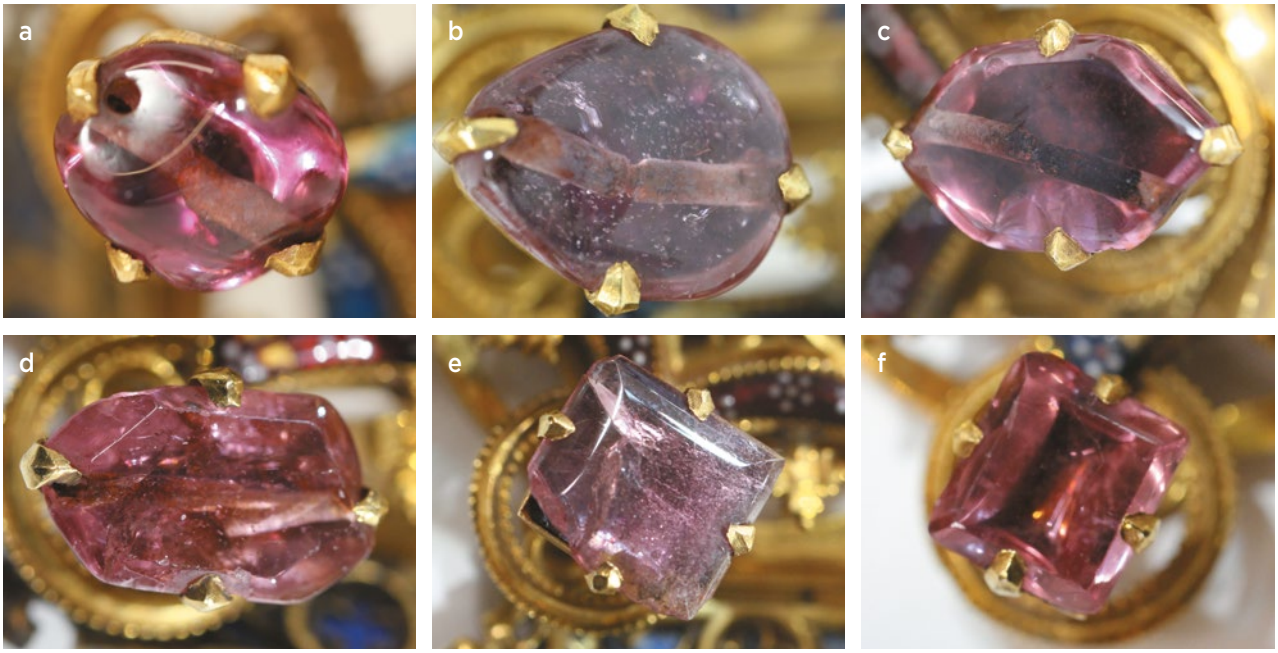

Figure 28: The majority of the pink spinels are irregular and pebble-like (**a**), frequently with surface indentations and drill holes containing foreign fillers. In only a few instances is a flat or near-planar table added to truncate the curved upper surfaces (**b**). More-regular polygons include hexagonal (**c**, **d**) and rectangular samples (**e**, **f**), either without distinct edges (c, e) or with sharp planar facets (d, f). Photos by H. A. Gilg.

Figure 29: The garnets comprise irregularly shaped pebbles (**a**, **b**) and a single oval cabochon truncated by a planar table (**c**). Chemically, the samples were identified as almandines (a, c) and pyropes (b). Photos by H. A. Gilg.

Garnets. Five garnets were used in the crown. Four were irregularly shaped, polished pebbles (e.g. Figure 29a, b), including one with a drill hole (Figure 17d) and one with surface indentations (Figure 20d). The fifth was oval with a planar table (Figure 29c). EDXRF analysis established that they consisted of two pyropes (Figures 17d and 29b) and three almandines (Figures 20d, 29a and 29c). The ranges of chemical composition are as follows:

- Pyropes: 19.1–20.1 wt.% MgO, 16.0–18.8 wt.% FeO, 1.3–1.9 wt.% CaO, 0.4–0.9 wt.% MnO
- Almandines: 2.4–4.9 wt.% MgO, 30.7–32.2 wt.% FeO, 1.7–4.1 wt.% CaO, 1.5–2.0 wt.% MnO

Pink Potassium-Lead Glass. One of the pink specimens proved to be an irregularly shaped piece of potassium-lead glass (Figure 30). The measured Pb content was higher than that for the green lead glass described below.

Figure 30: One irregularly shaped piece of pink lead glass is incorporated in the crown's embellishment. Photo by H. A. Gilg.

Green Gem Materials in Detail

Emeralds. The nine emeralds fell within two size categories: three larger, including two irregular pebbles (e.g. Figure 31a) and one oval cabochon; and six smaller, including five squares (Figure 31b) and one triangle (Figure 31c), each with a curved upper surface or dome. All the emeralds were of intense green colour, but most were only translucent due to numerous inclusions and partially healed or unhealed fractures. EDXRF analysis showed that the emeralds contained some Mg and no V.

Green Potassium-Lead Glass. Mirroring the use of the smaller emeralds and obviously imitating them were one square (Figure 32a) and five triangular (e.g. Figure 32b) samples of green potassium-lead glass. All of them had curved tops and were only translucent, appearing somewhat grainy and non-homogeneous.

Diamonds and Diamond Imitations in Detail

The 14th-century inventories of the crown characterised 33 gems as 'diamonds' (i.e. three in each of 11 base segments present at the time), eight of them being imitations. During the present investigation, these same 11 segments contained 32 purported 'diamonds' (one having been broken away from segment II) that were found to include 10 imitations. The three 'diamonds' in segment IV were all imitations (see Figure 14).

Diamonds. All the diamonds consisted of natural crystals with octahedral habit. More specifically, the main crystal form was the octahedron {111}, often modified by stepped development of the octahedral faces. Most crystals also displayed dissolution structures, as seen by the development of pseudo rhombic-dodecahedral, somewhat rounded or curved facial surfaces (Figure 33).

Diamond Imitations. The materials imitating diamonds exhibited a basic structure of four planar or near-planar gold faces forming a four-sided pyramid, covered completely or partially by a black substance (Figure 34). The initial impression was broadly akin to that of a diamond octahedron (Figure 35).

EDXRF analysis of several such imitations yielded

Figure 31: The emeralds comprise irregularly shaped (**a**), oval, square (**b**) or triangular (**c**) stones, each displaying a curved upper surface or dome. Photos by H. A. Gilg.

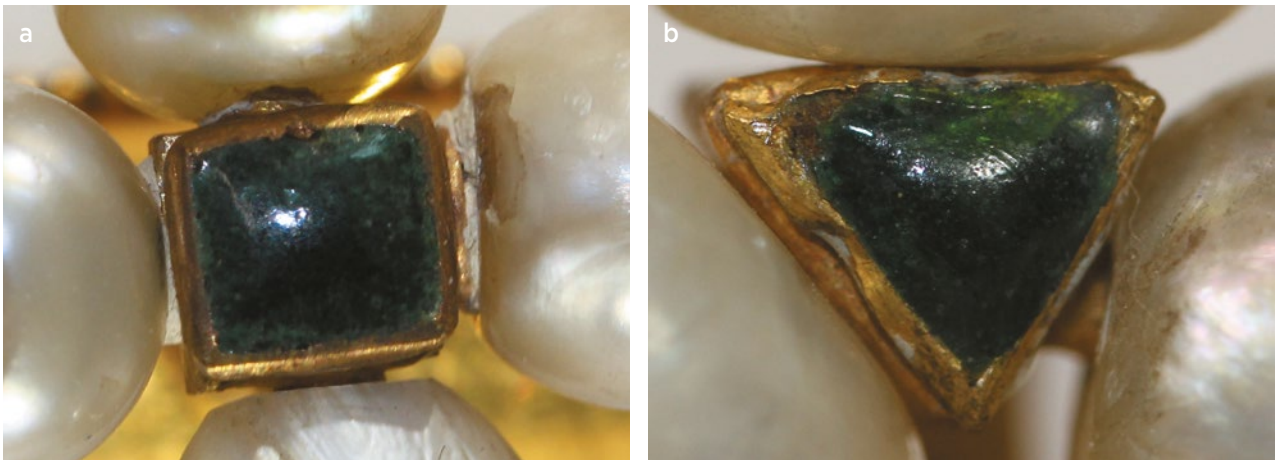

Figure 32: The samples of green lead glass imitating emeralds are square (**a**) or triangular (**b**), with curved upper surfaces. Photos by H. A. Gilg.

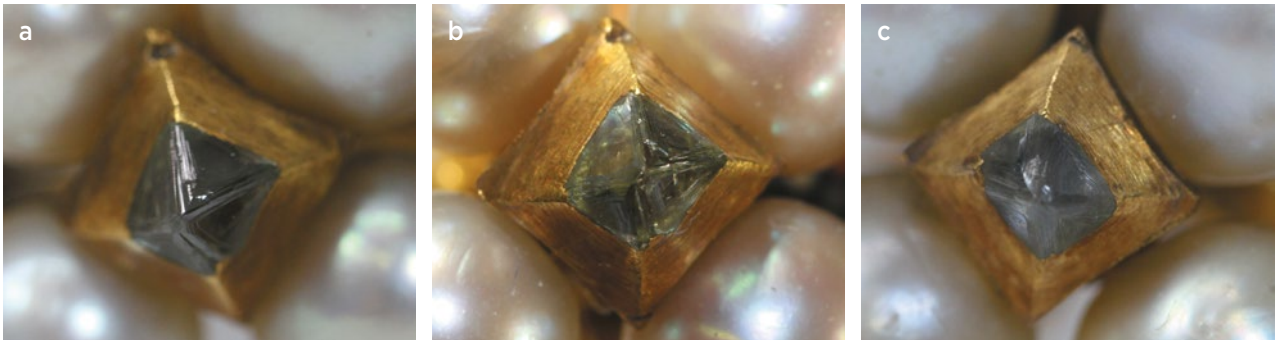

Figure 33: All the diamonds consist of natural octahedra, rarely with planar surfaces (**a**), but frequently showing stepped development of the octahedral faces (**b**) and/or somewhat rounded pseudo rhombic-dodecahedral forms (**c**). Photos by H. A. Gilg.

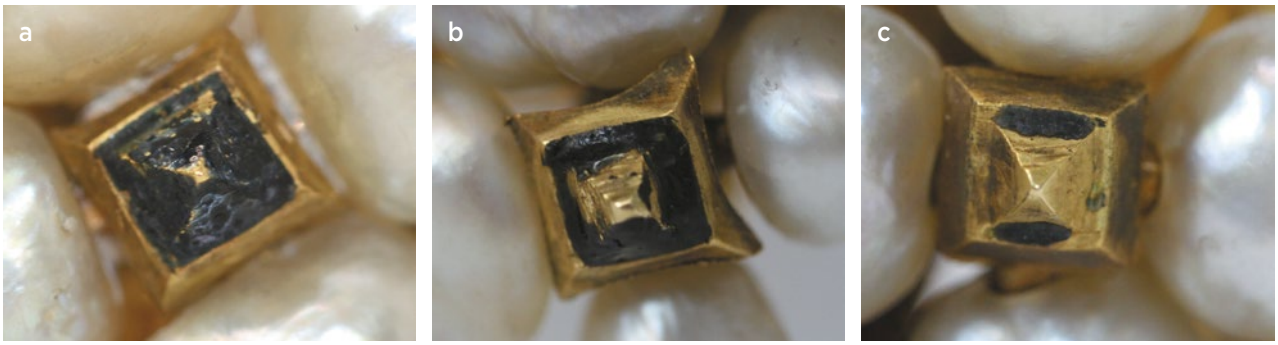

Figure 34: Diamond imitations were manufactured as a four-sided gold pyramid covered (at least partially, in some cases likely having worn away) by a layer of black K-Pb glass or enamel. Photos by H. A. Gilg.

signals for the major components of the alloyed gold (Au, Ag and Cu) and of the surrounding pearls (Ca and Sr). Additional signals were detected for K, Pb, Fe, Mn and minor amounts of Co. This combination indicates that an Fe-Mn-Co-bearing K-Pb glass or K-Pb enamel served as the black coating over the gold pyramids. Under the experimental conditions employed, Na could not be measured (especially in low concentrations) and, therefore, its presence cannot be excluded from the black layer (which would suggest a Na-K-Pb glass).

Settings in Detail

In general, the gems were set in closed-back, cup- or cone-like mountings adapted to their particular sizes and shapes (Figure 36). With one exception, all the larger gems with irregular, oval, rectangular, hexagonal or octagonal shapes were then affixed in the mountings with four prongs, occasionally taking the form of more extended curved claws (Figures 17–22, 25–30 and 31a). In some cases, the prongs corresponded with individual grooves or surface indentations on the stones. Smaller

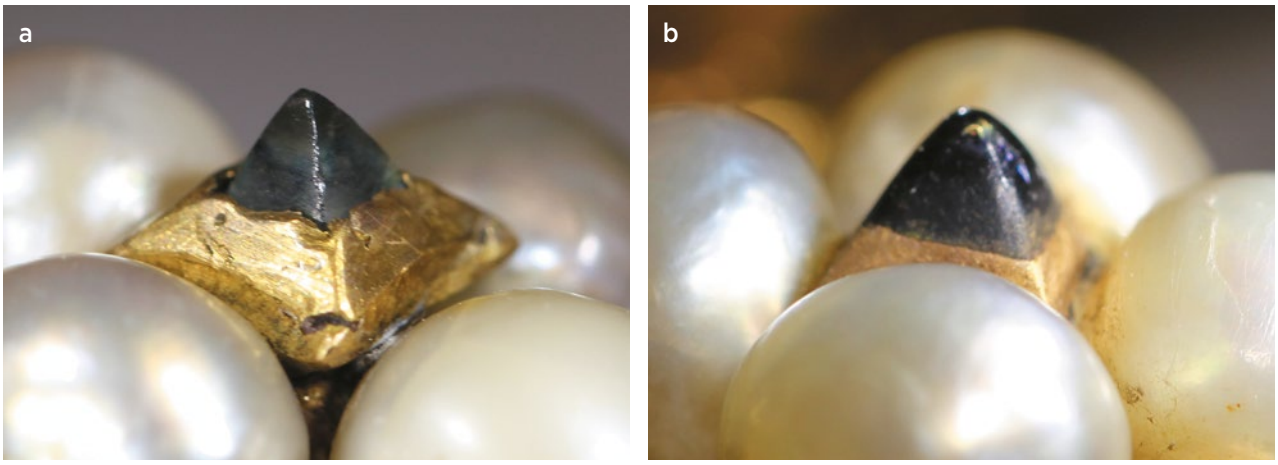

Figure 35: The visual appearance of the diamond octahedra (**a**) and diamond imitations (**b**) can be quite similar, rendering substitution of the latter for the former relatively convincing. Photos by H. A. Gilg.

Figure 36: The gem settings were adapted to the individual sizes and shapes of the available stones. Most of the larger gems are set with four prongs in a closed-back, cup- or cone-shape mounting. Photos by H. A. Gilg.

gems, such as the diamond octahedra, square and triangular emeralds, and green glass pieces, were typically secured in the mountings with a simple bezel setting (Figures 31b, 31c, 32 and 33). Only one larger garnet in the replaced segment IV showed a similar bezel setting without prongs (Figure 20d). The mountings are typical of the closed settings used for gems during the High and Late Middle Ages (Bethe 1956; Falk 1975).

DISCUSSION

The crown offers a unique window into how craftspeople of the late 14th century utilised the materials and techniques at their disposal. Each of its components, and their potential modification, can be instructive when considered within the context of the era.

Metalwork Composition

Chemical analysis yielded a composition for the metal framework comparable to 18-carat gold, a result in agreement with previous studies of the crown undertaken in the early 20th century (Deibel 1927, 1928). Notably, the compositional range of the Au-Ag-Cu alloy falls within that shown by numerous gold objects dated from the High to Late Middle Ages, thereby offering a strong indication for the crown's age (see Mecking 2010 and references cited therein).

Gem Sourcing

The crown is resplendent with multiple varieties of natural inorganic gem materials: blue and pink sapphires, pink spinels, garnets, emeralds and diamonds. Although it is beyond the scope of the present study to discuss the possible geographic provenance of the gems in detail (e.g. by comparing trace elements and inclusions with those of gems from known sources), certain general observations are relevant.

The origin of the individual gems can be considered from two distinct yet interrelated perspectives: the primary vs. secondary type of deposit and its geographic location. Regarding the deposit type, the condition of the gems in terms of their fashioning provides some insight (Figure 37a). As explained above, the degree of apparent fashioning work spans an entire spectrum from irregular, rounded and pebble-like polished shapes to sharply faceted geometric forms. A significant percentage of the sapphires, spinels and garnets showed irregular or pebble-like forms that are highly indicative of secondary deposits. It may also be reasonable to assume that the stones of these varieties that were preformed and/or faceted also originated from the same secondary deposits, given their similar visual appearance. Nonetheless, the possibility of a primary deposit, such as one of the marble-hosted deposits in Asia, cannot be excluded, particularly for some of the faceted samples. The majority of the emeralds are fashioned with a geometric shape (square or triangular), leaving both primary and secondary deposits equally possible as sources (Figure 37b). The appearance of the diamonds, being all octahedral crystals that reflect no further processing, is likewise theoretically consistent with either a primary or secondary source (Figure 37a).

With respect to potential geographic locations for the deposits, Sri Lanka is a strong candidate for the transparent pale-to-intense blue sapphires. As early as the 3rd century BCE, the great chronicle of Ceylon, the Mahavamsa, referenced sapphires amongst the known gem materials (Geiger & Bode 1912). In the Mediterranean region, the presence of blue sapphires from Ceylon has been documented from the era of the Roman Empire (Foster 1988), and the gems were an important part of the Eastern sea trade during the Roman and Byzantine periods (Bopearachchi 1997). Concerning the specific timing and quantities, present knowledge suggests that blue sapphires were extremely rare before the late 1st century BCE/early 1st century CE but became more widely known from the 2nd century CE onwards (Thoresen 2017).

Inventories from the 14th and 15th centuries frequently

differentiated between higher-quality, lighter-coloured sapphires and dark blue sapphires of inferior quality. The former were often labelled *saphirs d'orient*, a term describing mainly Sri Lankan material (Holmes 1934), characteristically traded via Arabic middlemen (Mahroof 1989). The latter were characterised as *saphirs de Puy*, indicating basaltic sapphires from Le Puy en Velay in France (Schulz 1897). The Le Puy en Velay locality was recognised at least by the mid-14th century, as it was explicitly mentioned in a text by Conrad von Megenberg written circa 1350 (Schulz 1897). These early descriptions and understandings have also been borne out in modern gemmological examinations, which have identified sapphires in numerous objects of medieval jewellery as having come from either Le Puy en Velay or Sri Lanka (e.g. Hyršl 2001). Such factors could point towards the same two sources for the dark and light sapphires, respectively, in the present crown.

The options for the pink to red gems, however, are multiple. The gem gravels of Sri Lanka, given their role in furnishing blue sapphires, would be one logical suggestion for at least some of the pink sapphires, pink spinels and garnets decorating the crown. Sri Lanka has historically been recognised as a source of such materials. Venetian merchant Marco Polo mentioned rubies from Ceylon at the end of the 13th century (Moule & Pelliot 1938). The island was similarly referenced in a text written by the Franciscan friar Odoric of Pordenone around 1330, as well as by the Moroccan traveller Ibn Battuta, who visited Ceylon circa 1340 (Yule 1866; Gray 1883). Yet little exists to rule out various other primary and secondary deposits in India and elsewhere in Asia or in Europe. For example, the Badakhshan deposits of pink spinels at Kuh-i-Lal in present-day Tajikistan have been known since the 10th century. They were first reported in Arabic texts (e.g. by Al-Beruni) and later mentioned by Western travellers such as Marco Polo (Yule 1871; Said 1989; Hughes 1994; Bowersox & Chamberlin 1995).

More questionable are the Burmese deposits of rubies, pink sapphires and spinels. Insofar as the earliest report of gems (not gem mines) in the area dates from the Venetian traveller Nicolò de' Conti, who reached Burma in the late 1420s or early 1430s (Frampton 1579), there is no clear indication that Burmese materials would have entered Western trade before the end of the 14th century. Only later would they have a meaningful presence, as evidenced by early 16th-century reports of Italian and Portuguese travellers, including Ludivico di Vartherma, Tomé Pires and Duarte Barbosa. For instance, a 1516 letter from Tomé Pires to the King of Portugal referenced rubies from Burma as well as dark red rubies and *baleis* rubies from Ceylon (Cortesão 1944). Similarly, by 1518 Duarte Barbosa was differentiating between rubies from Burma and Ceylon while also noting spinels from

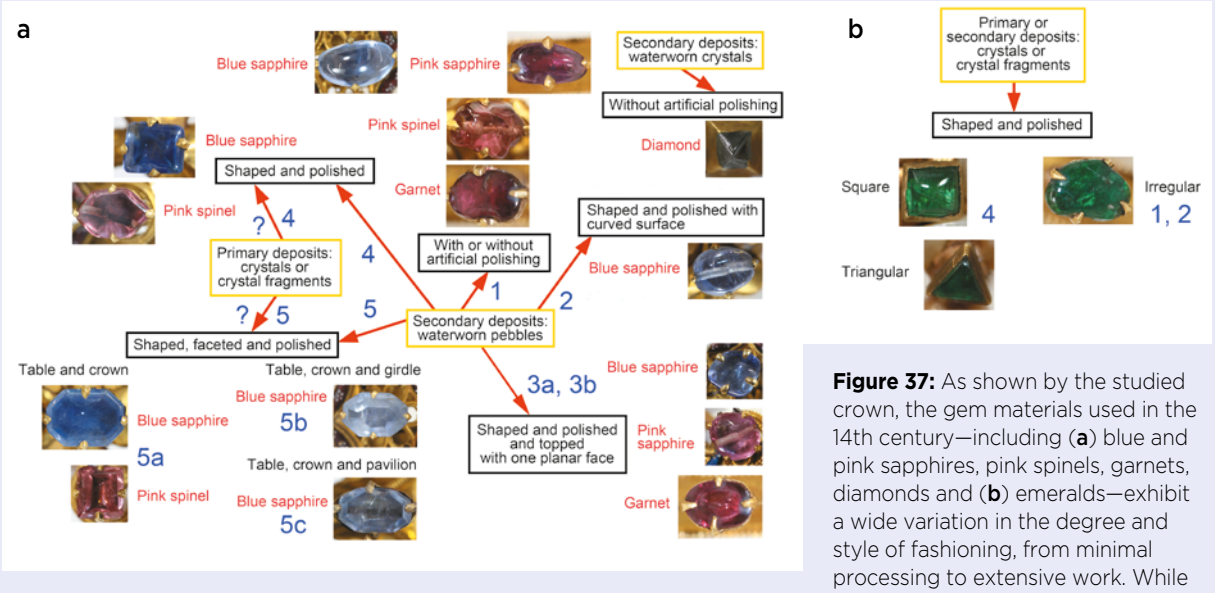

Figure 37: As shown by the studied crown, the gem materials used in the 14th century—including (**a**) blue and pink sapphires, pink spinels, garnets, diamonds and (**b**) emeralds—exhibit a wide variation in the degree and style of fashioning, from minimal processing to extensive work. While the diamonds were left as natural crystals, the coloured stones consist of: (**1**) irregular, pebble-like forms, most with polished surfaces, likely from secondary deposits; (**2**) rounded cabochon forms, shaped or preformed and polished, with a domed top; (**3**) irregular pebble (classified as **3a**) or cabochon (classified as **3b**) forms with an added planar table surface; (**4**) regular polygonal forms, shaped or preformed and polished, without sharp edges; and (**5**) regular polygonal forms, preformed, faceted and polished, with sharp edges, showing table and crown facets (see **5a**), table, crown and girdle facets (see **5b**), table, crown and pavilion facets (see **5c**), or more complex scissor-cut crown facets (not shown).

these localities and *balaches* (as a variety of ruby) from Badakhshan (Dames 1921; Mugler 1928).

Identifying possible sources for the emeralds suffers from similar complexity in the context of the Middle Ages. The deposits in Egypt, incorporating several ancient mines, have been known from antiquity (Jennings *et al.* 1993), although the principal old workings themselves were rediscovered only in the early 1800s (Cailliaud 1822). The main locality—Wadi Sikait (Mons Smaragdus area)—was operated primarily in Roman and early Byzantine times, up to the 5th or 6th century CE (Harrell 2004, 2006; Foster *et al.* 2007; Sidebotham *et al.* 2018). Excavations at neighbouring mines, including Wadi Nuqrus and Gebel Zabara, have suggested that activities there extended later into the Islamic period (e.g. from the 6th to the 9th century or from the 12th to the 16th century; Shaw *et al.* 1999). Emerald mining in the region from the late-9th to the mid-17th century is supported by the Arabic literature, although the texts do not differentiate between specific localities (Schneider & Arzruni 1892; Power 2012).

However, problems arise in that these Egyptian sources lack a demonstrated connection, based upon chemical and gemmological properties, to materials used in the Late Middle Ages. Most emeralds in pieces of the High and Late Middle Ages were, according to modern standards, of low quality, often not even translucent (Kržič *et al.* 2013), notwithstanding a few examples of better quality, such as in the treasure of Preslav, Bulgaria, dated to the 10th century (see Strack & Kostov 2010 and references therein). Compounding these difficulties are the ever-present challenges posed by nomenclature and failure to distinguish between gems of the same colour. For instance, concerning the Arabic literature, the 13th-century work of Al Tifaschi was the first to give separate descriptions for emerald and peridot, and discrepancies are replete in the mineralogical identification of the various green gems mentioned in older Arabic treatises (Abul Huda 1998).

Other sources proposed for the emeralds found in Middle Ages ornaments include Austria, Afghanistan and Pakistan (Giuliani *et al.* 2000). Nonetheless, as with the Egyptian material, a demonstrated scientific connection is lacking. Studies aiming to establish an empirical link between emeralds in historical jewellery and recently mined gems from these localities (through trace elements, inclusions, etc.) have been performed on only a few samples (see, e.g., Calligaro *et al.* 2000; Kržič *et al.* 2013). Moreover, a key concern is that early mining or use of such materials has not been documented, a shortcoming well illustrated with regard to the Austrian deposits. Danish scientist Niels Stensen (Nicolaus Steno) is reported to have travelled to the Habachtal (Heubachtal) emerald locality in 1669 (Scherz 1955). A worldwide mining list published by Brückmann (1727) broadly referenced Tyrol as the sole emerald source in Austria, and the first real published description of emeralds from Habachtal did not appear until 1797 (Schroll 1797).

The prolific Colombian deposits can be readily excluded as a source for the emeralds in Blanche's crown. Both the later 'discovery' by Europeans in the mid-16th century and their distinct chemical properties exclude them. In particular, the lack of V and the presence of Mg in the crown's emeralds is telling.

Finally, tracing the diamonds offers perhaps the highest degree of probability. The only sources for diamonds known in Europe at the end of the 14th century were the various secondary deposits in India (Bagchi & Ghose 1980; Harlow 1998; Levinson 1998; Coulson 2012; Ogden 2013). While deposits in Borneo were reportedly active from the 6th century, with gems having been traded to China (Spencer *et al.* 1988; Tay *et al.* 2005), those diamonds were not acknowledged in European texts until the mid-16th century, via descriptions by Portuguese travellers such as Gonçalo Pereira in 1530 (Lopes de Castanheda 1561; Dames 1921).

Gem Enhancements

The historical record strongly supports the use of foil-backing as a common and accepted practice during, and after, the era of the crown's creation. The Early Middle Ages witnessed extensive application of foil-backing in cloisonné-type jewellery, where doubly polished garnet plates were set in a metal framework on top of thin gold or silver foils (Gilg *et al.* 2010). In the following centuries, the widespread use of closed-back settings prolonged the popularity of the technique. By the Renaissance, sophistication had reached a level to yield publication of different compositional formulas for the foils used to enhance gems of specific colours. For example, in 1568 Italian goldsmith Benvenuto Cellini specified Au-Ag-Cu alloys to enhance yellow, red, blue and green gems (Table II; see German translations by Brinckmann 1867 and Brepohl 2005).

Table II: Alloys used for foils to enhance gems of various colours, specified by Benvenuto Cellini in 1568.

Element (wt.%)	Yellow	Red	Blue	Green
Au	9.1	37.0	18.2	5.9
Ag	18.2	29.6	9.1	35.3
Cu	72.7	33.3	72.7	58.8

Other authors, such as Agricola (in 1546; German translation by Lehmann 1810), Della Porta (in 1589; English translation attributed to Porta 1658 and German translation by Peganium 1680) and Smith (1750), described the use of foils consisting of pure copper, pure gold, gold-silver alloys and gold-silver-copper alloys. The foils, in turn, could themselves be modified to further enhance the visual effect, depending on the gem variety involved and the colour sought, by methods such as oxidation in air. The potential effectiveness of such methods is corroborated in historical pieces by the results of long-term exposure to air of portions of such foils, especially those with a high Cu content. Foil colour has frequently been influenced by partial decomposition and heavy oxidation forming cuprous oxide Cu_2O (cuprite, red) or cupric oxide CuO (tenorite, black; Cretu & van der Lingen 1999; Lee *et al.* 2016).

Foil-backing started to decline in the 18th century before largely disappearing in the 19th century, as new cuts and open settings increasingly came into vogue (Blum 1828; Bauer 1896; Kornbluth 2003; Brepohl 2005; Whalley 2012). Notably, throughout its many decades of broad application, foil-backing was not considered a fraudulent practice but an accepted and even necessary method to bring out and best display a gem's optical properties and beauty.

The foregoing indicates that observation of a dark layer or foil between many of the crown's sapphires and spinels and their closed-back mountings fits well within the context of a 14th-century creation, following established traditions of the time, and would not be out of place for the few later substitutions (see, e.g., Otavsky 1992).

The use of filler materials or dyes in drill holes to enhance gem colour and hide the holes also finds historical analogue in other examples from the Middle Ages. As noted above, Blanche's crown exhibited drill holes in blue sapphires with a dark and light mosaic-like pattern and in pink sapphires and spinels with a reddish brown hue. A similar appearance for blue sapphires in medieval jewellery objects was mentioned briefly by Hyršl (2001), and nothing suggests that the dark-appearing drill holes in the pink gems would be unusual for the time.

Gem Imitations

Imitations incorporated in the crown's decoration included green and pink samples made from lead glass and black-coated gold pyramids. The green pieces imitated emeralds while the pyramids imitated diamond crystals. These were likely used because insufficient natural emeralds and diamonds were available, both at the time of the crown's creation and when it was later repaired, to complete the intended design with the requisite symmetry. The single pink glass sample was visually similar to the other pink stones (sapphires and spinels).

Green and Pink Lead Glass. The history and use of glass to imitate gems spans almost 3,500 years. Chemical composition is key for understanding and classifying the different types of glass, their manufacture and their age. Lead glass with widely varying compositions has been employed in different cultures since antiquity and was widespread in medieval times (Wedepohl *et al.* 1995; Wedepohl 2003).

Use of lead glass for jewellery purposes in central Europe can be dated back at least to the 8th or 9th century, based on the age of lead glass beads excavated from a site in northern Germany (Pöche 2001). An early written account of the practice can be found in the text *Upon Various Arts* by the monk Theophilus, dated circa 1120 (see English translation by, e.g., Hendrie 1847 or Dodwell 1961). The treatise describes the preparation of finger rings from lead glass, including mention of Cu as an additive. Chapters of the manuscript that might have addressed the specific colour(s) of the glass have been lost (Brepohl 1999), although several extant treatises from later in the Middle Ages dealt with the topic. One, referred to as the *Manuscripts of Eraclius* and dated to the 12th or 13th century, expounds methods for preparing green lead glass with Cu added for colouration (see English translation by Merrifield 1849). Another penned by Jean d'Outremeuse at the end of the 14th century contains a similar formula for manufacturing imitation gems from green glass (Canella 2006). More than two centuries later, in 1612, a number of recipes for making lead-glass imitation gems in a variety of colours were presented in *L'Arte Vetraria* by Antonio Neri (with an English translation provided by Merrett 1662).

Potassium-bearing lead glass was among several types that were produced in different parts of Europe during the 10th–14th centuries. It was used, for example, by a 13th-century workshop in Erfurt, Germany, to produce lead-glass rings and beads (Mecking 2013).

As discussed in the Gemstone Replacement section below, the pink glass sample, with its relatively high Pb content, is assumed to have been included to replace an emerald in one of the smaller fleurons after 1568, long after the crown was originally manufactured. By contrast, the green glass pieces with lower Pb contents are thought to be part of the original decoration on the basis of both their positions and their mountings in the crown. Specifically, their locations in the design

are consistent with those of the natural emeralds, and they are properly encased by well-fit bezel settings. These contrasting conclusions regarding the pink and green samples align with the technological progress documented throughout the Middle Ages.

In summary, information about the manufacture and use of green lead glass for jewellery purposes was state of the art in the 12th–14th centuries. Conversely, the preparation and use of lead glass in a greater variety of colours for gem imitations was described only centuries later, with general reference first available at the beginning of the 17th century.

Diamond Imitations. The diamond imitations were composed of four-sided gold pyramids coated with a black layer made of K-Pb glass or enamel with Fe, Mn and traces of Co as colour-causing components. Although quantitative chemical data for similar materials are lacking, there appears to be some precedent for applying dark coatings, including black glass or enamel, to decorative objects in the Middle Ages. Notably, the three 'diamonds' in base segment IV, added during the 1402 repair in London, are all imitations, thereby demonstrating that the practice of constructing such black-coated gold pyramids as simulants was widely understood by that time.

One well-known technique for achieving a dark coating, that of niello, can be promptly excluded as a possibility. The practice had been in use since Roman times and was described in Theophilus's *Upon Various Arts* as a process of heating mixtures of silver, copper, lead and sulphur (English translation by, e.g., Hendrie 1847 or Dodwell 1961; see also Wolters 1997, for a detailed explanation of the process). While analytical data of lustrous black layers covering silver or gold art objects from the Middle Ages have confirmed its use during the period (Newman *et al.* 1982), the chemical data from the diamond imitations in the crown cannot support interpretation of the black material as niello.

With respect to black glasses and enamels, chemical analyses of artefacts from the High and Late Middle Ages show wide variations in composition, including low, moderate and extremely high Pb contents (Biron *et al.* 1996). Although research has not revealed any direct parallel in Middle Ages literature to the composition determined for the diamond imitations in the Munich crown, information on the general practice of applying such a dark lead glass or enamel layer suggests that the crown fits within the temporal context. For instance, the *Manuscripts of Eraclius* (English translation by Merrifield 1849) discussed manufacture of a special (black?) lead glass to be used for painting on other glass pieces, wherein an Fe-bearing component was added to the 'normal' green lead glass. Similarly, *Upon Various Arts* (English translation by, e.g., Hendrie 1847 or Dodwell 1961; see also Brepohl 1999, for a detailed discussion) reported preparation of a (lead?) glass with a low melting temperature that was applied to form a black layer on another glass surface, again via painting. These two sources thus indicate that techniques to create layers of iron-bearing lead glass or enamel were known in the 12th–13th centuries.

The technique continued to be employed in the following centuries and increasingly came to be referred to as *schwarzlot* (black lead), *schwarzlot painting* or *schwarzlot decoration* (see Strobl 1990; Müller 1997). These expressions derived from the 16th-century German word *loit* (meaning solder), first used in a text on glass technology written by C. Greitzer and appearing in a codex from 1565 (see also reprint published by Heyen 1963). As time progressed, references to *schwarzlot* continued to appear (Kunckel 1689), but the material was additionally designated simply as *black enamel*, especially in English texts. Numerous glass objects decorated with the technique are known from the Late Middle Ages in Germany, Flanders and Burgundy (Hahn *et al.* 2009a, b). According to analyses published for this material, it normally contained Fe or Fe and Cu, but a Mn-bearing example has been reported as well (Hahn *et al.* 2009a, b; Mantouvalou 2009; Bretz *et al.* 2016).

The only specific information published to date on the layer covering the four-sided gold pyramids in Blanche's crown was offered by Ogden (2018), who described the black layer by visual estimation as enamel. Given the foregoing, such a characterisation appears reasonable.

Gemstone Replacement

Multiple factors, alone or in combination, indicate that certain gems now embellishing the crown are replacements of the original pieces. The most explicit evidence comes from comparing the descriptions in the inventories from the Late Middle Ages onward. Other circumstantial evidence derives from features such as ill-fitting settings, lack of parallelism in design, or temporally incorrect fashioning. Taken together, these support a conclusion that a small number of blue (sapphires), pink (sapphires and spinels) and green (emeralds) stones were lost and replaced, particularly in the time frame after the crown arrived in Heidelberg as part of the dowry of Blanche of Lancaster in 1402. Moreover, corroboration for a general pattern of occasional loss and practice of replacement comes from the references in several of the crown's inventories to absent blue sapphires still being

available as loose stones, yet apparently later restored to their mountings.

With respect to specific gems, clues from the inventories suggest that three emeralds in the smaller fleurons were replaced after 1568 by three pink to red samples, now identified as two garnets and one piece of pink lead glass. By contrast, two other garnets have features, namely a drill hole and surface indentations, from which it can be inferred that they were in place on the crown by at least 1402.

Also instructive are mentions in inventories from 1783, 1818/1820 and 1833 that amongst the sapphires was one imitation or one glass piece. A logical interpretation would therefore be that the sapphire doublet (Figure 26) was characterised in the late 18th and early 19th centuries either as an imitation or as glass.

Nonetheless, the accuracy of the inventories is sometimes problematic. The 1544 text described two of the smaller fleurons as having one emerald and five *baleis* (instead of one sapphire surrounded by four pink to red gems), while the 1745 documentations noted that one sapphire had been replaced by an amethyst. In these instances, it could be that the dark basaltic sapphires in the crown were mistaken for other gem varieties, but other scenarios are possible.

Considering cases where circumstantial clues such as cut and setting weigh most heavily, the sapphire with a scissor-cut crown presents a strong candidate for replacement after 1402 or even 1700, simply because such complex cuts belong to the Renaissance or later (i.e. Baroque style), and not to the Late Middle Ages (see, for diamonds, Falk 1975; Tillander 1995; Ogden 2018). Similarly, the only sapphire exhibiting table, crown and pavilion facets (Figure 25b) is too small for its setting, again pointing to a later replacement for a lost gemstone.

The mounting of two other sapphires also implies at least reattachment, if not outright substitution. The dark sapphire surrounded by the blue wax-like mass at minimum experienced breakage and was reaffixed (Figure 21b). Likewise, one sapphire is presently attached so as to display a rounded top and 'pavilion' facets. Given the absence of logic in such an approach in the context of the closed-back settings and foiling, a more reasonable explanation might be that the stone is in a position rotated 180° from the original mounting.

Gem Cuts and Development of Faceting

Use of gems for adornment began primarily with naturally polished pebbles, which were included in jewellery objects for hundreds of years. Evidence of early developments in shaping and faceting gems can be found in 13th- and 14th-century European jewellery (Hahnloser & Brugger-Koch 1985; Jülich 1986–1987). A limited number of coloured stones exhibiting planar or near-planar surfaces have been documented in pieces from the era (Falk 1975; Lightbown 1992; Content 2016), and the beginning of gem faceting in Europe is thought to date from this period. The transition, however, was in no sense abrupt, as items dated to the Late Middle Ages tended to incorporate gems with a range of processing, from irregular pebbles, to cabochons, to those with varying degrees of further shaping or preforming and faceting.

Initially, such shaping or preforming and faceting operations were done solely with handheld tools (Figure 38), with the first more complex instruments in which the gems were fixed and/or oriented for faceting appearing in 15th-century codices (Schmetzer 2019). Hence, it must be assumed that most processing in the 13th and 14th centuries was accomplished with simple handheld techniques, thereby explaining the common presence of merely near-planar surfaces and rounded edges.

As time progressed, more examples with a symmetrical cut layout and a regular facet arrangement began to appear, featuring in 14th- and 15th-century royal regalia.

Figure 38: One of the first printed representations of gem cutting by means of a rotating wheel is found in the *Buch der Natur* (*Book of Nature*) by Conrad von Megenberg (1482).

Notably, these developments were largely exclusive to the European realm. Even through the Mughal period in India, which began in the early 16th century, faceting of coloured stones was not common in Asia and especially not in the Islamic world. Use of naturally polished pebbles continued to predominate, although some gems imported into trade centres such as Venice, Genoa or Lisbon were occasionally re-exported to the East after faceting (Byrne 1935; Keene 1981; Spink & Ogden 2013; Ogden 2013, 2014), and archaeological excavations provide only limited evidence of faceted stone use.

With respect to the European Late Middle Ages period in focus here, and as highlighted above, pieces tended to incorporate gems reflective of a range of processing levels. Nonetheless, a substantial percentage of pieces dated from the time, such as finger rings and brooches seen in the treasuries of Colmar, Erfurt and Wiener Neustadt, typically had only a single stone or a few gems (Pasch 2010; Stürzebecher 2010; Singer 2014). Items with a relatively rich embellishment—such as the crowns of Margaret of York (see Figure 4), Charles V of France, Charles IV of Bohemia, and Blanche—were far rarer, and many have been lost. For instance, one of Charles V's crowns was described in a 1380 inventory as '*très grant, très belle et la meilleure couronne du Roy*' and contained cabochons together with octagonal and square sapphires and *balaiz* (Labarte 1879), but further details are no longer available.

Comparison with the Crown of Saint Wenceslaus. Of the extant examples, Charles IV's and Blanche's crowns share sufficient parallels to provide an elucidating recapitulation of centuries of gem processing history. A comparative summary of how their components were fashioned is given in Table III.

Charles IV's crown was originally made for his coronation in 1347 as King of Bohemia and was dedicated to Saint Wenceslaus (about 907–935), becoming known as the Crown of Saint Wenceslaus (Figure 39). Charles IV would later be crowned Holy Roman Emperor by the pope in Rome as well (having previously been elected King of the Romans in 1346, a title then used for the King of Germany). The crown was reworked several times prior to his death in 1378 (Hyršl & Neumanova 1999; Šumbera 2008). As can be deduced from detailed inventories dated 1355 and 1387, a final comprehensive remodelling occurred between 1374 and 1378 (Podlaha & Sittler 1903; Otavsky 1992), bringing the piece into its present state.

Several gems in Charles IV's crown display rounded irregular, pebble-like or oval forms, occasionally with drill holes, and might have been reused from older pieces during the crown's original construction in 1347. These include both sapphires and spinels. Also quite possibly reused was one blue sapphire shaped as a four-sided flat pyramid (Figure 40a). Similar stones are found in 13th- and early 14th-century jewellery

Table III: General survey of gem fashioning in the crowns of Saint Wenceslaus and Blanche of Lancaster.

Outline shape as mounted	Irregular/ pebble-like		Oval, square, triangle		Pyramid	Rectangle, hexagon, octagon					
Characteristics	—	With planar table	Curved upper surface or dome	With planar table	Without sharp edges	Without sharp edges	Table and crown facets	Table, crown and girdle facets	Pavilion facets	Table, crown and pavilion facets	More complex scissor-cut crown facets
Crown of Saint Wenceslaus[a]	X	X	X	X	X	X	?	—	—	—	—
Crown of Blanche of Lancaster[b]	X	X	X	X	—	X	X	X	X[c]	X[d]	X[d]
Cutting and polishing processes[e]	Only surface polish (1)	Shaped or preformed and polished (3a)	Shaped or preformed and polished (2)	Shaped or preformed and polished (3b)	Shaped or preformed and polished (4)		Preformed, faceted and polished (5a)	Preformed, faceted and polished (5b)	Preformed, faceted and polished	Preformed, faceted and polished (5c)	Preformed, faceted and polished

[a] From descriptions and photos given by Otavsky (1992), Hyršl & Neumanova (1999) and Šumbera (2008).
[b] From this study.
[c] This sapphire apparently is not oriented as originally mounted in the setting, having been rotated 180°.
[d] Added later.
[e] The numbers in parentheses refer to the categories shown in Figure 37.

Figure 39: The Crown of Saint Wenceslaus was originally created for Charles IV in 1347 apparently by using, at least in part, gems from older jewellery or crowns. The crown was substantially reworked between 1374 and 1378, with various substitutions made throughout that period. The crown is richly jewelled with blue sapphires, pink to red spinels, one red tourmaline, one aquamarine, rubies, emeralds and pearls. The diameter of the headband is 19 cm and the crown's height is approximately 19 cm. The piece is in the collection of St Vitus Cathedral, Prague. Photo and stone identification by Jaroslav Hyršl.

but seldom thereafter. Other regular polygons included rectangles (two blue sapphires and two pink to red spinels) and octagons (one blue sapphire and one red spinel; Figure 40b, c). Precisely deciphering the degree of processing, insofar as concerns the sharpness of facets, is somewhat difficult from the available literature and photos (the crown is not displayed publicly), but a description by Otavsky explicitly mentioned rounded corners for the rectangular spinels, and photos from Šumbera and Hyršl show an absence of sharp edges for the rectangular and octagonal spinels and sapphires (Otavsky 1992; Šumbera 2008; J. Hyršl, pers. comm. 2018 and 2019).

Thus, taken together, the crowns of Charles IV and Blanche of Lancaster, which were manufactured within a span of one or two decades, show decorative practices for the Late Middle Ages while also demonstrating a full panoply of developments in gem processing. Although the advancements were doubtlessly nonlinear, with similar or parallel developments taking place at different places throughout the globe, a certain progression from polished pebbles to complex faceted cuts is discernible within the confines of just these two crowns (again as illustrated in Figure 37).

Figure 40: Gemstones from the Crown of Saint Wenceslaus exhibit a variety of shapes and represent early developments in gem cutting. They include: (**a**) a blue sapphire in the form of a four-sided flat pyramid, 39 × 36 mm; (**b**) one octagon, 31 × 22.5 mm, and two rectangular blue sapphires; and (**c**) an octagonal spinel, 32.5 × 23 mm. Stone identification by Hyršl & Neumanova (1999); photos by Jaroslav Hyršl.

In both crowns, gems with entirely rounded forms, either irregular pebble-like specimens or domed cabochons, were prevalent. The next stages of advancement began with the addition of near-planar to planar tables, but without altering the remainder of the rounded shapes. Another early type of modification is represented by the four-sided flat blue sapphire pyramid in Charles IV's crown (again, see Figure 40a). With no similar examples appearing in Blanche's crown, the popularity of this style may have waned by the second half of the 14th century. Such pyramidal forms might have served as a prelude to later polygonal stones with planar tables or to the various six-fold rose cuts developed in the Renaissance period and thereafter (Tillander 1995; Ogden 2018).

Both crowns likewise incorporate gems showing regular geometric forms (e.g. rectangular, hexagonal or octagonal) with near-planar tables and rows of slightly rounded crown surfaces inclined thereto, without sharp edges. Only Blanche's jewel, however, clearly reflects further developments toward planar facets and sharp edges. Then, presumably represented by replacements after 1402 or even 1700, advancements in the Renaissance and beyond can be witnessed in the more complex patterns with scissor-cut crown facets or with table, crown and pavilion facets.

Hence, by taking into account the decoration of both crowns and what is seen in many historical pieces that followed them, it becomes clear that irregularly shaped pebbles and cabochons with one near-planar face, as well as polygons with multiple inclined surfaces but without sharp edges, would disappear. What would survive from early forms would be cabochons with curved domes in a variety of shapes, and further developments would continue to yield more complex rose cuts and stones with sharply faceted crowns and pavilions.

CONCLUSIONS

The crown of Princess Blanche facilitates a rare view into the gem materials and imitations used in the last decades of the 14th century and the progression towards modern gemstone fashioning. The historical record supports that the crown was initially created for and used by Anne of Bohemia at the court of Richard II in London, before it arrived in Heidelberg as part of the dowry of Blanche of Lancaster at the time of her marriage to the future Louis III, Elector Palatine. It has since been preserved in Heidelberg, in Mannheim and, from the late 18th century, in Munich. Comparisons between inventories from the Middle Ages and new scientific data identifying the gems and materials used in the crown show remarkable consistency, confirming that only a limited number of replacements have altered the jewel's appearance. Diamonds are present as rough octahedra, and coloured stones include blue and pink sapphires, pink spinels, garnets and emeralds; imitations comprise black-coated gold pyramids and lead glass samples. Consideration of the forms of the gems further reveals an ongoing transition from the use of merely polished pebbles derived from secondary gem gravels to manufacturing complex, sharply faceted cuts. As such, centuries of history are encapsulated within a single artefact.

REFERENCES

Abul Huda, S.N. 1998. *Arab Roots of Gemology. Ahmad ibn Yusuf Al Tifaschi's Best Thoughts on the Best of Stones*. Scarecrow Press Inc., Lanham, Maryland, USA, 271 pp.

Alexander, J.J.G. 1987. Kingship. *In*: Alexander, J.J.G. & Binski, P. (eds) *Age of Chivalry: Art in Plantagenet England 1200–1400*. Royal Academy of Arts, London, 194–204.

Auge, O. 2005. Ruprecht von der Pfalz. *Neue Deutsche Biographie*, **22**, 283–285, www.deutsche-biographie.de/pnd118750410.html#ndbcontent.

Bagchi, S. & Ghose, A.K. 1980. History of mining in India—circa 1400–1800 and technology status. *Indian Journal of History of Science*, **15**(1), 25–29, www.insa.nic.in/writereaddata/UpLoadedFiles/IJHS/Vol15_1_4_SBagchi.pdf.

Bauer, M. 1896. *Edelsteinkunde*. Chr. Herm. Tauchnitz, Leipzig, Germany, 711 pp.

Bethe, H. 1956. Edelsteine. *In*: Schmitt, O. (ed) *Reallexikon zur Deutschen Kunstgeschichte*, Band IV. Alfred Druckenmüller Verlag, Stuttgart, Germany, 714–742.

Binski, P. 1997. The *Liber Regalis*: Its date and European context. *In*: Gordon, D., Monnas, L. & Elam, C. (eds) *The Regal Image of Richard II and the Wilton Diptych*. Harvey Miller Publishers, London, 233–246.

Biron, I., Dandridge, P. & Wypyski, M.T. 1996. Techniques and material in Limoges enamels. *In*: O'Neill, J.P. (ed) *Enamels of Limoges, 1100–1350*. The Metropolitan Museum of Art, New York, New York, USA, 445–450.

Blum, J.R. 1828. *Die Schmuck-Steine und deren Bearbeitung*. J.C.B. Mohr, Heidelberg, Germany, 72 pp.

Bopearachchi, O. 1997. Foreword. *In*: Weerakkody, D.P.M. (ed), *Taprobanê: Ancient Sri Lanka as Known to Greeks and Romans*. Brepols Publishers, Turnhout, Belgium, IX–XXII.

Bowers, J.M. 2001. *The Politics of Pearl: Court Poetry in the Age of Richard II*. D.S. Brewer, Cambridge, 236 pp.

Bowersox, G.W. & Chamberlin, B.E. 1995. *Gemstones of Afghanistan*. Geoscience Press, Tucson, Arizona, USA, 220 pp.

Brandenstein, C. (Freiherr von) 1983. *Urkundenwesen und Kanzlei, Rat und Regierungssystem des Pfälzer Kurfürsten Ludwig III. (1410–1436)*. Vandenhoeck & Ruprecht, Göttingen, Germany, 448 pp.

Brepohl, E. 1999. *Theophilus Presbyter und das mittelalterliche Kunsthandwerk*, Band 1: Malerei und Glas. Böhlau Verlag, Cologne, Germany, 221 pp. (see pp. 156–158, 187–194, 206–208).

Brepohl, E. 2005. *Benvenuto Cellini. Traktate über die Goldschmiedekunst und die Bildhauerei*. Böhlau Verlag, Cologne, Germany, 208 pp.

Bretz, S., Hagnau, C., Hahn, O. & Ranz, H.-J. 2016. Kunsthistorische, kunsttechnologische und materialanalytische Untersuchungen an deutscher und niederländischer Hinterglasmalerei von 1300 bis 1600. *In*: Bretz, S., Hagnau, C., Hahn, O. & Ranz, H.-J. (eds) *Deutsche und niederländische Hinterglasmalerei vom Mittelalter bis zur Renaissance*. Deutscher Kunstverlag, Berlin, Germany, 46–67.

Brinkmann, J. 1867. *Abhandlungen über die Goldschmiedekunst und die Skulptur von Benvenuto Cellini*. Verlag von E.A. Seemann, Leipzig, Germany, 193 pp.

Brückmann, F.E. 1727. *Magnalia Dei in Locis Subterraneis oder Unterirdische Schatz-Kammer aller Königreiche und Länder, in ausführlicher Beschreibung*. Braunschweig, Germany, 368 pp., https://archive.org/details/magnaliadeiinloc00brck.

Brunner, H. 1968. *Schatzkammer der Residenz München*. Hirmer Verlag, Munich, Germany, 15 pp.

Brunner, H. 1971. *Kronen und Herrschaftszeichen in der Schatzkammer der Residenz München (Aus bayerischen Schlössern)*. Schnell & Steiner, Munich, Germany, 47 pp.

Byrne, E.H. 1935. Mediaeval gems and relative values. *Speculum*, **10**(2), 177–187, https://doi.org/10.2307/2849464.

Cailliaud, F. 1822. *Travels in the Oasis of Thebes, and in the Deserts Situated East and West of the Thebaid; in the Years 1815, 16, 17, and 18*. Sir Richard Phillips & Co., London, 72 pp.

Calligaro, T., Dran, J.C., Poirot, J.P., Querré, G., Salomon, J. & Zwaan, J.C. 2000. PIXE/PIGE characterisation of emeralds using an external micro-beam. *Nuclear Instruments and Methods in Physics Research Section B: Beam Interactions with Materials and Atoms*, **161–163**, 769–774, https://doi.org/10.1016/s0168-583x(99)00974-x.

Campbell, M. 1997. 'White harts and coronets': The jewellery and plate of Richard II. *In*: Gordon, D., Monnas, L. & Elam, C. (eds) *The Regal Image of Richard II and the Wilton Diptych*. Harvey Miller Publishers, London, 95–114.

Cannella, A.-F. 2006. *Gemmes, Verre Coloré, Fausses Pierres Précieuses au Moyen Âge*. Dissertation, Université de Liège, France, Librairie Droz S.A., Geneva, Switzerland, 480 pp.

Cherry, J. 1988. Late fourteenth-century jewellery: The inventory of November 1399. *Burlington Magazine*, **130**(1019), 137–140, www.jstor.org/stable/883320.

Content, D.J. 2016. *Ruby, Sapphire & Spinel: An Archaeological, Textural and Cultural Study. Part I: Text*. Brepols Publishers, Turnhout, Belgium, 191 pp.

Cortesão, A. 1944. Appendix I: Letter of Tomé Pires to King Manuel. *In*: *The Suma Oriental of Tomé Pires*, Vol. II. Ashgate Publishing for The Hakluyt Society, London, 512–518.

Coulson, M. 2012. The Middle Ages to the Industrial Revolution (1066–1800)—12. Diamond mines in India and Brazil. *In*: *The History of Mining*. Harriman House Ltd, Petersfield, Hampshire, 75–78.

Cretu, C. & van der Lingen, E. 1999. Coloured gold alloys. *Gold Bulletin*, **32**(4), 115–126, https://doi.org/10.1007/BF03214796.

Dames, M.L. 1921. *The Book of Duarte Barbosa*, Vol. II. The Hakluyt Society, London, 286 pp.

Deibel, U. 1927. Eine pfälzische Krone in der Münchener Schatzkammer. *Pfälzisches Museum—pfälzische Heimatkunde*, **44**(7/8), 157–162.

Deibel, U. 1928. Eine pfälzische Krone in der Münchener Schatzkammer. *Korrespondenzblatt des Gesamtvereins der deutschen Geschichts- und Altertumsvereine*, **76**(1–3), 32–40.

Devon, F. 1837. *Issues of the Exchequer; Being a Collection of Payments Made out of His Majesty's Revenue, from King Henry III to King Henry VI Inclusive*. John Murray, London, 664 pp., https://archive.org/details/b29340135.

Dodwell, C.R. 1961. *Theophilus, De Diversis Artibus (The Various Arts)*. Thomas Nelson and Sons, London, 178 pp.

Dürschner, K. 2003. *Der wacklige Thron: Politische Opposition im Reich von 1378 bis 1438*. Peter Lang GmbH, Frankfurt, Germany, 404 pp.

Eikelmann, R. 1980. *Mittelalterliche Kronen in der Schatz kammer der Residenz München.* Master's thesis, Ludwig-Maximilians-University, Munich, Germany, 355 pp.

Eikelmann, R. 1984. *Franko-flämische Emailplastik des Spätmittelalters.* Dissertation, Ludwig-Maximilians-University, Munich, Germany, 784 pp.

Emerson, O.F. 1910. The suitors in Chaucer's "parlement of foules". *Modern Philology*, **8**(1), 45–62, www.jstor.org/stable/432497.

Falk, F. 1975. *Edelsteinschliff und Fassungsformen im späten Mittelalter und im 16. Jahrhundert: Studien zur Geschichte d. Edelsteine u. d. Schmuckes*. Verlag Wilhelm Kempter KG, Ulm, Germany, 150 pp.

Foster, B.C., Rivard, J.-L., Sidebotham, S.E. & Cuvigny, H. 2007. Survey of the emerald mines at Wadi Sikait 2000/2001 seasons. *In*: Sidebotham, S.E. & Wendrich, W. (eds) *Berenike 1999/2000: Report on the Excavations at Berenike, Including Excavations in Wadi Kalalat and Siket, and the Survey of the Mons Smaragdus Region*. Cotsen Institute of Archaeology Press, University of California Los Angeles, California, USA, 304–349.

Foster, G.V. 1988. Working of gem materials: Consequences of the Indian and Sri Lankan sea trade. *In*: Sayre, E.V. (ed) *Materials Research Society Symposium Proceedings Vol. 123 (Symposium L – Materials Issues in Art and Archeology I)*. Materials Research Society, Pittsburgh, Pennsylvania, USA, 153–158, https://doi.org/10.1557/PROC-123-153.

Frampton, J. 1579 (reprinted 2004). Early fifteenth century travels in the East. *SOAS Bulletin of Burma Research*, **2**(2), 110–117, www.soas.ac.uk/sbbr/editions/file64309.pdf (translation of original text of Nicolò de' Conti, with notes by Kennon Breazeale).

Geiger, W. & Bode, M.H. 1912. *The Mahavamsa or the Great Chronicle of Ceylon*. The Pali Text Society, London, 300 pp.

Gilg, H.A., Gast, N. & Calligaro, T., 2010. Vom Karfunkelstein. *In*: Wamser, L. (ed), *Karfunkelstein und Seide: neue Schätze aus Bayerns Frühzeit*. Ausstellungskataloge der Archäologischen Staatssammlung, **37**, Pustet, Munich, Germany, 87–100.

Giuliani, G., Chaussidon, M., Schubnel, H.-J., Piat, D.H., Rollion-Bard, C., France-Lanord, C., Giard, D., *et al.* 2000. Oxygen isotopes and emerald trade routes since antiquity. *Science*, **287**(5453), 631–633, https://doi.org/10.1126/science.287.5453.631.

Gray, A. 1883 (reprinted 1999). *Ibn Batuta in the Maldives and Ceylon*. Asian Educational Services, New Delhi, India, 60 pp. (translation of original text of C. Defrémery).

Gray, A. 1989. A fourteenth century crown. *Journal of Gemmology*, **21**(7), 431–432, https://doi.org/10.15506/JoG.1989.21.7.431.

Green, M.A.E. 1857. *Lives of the Princesses of England from the Norman Conquest*, Vol. 3. Longman, Brown, Green, Longman, & Roberts, London, 456 pp.

Greitzer, C. 1565. Glasmalerei. *Kölner Domblatt*, No. 103, 3–4, https://doi.org/10.11588/diglit.1513#0035; No. 104, 3–4, https://doi.org/10.11588/diglit.1513#0039.

Gübelin, E. 1990. The jewels of the Bavarian crown. *In*: *Gemmologia Europa II*. Centro Informazione e Servizi Gemmologici (CISGEM), Milan, Italy, 115–145.

Hahn, O., Bretz, S., Hagnau, C., Ranz, H.-J. & Wolff, T. 2009a. Pigments, dyes, and black enamel—The colorants of reverse paintings on glass. *Archaeological and Anthropological Sciences*, **1**(4), 263–271, https://doi.org/10.1007/s12520-009-0021-4.

Hahn, O., Bretz, S., Hagnau, C., Ranz, H.-J. & Wolff, T. 2009b. Das Schwarzlot in der Hinterglasmalerei. Zerstörungsfreie Untersuchung von Kunst- und Kulturgut. *ZfP-Zeitung*, **113**, 38–40, www.ndt.net/article/dgzfp/pdf/zfp113-Hahn.pdf.

Hahnloser, H.R. & Brugger-Koch, S. 1985. *Corpus der Hartsteinschliffe des 12.-15. Jahrhunderts*. Deutscher Verlag für Kunstwissenschaften, Berlin, Germany, 278 pp.

Hammond, P.W. 1984. The coronet of Margaret of York. *The Ricardian*, **6**(86), 362–365.

Harlow, G.E. 1998. Following the history of diamonds. *In*: Harlow, G.E. (ed) *The Nature of Diamonds*. Cambridge University Press, Cambridge, 116–136.

Harrell, J.A. 2004. Archaeological geology of the world's first emerald mine. *Geoscience Canada*, **31**(2), 69–76, https://journals.lib.unb.ca/index.php/gc/article/view/2752/3212.

Harrell, J.A. 2006. Archaeological geology of Wadi Sikait. *PalArch's Journal of Archaeology of Egypt/Egyptology*, **4**(1), 1–12, www.palarch.nl/wp-content/harrell_ja_archaeological_geology_of_wadi_sikait_palarchs_journal_of_archaeology_of_egypt_egyptology_4_1_2006.pdf.

Heeren, J.J. 1910. *Das Bündnis zwischen Richard II. Von England und König Wenzel vom Jahre 1381*. Dissertation Universität Halle-Wittenberg, Wischan und Burkhardt, Halle, Germany, 87 pp.

Hendrie, R. 1847. *An Essay upon Various Arts, in Three Books, by Theophilus, Called also Rugerus, Priest and Monk, Forming an Encyclopaedia of Christian Art*. John Murray, London, 447 pp., https://babel.hathitrust.org/cgi/pt?id=gri.ark:/13960/t9573n59t.

Heyen, F.-J. 1963. Ein clarlicher bericht und lere der schoner kunst des glas malen und bernen mitsamt vilen cautelen und unterwisungen darzu denenden mit gruntlicher anzeigung. *Allgemeine Glaserzeitung*, **1963**(11), 197–200 (reprint of C. Greitzer's original 1565 text with comments).

Hilton, L. 2008. *Queens Consort: England's Medieval Queens*. Weidenfeld & Nicolson, London, 482 pp.

Höfler, K.A.K. 1861. *Ruprecht von der Pfalz genannt Clem römischer König 1400–1410*. Herder'sche Verlagsbuchhandlung, Freiburg im Breisgau, Germany, 484 pp.

Holmes, M.R. 1937. The crowns of England. *Archaeologia*, **86**, 73–90, https://doi.org/10.1017/s0261340900015356.

Holmes, U.T. 1934. Mediaeval gem stones. *Speculum*, **9**(2), 195–204.

Holtzmann, W. 1930. Die englische Heirat Pfalzgraf Ludwigs III. *Zeitschrift für die Geschichte des Oberrheins*, No. 43, 1–22.

Huffschmid, M. 1910. Ein französischer Reisebericht über Heidelberg von 1664. *Neues Archiv für die Geschichte der Stadt Heidelberg und der rheinischen Pfalz*, **8**, 59–71.

Hughes, R.W. 1994. The rubies and spinels of Afghanistan – A brief history. *Journal of Gemmology*, **24**(4), 256–267, https://doi.org/10.15506/JoG.1994.24.4.256.

Hyršl, J. 2001. Sapphires and their imitations on medieval art objects. *Gemmologie: Zeitschrift der Deutschen Gemmologischen Gesellschaft*, **50**(3), 153–162.

Hyršl, J. & Neumanova, P. 1999. Eine neue gemmologische Untersuchung der Sankt Wenzelskrone in Prag. *Gemmologie: Zeitschrift der Deutschen Gemmologischen Gesellschaft*, **48**(1), 29–36.

Jennings, R.H., Kammerling, R.C., Kovaltchouk, A., Calderon, G.P., El Baz, M.K. & Koivula, J.I. 1993. Emeralds and green beryls of Upper Egypt. *Gems & Gemology*, **29**(2), 100–115, https://doi.org/10.5741/gems.29.2.100.

Jülich, T. 1986–1987. Gemmenkreuze. Die Farbigkeit ihres Edelsteinbesatzes bis zum 12. Jahrhundert. *Aachener Kunstblätter*, **54–55**, 99–258, https://doi.org/10.11588/akb.1986.0.36211.

Keddigkeit, J., Untermann, M., Ammerich, H., Heberer, P. & Lagemann, C. 2015. Neustadt, Unserer Lieben Frauen und St. Ägidius Kollegialstift, später Jesuitenkirche, dann Lazaristenkirche – Stadt Neustadt an der Weinstraße. *In*: *Pfälzisches Klosterlexikon: Handbuch der pfälzischen Klöster, Stifte und Kommenden*, Vol. 3. Institut für Pfälzische Geschichte und Volkskunde, Kaiserslautern, Germany, 231–272.

Keene, M. 1981. The lapidary arts in Islam. An underappreciated tradition. *Expedition*, **24**(1), 24–39, www.penn.museum/sites/expedition/the-lapidary-arts-in-islam.

Kornbluth, G. 2003. Bibliothèque Nationale MS Lat. 9383: Archaeology and function of a Carolingian treasure binding. *Aachener Kunstblätter*, **62**, 185–201, www.academia.edu/5488068/Biblioth%C3%A8que_Nationale_MS_Lat._9383_archaeology_and_function_of_a_Carolingian_treasure_binding.

Kržič, A., Šmit, Ž., Fajfar, H., Dolenec, M., Činč Juhant, B. & Jeršek, M. 2013. The origin of emeralds embedded in archaeological artefacts in Slovenia. *Geologija*, **56**(1), 29–46, https://doi.org/10.5474/geologija.2013.003.

Kunckel II, J. 1689. *Ars vitraria experimentalis oder vollkommene Glasmacher-Kunst*. Verlegung Christoph Riegels, Frankfurt, Germany, 472 pp., https://books.google.com/books?id=4AVdAAAAcAAJ.

Labarte, J. 1879. *Inventaire du Mobilier de Charles V, Roi de France*. Imprimerie Nationale, Paris, France, 423 pp., https://archive.org/details/inventairedumobi181labauoft.

Lawrance, H. 1840. *Historical Memoirs of the Queens of England from the Commencement of the Twelfth Century*, Vol. II. Edward Moxon, London, 456 pp.

Lee, S.-K., Hsu, H.-C. & Tuan, W.-H. 2016. Oxidation behavior of copper at a temperature below 300°C and the methodology for passivation. *Materials Research*, **19**(1), 51–56, https://doi.org/10.1590/1980-5373-mr-2015-0139.

Lehmann, E.J.T. 1810. *Georg Agricola's Mineralogische Schriften, übersetzt und mit erläuternden Anmerkungen begleitet, Zweyter Band*. Craz und Gerlach, Freiberg, Germany, 335 pp.

Levinson, A.A. 1998. Diamond sources and their discovery. *In*: Harlow, G.E. (ed) *The Nature of Diamonds*. Cambridge University Press, Cambridge, 72–104.

Lightbown, R.W. 1992. *Mediaeval European Jewellery*. Victoria & Albert Publications, London, 589 pp.

Lindner, T. 1896. Wenzel, Herzog. *Allgemeine Deutsche Biographie*, **41**, 726–732, www.deutsche-biographie.de/sfz85051.html.

Lopes de Castanheda, F. 1561 (reprinted 1833). *Ho Octavo Livro da Historia do Descobrimento e Conquista da India Pelos Portugueses*. Typographia Rollandiana, Lisbon, Portugal, 474 pp.

Mahroof, M.M.M. 1989. The Muslim lapidary – Some aspects of the gem folkways in Sri Lanka. *Journal of Gemmology*, **21**(7), 405–410, https://doi.org/10.15506/JoG.1989.21.7.405.

Mantouvalou, I. 2009. *Quantitative 3D micro X-ray fluorescence spectroscopy.* Dissertation, Technische Universität, Berlin, Germany, 117 pp., https://pdfs.semanticscholar.org/9a27/15d66928a8964b4d2cf51849dfbc4f678e14.pdf.

Mecking, O. 2010. Goldlegierungen. *In*: Ostritz, S. (ed) *Die mittelalterliche jüdische Kultur in Erfurt. Band 2. Der Schatzfund: Analysen – Herstellungstechniken – Rekonstruktionen*. Thüringisches Landesamt für Denkmalpflege und Archäologie, Weimar with Verlag Beier & Beran, Langenweißbach, Germany, 59–65.

Mecking, O. 2013. Medieval lead glass in central Europe. *Archaeometry*, **55**(4), 640–662, https://doi.org/10.1111/j.1475-4754.2012.00697.x.

Merrifield, M.P. 1849. Manuscripts of Eraclius. *In*: *Original Treatises Dating from the XIIth to XVIIIth Centuries, on the Arts of Painting*, Vol. 1. John Murray, London, 166–257, https://archive.org/details/originaltreatis00merrgoog.

Moraw, P. 2001. Ruprecht von der Pfalz – ein König aus Heidelberg. *Zeitschrift für die Geschichte des Oberrheins*, **149**, 97–110.

Morley, H. 1873. *First Sketch of English Literature*. Cassell, Petter & Galpin, London, 912 pp., https://archive.org/details/firstsketchofeng00morl.

Moule, A.C. & Pelliot, P. 1938. *Marco Polo: The Description of the World*. George Routledge & Sons Ltd, London, 595 pp.

Mugler, O. 1928. *Edelsteinhandel im Mittelalter und im 16. Jahrhundert mit Excursen über den Levante- und asiatischen Handel überhaupt*. Dissertation, Ludwig-Maximilians-University, Munich, Germany, 154 pp.

Müller, W. 1997. Glasherstellung und Bleiverglasung. *In*: Lindgren, U. (ed) *Europäische Technik im Mittelalter: 800 bis 1400; Tradition und Innovation; ein Handbuch*. Gebr. Mann Verlag, Berlin, Germany, 289–292.

Neri, A. (transl. by C. Merret) 1662. *The Art of Glass*. Octavian Pulleyn, London, 366 pp., https://archive.org/details/TheArtOfGlassWhereinAreShownTheWayesToMakeAndColourGlass.

Newman, R., Dennis, J.R. & Farrell, E. 1982. A technical note on niello. *Journal of the American Institute for Conservation*, **21**(2), 80–85, https://doi.org/10.1179/019713682806028568.

Oberndorff, G.L. von 1912. *Regesten der Pfalzgrafen am Rhein 1214–1508*, Zweiter Band. 1. Lieferung. Verlag der Wagner'schen K.K. Universitäts-Buchhandlung, Innsbruck, Austria, 683 pp., https://bildsuche.digitale-sammlungen.de/?c=viewer&bandnummer=bsb00009261.

Ogden, J. 2013. Gems and the gem trade in India. *In*: Jaffer, A. (ed) *Beyond Extravagance: A Royal Collection of Gems and Jewels*. Assouline Publishing, New York, New York, USA, 346–377.

Ogden, J. 2014. Mughal gems in context. *InColor*, No. 26, 36–47.

Ogden, J. 2018. *Diamonds: An Early History of the King of Gems*. Yale University Press, New Haven, Connecticut, USA, 388 pp.

Otavsky, K. 1992. *Die Sankt Wenzelskrone im Prager Domschatz und die Frage der Kunstauffassung am Hofe Kaiser Karls IV*. Peter Lang, Bern, Switzerland, 200 pp.

Palgrave, F. 1836. Henry IV. *In*: *The Antient Kalendars and Inventories of the Treasure of His Majesty's Exchequer, Together with Other Documents Illustrating the History of that Repository*, Vol. III. G. Eyre and A. Spottiswoode, London, 313–358, https://hdl.handle.net/2027/gri.ark:/13960/t3mw7bb3w.

Pasch, A. 2010. Zur Herstellungstechnik der Schatzfunde. *In*: Ostritz, S. (ed) *Die mittelalterliche jüdische Kultur in Erfurt. Band 2. Der Schatzfund: Analysen – Herstellungstechniken – Rekonstruktionen*. Thüringisches Landesamt für Denkmalpflege und Archäologie, Weimar with Verlag Beier & Beran, Langenweißbach, Germany, 226–427.

Pelzel, F.M. 1788. *Lebensgeschichte des Römischen und Böhmischen Königs Wenceslaus*. Erster Theil, Prague, Austria, 304 pp., https://books.google.com/books?id=PuJdAAAAcAAJ.

Peganium, C. (ed) 1680. *Des Vortrefflichen Herren Johann Baptista Portae von Neapolis Magia Naturalis, oder Haus-Kunst-und Wunder-Buch*, Vol. 1. Johann Zieger, Nürnberg, Germany, 990 pp., https://archive.org/details/bub_gb_AZ6cYsKKMtwC.

Percival, F. 1998. *Chaucer's Legendary Good Women*. Cambridge University Press, Cambridge, 338 pp.

Pöche, A. 2001. *Die Glasfunde des frühmittelalterlichen Handelplatzes von Groß Stömkendorf bei Wismar*. Dissertation, Christian-Albrechts-University, Kiel, Germany, 227 pp., https://d-nb.info/969953267/34.

Podlaha, A. & Sittler, E. 1903. *Die königl. Hauptstadt Prag: Hradschin. Der Domschatz und die Bibliothek des Metropolitancapitels*. Verlag der archaeologischen Commission bei der böhmischen Kaiser-Franz-Josef-Akademie für Wissenschaften, Literatur und Kunst, Prague, Austria, 216 pp.

Porta, J.B. 1658. *Natural Magick*. Thomas Young and Samuel Speed, London, 409 pp., https://archive.org/details/naturalmagickbyj00port.

Power, T. 2012. *The Red Sea from Byzantium to the Caliphate: AD 500–1000*. American University in Cairo Press, Cairo, Egypt, 363 pp.

Rall, H. 1965. Die ältesten erhaltenen Urkunden über Kleinodien, die durch Heirat in das Wittelsbacher Haus kamen. *Mitteilungen für die Archivpflege in Bayern*, **11**(1), 5–8.

Reitemeier, A. 1999. *Aussenpolitik im Spätmittelalter: die diplomatischen Beziehungen zwischen dem Reich und England 1377–1422*. Ferdinand Schöningh, Paderborn, Germany, 473 pp.

Riley, H.T. 1868. Deposit of royal jewels with the City, as security for a loan of two thousand pounds. *In*: Riley, H.T. (ed) *Memorials of London and London Life in the 13th, 14th and 15th Centuries*. Longmans, Green, and Co., London, 443–444, www.british-history.ac.uk/no-series/memorials-london-life/pp438-447.

Rödel, V. 2000. *Mittelalter. Der Griff nach der Krone. Die Pfalzgrafschaft bei Rhein im Mittelalter*. Schnell & Steiner, Regensburg, Germany (see pp. 218–221).

Said, H.M. 1989. *Al-Beruni's Book on Mineralogy. The Book Most Comprehensive in Knowledge on Precious Stones.* Pakistan Hijra Council, Islamabad, Pakistan, 355 pp. (see pp. 29–75).

Sandrart, J. von 1679. Scvltura oder Bildereykvnst. *In*: *Teutsche Academie der Edlen Bau- Bild- und Mahlerey-Künste*, Vol. 2.2. Christian Sigismund Frohberger, Nürnberg, Germany, 74–76, https://doi.org/10.11588/diglit.1285.

Saul, N. 1997. *Richard II*. Yale University Press, New Haven, Connecticut, USA, 514 pp.

Scharf, G. 1867. The Westminster portrait of Richard II. *Fine Arts Quarterly Review*, **II N.F.**, 29–63.

Schauss, E. von 1879. Die Sogen. Böhmische Krone. *In*: *Historischer und beschreibender Catalog der königlich bayerischen Schatzkammer zu München*. Druck des literar. Instituts von M. Huttler, Munich, Germany, 184 pp., https://archive.org/details/historischerundb00resi.

Scherz, G. 1955. Niels Stensens Smaragdreise. *Centaurus*, **4**(1), 51–57, https://doi.org/10.1111/j.1600-0498.1955.tb00468.x.

Schmetzer, K. 2019. A 15th-century polishing machine for gemstones attributed to Henri Arnaut. *Journal of Gemmology*, **36**(6), 544–550, https://doi.org/10.15506/JoG.2019.36.6.544.

Schneider, O. & Arzruni, A. 1892. Der aegyptische Smaragd, nebst einer vergleichenden mineralogischen Untersuchung der Smaragde von Alexandrien, vom Gebel Sabara und vom Ural. *Zeitschrift für Ethnologie*, **24**, 41–100.

Schneidmüller, B. 2011. Ruprecht 1410–2010. Der König aus Heidelberg. *Heidelberg. Jahrbuch zur Geschichte der Stadt*, **15**, 51–65, https://doi.org/10.11588/heidok.00024437.

Schramm, P.E. 1956. Englische Frauenkronen aus dem 15. Jahrhundert, mit Ausblicken auf die Kronen, besonders die Madonnenkronen, des späten Mittelalters. *In*: *Herrschaftszeichen und Staatssymbolik*, Vol. III. Anton Hiersemann, Stuttgart, Germany, 991–1003.

Schreibmüller, H. 1959. Krankheit und Tod der Kurprinzessin Blanka aus England (1409). *In*: Schreibmüller, H. & Baumann, K. (eds) *Von Geschichte und Volkstum der Pfalz. Ausgewählte Aufsätze*. Verlag der Pfälzischen Gesellschaft zur Förderung der Wissenschaften, Speyer, Germany, 99–102.

Schroll, K.M. 1797. Grundriss einer Salzburgischen Mineralogie. *Jahrbücher der Berg- und Hüttenkunde*, **1**, 95–196.

Schulz, H. 1897. *Das Buch der Natur von Conrad von Megenberg: Die Erste Naturgeschichte in Deutscher Sprache*. Julius Abel, Greifswald, Germany, 445 pp.

Shaw, I., Bunbury, J. & Jameson, R. 1999. Emerald mining in Roman and Byzantine Egypt. *Journal of Roman Archaeology*, **12**, 203–215, https://doi.org/10.1017/s1047759400017980.

Sidebotham, S.E., Gates-Foster, J.E. & Rivard, J.-L.G. (eds) 2018. *The Archaeological Survey of the Desert Roads between Berenike and the Nile Valley: Expeditions by the University of Michigan and the University of Delaware to the Eastern Desert of Egypt, 1987–2015*. American Schools of Oriental Research, Boston, Massachusetts, USA, 480 pp.

Sillib, R. 1903. König Ruprechts Krone. *Mannheimer Geschichtsblätter*, **4**(10), 230–232.

Singer, M. 2014. Der Schatzfund von Wiener Neustadt. Eine kulturhistorische Analyse. *In*: Hofer, N. (ed) *Der Schatzfund von Wiener Neustadt*. Ferdinand Berger & Söhne, Horn, Austria, 130–237.

Smith, G. 1750. *The Laboratory; or, School of Arts*. James Hodges & T. Astley, London, 352 pp., https://openlibrary.org/books/OL26972559M.

Spencer, L.K., Dikinis, S.D., Keller, P.C. & Kane, R.E. 1988. The diamond deposits of Kalimantan, Borneo. *Gems & Gemology*, **24**(2), 67–80, https://doi.org/10.5741/gems.24.2.67.

Spink, M. & Ogden, J. 2013. Metals and gems in Islamic jewellery. *In*: Spink, M., Ogden, J., Rogers, J.M., Kramarovsky, M.G., Carvalho, P.M. & Bayani, M. (eds) *The Art of Adornment: Jewellery of the Islamic Lands*, Part 1. The Nour Foundation, London, 20–53.

Strack, E. & Kostov, R.I. 2010. Emeralds, sapphires, pearls and other gemological materials from the Preslav gold treasure (X century) in Bulgaria. *Bulletin of Mineralogy Petrology and Geochemistry*, **48**, 103–123, www.geology.bas.bg/mineralogy/gmp_files/gmp48/strack.pdf.

Stratford, J. 2012. *Richard II and the English Royal Treasure*. Boydell Press, Woodbridge, Suffolk, 470 pp.

Strickland, A. 1849. *Lives of the Queens of England from the Norman Conquest; With Anecdotes of Their Courts, Now First Published from Official Records and Other Authentic Documents, Private as Well as Public*, Vol. II. Lea and Blanchard, Philadelphia, Pennsylvania, USA, 222 pp., https://hdl.handle.net/2027/umn.31951d00705171q.

Strobl, S. 1990. *Glastechnik des Mittelalters*. A. Gentner Verlag, Stuttgart, Germany, 232 pp.

Stürzebecher, M. 2010. Der Schatzfund aus der Michaelisstraße in Erfurt. *In*: Ostritz, S. (ed) *Die mittelalterliche jüdische Kultur in Erfurt. Band 1. Der Schatzfund: Archäologie – Kunstgeschichte – Siedlungsgeschichte*. Thüringisches Landesamt für Denkmalpflege und Archäologie, Weimar with Verlag Beier & Beran, Langenweißbach, Germany, 60–323.

Šumbera, A. 2008. *The Bohemian Crown Jewels*. Olympus CS, Prague, Czech Republic, 60 pp.

Tay, T.S., Wathanakul, P., Atichat, W., Moh, L.H., Kem, L.K. & Hermanto, R. 2005. Kalimantan diamond: Morphology, surface features and some spectroscopic features. *Australian Gemmologist*, **22**(5), 186–195.

Thomas, A. 2007. *A Blessed Shore: England and Bohemia from Chaucer to Shakespeare*. Cornell University Press, Ithaca, New York, USA, 239 pp.

Thoresen, L. 2017. Archaeogemmology and ancient literary sources on gems and their sources. *In*: Hilgner, A., Greiff, S. & Quast, D. (eds) *Gemstones in the First Millennium AD: Mines, Trade, Workshops and Symbolism*. Verlag des Römisch-Germanischen Zentralmuseums, Mainz, Germany, RGZM – Tagungen, Vol. 30, 155–217.

Tillander, H. 1995. *Diamond Cuts in Historic Jewellery 1381–1910*. Art Books International, London, 248 pp.

Tuck, A. 1999. Richard II and the House of Luxemburg. *In*: Goodman, A. & Gillespie, J. (eds) *Richard II: The Art of Kingship*. Clarendon Press, Oxford, 203–229.

Twining, E.F. 1960. *A History of the Crown Jewels of Europe*. B.T. Batsford Ltd, London, 707 pp.

Twining, E.F. 1967. *European Regalia*. B.T. Batsford Ltd, London, 334 pp.

Van Dussen, M. 2009. Three verse eulogies of Anne of Bohemia. *Medium Ævum*, **78**(2), 231–260, https://doi.org/10.2307/43632839.

von Megenberg, C. 1482. *Buch der Natur*. Anton Sorg, Augsburg, Germany, 240 Blatt.

von Wiltmaister, J.K. 1783. *Churpfälzische Chronik*. Johann Baptist Haimerle, Sulzbach, Germany, 195–197.

Wedepohl, K.H. 2003. *Glas in Mittelalter und Antike: Geschichte eines Werkstoffs*. E. Schweizerbart'sche Verlagsbuchhandlung, Stuttgart, Germany, 227 pp.

Wedepohl, K.H., Krueger, I. & Hartmann, G. 1995. Medieval lead glass from northwestern Europe. *Journal of Glass Studies*, **37**, 65–82.

Weiß, J. 1911. Eine wiedergefundene wittelsbachische Königskrone. *Das Bayerland*, **22**(37), 617–618.

Weizsäcker, J. 1882. *Deutsche Reichstagsakten, Ältere Reihe, 4. Band, Deutsche Reichstagsakten unter König Ruprecht. Erste Abteilung, 1400–1401*. Friedrich Andreas Perthes, Gotha, Germany, 532 pp.

Weizsäcker, J. 1885. *Deutsche Reichstagsakten, Ältere Reihe, 5. Band, Deutsche Reichstagsakten unter König Ruprecht. Zweite Abteilung, 1401–1405*. Friedrich Andreas Perthes, Gotha, Germany, 851 pp.

Whalley, J. 2012. Faded glory: Gemstone simulants and enhancements. *Studies in Conservation*, **57**(Suppl. 1), S313–S321, https://doi.org/10.1179/2047058412y.0000000041.

Whittingham, S. 1971. The chronology of the portraits of Richard II. *The Burlington Magazine*, **113**(814), pp. 12, 14–21.

Wolters, J. 1997. Niello im Mittelalter. *In*: Lindgren, U. (ed) *Europäische Technik im Mittelalter: 800 bis 1400; Tradition und Innovation; ein Handbuch*. Gebr. Mann Verlag, Berlin, Germany, 169–186.

Yule, H. 1866. *Cathay and the Way Thither; Being a Collection of Medieval Notices of China*, Vol. 1. The Hakluyt Society, London, 250 pp., https://archive.org/details/CathayAndTheWayThitherVol1.

Yule, H. 1871. *The Book of Ser Marco Polo, the Venetian, Concerning the Kingdoms and Marvels of the East*, Vol. I. John Murray, London, 409 pp., https://archive.org/details/bookofsermarcopo01polo.

The Authors

Dr Karl Schmetzer
Taubenweg 16, 85238 Petershausen, Germany
Email: SchmetzerKarl@hotmail.com

Prof. Dr H. Albert Gilg
Chair of Engineering Geology, Technical University of Munich, Arcisstr. 21, 80333 Munich, Germany
Email: agilg@tum.de

Acknowledgements

The examination of the crown was initiated by Dr B. Graf (Bayerischer Rundfunk, Munich, Germany) and supported by Dr S. Heym (Bayerische Verwaltung der staatlichen Schlösser, Gärten und Seen, Munich), who also provided archival information regarding the crown's history. J. Jückstock (conservation department at Bayerische Verwaltung der staatlichen Schlösser, Gärten und Seen) is responsible for the Treasury at the Munich Residence and assisted with the on-site work and handling of the crown at the museum. Dr R. Eickelmann (Munich), Dr J. Ogden (London) and Dr J. Hyršl (Prague, Czech Republic) shared helpful discussions regarding various aspects of this research project.

An innovator in gemstone reporting

• Identification of colored gemstones • Country of origin determination • Full quality and color grading analysis

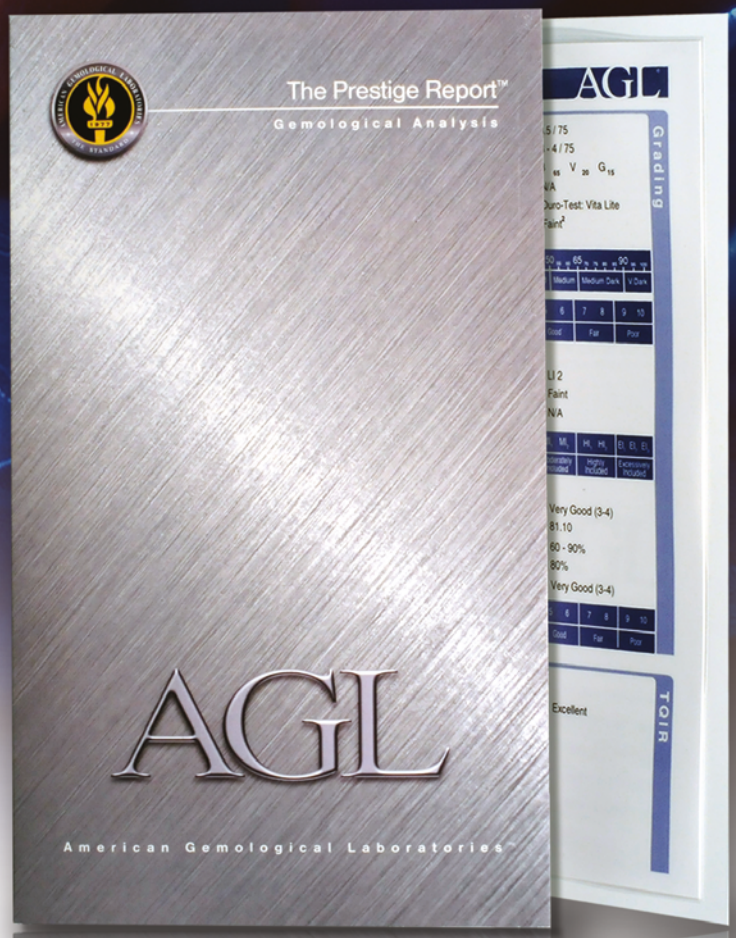

AMERICAN GEMOLOGICAL LABORATORIES AGL

580 5th Ave • Suite 706 • New York, NY 10036, USA
www.aglgemlab.com • +1 (212) 704 - 0727

Figure 1: These two specimens (167.4 ct pear shape and 30.3 ct carved turtle) show the deep black colour and high lustre of spinel from Bo Phloi, Thailand. Photo by M. Wildner.

Black Spinel—A Gem Material from Bo Phloi, Thailand

Ágnes Blanka Kruzslicz, Lutz Nasdala, Manfred Wildner, Radek Škoda, Günther J. Redhammer, Christoph Hauzenberger and Bhuwadol Wanthanachaisaeng

ABSTRACT: The Bo Phloi gem field in Kanchanaburi Province, western Thailand, is renowned mostly for its blue sapphire. Corundum production has now virtually ceased, so local gem cutters are focusing on high-quality black spinel, which is abundant from past stockpiles, to produce various jewellery items and carvings. A detailed mineralogical characterisation of this material showed that it is spinel *sensu stricto* ($MgAl_2O_4$) with elevated Fe contents (20.7 ± 0.9 wt.% FeO, or Mg:Fe atomic ratio about 2:1). The enriched Fe causes the dark colouration of the material. Based on Mössbauer spectroscopic results, Fe occurs in both divalent and trivalent states, the latter occupying both (four- and six-coordinated) cation sites in the crystal structure. The Fe^{3+} contributes to a 'partially inverse' occupation of the cation sites. As a result, the Raman spectrum of Bo Phloi material does not resemble that of 'normal' spinel, but rather is similar to the spectra of other spinel-group minerals that tend to show some inversion in their cation-site occupation, such as hercynite, magnetite and magnesioferrite.

The Journal of Gemmology, **37**(1), 2020, pp. 66–79, http://doi.org/10.15506/JoG.2020.37.1.66

Gem-quality spinel of various colours is mined from many deposits around the world. Famous localities include Myanmar, Sri Lanka, Tajikistan, Tanzania and Vietnam (e.g. Gübelin 1982; Dirlam *et al*. 1992; Ananyev & Konovalenko 2012; Huong *et al*. 2012; Malsy *et al*. 2012; Phyo *et al*. 2019). The black variety of this mineral is rarely used for jewellery purposes, and then only if it is homogeneously coloured, free of fractures and shows high lustre. Such high-quality black spinel is known to occur near the village of Acaponeta, Nayarit State, Mexico (Rohtert 2002), and in the Bo Phloi District of Kanchanaburi Province, Thailand (Limsuwan 1999; Srithai 2007; Saminpanya & Sutherland 2008; Sutthirat *et al*. 2010). Other Thai occurrences of black spinel are known in the Chanthaburi, Phetchabun, Phrae, Sukhothai and Trat provinces (Coenraads *et al*. 1995), but these are typically not of good gem quality.

After decades of mining, blue sapphire production from the Kanchanaburi area has dwindled, so local gem cutters are turning to black spinel (Figures 1 and 2). Faceted and carved black spinel gems have therefore become more widespread in local gem markets. Several terms have been used to describe the non-transparent black spinel, with *pleonaste* and *ceylonite* (Deer *et al*. 1996) being the best known. Thai names include *nin* (meaning 'black gem'), *nin-ta-go* and *nin-tan* (the last two meaning 'solid-looking'). Some local dealers call the material *spiderman* or use the misleading terms *black sapphire* or *onyx* to describe the black spinel.

In this article we present the results of a recent study aiming to comprehensively characterise black spinel from Bo Phloi, including its physical properties, its chemical composition (major, minor and trace elements, as well as Fe^{2+} and Fe^{3+} contents), and its optical absorption and Raman spectral features.

BACKGROUND

The mineral spinel (more precisely magnesium aluminate spinel: $MgAl_2O_4$) has cubic space group $Fd\bar{3}m$ (Sickafus *et al*. 1999; cf. also Grimes *et al*. 1983). It occurs commonly as idiomorphic (i.e. well-formed crystals) to hypidiomorphic (i.e. partially developed crystal habit) grains in basic igneous rocks, in regional and contact metamorphic rocks, and as waterworn pebbles in alluvial sediments.

The spinel structure is characterised by O^{2-} ions that

Figure 2: These seven crystals (4.8–6.7 g) and one faceted stone (32.7 ct) of black spinel are typical of material from Bo Phloi. The shapes of the crystals are dominated by octahedral faces, rarely in combination with rhombic dodecahedral faces (such as the top specimen). Some pieces (see, e.g., the one at the upper right) show surface striations. Photo by M. Wildner.

form a cubic close-packed arrangement, hosting two non-equivalent cation sites (four- and six-coordinated with oxygen). Within this framework two different site occupations exist. In 'normal' spinels—such as ideal $MgAl_2O_4$—divalent cations occupy the tetrahedral cation site (four-coordination) and trivalent cations occupy the octahedral site (six-coordination), resulting in the general formula $A^{2+[4]}B^{3+[6]}{}_2O_4$. By contrast, in 'inverse' spinels half the trivalent cations occupy the four-coordinated site, whereas the remaining trivalent cations and divalent cations are incorporated at the six-coordinated site, resulting in the general formula $B^{3+[4]}(A^{2+}B^{3+})^{[6]}O_4$. An example of the latter is magnetite: $Fe^{3+[4]}(Fe^{2+}Fe^{3+})^{[6]}O_4$. However, many natural spinels represent intermediate states characterised by a 'partially inverse' site occupation. In such cases, the general formula can be summarised as $(A_{1-i}B_i)^{[4]}(A_iB_{2-i})^{[6]}O_4$, where 'i' is the inversion parameter. The degree of inversion depends on several factors (see O'Neill & Navrotsky 1983), but it is mainly controlled by the fraction of trivalent cations at the four-coordinated cation sites.

GEOLOGY AND MINING AT BO PHLOI

Geological Setting

Starting about 10 million years ago (Ma) during the Late Cenozoic, regional uplift and decompression melting resulted in extensive basaltic eruptions in Thailand (Figure 3). In the Bo Phloi area, basaltic volcanism took place either in the Inthanon Zone developed within the East Malaya block (Stauffer 1983) or within the Shan-Thai craton (Barr & Macdonald 1978). The Bo Phloi basaltic body is located in a major fracture zone transecting Silurian-Devonian quartzite of the Bo Phloi Formation. The present surface expression of the basalt is a remnant small plug approximately 1 km² in size (Bunopas & Bunjitradulya 1975). According to the currently accepted classification, the Bo Phloi basalt has a nepheline-hawaiite composition (Barr & Macdonald 1978, 1981; Yaemniyom 1982). The magma originated in the upper mantle at pressures of approximately 18–25 kbar and temperatures of 1,340–1,475°C, and ascended

Figure 3: The black patches on this simplified map show the distribution of Late Cenozoic basalt bodies in Thailand, including the Bo Phloi occurrence. Modified after Limtrakun (2003).

rapidly without any significant crustal interaction from estimated depths of 36–79 km (Barr & Macdonald 1981; Yaemniyom 1982). The basalt has been dated to the Pliocene (3.14 ± 0.17 Ma according to Barr & Macdonald 1981, or 4.17 ± 0.11 Ma according to Sutthirat *et al*. 1994; see also Choowong 2002).

The Bo Phloi basalt is a dark, dense, extremely fine-grained rock with a porphyritic texture. It contains abundant mantle xenoliths and xenocrysts such as pyroxene, spinel (Figure 4a), sanidine, olivine, plagioclase and magnetite. Less common syngenetic constituents include zircon, rutile, sapphire and ruby.

Mining

The Bo Phloi gem field comprises an area of about 60 km^2 in western Thailand, and is located about 30 km north of the town of Kanchanaburi (again, see Figure 3). Most of the mining sites are situated in gravels along the western terrace of the Lam Ta Phoen River (Limsuwan 1999; Choowong 2002). The area is renowned for the gem-quality blue sapphire that was once produced there (Bunopas & Bunjitadulya 1975; Vichit *et al*. 1978). The deposits are related to the weathering of basalt flows, and the gems have been mined from residual basalt-derived soil or gravel deposits up to 3 m thick and located up to 16 m below the surface (Hansawek & Pattamalai 1997; Choowong 2002; Khamloet *et al*. 2014). The gem-bearing fluvial deposition dates to the Pleistocene (approximately 0.7 Ma; Udomchoke 1988).

Mining in Bo Phloi with simple hand tools started in 1918, and shortly thereafter the deposit was believed to be depleted. In 1987, the site was rediscovered and subsequently exploited using modern mining tools and machinery (Limsuwan 1999; Figure 4b). However, most of these large-scale activities lasted less than two decades. The peak was during 1998–2005, when an average of 140–250 kg of sapphire were produced yearly (with a maximum of 320 kg in 2002). In 2006, sapphire production declined to only 20 kg. Since the early 2000s, miners also began to collect the initially discarded black spinel (Figure 4c). During 2003 and 2005, spinel production averaged 135 t per year, but in 2006 it decreased to about 15 t (Anonymous 2008). These numbers indicate that, although it was only a by-product of sapphire mining, black spinel was produced in huge amounts during the 2000s. There was so much available that local people built a huge Buddha statue with 49 t of crushed black spinel (Figure 4d).

Currently, mining activities have nearly ceased. At present, only negligible quantities of sapphire and black spinel are still produced as by-products of river-sand exploitation in a gravel quarry. Most mining sites are being transformed for other purposes. For example, one of the formerly most productive gem areas is now located under a golf course (Figure 4e). With the decline in blue sapphire production, the focus of local gem cutters and carvers has shifted towards black spinel, which is abundantly available for lapidaries from stockpiles that resulted from previous mining activities.

MATERIALS AND METHODS

The Bo Phloi spinel samples investigated for this study were purchased from local dealers in September 2018. They include 23 rough, more-or-less idiomorphic specimens of predominantly octahedral shape (seven of them are shown in Figure 2) and six cut and polished specimens (faceted or carved; three of them are seen in Figures 1 and 2).

Two rough pieces were cut in half (at random orientation), and one half of each was embedded in epoxy and then ground and polished; these samples were carbon coated for electron-beam imaging and major-element analysis. Doubly polished thin slabs were also prepared for optical absorption spectroscopy. For Mössbauer and powder X-ray diffraction analysis, sample material was powdered with an agate mortar and pestle.

The Mohs hardness (i.e. the resistance to being scratched) was tested by scratching one cut and four rough spinel specimens with reference minerals. SG values (here reported as mass density) were measured hydrostatically on the same five specimens, and RI was determined from polished surfaces on four spinels with a Krüss ER601-LED refractometer equipped with a diode lamp emitting 589 nm light.

Powder X-ray diffraction analysis was performed on two samples to confirm their identity and obtain their unit-cell dimensions, using a Bruker D8 Advance Eco powder diffractometer coupled with a LynxEye XE-T energy-dispersive detector with Cu($K\alpha$) radiation. The system was operated at 40 kV and 25 mA with a fixed divergence slit and sample spinning setup. The scanning range was 5–140° 2θ with a 0.01° θ step width. TOPAS version 4.2 (Bruker AXS GmbH 2009) software was used for powder X-ray diffraction data refinement.

Major-element analyses were carried out on two samples with a Cameca SX100 electron probe microanalyser (EPMA). The instrument was operated in wavelength-dispersive mode with the following conditions: accelerating voltage 15 kV, current 20 nA, and electron beam diameter of 2 µm at the sample surface. The following calibrant materials were used (with respective

Figure 4: (**a**) Two spinel xenocrysts (16 mm and 5 mm long) are embedded in their basaltic host rock. (**b**) The sapphire and spinel mining site at Ban Bung Hua Waen, southwest of Bo Phloi, as seen in 2012. (**c**) Mine employees pick sapphires from a conveyor belt in March 2012. Most of the black material in this heavy mineral fraction consists of spinel, which was stockpiled. (**d**) This Buddha statue (Luang Por Nil) is located on a hill inside the town of Bo Phloi. It measures 9 m tall and is made from crushed black spinel mixed with cement. (**e**) This area along the Lam Ta Phoen River northwest of Bo Phloi hosted the former Ban Chong Dan mining area, which has been transformed into a golf course. Photos by B. Wanthanachaisaeng.

X-ray lines analysed shown in parentheses): $MgAl_2O_4$ (Al[*K*α], Mg[*K*α]), sanidine (Si[*K*α]), titanite (Ti[*K*α]), chromite (Cr[*K*α]), wollastonite (Ca[*K*α]), hematite (Fe[*K*α]), spessartine (Mn[*K*α]), vanadinite (V[*K*α]), gahnite (Zn[*K*α]) and Ni_2SiO_4 (Ni[*K*α]). Peak counting times were 10 s for major and 30 s for minor elements; the background counting times were half the respective peak counting times. An X-PHI matrix correction routine (Merlet 1994) was applied to the raw data. The Fe^{2+}:Fe^{3+} ratio was calculated from stoichiometry, assuming four oxygen atoms per formula unit. Prior to EPMA analysis, backscattered electron images (BSE) were acquired to check for possible zoning and other heterogeneity within the crystals.

Laser ablation inductively coupled plasma mass spectroscopy (LA-ICP-MS) measurements of minor and trace elements were carried out on two samples with an Agilent 7500cx quadrupole ICP-MS unit coupled with an ESI NWR193 laser-ablation system. The instrument was operated with a 193 nm laser, working at 8 Hz repetition

rate pulse frequency with an energy of approximately 8 mJ/cm^2 at the surface and a 75 µm spot size. A gas flow of 0.75 l/min He transported the ablated material to the spectrometer unit. After every seventh measurement, NIST standard glasses SRM610 and SRM612 (Jochum *et al.* 2011) were probed for drift correction. The USGS reference glass BCR-2G (Rocholl 1998) was measured for quality control and was reproduced within 10% relative error. Aluminium was used as an internal standard. The detection limits of this method are in the range of 0.01–0.1 ppm for most trace elements. For data reduction GLITTER 4.0 software (Griffin *et al.* 2008) was utilised. Data for all elements were reduced using the SRM612 standard, except for ^{49}Ti, for which the SRM610 standard was used.

Mössbauer spectroscopy was performed on two samples to investigate the valence state of iron (Fe^{3+} and/or Fe^{2+}) and its occupancy in the spinel structure. Measurements were done with an apparatus manufactured by Halder Electronics GmbH (Starnberg, Germany) using methodology described by Redhammer *et al.* (2012). Folded spectra were deconvoluted with the Voigt-based quadrupole-splitting distribution approach (Rancourt & Ping 1991; Lagarec & Rancourt 1997). Using this procedure, distributions of quadrupole splitting due to slightly different local distortion environments around the Fe-probe site can be adequately modelled.

An optical absorption spectrum was obtained from each of the two doubly polished thin slabs mentioned above in the near-ultraviolet, visible and near-infrared spectral ranges using a Bruker IFS 66v/S Fourier-transform spectrometer. Analytical details were analogous to those of Zeug *et al.* (2018).

Raman spectroscopic measurements were performed on all 23 rough and six polished samples to confirm mineral identification and evaluate the extent of 'structural inversion' in comparison with other spinels. Analyses were done by means of a Horiba LabRAM HR Evolution spectrometer, with the same measurement setups as in Zeug *et al.* (2018). Spectra were excited with a 532 nm Nd:YAG laser (10 mW at the sample surface), using a 50× objective (numerical aperture of 0.50). The resulting energy density was well below the threshold of any laser-beam-induced sample changes, as could possibly be caused by local heating due to intense light absorption (note that, e.g., the Fe-spinel magnetite is easily oxidised by a focused laser beam to form hematite; cf. figure 8 in Nasdala *et al.* 2004). Raman analyses were carried out prior to EPMA and LA-ICP-MS analysis to avoid any possible influence on the samples from the beams used by those instruments.

RESULTS AND DISCUSSION

General Properties

All samples were non-transparent and macroscopically black. The rough pieces appeared dull and greyish black, whereas polished specimens (faceted stones and carvings) were deep black with high lustre (Figures 1 and 2). The samples' Mohs hardness was about 8. This, along with the chemical stability and the lack of clear cleavage, explains their resistance to the chemical and mechanical weathering processes that acted upon the host basalt.

The X-ray diffraction pattern of the Bo Phloi material corresponded to that of Mg-Al spinel, which confirms the material's identity as spinel *sensu stricto*. This was not certain from the outset, as a good fraction of the 'black spinels' in the Thai gem markets actually are pyroxene or another black material. The unit-cell constant was determined as a_0 = 8.1363(1) Å, which corresponds well to literature data for spinel *sensu stricto* (a_0 = 8.103 Å; Putnis 1992). The resulting cell volume is 538.62(2) Å^3.

Samples were found to be optically isotropic, without any pleochroism. The RI was determined as about 1.770, which is somewhat higher than that of transparent gem-quality Mg-Al spinel (1.720; Tropf & Thomas 1991). Mass density averaged 3.85 ± 0.01 g/cm^3, which corresponds well to the 3.86 g/cm^3 determined by Saminpanya and Sutherland (2008) for black spinel from Bo Phloi. These values are notably higher compared to the mass density of near-end-member Mg-Al spinel (3.58–3.61 g/cm^3; Deer *et al.* 1996). This, along with the dark colour, points to the presence of elevated non-formula elements (e.g. Fe). The specimens were not attracted to an Alnico magnet.

Chemical Composition

The chemical composition of black spinel from Bo Phloi, as determined by EPMA and LA-ICP-MS analysis, is presented in Table I. Samples generally contained about 59 wt.% Al_2O_3, 19 wt.% MgO, and 21 wt.% FeO (with the total Fe expressed as FeO). The measured values agree with the results of a previous study on black spinel from Bo Phloi (Saminpanya & Sutherland 2008). With the exception of Fe and Ti, the Bo Phloi spinel contains low amounts of non-formula elements (below 0.2 wt.%). The BSE images of the samples (not shown) were virtually without any internal contrast. This, and generally low variations of EPMA results within and among samples, indicate that the Bo Phloi spinel has a fairly homogeneous chemical composition.

Table I: Average chemical composition of black spinel from Bo Phloi determined by EPMA and LA-ICP-MS, and calculated mineral formula units.

EPMA results (n = 34)				LA-ICP-MS results (n = 14)					
Oxide	Concentration (wt.%)[a]	Element	Content (apfu)[b]	Element	Isotope measured	Concentration (ppm)[a]	Element	Isotope measured	Concentration (ppm)[a]
SiO_2	0.16 ± 0.02	Si	0.004	Li	7	0.74 ± 0.14	Ga	71	209 ± 3
TiO_2	0.66 ± 0.05	Ti	0.013	Be	9	0.14 ± 0.04	Sr	88	0.02 ± 0.01
Al_2O_3	59.0 ± 0.6	Al	1.801	P	31	20.6 ± 3.4	Y	89	0.01 ± 0.01
MgO	18.7 ± 0.3	Mg	0.720	Ti	49	3440 ± 34	Zr	90	0.80 ± 0.18
Cr_2O_3	0.05 ± 0.05	Cr	0.001	V	51	705 ± 7	Nb	93	0.03 ± 0.01
MnO	0.13 ± 0.02	Mn	0.003	Cr	53	253 ± 5	Sn	118	0.29 ± 0.05
V_2O_3	0.12 ± 0.02	V	0.002	Mn	55	1025 ± 9			
ZnO	0.11 ± 0.02	Zn	0.002	Co	59	283 ± 3			
NiO	0.15 ± 0.03	Ni	0.003	Ni	60	1290 ± 19			
FeO[c]	20.7 ± 0.9	Fe^{2+}	0.289	Cu	63	2.94 ± 0.38			
Total	99.8 ± 0.3	Fe^{3+}	0.161	Zn	66	1290 ± 23			

[a] All errors are quoted at the 1σ level.
[b] General chemical formula units calculated assuming three cations and four oxygen atoms per formula unit. Fe^{2+}/Fe^{3+} was recalculated to maintain charge neutrality.
[c] Total Fe is quoted here as FeO.

Mössbauer Spectroscopy

Mössbauer spectra exhibited a broad resonance absorption that could be resolved into three principal sites (Figure 5), based on their isomer shift and quadrupole splitting values. Two of these sites belonged to Fe^{3+} and the third to Fe^{2+}. As is typically found in Al-rich spinel samples, the Fe^{2+} contribution was broad and consisted of three sub-components. This is in accordance with literature data (Larsson *et al.* 1994; Carbonin *et al.* 1996, 1999; Jastrzebska *et al.* 2017).

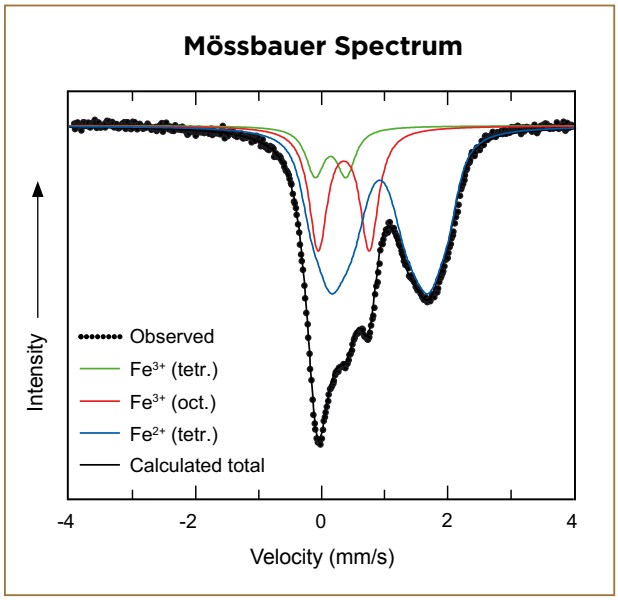

Figure 5: The Mössbauer spectrum of Bo Phloi spinel indicates the presence of three different iron site occupancies: Fe^{2+} in four-coordination, and Fe^{3+} in four- and six-coordination.

Refinement of the Mössbauer spectra showed that the broad component (being the sum of three sub-components) at the isomer shift of around 0.92 mm/s (Figure 5) is characteristic for Fe^{2+} in four-coordination. The component with an isomer shift of about 0.35 mm/s is ascribed to Fe^{3+} in six-coordination. The remaining component has isomer shifts and quadrupole splitting values typical of Fe^{3+} in four-coordination. Fits were also done without assuming the presence of this last component ($Fe^{3+[4]}$). As the results were distinctly worse for these fits, it can be assumed that a small amount of $Fe^{3+[4]}$ is present. The fit results are presented in Table II. Note that Mössbauer spectra do not yield an independent indication for the presence of Fe^{2+} in the octahedral position.

Table II: Mössbauer parameters for black spinel from Bo Phloi.

Iron species	Isomer shift (mm/s)	Quadrupole splitting (mm/s)	Fraction* (%)
Fe^{3+}; four-coordinated	0.13 ± 0.2	0.5 ± 0.3	9 ± 1
Fe^{3+}; six-coordinated	0.35 ± 0.2	0.8 ± 0.1	24 ± 2
Fe^{2+}; four-coordinated	0.92 ± 0.2	0.9 ± 0.1 1.6 ± 0.1 2.2 ± 0.1	67 ± 1

*Fractions of Fe species were determined from the ratios of integrated areas of the respective doublets and normalised to 100%.

Considering the Mössbauer results, the EPMA data (Table I) were converted to end-member fractions, which resulted in a nominal composition of the following components: 72 mol.% spinel (Mg-Al), 18 mol.% hercynite (Fe^{2+}-Al^{3+}), 8.1 mol.% magnetite (Fe^{2+}-Fe^{3+}) and 1.3 mol.% ulvöspinel (Ti^{4+}-Fe^{2+}). Despite the significant $Fe_{(total)}$ content, the material is assigned to spinel *sensu stricto* (that is, Mg-Al spinel; Figure 6). Correspondingly, the data plot near the spinel end member of the (Mg-Al) spinel-hercynite-magnetite triangle (Figure 6). The chemical formula is estimated, based on four O atoms per formula unit, as $(Mg_{0.66}Fe^{2+}_{0.30}Fe^{3+}_{0.04})^{[4]}{}_{\Sigma=0.99}(Al_{1.80}Fe^{3+}_{0.11}Mg_{0.06}Ti_{0.01})^{[6]}{}_{\Sigma=1.98}O_4$. Here, a small fraction of the Mg is assumed to be incorporated at the six-coordinated site, as otherwise there would be a significant imbalance in the occupations of A and B sites. The small but significant amounts of $Fe^{3+[4]}$ and $Mg^{2+[6]}$ characterise the cation occupation as 'partially inverse'.

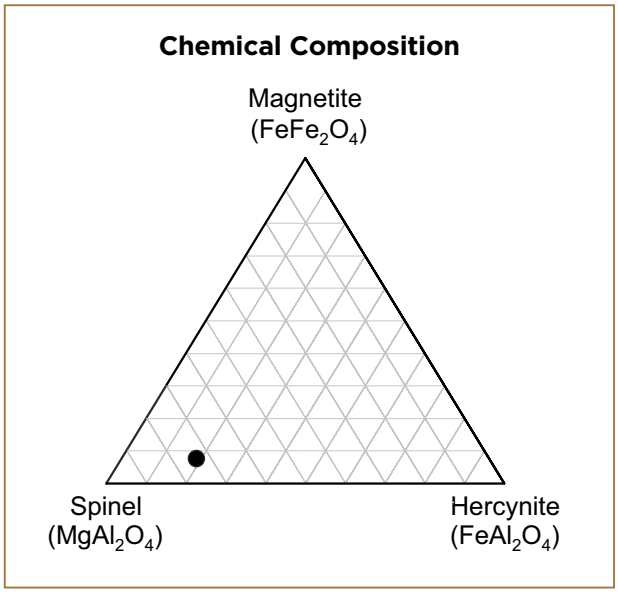

Figure 6: Results of chemical analyses of the Bo Phloi spinel (converted to nominal end-member fractions in mol.%) are plotted in the spinel end-member triangle. Note that an 0.8 mol.% ulvöspinel ($TiFe_2O_4$) component is also present in the material but is not shown in this plot.

Optical Absorption Spectroscopy

The optical absorption spectrum is shown in Figure 7 as linear absorption coefficient plotted against wavenumber (lower x-axis) and wavelength (top x-axis). Note, however, that even a 27-µm-thick slab (see transmitted-light image in Figure 7, inset) turned out to be too thick to obtain an optical absorption spectrum with adequate signal-to-noise ratio. The spectrum presented in Figure 7 was, therefore, obtained from a thinned edge of the slab (10 µm thickness). As the material's chemical composition is very homogeneous, the small sample volume that was effectively analysed in the absorption spectrometer is not believed to cause any bias.

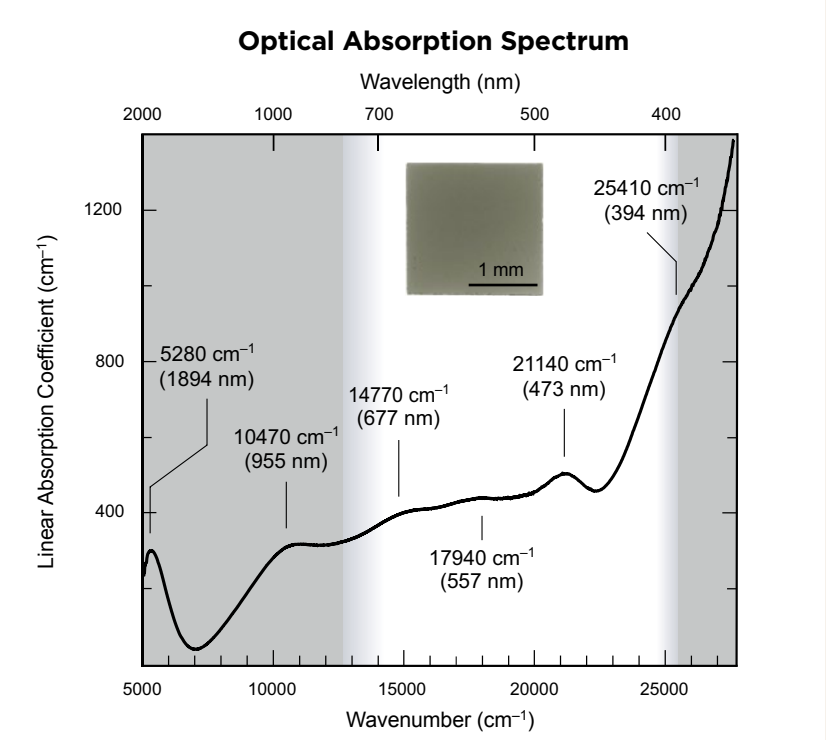

Figure 7: This optical absorption spectrum of spinel from Bo Phloi was measured in transmission mode from a 10-µm-thick slab. Spectral ranges invisible to the human eye are shaded in grey. All of the absorption features are due to iron. The inset shows a 27-µm-thick slab (transmitted-light photomicrograph), which reveals the brownish grey colour. Photomicrograph by B. Kruzslicz.

To quantify specific band positions, a twofold procedure was applied. First, several versions of 'rubber-band corrections' based on polynomials with manually selected anchor points were performed, to account for the assumed shape of the absorption edge and for linear background absorption. Second, band deconvolution implying six Gaussian band profiles was performed for each version of the resulting background-subtracted spectrum. It was found that different background corrections did not result in significant variations of fitted band positions, whereas the fitted bandwidths were quite different in some cases. The final band positions were obtained by averaging these band-fitting results, and are presented in Table III. Overall, the intense dark colouration of the black spinel from Bo Phloi is caused by a strong absorption edge that increases toward the UV range, with a number of Fe-related absorption bands in the visible range. For more details on the band assignments pertaining to the optical absorption spectra, see Box A.

Box A: Band Assignments for Optical Absorption Features in Black Spinel from Bo Phloi

A summary of the band assignments for the optical absorption spectral features in Bo Phloi black spinel is included in Table III and described below.

The comparatively sharp lowest-energy band at 5280 cm^{-1} (1894 nm; full width at half maximum about 1700 cm^{-1}) is the result of the spin-allowed d–d crystal-field transition of $Fe^{2+[4]}$, that is $^5E(D) \rightarrow {}^5T_2(D)$. Since this transition is affected by dynamic Jahn–Teller splitting, the observed band represents the high-energy component of the $^5T_2$ set only. Skogby and Hålenius (2003) identified three weaker split components at lower energies in infrared absorption spectra of spinel-hercynite mixed crystals, with the major one located at 3430 cm^{-1}.

The assignment of the broad band at 10470 cm^{-1} (955 nm) is less clear than that of the lowest-energy band. Here, no major crystal-field transition is to be expected due to the rather evidently low content of $Fe^{2+[6]}$, which was not detected in the Mössbauer spectra. However, even limited contents of $Fe^{2+[6]}$ might cause the transition of exchange-coupled six-coordinated Fe^{2+}–Fe^{3+} pairs, in accordance with the assignment of a comparable band by Hålenius *et al.* (2002). The quite flat and broad band at 14770 cm^{-1} (677 nm) is assigned, again in agreement with Hålenius *et al.* (2002), to electronic intervalence charge transfer (IVCT) between neighbouring $Fe^{2+[6]}$–$Fe^{3+[6]}$ ions. The latter interpretation too is in apparent contrast with the Mössbauer results, as it also assumes some Fe^{2+} ions in the octahedral site. It should be noted, however, that even minute amounts of Fe^{2+} in the octahedral site, well below the Mössbauer detection limit, can be enough to activate the IVCT process.

Bands at higher energies are most likely related to spin-forbidden d–d transitions of $Fe^{2+[4]}$ and/or $Fe^{3+[6]}$. The apparently weak band at 17940 cm^{-1} (557 nm) might be attributed to the (more-or-less field-independent) spin-forbidden $^3T_2(H)$ level of $Fe^{2+[4]}$, probably $^3E(G) \rightarrow {}^3T_2(H)$ with additional contributions from $^3T_1(H)$ and/or $^3T_1(G)$. A comparable assignment was proposed by Gaffney (1973) for $Fe^{2+[4]}$ in $MgAl_2O_4$. The pronounced band at 21140 cm^{-1} (473 nm) typically results from spin-forbidden d–d transitions in $Fe^{3+[6]}$, that is $^6A_{1g}(S) \rightarrow {}^4A_{1g}/{}^4E_g(G)$ (cf. Andreozzi *et al.* 2001, 2018; Taran *et al.* 2005), probably with a contribution of spin-forbidden d–d transitions of $Fe^{2+[4]}$, such as $^5E(D) \rightarrow {}^3T_2(G)$. The shoulder centred at about 25410 cm^{-1} (394 nm) within the ligand-metal charge-transfer absorption edge is also assumed to be related to a combination of spin-forbidden d–d transition of $Fe^{2+[4]}$ and $Fe^{3+[6]}$ positions, tentatively $^5E(D) \rightarrow {}^3T_2(D)/{}^3T_2(P2)$ of $Fe^{2+[4]}$ (e.g. Andreozzi *et al.* 2018) and $^6A_{1g}(S) \rightarrow {}^4T_{2g}(D)$ of $Fe^{3+[6]}$.

In summary, the interpretation of the bands at 5280 cm^{-1} (1894 nm), 10470 cm^{-1} (955 nm) and 14770 cm^{-1} (677 nm) goes along with the findings of Hålenius *et al.* (2002), who analysed samples with roughly comparable composition to this study's material. However, due to distinct differences in the composition and Fe distribution of the two studied materials (especially concerning significantly higher octahedral Fe^{3+} in our samples), assignments by analogy of the bands at 10470 cm^{-1} (955 nm) and 14770 cm^{-1} (677 nm) are not straightforward. According to Taran *et al.* (2005), an absorption band around 10500 cm^{-1} (952 nm) could also be assigned to electronic spin-forbidden transitions $^6A_{1g} \rightarrow {}^4T_{1g}$ of $Fe^{3+[6]}$. Higher-energy bands at 17940 cm^{-1} (557 nm), 21140 cm^{-1} (473 nm) and 25410 cm^{-1} (394 nm) can be attributed to spin-forbidden transitions of Fe in general (e.g. Andreozzi *et al.* 2001), but due to the complex distribution of Fe in the black spinel from Bo Phloi, singular assignments naturally bear some uncertainty.

Table III: Band positions and assignment of optical absorption bands* for black spinel from Bo Phloi.

Band position (cm^{-1})	Band position (nm)	Assignment
5280	1894	Spin-allowed d-d transition of $Fe^{2+[4]}$: $^5E(D) \rightarrow {}^5T_2(D)$
10470	955	Transition of exchange-coupled $Fe^{2+[6]}$ –$Fe^{3+[6]}$ pairs
14770	677	Intervalence charge transfer (IVCT) between neighbouring $Fe^{2+[6]}$ –$Fe^{3+[6]}$ ions
17940	557	Spin-forbidden d-d transition of $Fe^{2+[4]}$: $^5E(D) \rightarrow {}^3T_2(H)$ etc. (assignment uncertain)
21140	473	Spin-forbidden d-d transition of $Fe^{3+[6]}$: $^6A_{1g}(S) \rightarrow {}^4A_{1g}/{}^4E_g(G)$, probably with contribution of $Fe^{2+[4]}$: $^5E(D) \rightarrow {}^3T_2(G)$
25410	394	Spin-forbidden d-d transitions of $Fe^{2+[4]}$: $^5E(D) \rightarrow {}^3T_2(D)/{}^3T_2(P2)$ and $Fe^{3+[6]}$: $^6A_{1g}(S) \rightarrow {}^4T_{2g}(D)$ (assignment uncertain)

*Superimposed on the O–$Fe^{2+,3+}$ ligand-metal charge-transfer UV absorption edge.

Raman Spectroscopy

The Raman spectrum of Bo Phloi black spinel is shown in Figure 8, along with reference spectra of spinel *sensu stricto* (Nasdala *et al.* 2001), magnesioferrite, hercynite (D'Ippolito *et al.* 2015) and magnetite (Stähle *et al.* 2017). The spectrum is dominated by intense bands at 542 and 750 cm^{-1}, which concurs well with a Raman spectrum obtained for Bo Phloi spinel by Saminpanya and Sutherland (2008).

A most remarkable finding is that the Raman spectrum of the Bo Phloi spinel does not resemble the spectrum of natural, 'normal' Mg-Al spinel, which is dominated by an intense, narrow E_g-type band at 408 cm^{-1} (Cynn *et al.* 1992; Nasdala *et al.* 2001; Slotznick & Shim 2008; cf. also Schubnel *et al.* 1992). Instead, the most intense bands in the Raman pattern of the Bo Phloi spinel are at different spectral positions and with different relative intensities. However, the Raman spectrum of the Bo Phloi spinel does show similarities to those of other spinel-group minerals, such as hercynite and magnesioferrite, which often tend to be 'partially inverse'. Andreozzi *et al.* (2001), D'Ippolito (2013), Lenaz & Lughi (2017) and Granone *et al.* (2018) have discussed that the Raman spectra of natural spinel-group minerals and synthetic spinels are controlled predominantly by the degree of 'inversion' in the occupation of the two non-equivalent cation sites, rather than by chemical composition alone. Lenaz & Lughi (2017) found that at low inversion degrees ($i \leq 0.14$), spinel spectra are dominated by the strong 400–410 cm^{-1} Raman band of 'normal' spinel (again, see Figure 8). The low intensity or even absence of this band in the Raman spectrum of the Bo Phloi spinel suggests that its degree of 'partial inversion' must be significant, even higher than in the estimated chemical formula ($i \approx 0.04$–0.06).

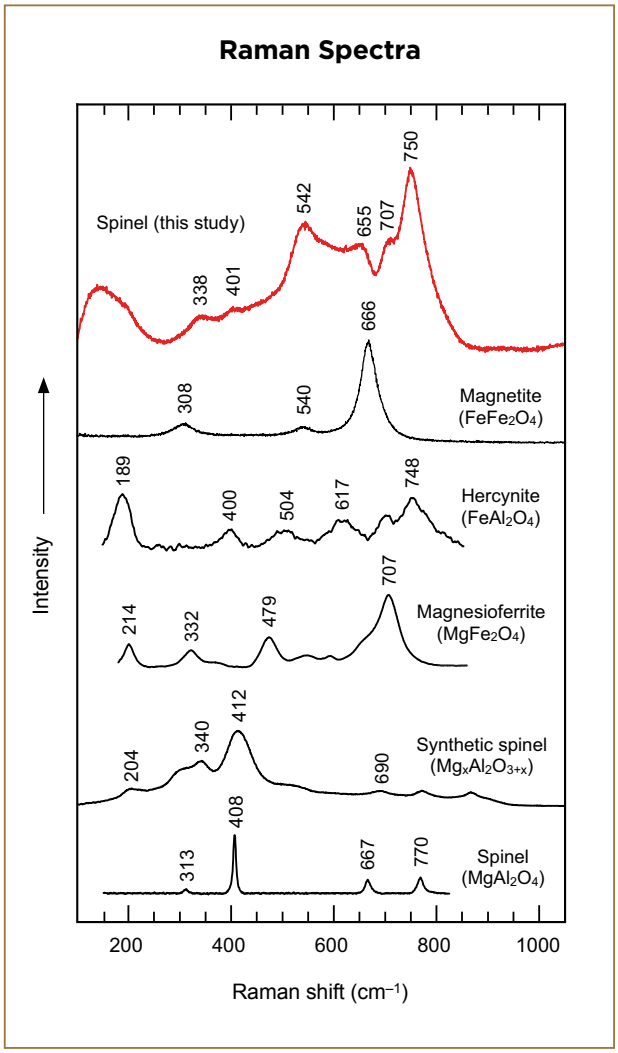

Figure 8: The Raman spectrum of Bo Phloi spinel in comparison with reference spectra for spinel-group minerals shows dissimilarity to natural and synthetic Mg-Al spinel references but similarity to the principal 'fingerprint' patterns of magnetite, hercynite and magnesioferrite. These can be explained by the degree of inverse cation occupation. Differences between natural and synthetic Mg-Al spinel are explained by the non-stoichiometry and disorder in the latter (Erukhimovitch *et al.* 2015). The reference spectrum for magnetite was obtained from a natural sample from Rumpersdorf, Austria (courtesy E. Libowitzky), and the synthetic Mg-Al spinel was provided by G. Giester. The other reference spectra were extracted from D'Ippolito *et al.* (2015; synthetic $FeAl_2O_4$ and $MgFe_2O_4$) and Nasdala *et al.* (2001; natural Mg-Al spinel from Mogok, Myanmar).

CONCLUSIONS

Black spinel from Bo Phloi, Thailand, is characterised by a remarkably homogenous chemical composition, corresponding to $MgAl_2O_4$ with particularly high Fe content. Mössbauer spectroscopic results indicate the iron consists of $Fe^{2+[4]}$ 67%, $Fe^{3+[6]}$ 24% and $Fe^{3+[4]}$ 9%. The additional presence of $Fe^{2+[6]}$ is indicated by the optical absorption spectrum, but the amount is below the detection limit of Mössbauer spectroscopy. The chemical formula (based on four O per formula unit), estimated from EPMA and Mössbauer spectroscopic data, is $(Mg_{0.66}Fe^{2+}_{0.30}Fe^{3+}_{0.04})^{[4]}{}_{\Sigma=0.99}(Al_{1.80}Fe^{3+}_{0.11}Mg_{0.06}Ti_{0.01})^{[6]}{}_{\Sigma=1.98}O_4$. This correlates to a 'partially inverse' occupation of the two principal cation sites. The Raman spectrum also indicates that the Bo Phloi spinel does not represent a 'normal' but rather a 'partially inverse' cation occupation, which suggests that it might contain some additional amounts of $Mg^{2+[6]}$ and $Al^{3+[4]}$.

The brownish grey colour of the Bo Phloi spinel can be observed only in samples with thicknesses well below 0.1 mm. Gemmologists would hence call the material 'opaque', whereas geoscientists would describe it as 'non-transparent'. For the latter, materials are considered opaque only if they are still fully non-transparent at the thickness of a petrological thin section (i.e. 25 μm). Optical absorption spectroscopy indicated that the intense dark colouration that makes the material appear black and non-transparent (Figure 9) is caused by a strong absorption edge that increases toward the UV range, with a number of Fe-related absorption bands in the visible range.

Distinguishing black spinel, especially when already faceted, from similar black, non-transparent materials such as pyroxenes and amphiboles is challenging (Johnson *et al*. 1996). Measuring RI and SG might not suffice for definitive identification. Here, Raman spectroscopy allows for quick, non-destructive mineral identification, even though the spectrum of black spinel and that of 'common' gem spinel (i.e. transparent, coloured material) differ appreciably.

Mining of black spinel in the Bo Phloi area has almost ended in recent years. Nevertheless, we should expect to continue seeing Bo Phloi black spinel in gem markets as existing stockpiles are processed into faceted stones and carvings.

Figure 9: Black spinel from Bo Phloi is being set into attractive jewellery, as shown by this sterling silver ring featuring a 35 ct centre stone surrounded by cubic zirconia accent stones. Photo by Tidarat Pruttipako.

REFERENCES

Ananyev, S.A. & Konovalenko, S.I. 2012. Morphological and gemmological features of gem-quality spinel from the Goron deposit, southwestern Pamirs, Tajikistan. *Journal of Gemmology*, **33**(1), 15–18, https://doi.org/10.15506/JoG.2012.33.1.15.

Andreozzi, G.B., Hålenius, U. & Skogby, H. 2001. Spectroscopic active $^{IV}Fe^{3+}$–$^{VI}Fe^{3+}$ clusters in spinel-magnesioferrite solid solution crystals: A potential monitor for ordering in oxide spinels. *Physics and Chemistry of Minerals*, **28**(7), 435–444, https://doi.org/10.1007/s002690100178.

Andreozzi, G.B., D'Ippolito, V., Skogby, H., Hålenius, U. & Bosi, F. 2018. Color mechanisms in spinel: A multi-analytical investigation of natural crystals with a wide range of coloration. *Physics and Chemistry of Minerals*, **46**(4), 343–360, https://doi.org/10.1007/s00269-018-1007-5.

Anonymous 2008. *Area Classification for Management of Geological and Mineral Resources, Kanchanaburi Province*, Department of Mineral Resources, Ministry of Natural Resources and Environment, Bangkok, Thailand, 96 pp. (in Thai).

Barr, S.M. & MacDonald, A.S. 1978. Geochemistry and petrogenesis of Late Cenozoic alkaline basalts of Thailand. *Bulletin of the Geological Society of Malaysia*, **10**, 25–52, https://doi.org/10.7186/bgsm10197803.

Barr, S.M. & MacDonald, A.S. 1981. Geochemistry and geochronology of Late Cenozoic basalts of Southeast Asia. *GSA Bulletin*, **92**(8), Part II, 1069–1142, https://doi.org/10.1130/gsab-p2-92-1069.

Bruker AXS GmbH 2009. *DIFFRACplus TOPAS - TOPAS 4.2 User Manual*. Bruker AXS GmbH, Karlsruhe, Germany, 72 pp., http://algol.fis.uc.pt/jap/TOPAS%204-2%20Users%20Manual.pdf.

Bunopas, S. & Bunjitradulya, S. 1975. Geology of Amphoe Bo Ploi, north Kanchanaburi, with special notes on the "Kanchanaburi Series". *Journal of the Geological Society of Thailand*, **1**, 51–67.

Carbonin, S., Russo, U. & Della Giusta, A. 1996. Cation distribution in some natural spinels from X-ray diffraction and Mössbauer spectroscopy. *Mineralogical Magazine*, **60**(399), 355–368, https://doi.org/10.1180/minmag.1996.060.399.10.

Carbonin, S., Menegazzo, G., Lenaz, D. & Princivalle, F. 1999. Crystal chemistry of two detrital Cr-spinels with unusually low values of oxygen positional parameter: Oxidation mechanism and possible origin. *Neues Jahrbuch für Mineralogie, Monatshefte*, **8**(8), 359–371.

Choowong, M. 2002. Quaternary geology and sapphire deposits from the Bo Phloi gem field, Kanchanaburi Province, western Thailand. *Journal of Asian Earth Sciences*, **20**(2), 119–125, https://doi.org/10.1016/s1367-9120(01)00032-3.

Coenraads, R.R., Vichit, P. & Sutherland, F.L. 1995. An unusual sapphire–zircon–magnetite xenolith from the Chanthaburi gem province, Thailand. *Mineralogical Magazine*, **59**(396), 465–479, https://doi.org/10.1180/minmag.1995.059.396.08.

Cynn, H., Sharma, S.K., Cooney, T.F. & Nicol, M. 1992. High-temperature Raman investigation of order-disorder behavior in the $MgAl_2O_4$ spinel. *Physical Review B*, **45**(1), 500–502, https://doi.org/10.1103/PhysRevB.45.500.

Deer, W.A., Howie, R.A. & Zussman, J. 1996. *An Introduction to the Rock-Forming Minerals*, 2nd edn. Pearson Education Limited, Harlow, 712 pp.

D'Ippolito, V. 2013. *Linking crystal chemistry and physical properties of natural and synthetic spinels: An UV–VIS–NIR and Raman study.* PhD thesis, Sapienza University of Rome, Italy, 237 pp.

D'Ippolito, V., Andreozzi, G.B., Bersani, D. & Lottici, P.P. 2015. Raman fingerprint of chromate, aluminate and ferrite spinels. *Journal of Raman Spectroscopy*, **46**(12), 1255–1264, https://doi.org/10.1002/jrs.4764.

Dirlam, D.M., Misiorowski, E.B., Tozer, R., Stark, K.B. & Bassett, A.M. 1992. Gem wealth of Tanzania. *Gems & Gemology*, **28**(2), 80–102, https://doi.org/10.5741/gems.28.2.80.

Erukhimovitch, V., Mordekoviz, Y. & Hayun, S. 2015. Spectroscopic study of ordering in non-stoichiometric magnesium aluminate spinel. *American Mineralogist*, **100**(8–9), 1744–1751, http://doi.org/10.2138/am-2015-5266.

Gaffney, E.S. 1973. Spectra of tetrahedral Fe^{2+} in $MgAl_2O_4$. *Physical Review B*, **8**(7), 3484–3486, https://doi.org/10.1103/PhysRevB.8.3484.

Granone, L.I., Ulpe, A.C., Robben, L., Klimke, S., Jahns, M., Renz, F., Gesing, T.M., Bredow, T., Dillert, R. & Bahnemann, D.W. 2018. Effect of the degree of inversion on optical properties of $ZnFe_2O_4$. *Physical Chemistry Chemical Physics*, **20**, 28267–28278, https://doi.org/10.1039/c8cp05061a.

Griffin, W.L., Powell, W., Pearson, N.J. & O'Reilly, S.Y. 2008. GLITTER: Data reduction software for laser ablation ICP-MS. *In*: Sylvester, P. (ed) *Laser Ablation ICP–MS in the Earth Sciences: Current Practices and Outstanding Issues*. Mineralogical Association of Canada, Québec, Canada, 308–311.

Grimes, N.W., Thompson, P. & Kay, H.F. 1983. New symmetry and structure for spinel. *Proceedings of the Royal Society A: Mathematical, Physical and Engineering Sciences*, **386**(1791), 333–345, https://doi.org/10.1098/rspa.1983.0039.

Gübelin, E.J. 1982. Gemstones of Pakistan: Emerald, ruby, and spinel. *Gems & Gemology*, **18**(3), 123–139, https://doi.org/10.5741/gems.18.3.123.

Hålenius, U., Skogby, H. & Andreozzi, G.B. 2002. Influence of cation distribution on the optical absorption spectra of Fe^{3+}-bearing spinel s.s.-hercynite crystals: Evidence for electron transitions in $^{VI}Fe^{2+}$–$^{VI}Fe^{3+}$ clusters. *Physics and Chemistry of Minerals*, **29**(5), 319–330, https://doi.org/10.1007/s00269-002-0240-z.

Hansawek, R. & Pattamalai, K. 1997. Kanchanaburi sapphire deposits. *Mineral Resources Gazette*, **45**(1), 17–38.

Huong, L.T.-T., Häger, T., Hofmeister, W., Hauzenberger, C., Schwarz, D., Van Long, P., Wehrmeister, U., *et al.* 2012. Gemstones from Vietnam: An update. *Gems & Gemology*, **48**(3), 158–176, https://doi.org/10.5741/gems.48.3.158.

Jastrzębska, I., Bodnar, W., Witte, K., Burkel, E., Stoch, P. & Szczerba, J. 2017. Structural properties of Mn-substituted hercynite. *Nukleonika*, **62**(2), 95–100, https://doi.org/10.1515/nuka-2017-0013.

Jochum, K.P., Weis, U., Stoll, B., Kuzmin, D., Yang, Q., Raczek, I., Jacob, D.E., Stracke, A., *et al.* 2011. Determination of reference values for NIST SRM 610-617 glasses following ISO guidelines. *Geostandards and Geoanalytical Research*, **35**(4), 397–429, https://doi.org/10.1111/j.1751-908X.2011.00120.x.

Johnson, M.L., McClure, S.F. & DeGhionno, D.G. 1996. Some gemological challenges in identifying black opaque gem materials. *Gems & Gemology*, **32**(4), 252–261, https://doi.org/10.5741/gems.32.4.252.

Khamloet, P., Pisutha-Arnond, V. & Sutthirat, C. 2014. Mineral inclusions in sapphire from the basalt-related deposit in Bo Phloi, Kanchanaburi, western Thailand: Indication of their genesis. *Russian Geology and Geophysics*, **55**(9), 1087–1102, https://doi.org/10.1016/j.rgg.2014.08.004.

Lagarec, K. & Rancourt, D.G. 1997. Extended Voigt-based analytic lineshape method for determining N-dimensional correlated hyperfine parameter distributions in Mössbauer spectroscopy. *Nuclear Instruments and Methods in Physics Research Section B: Beam Interactions with Materials and Atoms*, **129**(2), 266–280, https://doi.org/10.1016/s0168-583x(97)00284-x.

Larsson, L., O'Neill, H.S.C. & Annersten, H. 1994. Crystal chemistry of synthetic hercynite ($FeAl_2O_4$) from XRD structural refinements and Mössbauer spectroscopy. *European Journal of Mineralogy*, **6**(1), 39–52, https://doi.org/10.1127/ejm/6/1/0039.

Lenaz, D. & Lughi, V. 2017. Raman spectroscopy and the inversion degree of natural Cr-bearing spinels. *American Mineralogist*, **102**(2), 327–332, https://doi.org/10.2138/am-2017-5814.

Limsuwan, R. 1999. "Bore-pile drilling" a new choice for deep sampling for placer deposits of gemstone. *Symposium on Mineral, Energy, and Water Resources of Thailand: Towards the Year 2000*, Bangkok, Thailand, 28–29 October, 485–495.

Limtrakun, P. 2003. *Origin and distribution of corundum from an intraplate alkali basaltic province in Thailand: Evidence from field and inclusion studies.* PhD thesis, University of Tasmania, Hobart, Australia, 276 pp, https://core.ac.uk/download/pdf/33332094.pdf.

Malsy, A.K., Karampelas, S., Schwarz, D., Klemm, L., Armbruster, T. & Tuan, D.A. 2012. Orangey-red to orangey-pink gem spinels from a new deposit at Lang Chap (Tan Huong-Truc Lau), Vietnam. *Journal of Gemmology*, **33**(1–4), 19–27, https://doi.org/10.15506/JoG.2012.33.1.19.

Merlet, C. 1994. An accurate computer correction program for quantitative electron probe microanalysis. *Mikrochimica Acta*, **114/115**(1), 363–376, https://doi.org/10.1007/bf01244563.

Nasdala, L., Banerjee, A., Häger, T. & Hofmeister, W. 2001. Laser-Raman micro-spectroscopy in mineralogical research. *Microscopy and Analysis, European Edition*, **70**, 7–9.

Nasdala, L., Smith, D.C., Kaindl, R. & Ziemann, M.A. 2004. Raman spectroscopy: Analytical perspectives in mineralogical research. *In*: Beran, A. & Libowitzky, E. (eds) *Spectroscopic Methods in Mineralogy*. Eötvös University Press, Budapest, Hungary, EMU Notes in Mineralogy **6**, 281–343, https://doi.org/10.1180/EMU-notes.6.7.

O'Neill, H.S.C. & Navrotsky, A. 1983. Simple spinels: Crystallographic parameters, cation radii, lattice energies, and cation distribution. *American Mineralogist*, **68**(1–2), 181–194.

Phyo, M.M., Franz, L., Bieler, E., Balmer, W. & Krzemnicki, M.S. 2019. Spinel from Mogok, Myanmar—A detailed inclusion study by Raman microspectroscopy and scanning electron microscopy. *Journal of Gemmology*, **36**(5), 418–435, https://doi.org/10.15506/JoG.2019.36.5.418.

Putnis, A. 1992. *Introduction to Mineral Sciences*. Cambridge University Press, Cambridge, 457 pp., https://doi.org/10.1017/cbo9781139170383.

Rancourt, D.G. & Ping, J.Y. 1991. Voigt-based methods for arbitrary-shape static hyperfine parameter distributions in Mössbauer spectroscopy. *Nuclear Instruments and Methods in Physics Research Section B: Beam Interactions with Materials and Atoms*, **58**(1), 85–97, https://doi.org/10.1016/0168-583x(91)95681-3.

Redhammer, G.J., Tippelt, G., Amthauer, G. & Roth, G. 2012. Structural and ^{57}Fe Mössbauer spectroscopic characterization of the synthetic $NaFeSi_2O_6$ (aegirine) – $CaMgSi_2O_6$ (diopside) solid solution series. *Zeitschrift für Kristallographie*, **227**(7), 396–410, https://doi.org/10.1524/zkri.2012.1514.

Rocholl, A. 1998. Major and trace element composition and homogeneity of microbeam reference material: Basalt glass USGS BCR-2G. *Geostandards and Geoanalytical Research*, **22**(1), 33–45, https://doi.org/10.1111/j.1751-908X.1998.tb00543.x.

Rohtert, W. 2002. Gem News International: Black spinel from Mexico. *Gems & Gemology*, **38**(1), 98–99.

Saminpanya, S. & Sutherland, F.L. 2008. Black opaque gem minerals associated with corundum in the alluvial deposits of Thailand. *Australian Gemmologist*, **23**, 242–253.

Schubnel, H.-J., Pinet, M., Smith, D.C. & Lasnier, B. 1992. *La Microsonde Raman en Gemmologie*. Association Française de Gemmologie, Paris, France, 60 pp. (in French).

Sickafus, K.E., Wills, J.M. & Grimes, N.W. 1999. Structure of spinel. *Journal of the American Ceramic Society*, **82**(12), 3279–3292, https://doi.org/10.1111/j.1151-2916.1999.tb02241.x.

Skogby, H. & Hålenius, U. 2003. An FTIR study of tetrahedrally coordinated ferrous iron in the spinel-hercynite solid solution. *American Mineralogist*, **88**(4), 489–492, https://doi.org/10.2138/am-2003-0402.

Slotznick, S.P. & Shim, S.H. 2008. In situ Raman spectroscopy measurements of $MgAl_2O_4$ spinel up to 1400°C. *American Mineralogist*, **93**(2–3), 470–476, https://doi.org/10.2138/am.2008.2687.

Srithai, B. 2007. *Geochemistry and petrogenesis of corundum from the Bo Ploi deposit, Kanchanaburi, Thailand.* PhD thesis, University College London, 337 pp., https://discovery.ucl.ac.uk/id/eprint/1445108/1/U592422.pdf.

Stähle, V., Altherr, R., Nasdala, L., Trieloff, M. & Varychev, A. 2017. Majoritic garnet grains within shock-induced melt veins in amphibolites from the Ries impact crater suggest ultrahigh crystallization pressures between 18 and 9 GPa. *Contributions to Mineralogy and Petrology*, **172**(10), article 86 (21 pp.), https://doi.org/10.1007/s00410-017-1404-7.

Stauffer, P.H. 1983. Unraveling the mosaic of Paleozoic crustal blocks in Southeast Asia. *Geologische Rundschau*, **72**(3), 1061–1080, https://doi.org/10.1007/bf01848354.

Sutthirat, C., Charusiri, P., Farrar, E. & Clark, A.H. 1994. New $^{40}Ar/^{39}Ar$ geochronology and characteristics of some Cenozoic basalts in Thailand. *International Symposium on Stratigraphic Correlation of Southeast Asia*, Bangkok, Thailand, 15–20 November, 306–321.

Sutthirat, C., Namphet, Y. & Shitangkool, N. 2010. Felsic xenoliths in corundum-related basalt at Khao Lun Tom, Bo Phloi District, Kanchanaburi Province, western Thailand. *Bulletin of Earth Sciences Thailand*, **3**(1), 28–37, www.geo.sc.chula.ac.th/BEST/volume3/Number1/4_BEST_3_1_004_Sutthirat%20et%20al.pdf.

Taran, M.N., Koch-Müller, M. & Langer, K. 2005. Electronic absorption spectroscopy of natural (Fe^{2+}, Fe^{3+})-bearing spinels of spinel s.s.-hercynite and gahnite-hercynite solid solutions at different temperatures and high-pressures. *Physics and Chemistry of Minerals*, **32**(3), 175–188, https://doi.org/10.1007/s00269-005-0461-z.

Tropf, W.J. & Thomas, M.E. 1991. Magnesium aluminium spinel ($MgAl_2O_4$). *In*: Palik, E.D. (ed) *Handbook of Optical Constants of Solids*. Academic Press Inc., New York, New York, USA, 883–898.

Udomchoke, V. 1988. Quaternary stratigraphy of the Khorat Plateau area, northeastern Thailand. *Workshop on Correlation of Quaternary Succession in South, East and Southeast Asia*, Bangkok, Thailand, 21–24 November, 69–94.

Vichit, P., Vudhichativanich, S. & Hansawek, R. 1978. The distribution and some characteristics of corundum-bearing basalts in Thailand. *Journal of the Geological Society of Thailand*, **3**, M4–M38.

Yaemniyom, N. 1982. *The petrochemical study of corundum-bearing basalts at Bo Phloi District, Kanchanaburi.* MSc thesis, Chulalongkorn University, Bangkok, Thailand, 100 pp., http://library.dmr.go.th/Document/DMR_Technical_Reports/1982/4523.pdf.

Zeug, M., Nasdala, L., Wanthanachaisaeng, B., Balmer, W.A., Corfu, F. & Wildner, M. 2018. Blue zircon from Ratanakiri, Cambodia. *Journal of Gemmology*, **36**(2), 112–132, https://doi.org/10.15506/JoG.2018.36.2.112.

The Authors

Ágnes Blanka Kruzslicz,
Prof. Dr Lutz Nasdala
and Prof. Dr Manfred Wildner
Institut für Mineralogie und Kristallographie,
University of Vienna, Althanstraße 14,
1090 Vienna, Austria
Email: lutz.nasdala@univie.ac.at

Dr Radek Škoda
Department of Geological Sciences,
Faculty of Science, Masaryk University,
Kotlářská 267/2,
61137 Brno, Czech Republic

Prof. Dr Günther J. Redhammer
Department of Chemistry and
Physics of Materials, University of Salzburg,
Jakob-Haringer-Strasse 2a,
5020 Salzburg, Austria

Prof. Dr Christoph Hauzenberger
NAWI Graz Geozentrum, Petrologie und
Geochemie, Universitätsplatz 2,
8010 Graz, Austria

Dr Bhuwadol Wanthanachaisaeng
College of Creative Industry,
Srinakharinwirot University,
114 Sukhumvit 23, Bangkok 10110,
Thailand; and Faculty of Gems, Burapha
University, Chanthaburi 22170, Thailand

Acknowledgements

Sample preparation was done by Andreas Wagner. We are indebted to Prof. Dr Eugen Libowitzky and Prof. Dr Gerald Giester for providing reference samples, Prof. Dr Christian L. Lengauer for help with the powder X-ray diffraction analysis, and Wolfgang Zirbs for technical assistance. Thanks are also due to Dr Chutimun Chanmuang N., Dr Christoph Lenz and Dr Manuela Zeug for fruitful discussions, and to Tidarat Pruttipako for the photo of the sterling silver ring in Figure 9. Constructive comments by three anonymous experts are greatly appreciated. Author ÁBK acknowledges support from the Institut für Mineralogie und Kristallographie (University of Vienna). Author BW acknowledges support from the Gem and Jewelry Institute of Thailand (Public Organisation), Bangkok.

Gem Exploration Using a Camera Drone and Geospatial Analysis: A Case Study of Peridot Exploration in British Columbia, Canada

Philippe Maxime Belley, Pattie Shang and Donald John Lake

ABSTRACT: This case study examines the use of a consumer-grade unmanned aerial vehicle (UAV, or drone) and geospatial analysis for peridot exploration. Gem-quality olivine occurs in peridotite xenoliths hosted by Chilcotin Group basalts in south-central British Columbia, Canada. Geographic information system (GIS) geospatial analysis and satellite image verification identified 73 exploration targets consisting of basalt outcrops and talus slopes in the southern Monashee Mountains near the cities of Kelowna and Vernon. A DJI Mavic Pro drone was used in conjunction with high-definition (HD) first-person-view goggles to assess 15 localities for peridot potential. Six of them contained peridotite xenoliths, but at concentrations (1–2 vol.%) far below that of economically viable peridot deposits (30–50 vol.%). The use of the drone saved considerable time in the field, and the combined GIS-UAV approach could be applied in the future to facilitate peridot exploration throughout a large area of central British Columbia. Camera-drone remote exploration could also be applied to other types of gem deposits, such as lapis lazuli and those hosted by granitic pegmatites.

The Journal of Gemmology, **37**(1), 2020, pp. 80–90, http://doi.org/10.15506/JoG.2020.37.1.80

Recent technological advances have significantly improved the range, flight time and camera quality of consumer-grade UAVs, and mass production has made them considerably more affordable. These improvements have made camera drones feasible, cost effective and potentially useful for the exploration and field reconnaissance of gem and mineral deposits. More-sophisticated drones capable of conducting hyperspectral imaging, aerial magnetic and photogrammetric surveys are already being employed in mining and exploration for various commodities (e.g. Kirsch *et al*. 2018; Jackisch *et al*. 2019). We present a case study demonstrating the use of GIS geospatial analysis combined with observations made with a camera drone and on-site in conjunction with basic exploration criteria to efficiently explore for basalt-hosted gem-quality peridot (e.g. Figures 1 and 2) in British Columbia (BC), Canada.

Production of peridot gems from BC has been sporadic and occasional, being primarily extracted by hobbyist collectors. The first record of peridot in BC was published by Galloway (1918), who noted that a prospector sent a number of stones from Timothy Mountain (also called Takomkane Mountain; Wilson 2014) to Tiffany & Co. for examination, but that they were too flawed to have significant value as a gem material. What is perhaps the most well-known peridot locality in BC, Lightning Peak, was first reported in a guidebook for mineral collectors by Sabina (1964). Several peridot occurrences have since been discovered (Wilson 2014; present article), and they

Figure 1: This basalt-hosted peridotite xenolith was found during field exploration in British Columbia, Canada. Several fragments of gem-quality peridot are visible on the surface of the broken xenolith, which is approximately 15 cm long. Photo by P. M. Belley.

have produced small amounts of rough material that yielded several dozen faceted stones weighing >1 ct. The largest peridot gems reported from the region weigh over 4 ct (or 3.52 ct for Lightning Peak specifically; Wilson 2014). Overall, gem-quality peridot is rare relative to the total amount of olivine present, since most xenoliths are generally too fine grained to yield facetable material (Wilson 2014).

BACKGROUND

Geology

Gem-quality peridot (Fe-bearing forsterite olivine) is primarily produced from two types of host rocks. In the first type, peridot typically forms euhedral crystals in open cavities or in talc/serpentine within peridotites or coarse-grained olivine dykes cutting peridotite (e.g.

Figure 2: The peridot in the xenolith shown in Figure 1 was faceted into numerous gemstones. The gems in this selection weigh up to 1.65 ct. Photo by P. M. Belley.

Egypt, Kurat *et al*. 1993; Myanmar, Kammerling *et al*. 1994; and Pakistan, Qasim Jan & Asif Khan 1996). In the second type, peridot occurs as crystalline aggregates in peridotite xenoliths that are hosted by alkali basalt (e.g. western Canada, Wilson 2014; China and North Korea, Koivula & Fryer 1986 and Zhang *et al*. 2019; Italy, Adamo *et al*. 2009; USA, Koivula 1981 and Fuhrbach 1992; and Vietnam, Thuyet *et al*. 2016).

In Canada, gem-quality peridot occurs within peridotite xenoliths in the Chilcotin Group basalts (CGB) of south-central British Columbia (Figure 3). The CGB are spread relatively thinly (averaging 70 m thick; Dostal *et al*. 1996) over an area of 25,000 km^2 in the intermontane super-terrane of central and southern BC (again, see Figure 3; Dostal *et al*. 1996; Dohaney 2009). The basalts erupted from 24 to 0.74 million years ago (Dostal *et al*. 1996 and references therein). They overlay various rock types, including Proterozoic orthogneiss, Devonian–Triassic basalt of the Nicola Group, Carboniferous–Permian greenschist, Jurassic granite, the Cretaceous Okanagan batholith, and Eocene volcanic rocks of the Kamloops and Penticton Groups (see Massey *et al*. 2005). Bevier (1983) concluded that the CGB were generated in a back-arc tectonic setting, possibly due to upwelling of the asthenosphere, in addition to possible influence from a mantle hot spot. The peridotite xenoliths (classified petrographically as primarily spinel lherzolite) were transported from the upper mantle to the earth's

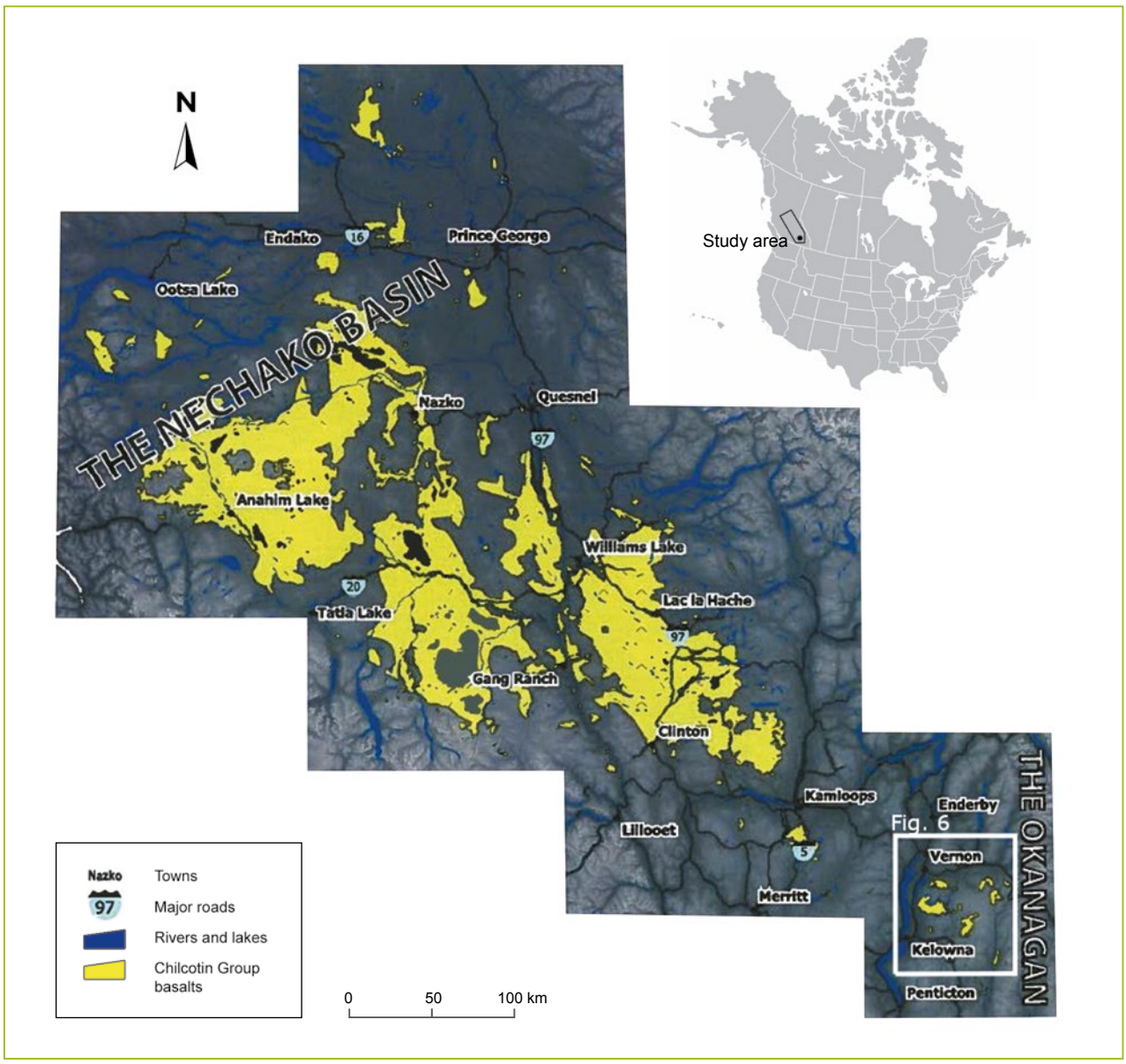

Figure 3: The study area is situated in south-central British Columbia, Canada, near the cities of Kelowna and Vernon. The distribution of Chilcotin Group basalts is shown in yellow-green. After Dohaney (2009); used with permission.

Figure 4: This view looking west from the basalt talus at Lightning Peak shows the typical terrain of the southern Monashee Mountains, where active logging takes place. See person for scale. Photo by P. M. Belley.

surface by the basaltic magma, which itself originated due to partial melting of upper mantle rocks. Only some flows contain peridotite xenoliths (e.g. Fujii & Scarfe 1982). The composition of olivine in the xenoliths from one locality in the study area was reported in the range of 87–92 mol.% forsterite (Fujii & Scarfe 1982).

The distribution and elevation of basalt exposures was influenced by the paleotopography (pre-existing hills and valleys) at the time of volcanism, with some flows having a 400 m difference in elevation (Mathews 1988). The landscape and rock outcrops were physically transformed by glacial erosion in the Pleistocene (Nasmith 1962) and subsequent erosion from freeze-thaw and gravitational forces, resulting in the formation of rock talus (e.g. Figure 4) below steep basalt outcrops.

Description of the Study Area

The study area is situated in the southern portion of the Monashee Mountains, just east of the cities of Kelowna and Vernon. It was selected because it is known to contain peridot and is in closest proximity to the authors' location in Vancouver. The elevation ranges between 1,200 and 2,140 m above sea level, and the region largely consists of hills and valleys covered primarily by coniferous forests (Figure 4). Active logging is ongoing and, as a result, gravel roads are locally present in the region. Talus can be present in steeper areas, especially along the sides of valleys. The challenging terrain, expansive forests and sparse roads make fieldwork in this area time consuming. The forests are home to numerous animals, including deer, moose, elk, cougars, wolverines, black bears and grizzly bears. Moose, deer and both species of bear were seen on several occasions during the authors' fieldwork.

MATERIALS AND METHODS

Exploration Criteria

Commercially significant basalt-hosted peridot deposits contain a high content of peridotite xenoliths: 30–50 vol.% at San Carlos, Arizona, USA (Vuich & Moore 1977) and Jilin, China (Wang 2017). Since only a small portion of peridotite xenoliths contain gem-quality material, and due to the gem's relatively low per-carat value, a high concentration of peridotite xenoliths is a key factor in the economic feasibility of a deposit.

Basalt containing about 5% or more of peridotite by volume will appear noticeably different when observed from a short distance in the field, which the authors confirmed in a camera-drone feasibility test (described below). Peridotite xenoliths can be identified in photographs and videos by their yellowish green colour and their blocky/subangular shapes within the dark basaltic matrix. For more effective exploration, the basalt needs to be well-exposed. Furthermore, the locality must be relatively accessible, since mining costs can become prohibitive in remote areas.

Therefore, the exploration criteria for basalt-hosted peridot can be summarised as: (1) occurrence of a basalt unit known to contain peridotite xenoliths, (2) good physical exposure of the rock unit, (3) relative ease of access and (4) high concentrations of peridotite within the basalt.

Geospatial Analysis

The first three exploration criteria mentioned above were employed to locate potential targets within the study area. Government of British Columbia data were used together with ESRI ArcGIS software to identify

exploration targets in the region. Several well-exposed examples of basalt-bearing talus in the study area have slopes equal to or greater than 30°, so slopes of such steepness were used to target talus for exploration. Slope was determined using the BC digital elevation model (0.75 arcsec x-y resolution, or 20–30 m). Locations of interest were determined by having the following conditions: (1) slope ≥30°, (2) bedrock geology consisting of CGB and (3) less than 10 km proximity to major roads or less than 2 km from local or logging roads. Exploration targets were then selected using Google Earth satellite imagery to filter out false positives, such as where a steep slope occurred in unconsolidated glacial sediment which, in areas, covers the older bedrock.

Camera Drone Exploration

Concentrations of peridotite within the basalt were evaluated using a DJI Mavic Pro drone (Figure 5), which weighs 734 g, has a maximum speed of 65 km/h, an overall flight time of 21 minutes (27 minutes maximum), a maximum transmission distance of 7 km (under ideal conditions), a GPS receiver and a 12.35 megapixel (effective pixels) 4K video camera. The device communicates with a radio controller and supplies a live HD video feed to the user via a smartphone or DJI Goggles. The latter are first-person-view flight goggles that receive data from and communicate with the drone in real time, which allowed us to see in far greater detail than through a smartphone app or external screen. This proved useful for rapidly assessing exploration targets as well as piloting the aircraft in close proximity to rocky outcrops and trees. However, a spotter was required when using the goggles both for legal purposes and to watch for bears.

The camera includes a 1/2.3-inch CMOS (complementary metal-oxide semiconductor) sensor and a lens with 5 mm focal length, field of view of 78.8°, f/2.2, distortion <1.5% and focus from 0.5 m to infinity. The maximum image size is 4,000 × 3,000 pixels. At 15 m flight elevation, the ground-sampling distance—the actual length of ground captured per pixel—is 0.46 cm/pixel. Although error is introduced by uneven surface topography, lens distortion, movement during capture, inaccuracy of height measurements above ground level and other factors, the ground-sampling distance is well below the expected xenolith size (e.g. commonly 5–15 cm at the San Carlos, Arizona deposit: Vuich & Moore 1977; typically 1–20 cm in Chilcotin Group basalts: Fujii & Scarfe 1982 and Wilson 2014) at distances from exposures achievable by the DJI Mavic Pro in talus (4–15 m), so the xenoliths should be clearly visible under ideal conditions. Xenoliths were identified remotely by visually inspecting photographs and live video feeds. The presence of yellow lichen, which is common at Lightning Peak, can obscure xenoliths. The xenoliths are differentiated upon closer examination of photographs by their green colour and subangular shape. While a quantitative, automated method of xenolith detection could be developed, the qualitative inspection of images required no complex development, minimal training and was extremely cost effective.

Figure 5: The DJI Mavic Pro foldable quadcopter camera drone was used for this study. It measures 33.5 cm diagonally (propellers excluded) and weighs 734 g. Photo courtesy of DJI.

RESULTS

Geospatial analysis with ArcGIS yielded 73 exploration targets in the study area (Figure 6). False positives were rare, and typically occurred in creek or river valleys that steeply cut through a top layer of unconsolidated sediment. At least four false negatives (where CGB outcrops were not successfully identified with geospatial analysis) were either found during fieldwork or seen in satellite images near identified targets. They tended to be in flatter areas that contain smaller talus slopes.

The camera drone was first tested at a location known to contain peridotite xenoliths in basalt: Lightning Peak (2,139 m elevation). At the time (4 June 2017) the locality was not readily accessible due to snow, so the drone was flown from a point more than 2 km away (Figure 7). Basalt blocks at Lightning Peak contain 3–5 vol.% peridotite (visually estimated from a previously done on-foot traverse across the talus). Yellowish green peridotite xenoliths were successfully resolved by the drone camera hovering approximately 17 m above the talus with the camera pointing straight down (Figure 8).

The drone was then used to evaluate exploration targets in other areas that ranged from 0.2 to 2.1 km away

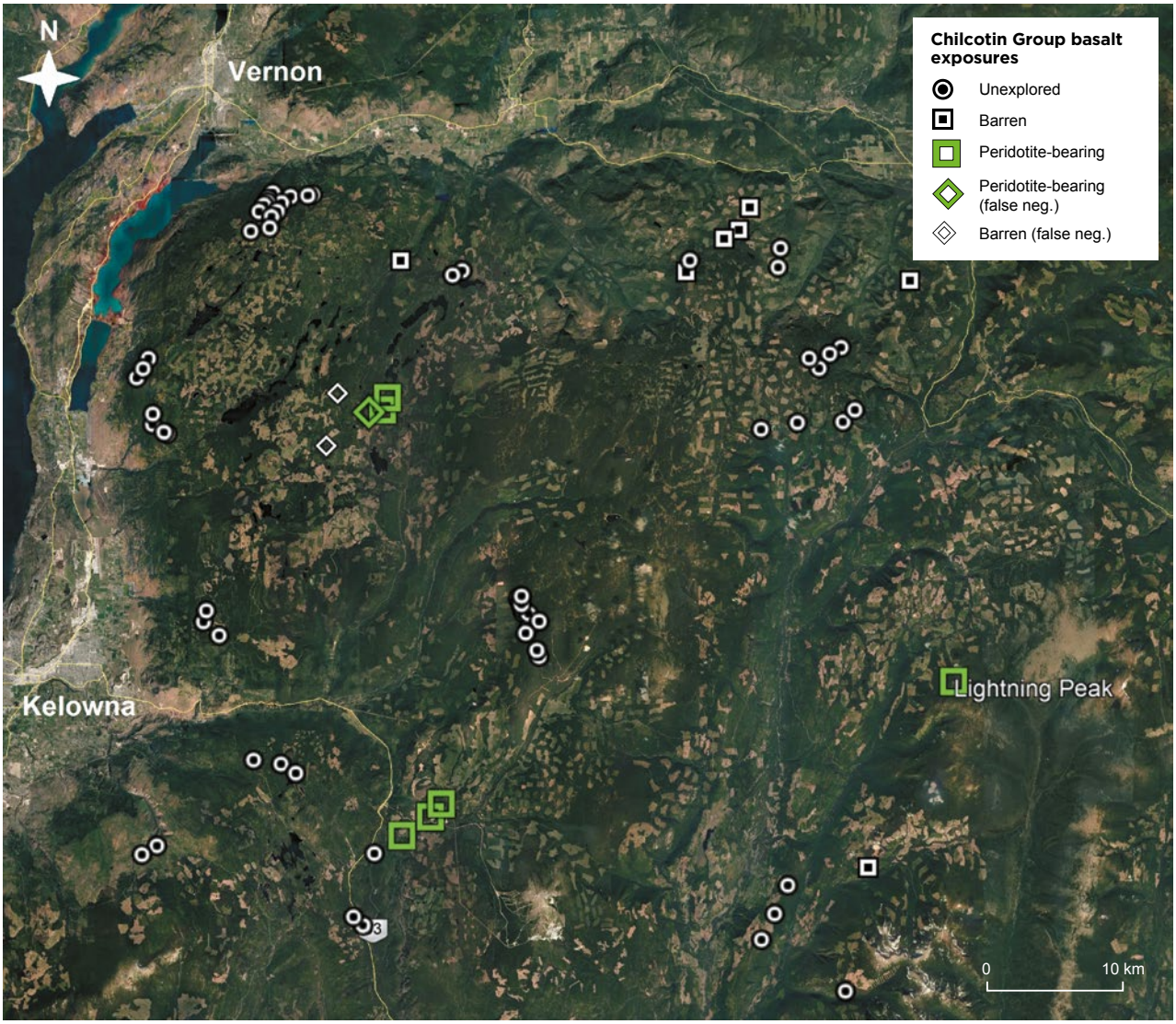

Figure 6: Exploration target results from geospatial analysis of Chilcotin Group basalt exposures in the study area are shown together with proximity to roads (yellow lines). Camera-drone exploration of some of these localities indicated those that were barren of peridotite xenoliths, as well as those containing peridotite xenoliths. Also shown are a few false negatives (i.e. those not identified via the ArcGIS analysis), as well as unexplored exposures. Satellite imagery from Landsat/Google Earth.

by air from the nearest road access point (e.g. Figure 9), with single-flight paths reaching 4.35 km in total distance. Fieldwork consisted of a total of six days in late spring and summer of 2017–2019, during which 16 targets were examined (three of which were false negatives). Excluding the previously mentioned Lightning Peak locality, six of the targets contained peridotite xenoliths and gem-quality peridot, while the other nine did not contain peridotite (again, see Figure 6). We found that peridotite xenoliths are more difficult to resolve with the drone at lower-elevation localities (e.g. at about 1,350 m) because the rocks have significantly more lichen cover than at higher elevations (e.g. at Lightning Peak), and because the peridotite at lower elevations is usually significantly more weathered. In basalt blocks that have been extensively exposed to the elements, xenoliths can be completely weathered out (Figure 10a). Xenoliths in basalt from more recent talus may show brownish surficial weathering (Figure 10b), while rare, very recent rock slides may expose fresh peridotite (Figure 1). Xenoliths in all stages of weathering were identified in drone images.

A low abundance of peridotite xenoliths typified all six targets (about 1–2 vol.% as confirmed by in-person visual estimation, compared to about 3–5 vol.% at Lightning Peak). Approximately 1–2% of the xenoliths contained facetable material (expected finished weight >0.5 ct). The cluster of localities in the southern part of the study area (again, see Figure 6) contained sparse, coarse-grained olivine crystals (2–5 cm) within peridotite xenoliths, but these crystals were generally non-transparent (the largest transparent stone faceted from this material weighed 1 ct). In the northernmost cluster of

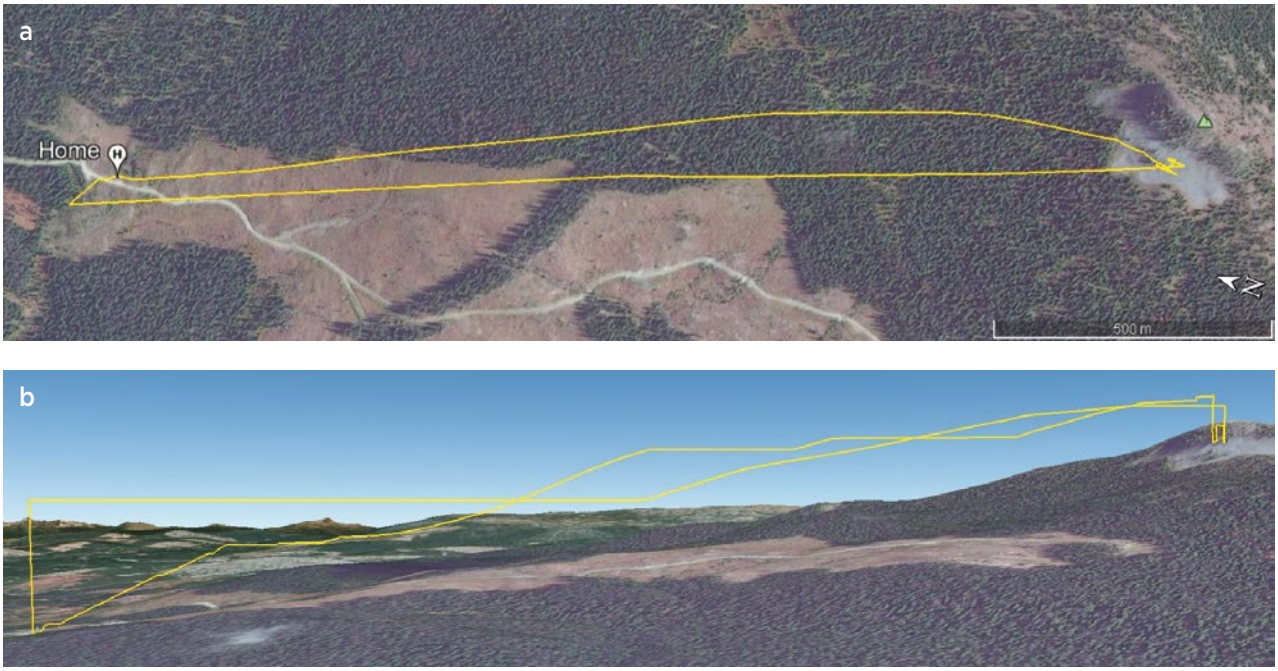

Figure 7: The flight path for the Lightning Peak test run is shown as yellow lines, in both top (**a**) and side (**b**) views. An enlarged side view (**c**) depicts the flight path over the talus slope on the western side of Lightning Peak. The 'home' (take-off) point is at an elevation of 1,766 m above sea level, and the top of Lightning Peak is at 2,139 m. The lowest part of the talus is at 2,050 m. Satellite imagery and terrain from Landsat/Google Earth; flight data processed by Airdata.com.

peridot-bearing localities, we found a few xenoliths containing gem-quality material. At one of these localities, a recent slide exposed a very large xenolith (originally about 30 × 20 × 20 cm) that broke into five pieces (e.g. Figure 1), which we found loose and within basalt blocks on the surface of the talus during an in-person traverse. Faceting of rough material from this xenolith produced 22 carats of commercial-grade cut stones weighing 0.80–1.65 ct (Figure 2), but this occurrence produced no significant gem material outside of this find.

A small portion of the xenoliths consisted of pyroxenite with very minor or no olivine. At one locality, gemmy dark green pyroxene xenocrysts up to 2 cm across occurred in low concentrations within basalt that was devoid of peridotite xenoliths. The pyroxene xenocrysts were observed in person and were too small to be identified in drone images.

DISCUSSION

Suitability of Geospatial Analysis

While geological maps could be cross-referenced to satellite images manually to locate exposures of Chilcotin Group basalt, the process is very time consuming. Geospatial analysis using ArcGIS proved extremely effective at identifying these exposures in a large-scale, automated fashion in minimal time. This process may immensely facilitate the identification of CGB outcrops over a 500 × 250 km region of central BC to the northwest of the study area. Satellite images also proved very useful both to confirm the occurrence of CGB talus and to plan navigation on logging roads. False negatives (where CGB outcrops were not successfully identified) occurred in more flat-lying areas, so geospatial analysis is most accurate in steep terrain.

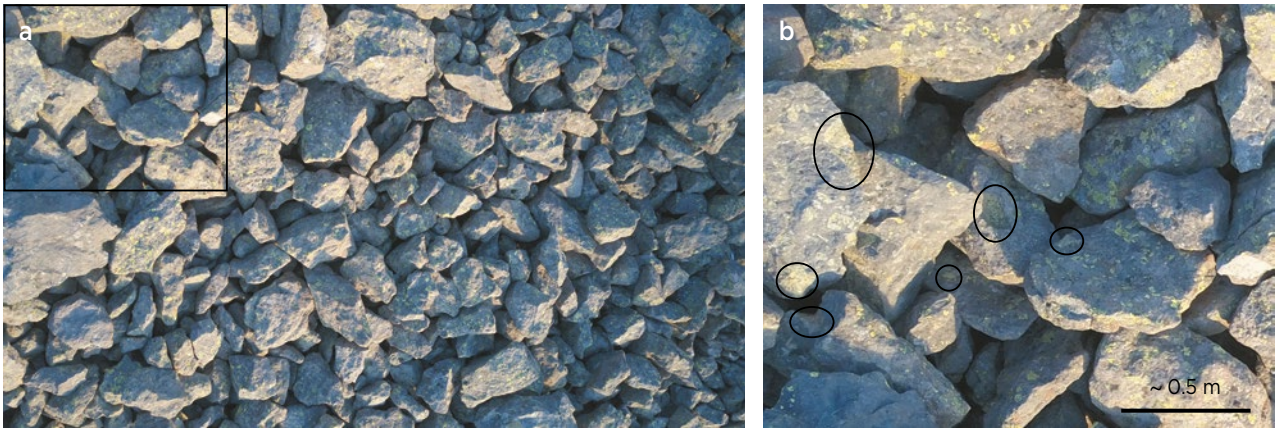

Figure 8: (**a**) This drone photograph of basalt talus at Lightning Peak (elevation 2,083 m) was taken from approximately 17 m above ground level. (**b**) A close-up of the upper left portion of (a) shows peridotite xenoliths (circled) in blocks of basalt. The locality could not be accessed by foot due to an abundance of snow, but snow-free parts of the talus could nonetheless be inspected with the drone. Photo taken 5 June 2017 with the camera oriented straight down (–90°) towards the ground.

Figure 9: An example flight path for a peridot target (here, barren basalt) is shown as yellow lines, in both top (**a**) and side (**b**) views. The 'home' (take-off) point is at an elevation of 1,407 m and the top of the basalt cliff is at approximately 1,550 m. Satellite imagery and terrain from Landsat/Google Earth; flight data processed by Airdata.com.

Figure 10: These two close-ups of the talus at a locality in the northernmost cluster of peridot occurrences (elevation approximately 1,350 m) show (**a**) holes resulting from the weathering of peridotite xenoliths and (**b**) weakly weathered brownish peridotite xenoliths in a boulder from a more recent rock fall. The weathering-out of the peridotite shown in photo (a) is not common at higher elevations (e.g. Lightning Peak). The camera was oriented straight down (–90°) towards the ground.

Camera Drone Exploration: Benefits and Limitations

Using the drone camera in the field saved considerable time and effort, since verifying targets remotely is significantly faster and easier than inspecting them in person. In addition, the telemetric and sensor capabilities of modern consumer-grade camera drones such as the DJI Mavic Pro make it possible to determine an approximate ground-sampling distance using altitude data; however, there is room for improvement. For one trip, we estimate that our three days of work would have taken two weeks with traditional prospecting (much time is lost setting up and taking down camp, and fewer sites can be verified in a day via hiking). The HD first-person-view goggles were useful for immediately assessing peridotite abundance, the alternative being the post-flight examination of photographs and video footage. More importantly, the goggles give a much clearer live view than a smartphone, which helped avoid obstacles (e.g. trees and branches) during the final approach. One limitation of the drone is that forest can sometimes obstruct communication with the drone, making a close approach to the talus (<15 m above surface) problematic due to difficulties in maintaining the live video feed. Since a close approach to talus is necessary for proper assessment, the exposure must be within (or close to being in) the line of sight. Vertical basalt exposures above talus were sufficiently above the tree line to enable target assessment in forested areas.

The presence of peridotite xenoliths in basalt—even at low concentrations (3–5 vol.%)—was easy to detect visually from images taken at approximately 15 m above ground level. However, some conditions make peridotite detection difficult: (1) weathering at lower elevations (about 1,350 m; causing round-shaped holes in the basalt that correspond to the locations of former peridotite xenoliths or a brownish appearance of less-weathered xenoliths; see Figure 10), (2) excessive lichen cover (more common at lower elevations and probably also on south-facing slopes) and (3) low peridotite concentrations. Nevertheless, it is probable that a viable peridot deposit (containing 30–50 vol.% peridotite in basalt) would be evident in drone-camera footage even under these conditions. Despite the effects of weathering, the presence of peridotite xenoliths was successfully detected from drone images. However, our field observations expanded the exploration criteria from locating only green subangular inclusions in basalt to include light brown weathered peridotite and holes left by the complete weathering of peridotite. It should be noted that open cavities or large vesicles in basalt could be mistaken for weathered xenoliths, although no such instances were observed during our fieldwork.

Assessment of Peridot Potential in the Kelowna Area

While the CGB in the Kelowna area of British Columbia has produced good-quality, albeit relatively small, peridot gemstones (e.g. Figure 11), the source material (peridotite xenoliths) was absent from more than half of the localities we examined. Even when present, the concentration of peridotite xenoliths (generally 1–2 vol.% and up to 5%) in the CGB is far below that at commercially mined deposits (30–50 vol.% at San Carlos, Arizona, and Jilin, China; Vuich & Moore 1977 and Wang 2017, respectively). Despite this, much of the CGB remains unexplored

Figure 11: South-central British Columbia, Canada, has produced small amounts of gem-quality peridot with good colour but typically in small sizes. Shown here is a rough piece (2.5 cm wide) from Lightning Peak and three faceted stones (1.1–1.25 ct) from the northernmost peridot-producing locality in Figure 6. Further gem exploration of basaltic terranes in this region using the remote-sensing techniques described in this article could result in additional production of gem-quality peridot. Photo by Michael Bainbridge.

for gem-quality peridot. Many more exploration targets identified during this study remain to be examined, and the potential for commercially viable peridot deposits may exist elsewhere in the CGB, which covers an area of 25,000 km^2 in south-central BC (Dostal *et al.* 1996). Potential also exists in other basalt units of the region, such as the Endako Group (Brearley *et al.* 1984).

Application to Other Gem Deposit Types

Qualitative camera-drone exploration is suitable for any deposit that features colours or textures easily recognisable from a distance, and the technique significantly increases productivity—particularly in steep terrain. Examples of gem deposits that might be prospected using camera drones include: (a) lapis lazuli, which is bright blue and requires large quantities to be economically viable for mining; and (b) granitic pegmatite dykes, which may be visible cross-cutting country rocks in mountainous terrain or exposed due to a relative lack of weathering. Qualitative visual examination of drone video/images is likely insufficient to detect gem deposits with a less characteristic appearance when observed from a distance. UAV exploration is most effective in areas with good surficial rock exposure, such as in polar regions (e.g. as suggested by Belley & Groat 2020) and in arid and alpine climates.

CONCLUSIONS

Geospatial analysis combined with the use of a camera drone dramatically improved the time and cost efficiency of exploring for peridot deposits in the CGB of south-central British Columbia. Peridotite xenoliths were resolved by the drone at an altitude of approximately 17 m, even at low concentrations (3–5 vol.%), but they were more difficult to observe at localities where weathering and lichen growth were more intense. However, these challenges are not expected to interfere with the remote detection of an important peridot gem deposit (i.e. basalt containing about 30–50 vol.% peridotite). Known peridot occurrences in the study area contained low peridotite concentrations (1–5 vol.%) relative to important deposits worldwide, but much of the CGB remain unexplored. The method outlined in this study could greatly facilitate exploration of the vast CGB flows located in a 500 × 250 km area of south-central BC. Drone-based visible-light imaging may also be useful for the exploration of lapis lazuli and pegmatite-hosted gem deposits.

REFERENCES

Adamo, I., Bocchio, R., Pavese, A. & Prosperi, L. 2009. Characterization of peridot from Sardinia, Italy. *Gems & Gemology*, **45**(2), 130–133, https://doi.org/10.5741/gems.45.2.130.

Belley, P.M. & Groat, L.A. 2020. Metamorphosed carbonate platforms and controls on the genesis of sapphire, gem spinel, and lapis lazuli: Insight from the Lake Harbour Group, Nunavut, Canada and implications for gem exploration. *Ore Geology Reviews*, **116**, article 103259 (10 pp.), https://doi.org/10.1016/j.oregeorev.2019.103259.

Bevier, M.L. 1983. Implications of chemical and isotopic composition for petrogenesis of Chilcotin Group basalts, British Columbia. *Journal of Petrology*, **24**(2), 207–226, https://doi.org/10.1093/petrology/24.2.207.

Brearley, M., Scarfe, C.M. & Fujii, T. 1984. The petrology of ultramafic xenoliths from Summit Lake, near Prince George, British Columbia. *Contributions to Mineralogy and Petrology*, **88**(1–2), 53–63, https://doi.org/10.1007/bf00371411.

Dohaney, J.A.M. 2009. *Distribution of the Chilcotin Group basalts, British Columbia.* M.S. thesis, University of British Columbia, Vancouver, Canada, 125 pp., https://doi.org/10.14288/1.0052663.

Dostal, J., Hamilton, T.S. & Church, B.N. 1996. The Chilcotin basalts, British Columbia (Canada): Geochemistry, petrogenesis and tectonic significance. *Neues Jahrbuch für Mineralogie, Abhandlungen*, **170**(2), 207–229.

Fuhrbach, J.R. 1992. Kilbourne Hole peridot. *Gems & Gemology*, **28**(1), 16–27, https://doi.org/10.5741/gems.28.1.16.

Fujii, T. & Scarfe, C.M. 1982. Petrology of ultramafic nodules from West Kettle River, near Kelowna, southern British Columbia. *Contributions to Mineralogy and Petrology*, **80**(4), 297–306, https://doi.org/10.1007/bf00378002.

Galloway, J.D. 1918. North–Eastern District (No. 2). *In*: Sloan, W. (ed) *Annual Report of the Minister of Mines for the Year Ending 31st December 1917 Being an Account of Mining Operations for Gold, Coal, etc. in the Province of British Columbia*. William H. Cullin, Victoria, British Columbia, Canada, F86–F136.

Jackisch, R., Yuleika, M., Zimmermann, R., Pirttijärvi, M., Saartenoja, A., Heincke, B.H., Salmirinne, H., Kujasalo, J.-P., *et al.* 2019. Drone-borne hyperspectral and magnetic data integration: Otanmäki Fe-Ti-V deposit in Finland. *Remote Sensing*, **11**(18), article 2084 (27 pp.), https://doi.org/10.3390/rs11182084.

Kammerling, R.C., Scarratt, K., Bosshart, G., Jobbins, E.A., Kane, R.E., Gübelin, E.J. & Levinson, A.A. 1994. Myanmar and its gems – An update. *Journal of Gemmology*, **24**(1), 3–40, https://doi.org/10.15506/JoG.1994.24.1.3.

Kirsch, M., Lorenz, S., Zimmermann, R., Tusa, L., Möckel, R., Hödl, P., Booysen, R., *et al.* 2018. Integration of terrestrial and drone-borne hyperspectral and photogrammetric sensing methods for exploration mapping and mining monitoring. *Remote Sensing*, **10**(9), article 1366 (31 pp.), https://doi.org/10.3390/rs10091366.

Koivula, J.I. 1981. San Carlos peridot. *Gems & Gemology*, **17**(4), 205–214, https://doi.org/10.5741/gems.17.4.205.

Koivula, J.I. & Fryer, C.W. 1986. The gemological characteristics of Chinese peridot. *Gems & Gemology*, **22**(1), 38–40, https://doi.org/10.5741/gems.22.1.38.

Kurat, G., Palme, H., Embey-Isztin, A., Touret, J., Ntaflos, T., Spettel, B., Brandstätten, F., Palme, C., *et al.* 1993. Petrology and geochemistry of peridotites and associated vein rocks of Zabargad Island, Red Sea, Egypt. *Mineralogy and Petrology*, **48**(2–4), 309–341, https://doi.org/10.1007/bf01163106.

Massey, N.W.D., MacIntyre, D.G., Desjardins, P.J. & Cooney, R.T. 2005. *Digital Geology Map of British Columbia: Whole Province*. British Columbia Geological Survey Geofile 2005-1, scale 1:250,000, British Columbia Ministry of Energy and Mines, Vancouver, Canada.

Mathews, W.M. 1988. Neogene geology of the Okanagan Highland, British Columbia. *Canadian Journal of Earth Sciences*, **25**(5), 725–731, https://doi.org/10.1139/e88–068.

Nasmith, H. 1962. *Late Glacial History and Surficial Deposits of the Okanagan Valley, British Columbia.* British Columbia Department of Mines and Petroleum Resources Bulletin 46, 46 pp.

Qasim Jan, M. & Asif Khan, M. 1996. Petrology of gem peridot from Sapat mafic–ultramafic complex, Kohistan, NW Himalaya. *Geological Bulletin, University of Peshawar*, **29**, 17–26.

Sabina, A.P. 1964. *Rock and Mineral Collecting in Canada, Volume 1: Yukon, Northwest Territories, British Columbia, Alberta, Saskatchewan, Manitoba*. Geological Survey of Canada Miscellaneous Report 8, 147 pp.

Thuyet, N.T.M., Hauzenberger, C., Nguyen, N.K., Cong, T.D., Chu, V.L., Nguyen, T.M., Nguyen, H. & Häger, T. 2016. Peridot from the Central Highlands of Vietnam: Properties, origin, and formation. *Gems & Gemology*, **52**(3), 276–287, https://doi.org/10.5741/gems.52.3.276.

Vuich, J.S. & Moore, R.T. 1977. Bureau studies olivine resources on San Carlos Apache Reservation. *Field Notes from the Arizona Bureau of Mines*, **7**(2), 1, 6–10.

Wang, J. 2017. Geological characteristics and metallogenic rules of peridotite gem mine in Yiqisong District, Dunhua City, Jilin Province (China). *Resource Information and Engineering*, **32**(4), 50–52, https://doi.org/10.19534/j.cnki.zyxxygc.2017.04.024 (in Chinese).

Wilson, B.S. 2014. Coloured gemstones from Canada. *In*: Groat, L.A. (ed) *Geology of Gem Deposits*. Mineralogical Association of Canada Short Course Series Vol. 44, Québec City, Québec, Canada, 375–405.

Zhang, Z., Ye, M. & Shen, A.H. 2019. Characterisation of peridot from China's Jilin Province and from North Korea. *Journal of Gemmology*, **36**(5), 436–446, https://doi.org/10.15506/JoG.2019.36.5.436.

The Authors

Dr Philippe Maxime Belley, Pattie Shang and Donald John Lake
University of British Columbia, Vancouver, British Columbia, Canada
Email: phil.belley@gmail.com

Acknowledgements

The authors thank Brad Wilson for granting access to his mineral claim on Lightning Peak. We are grateful to Xiaoyuan Chen for help with translating a Chinese-language reference. We thank three anonymous reviewers for helpful comments that improved the manuscript.

Conferences

THE PEARL SYMPOSIUM

DANAT, the Bahrain Institute for Pearls & Gemstones, hosted The Pearl Symposium on 14–15 November 2019 in Bahrain, a few days before the CIBJO Congress in Manama. This scientific event was promoted under the Pearl Revival Initiative, a programme that articulates historical, cultural, economic, biological and environmental knowledge to bring back the allure of the historically relevant natural pearl industry in Bahrain. The event was attended by more than 130 delegates from at least 28 countries. It started with a morning walk through the Pearling Trail in Muharraq (the former capital of Bahrain), a UNESCO world heritage site with a long-time tradition of pearl fishing, drilling and manufacturing.

Talks began that afternoon in the Sheik Ebrahim Center for Culture and Research with opening remarks by DANAT's CEO **Noora Jamsheer** and CIBJO president **Gaetano Cavalieri**. Keynote speaker **Dr Mohammed Bin Daina**, chief executive of the Supreme Council for Environment of the Kingdom of Bahrain, followed with an overview of Bahrain and its aquatic environment, focusing on historical and current pearling activities, in addition to the country's cultural, artistic, economic and tourism potential.

The technical presentations started with **Justin Hunter** (J. Hunter Pearls Fiji, Savusavu) on 'Pearling and the Environment – The Blue Pledge'. He pointed out the benefits of sustainable pearl farming for both local communities and the environment in regions with limited economic opportunities, which also host the greatest concentrations of marine biodiversity and are prone to the effects of climate change. The Blue Pledge for Sustainable Pearls is an initiative by three pearl-farming companies—J. Hunter Pearls Fiji, Jewelmer (Philippines) and Paspaley Pearls (Australia)—that merges conservation and economic opportunities, and seeks to raise awareness of sustainable luxury through cultured pearls, especially among eco-conscious millennials.

A well-documented overview on the 'The History and Archaeology of Pearl Fishing in Bahrain and the Gulf, 5500 BC to 1950 AD' was offered by **Dr Robert Carter** (London's Global University). He stressed that Bahrain has been the global centre of pearl production throughout most of recorded history, with archaeological evidence that pearling in the Gulf has been known for more than 7,500 years (i.e. since the Stone Age). Under the Greeks and Romans, Bahrain (then known as Tylos or Stoidis) was an important pearling area that also supplied the ancient Sasanian and Byzantine markets. There is evidence that great wealth was made in Bahrain during that period due to the pearl trade. For centuries, pearl fishing and trade were the main sources of income in Bahrain, especially in the Muharraq area after the early 1800s, with production peaking in the early 1900s. After the Great Depression started in the late 1920s and cultured pearls appeared on the international market, the value of the local natural pearls fell by nearly 90%.

Noura Al Sayeh (Architectural Affairs, Bahrain Authority for Culture and Antiquities, Manama) elaborated on the 'The History of the Pearling Trail', a project initiated in 2005 to document the cultural legacy of Bahrain's pearling activities—especially during the period when Muharraq was the capital (1810–1923)—including crafts and other activities related to pearl fishing, fashioning and trade. The initiative also seeks to preserve pearl-related buildings and their typical architecture. The economic impact of the pearl industry in Bahrain was quite significant to the urban development of Muharraq, until the 1930s when earnings related to pearling declined steeply. The project's goal is to translate the full cultural and urban legacy of pearling into a 3 km walking trail (which conference delegates visited that morning). The Pearling Trail encompasses 17 houses and public squares along the pedestrian path, including the homes of pearl divers and those of wealthy pearl merchants.

Dr Mohamed Al Rumaidh (marine biology and ocean science researcher) summarised investigations of pearl 'oyster' resources in Bahrain, especially regarding the local mollusc, *Pinctada radiata*. This research is based on studies from 1985 onward (i.e. 30 years after the last official pearl-fishing season in the mid-1950s), when a massive amount of data was collected on the pearl oyster resources. The research surveyed important oyster beds and provided statistical data on the yield and size of pearls from different locations, as well as the influence of fluctuations in pH, salinity and water temperature on

the breeding of the molluscs. The average number of shells was found to be 4–5.5 per square metre, totalling in excess of 200,000–400,000 per fishing area. The occurrence of pearls in the molluscs ranged from 1.9 to 7.9%, around 95% of which were below 3 mm, 4% were about 3 mm and only 1% measured 4+ mm.

Gina Latendresse (American Pearl Company Inc., Nashville, Tennessee, USA) reviewed the history of natural pearls from the Americas. Her father was John Latendresse, a key player in the production of shell beads for the cultured pearl industry. As his daughter, she witnessed not only the few natural pearls that were brought in by local fisherman but also her father's 20-year career producing beaded freshwater cultured pearls in America, an accomplishment that was first announced in 1983. Pearling in the Americas goes back to prehistoric times, according to 2,000-year-old archaeological evidence in Ohio. Latendresse described a pearl rush that occurred throughout the USA in the late 1800s to early 1900s, when significant quantities of natural freshwater pearls were obtained, including some of large size that were reportedly used by European Art Nouveau artists such as René Lalique.

The second day of The Pearl Symposium began with a panel discussion led by natural-pearl traders **Mohammed Al Mahmood** (Bahrain) and **Adi Al Fardan** (United Arab Emirates) and moderated by **Kenneth Scarratt** (ICA GemLab, Bangkok, Thailand). The discussion focused on specifics of pearl trading in the Gulf, a relatively unknown subject amongst the gemmological community. The current difficulty in sourcing fine-quality natural pearls (Figure 1), especially above certain sizes, contrasts with the relatively less-challenging times of the past. A fine, graduated necklace can take one or more years to assemble, considering that local pearl fishermen currently offer their findings on average only once a week. Amongst traders, pearls are measured by the *chaw* (an old Indian method to convert the weight of natural pearls into volume units for evaluation) rather than by the carat, although some still use ounces or pearl grains. The pricing of natural pearls is usually established through discussions within the very small pearl-traders' community spread throughout the Gulf, as well as in India and elsewhere in Asia.

Figure 1: These natural pearls from *Pinctada radiata* were presumably fished off Bahrain. The largest pearl is about 9 mm in maximum dimension. Photo © DANAT.

Kenneth Scarratt then delivered the second-day's keynote address, on the origins and modern trade usage of the term *keshi* ('poppy seed' in Japanese) in connection with natural and cultured pearls. The trade and consumers currently associate *keshi* with a non-beaded saltwater cultured pearl that resulted as an accidental by-product or intentional product of a culturing process. However, in Japan this term was originally used for the very small, rare natural pearls historically produced by *Pinctada fucata* (commonly known as the akoya pearl oyster) before the advent of pearl culturing research in the late 1890s to the early 20th century. The term was adopted by the trade and its meaning eventually corrupted to its current use worldwide. Thus, *keshi* has become a trade term for non-beaded saltwater cultured pearl by-products of various size and no longer refers to small natural seed pearls.

Abeer Al Alawi (DANAT) gave a well-illustrated presentation on the challenges presented by seed pearls in the laboratory. By law, Bahrain has prohibited the import of cultured pearls into the country since 1990. The vast majority of pearls entering Bahrain before then were seed pearls (typically 2 mm and below), which variously consisted of natural pearls or non-beaded saltwater or freshwater cultured pearls. Until 1997, testing at the former Gem & Pearl Testing Laboratory of Bahrain was performed by random sampling. If parcels or hanks had less than 10% cultured pearls, a 'pass' grade would enable them to enter the country. If they contained more than 10%, they would be returned to their origin. After 1997, the rules changed to require that each and every pearl be inspected, and the 'pass' grade for lots was reduced to 5%. Since its establishment in 2017, DANAT has played an important role in screening imported pearl products using modern testing equipment to detect undisclosed cultured or imitation pearls before being cleared through customs. As a consequence of this effective testing, a lower percentage of cultured pearls has entered Bahrain in recent years.

Nicholas Sturman (Gemological Institute of America [GIA], Bangkok, Thailand) recounted some of his interesting laboratory experiences with pearls, not only at GIA but also in his early career. He first reviewed the evolution of pearl identification techniques, from the endoscope (used by Basil Anderson at the Diamond, Pearl and Precious Stone Laboratory Branch of the London Chamber of Commerce, established in 1925) and old Lauegrams used to detect beaded cultured pearls, to custom-developed X-ray films, which were inspected under magnification to detect identifying features (a technique introduced in 1929). Today, pearl testing tackles new challenges (such as non-beaded cultured pearls) with sophisticated equipment like real-time X-radiography, X-ray computed microtomography, X-ray luminescence and energy-dispersive X-ray fluorescence, often supported by UV-Vis-NIR, Raman and photoluminescence spectroscopy, as well as chemical analysis by LA-ICP-MS. Occasionally, there are still divergent interpretations of the data collected, which demonstrates that pearl identification is not always a straightforward process. Laboratory experience is crucial when it comes to testing pearls, even when using the most sophisticated techniques.

Dr Hashim Al Sayed (University of Bahrain) offered a biological perspective on the existing pearl oyster banks in Bahrain, including their life cycle. He reminded the audience that pearl oysters are a renewable resource and more intensive scientific research is needed. He then presented a few facts related to the local molluscs. Different species of the *Pinctada* genus occur in the Gulf, but the most common is *P. radiata*, with densities that can reach up to 5–10 shells per square metre. Environmental conditions support their abundance around Bahrain, including the water temperature, abundant light (due to shallow water) and relatively high Ca content of the water. Dr Al Sayed elaborated on the ecological context of *P. radiata* (a filter-feeding organism), and described its nutritional properties, since local communities use this mollusc as meat. Its growth rate, according to regular measurements of shell length, was found to be about 58 mm in the first year (higher than in Japan).

This author presented a review of 'Antique and Museum Pearls' (Figure 2), starting with fossil pearls. While archaeological findings in the Gulf prove the antiquity of pearling activities there, even older finds have been reported from Baja California, Mexico, where worked pearls were radiocarbon dated to 8,500 years old. The significant use of pearls during ancient Roman times and the subsequent Byzantine period is illustrated by artefacts in various museums. The use of European freshwater pearls was significant in the Middle Ages

Figure 2: A presentation on famous and historic pearls was given at The Pearl Symposium by Rui Galopim de Carvalho. Photo © DANAT.

and after, notably in 19th-century jewellery from Russia. Important pearls of known historical provenance include La Peregrina, which was last seen at Elizabeth Taylor's estate auction at Christie's New York in 2011. La Peregrina has been erroneously represented as Mary Tudor's pearl, and recent research has shown that these two pear-shaped pearls are not one and the same. Other famous pearls include the Hope and Sleeping Lion pearls, the Mancini pearls, Marie Antoinette's pearl pendant and necklace, and Mae Plant's famous 1917 Cartier double-strand necklace.

Jean-Pierre Chalain (Swiss Gemmological Institute SSEF, Basel, Switzerland) delivered a talk prepared by **Dr Michael Krzemnicki** titled 'New Frontiers in Pearl Analysis: Age Dating, DNA Fingerprinting, and Novel Radiographic Methods'. He shared recent research conducted by SSEF on pearl testing, primarily on the separation of natural from cultured pearls that, for the most part, is straightforward. However, in some cases the results are a matter of opinion based on an educated interpretation of data collected from visual observations and advanced testing (e.g. X-radiography and EDXRF and Raman spectroscopy). In addition, radiocarbon dating has been successfully used on pearls. This quasi-non-destructive technique, which requires approximately 4 mg (0.02 ct) of powder (typically collected from a drill hole when possible), enables the dating of historically important samples and the separation of natural from cultured pearls based on their age. DNA fingerprinting has also proven useful, particularly for determining the species of pearl molluscs. Again, a very small amount of powdered sample is needed (as little as 2 mg). SSEF collaborates with ETH (Eidgenössische Technische Hochschule) and the Institute of Forensic Medicine at the University of Zurich to provide these services to the trade. Chalain also described two relatively new testing methods being developed to better visualise the internal structures of pearls: (1) simultaneous X-ray phase-contrast and darkfield imaging, and (2) neutron radiography and tomography.

Dr Stefanos Karampelas (DANAT) gave a well-illustrated talk on 'Pearl Species Determination: Possibilities and Limitations'. He pointed out that the availability of Central American pearls in the 1500s and 1600s (often called 'occidental pearls') made it possible to create necklaces by mixing them with Gulf pearls (often called 'Oriental pearls'), and he also noted that pearl-origin determination has traditionally been based on essentially historical information. In the 1980s, demand developed for the origin determination of cultured pearls. Today there is strong demand for the determination of mollusc origin (i.e. the host mollusc species and its location) for both nacreous and non-nacreous pearls, but only a few laboratories issue such reports. The methodology involves visual observation, radiographic (internal structure imaging) and DNA-sequencing techniques, supported by chemical and spectroscopic data (e.g. UV-Vis-NIR reflectance and Raman spectroscopy for organic pigment identification). DNA testing of pearls is not yet cost effective, but it may become so in the near future. A solid database is paramount to support the interpretation of the data collected during such testing, and must be built up by the collection and full documentation of samples from known localities. Limitations are related to the massive amount of data that has yet to be collected, and to specific issues pertaining to white pearls (no pigment information), treated pearls (e.g. bleached) and mounted or very small samples. In addition, pearls from different molluscs sometimes have overlapping data.

The 'Trade in Bahraini Pearls' was the subject of a presentation by notable natural-pearl dealer **Ali Safar** (formerly of the Gem & Pearl Testing Laboratory of Bahrain). He emphasised that Bahrain (particularly Muharraq) is still the capital of pearl trading in the Gulf, a position that has remained unchanged for centuries despite the ups and downs of the industry. The quality of the lustre, shape, size and orient of the Bahraini pearls became world famous. Due to their scarcity in larger and better qualities, their pricing is set according to the fact that each pearl is unique. With the support of DANAT, visitors to Bahrain can be assured that the pearls they buy are natural, since it is illegal to trade cultured pearls in the country. Recent efforts being undertaken to revive the pearl trade and industry are quite welcome, and have great symbolic and historical relevance to Bahrainis.

Kenneth Scarratt closed the symposium with the results of a 'Recent Expedition to Acquire and Characterise Natural Pearls from Australian *Pinctada maxima*', co-authored with **Ali Al-Atawi** (DANAT), which was also presented at the 7th European Gemmological Symposium (see *The Journal*, Vol. 36, No. 7, 2019, pp. 661–663).

The Pearl Symposium proceedings booklet, as well as videos of all the presentations and slides from some of them, are available at www.danat.bh/pearlsymposium-talks.

Rui Galopim de Carvalho FGA DGA
(ruigalopim@gmail.com)
Gem Education Consultant
Lisbon, Portugal

22ND FEEG SYMPOSIUM

The 22nd symposium of the Federation for European Education in Gemmology (FEEG) was organised by Zadkine Vakschool Schoonhoven in the Netherlands in celebration of their 125th anniversary. The event took place 25–27 January 2020 and was attended by 110 people.

Karin Voskamp (Zadkine Vakschool Schoonhoven) kicked off the symposium and introduced Zadkine, the only vocational school in the Netherlands providing education for goldsmiths, silversmiths, jewellers and watchmakers. **This author** then welcomed the delegates and pointed out that FEEG has two main objectives: to promote excellence in gemmological training and to connect gemmological education with the gem and jewellery sectors.

Rui Galopim de Carvalho (CIBJO and Portugal Gemas Academy, Lisbon, Portugal) presented a gemmological overview of precious coral and explained that it is critical to differentiate these eight species from the thousands of other common (i.e. reef-building) coral species. Considering the current emphasis on sustainability and corporate social responsibility, it is important to educate members of the trade and consumers that coral used in jewellery does not pose a threat to the coral reefs, although it does need to be sustainably harvested.

Dr J. C. (Hanco) Zwaan (Netherlands Gemmological Laboratory, National Museum of Natural History 'Naturalis', Leiden) elaborated on the use of geochemistry to study the geological formation of sapphires and determine their country of origin. Sapphires from primary deposits in Sri Lanka were compared to those from the main alluvial gem fields in that country, showing that not all data are consistent with the classic division between metamorphic and magmatic corundum. Because they show considerable overlap with other provenances, he demonstrated that evaluating polished sapphires of unknown origin may provide results with varying degrees of certainty. A statement on geographical origin is therefore, at best, a well-founded professional opinion based on scientific evidence.

John Benjamin (John C. Benjamin Ltd, Aylesbury, Buckinghamshire) delved passionately into jewellery history from Elizabeth I of England through Elizabeth Taylor, based on his 48 years of experience in the antique jewellery business. He illustrated his talk with numerous humorous anecdotes.

Menahem Sevdermish and **Guy Borenstein** (Gemewizard, Ramat Gan, Israel) discussed how, during the past decade, Gemewizard has devised a digitised, fully automated big-data analysis system geared towards large-scale gem and jewellery online platforms, based on image colour analysis and a contextual search engine. Both lecturers had the opportunity to examine the validity of the system from vast amounts of data that were obtained from a worldwide leading online retail marketplace and from major websites. The information gathered from these surveys, together with volumes of documented data collected from traders, have provided important insights on the perceptions of traders and laboratory personnel regarding commercial gem names such as 'pigeon blood', 'royal blue' and 'cornflower blue'. They concluded that the perception of the colours represented by each of these commercial names may differ according to geographical location and also between various leading gemmological laboratories.

Ya'akov Almor (Negev Heights, Israel) has been active in the diamond and coloured stone industry since the late 1980s. He offered his vision of how the diamond industry is facing some important challenges.

George Hamel (Schoonhoven) delved into the history of a sapphire diadem. During the coronation of King Willem-Alexander of the Netherlands in 2013, his wife Máxima wore the beautiful sapphire diadem from the crown jewels of the Oranges, a Christmas present from King Willem III to his second wife, Emma, in 1881. The diadem was previously attributed to Oscar Massin, working for Mellerio in Paris, with sapphires originating from the legacy of Willem III's mother, Anna Paulowna. Further research, however, has provided evidence that the jewel was made in Amsterdam, the Netherlands, by Maison Van der Stichel with diamonds and sapphires supplied by broker Vita Israëls.

Dr Lore Kiefert (Gübelin Gem Lab, Lucerne, Switzerland) gave an extensive update on the treatment of rubies and sapphires, from the traditional heating process to the more recent high-pressure method used to enhance sapphires and the low-temperature treatment of rubies. She focused on the development and detectability of these treatments, including what to look out for and how to interpret inclusion features and spectra.

Tom Stephan (German Gemmological Association, Idar-Oberstein, Germany) gave an overview of recent heat-treatment experiments on gem corundum at the German Gemmological Association. He heated rubies and sapphires at various temperatures and documented the changes in colour, inclusion features, spectroscopic characteristics and fluorescence with increasing temperature. The experiments were successful at intensifying yellow and removing blue colouration between 600 and 1,200°C, while at higher temperatures it was possible to intensify blue colour again. With photomicrographs

Figure 3: New FEEG diploma holders gather with (in the left foreground) CIBJO Coral Commission president Enzo Liverino (tan jacket), FEEG president Guy Lalous (wearing glasses) and Dr Ilaria Adamo (next to handrail). Photo courtesy of Rob Glastra.

before and after treatment, he demonstrated how mineral and fluid inclusions were affected at various temperatures and illustrated changes in Raman, FTIR and UV-Vis-NIR absorption spectra of the samples.

On 26–27 January several workshops were held: coloured stone grading and pricing (by **Richard Drucker** of Gemworld International Inc., Glenview, Illinois, USA); coloured stone grading and coloured diamond grading (by **Menahem Sevdermish** and **Guy Borenstein**); appraising gemstone jewellery (by **Wouter Abbestee**, jewellery and silverware valuer, The Haag, The Netherlands); diamond grading (by **George Hamel**); pearl stringing (by **Monique Konst-Kurstjens** of Zadkine Vakschool Schoonhoven); visual optics (by **Alan Hodgkinson**, Whinhurst, West Kilbride, Scotland); silver jewellery making (by **Femke Toele** of Zadkine Vakschool Schoonhoven); designing and shaping your own gemstone ring (by **Ornella Schavemaker-Piva** of Lapidarists Club, The Haag); hands-on identification of red, white and blue gemstones and diamonds (by **Leone Langeslag**, Sole Leone, Amsterdam); and precious coral (by **Rui Galopim de Carvalho**).

The evening of 26 January marked the FEEG diploma ceremony (Figure 3), which celebrated 78 new graduates. The ceremony was opened by **this author** and **Dr Ilaria Adamo** (Italian Gemmological Institute, Milan, Italy). The graduation address was given by **Richard Drucker**, who spoke about following one's passion and participating in a business full of interesting people. Meeting acquaintances at gemmological conferences and other events often results in lifelong friendships.

The next FEEG symposium will be held in Paris, France, in January 2021 and will celebrate the 25th Anniversary of FEEG.

Guy Lalous (guy.lalous@outlook.com)
President, FEEG
Brussels, Belgium

AGA TUCSON CONFERENCE

The 2020 Accredited Gemologists Association (AGA) Conference in Tucson, Arizona, USA, took place 5 February and was attended by 144 people from more than 10 countries. The event was moderated by outgoing AGA president **Stuart Robertson** (Gemworld International Inc., Glenview, Illinois, USA) and featured six presentations covering the theme 'Awareness of Our Gem Environment and People—Challenges in Technology and Culture'. The day closed with the AGA Gala and presentation of the 2020 Antonio C. Bonanno Award for Excellence in Gemology to **Robert Weldon** (Figure 4).

The conference was opened by **Stuart Robertson**,

who welcomed the new AGA board and incoming AGA president **Teri Brossmer** (Gem Appraisals Unlimited LLC, Glendora, California, USA). Then AGA Diamond Sponsor **Art Samuels** (EstateBuyers.com, Miami, Florida, USA) gave some further remarks.

The first conference speaker was **Richard Hughes** (Lotus Gemology, Bangkok, Thailand), who described his research on jade through trips to Myanmar, New Zealand, Guatemala, Russia and China, where most recently (in 2019) he visited the Xinyuan nephrite deposits near the Korean border and mining areas for 'Dushan jade' in Henan Province. He then focused on the mining, trading and treatments of nephrite in China, before highlighting contemporary jade carving by Chinese artists. There are now more than 100 'master' carvers in China who are using their talents and modern tools to pursue a variety of carving styles, including those that use negative space, reproduce the appearance of bronze statues or create delicate 'eggshell' carvings of just 1 mm in thickness.

Dr Jeffrey Post (Smithsonian Institution, Washington DC, USA) described his studies on environmental mineralogy, which deals with interactions between the solid earth and the environment in which we live (e.g. pertaining to soils and coatings on rocks), and showed that geology and biology are not necessarily entirely separate disciplines but may be interdependent. He then described some recent acquisitions for the Smithsonian Institution's National Gem Collection, including the 55.08 ct Kimberley diamond (see Gem Note on pp. 14–15 of this issue); the 48.86 ct 'Whitney Flame' red Imperial topaz; a 1,401 ct aquamarine from Brazil; a 568 ct black opal called 'The Eternal Flame', from the Tintenbar volcanic opal field in Australia; a 68 kg lapis lazuli carving called the 'Blue Flame'; two spodumene gemstones from Afghanistan weighing 396 and 127 ct; and many more.

Eric Fritz (University of Arizona Gem and Mineral Museum, Tucson) reviewed biogenic gem materials, including their identification and trade restrictions. He focused on coral and ivory, and had many examples from his collection available for hands-on viewing after his presentation. He covered the identifying features of the different types of precious coral and also highlighted the characteristics of dyed material. Regarding ivory, he showed how it is relatively straightforward to separate elephant from mammoth tusks when they are whole, but distinguishing between smaller pieces of these materials (as encountered in jewellery or as carvings) can be quite challenging when considering the orientation of Schreger lines: Their angles may vary (and potentially overlap) from the outer to inner portions of the tusks.

Dr Laurent E. Cartier (Swiss Gemmological Institute SSEF, Basel, Switzerland) examined the traceability of gemstones and pearls. He covered both the challenges (e.g. 'conflict' minerals) and opportunities

Figure 4: Antoinette Matlins, Karen Bonanno DeHaas and Kathryn Bonanno (from left to right) present the 2020 Antonio C. Bonanno Award for Excellence in Gemology to Robert Weldon. Photo by B. M. Laurs.

Figure 5: Previous Bonanno Award winners who were present at this year's AGA Gala include (from left to right) Stuart Robertson, Thom Underwood, Donna Hawrelko, Dr Thomas Hainschwang, Shane McClure, Richard Drucker, Al Gilbertson, Robert Weldon (2020 awardee), Dr Jim Shigley, Dr Çiğdem Lüle, Dr W. William Hanneman, Mikko Åström, John Koivula, Alberto Scarani, Richard Hughes and Dr John Emmett (with Antoinette Matlins). Photo by B. M. Laurs.

(e.g. sustainability initiatives) regarding traceability, and reviewed new technological advances such as DNA fingerprinting as applied to coral, ivory and pearls. He then treated the audience to a screening of a new documentary film (which he initially showed at the November 2019 Gem-A Conference) that he produced on artisanal miners who dive for diamonds in the Sewa River of Sierra Leone.

Dr Aaron Palke (GIA, Carlsbad, California) covered treatments of spinel and garnet, which are typically assumed to be untreated. He described experiments aimed at addressing recent claims in the trade that pink-to-red spinel from Mahenge, Tanzania, can be heated to shift the colour from orangey red to more red and also potentially improve transparency. So far, Palke has been unable to reproduce these effects in his experiments. Moreover, photoluminescence (PL) spectroscopy indicates that very few of the stones in the trade are heated (i.e. show broader PL lines). Palke was able to slightly improve the colour of demantoid from Russia's Karkodin (or Karkodino) mine by removing some brown component to make the colour appear slightly brighter and greener, by heating under reducing conditions to around 700°C for 16 hours. However, heat treatment cannot remove the brown colouration from Namibian or Malagasy demantoid.

Robert Weldon (GIA, Carlsbad) described an ongoing project to help educate artisanal miners in East Africa (particularly Tanzania) about sorting and evaluating the rough stones they recover according to important value factors (e.g. size, shape, transparency and colour). Through the use of a well-illustrated booklet that is written in Swahili and English, and a translucent tray for viewing the stones, the programme empowers miners with knowledge and abilities that allow them to bargain more effectively with their buyers and realise greater financial gain for their families and communities. The project has also brought Western buyers directly to the miners while also including local brokers in the supply chain.

The AGA Conference also featured two hands-on workshops, by **Samantha Lloyd** (Gem-A, London) on using filters and **Claire Scragg** (JTV, Knoxville, Tennessee, USA) on using the spectroscope.

The AGA Gala took place that evening and was attended by 167 people. **Stuart Robertson** opened the ceremony for the 2020 Antonio C. Bonanno Award for Excellence in Gemology, and **this author** introduced honouree **Robert Weldon**, who was then presented with the award by Bonanno's daughters **Antoinette Matlins**, **Karen Bonanno DeHaas** and **Kathryn Bonanno** (again, see Figure 4). This was followed by a presentation by Weldon on his early development as a gem aficionado and journalist, as well as a gathering of all the previous Bonanno Award winners who were present at this year's gala (Figure 5).

Brendan M. Laurs FGA

Gem-A Notices

Gifts to the Association

Gem-A is most grateful to the following for their generous donations that will support continued research and teaching:

Avant Chordia, Chordia Inc., India, for 42.87 g of Aquaprase (chalcedony) specimens.

Ian Kalway, Thailand, for specimens of cobalt-blue spinel from Vietnam, including 0.53 g of crystals and a 0.05 ct faceted stone.

Mineração Costa Marques, Brazil, for several pieces of heated and unheated amethyst from the Costa Marques mine, Amazonas State, Brazil.

Leonardo Silva Souto, Gems in Gems, Brazil, for two polished pieces of amazonite in quartz from Bahia, Brazil, and for three polished samples of Aquafire (aquamarine with inclusions) from Minas Gerais, Brazil.

Martin Steinbach, Steinbach – Gems with a Star, Germany, for a sample of hauyne in matrix from Germany and for several pieces of rough ruby from Bo Rai, Thailand.

Indra Man Sunuwar, Nepali Bazaar Co. Ltd, Japan, for three demantoid crystal slices from Iran.

Steve Ulatowski, New Era Gems, USA, for four pieces of heat-treated beryl from Brazil.

Abdiaziz Mohamed Yousuf, Ethiopia, for a parcel of rough and cut hessonite from Somaliland.

Donation from European Art & Antiques

Gem-A is delighted to report that Gem-A USA has received a donation of almost 7,000 gemstones from Robert Sadian of New York-based European Art & Antiques. The extensive collection of gems, which includes more than 30 species and 50 gem varieties ranging from less than 1 ct to more than 100 ct, will be used to educate Gem-A USA students taking the Gemmology Foundation and Gemmology Diploma courses. The collection will also be made available to assist gemmological research being carried out by current FGAs.

Commenting on the recent donation, Gem-A CEO Alan Hart FGA stated: 'All at Gem-A would like to express the greatest thanks to European Art & Antiques and to owner Robert Sadian for this extremely kind gift, which marks the beginning of a very bright future for the work of Gem-A USA.' Read the full press release here: https://gem-a.com/news-publications/gem-a-press-releases.

A selection of garnet specimens from Gem-A USA's new gem collection donated by Robert Sadian of European Art & Antiques.

Scottish Gemmological Association (SGA) Conference 2020

Gem-A will be returning to the Scottish Gemmological Association's annual conference on 1–4 May 2020. This year, two Gem-A Tutors will be hosting workshops during the Sunday session. From 13:30 to 15:00, Sam Lloyd FGA DGA EG will host 'Fun with Filters', a hands-on workshop that will guide participants through some of Gem-A's favourite filters and how to use them. Directly after, from 15:30 to 17:00, Lily Faber FGA DGA EG will present 'Seeing Colour: Succeed with the Spectroscope', an entry-level workshop that will teach the basic principles of colour and selective absorption, and enable participants to get to grips with different types of portable spectroscopes.

Gem-A Instruments will also be selling gemmological tools; Gem-A Members and Students will receive 10% off instruments and 5% off books as per their usual benefits. For more information and to book tickets, visit: https://scottishgemmology.org/registration-and-student-sponsorship.

Obituary

Anthony de Goutière

23 November 1927–25 December 2019

Gem-A regrets the passing of Anthony de Goutière on 25 December 2019. He was an esteemed gemmologist, photographer and long-standing Gem-A Member who contributed to many issues of *The Journal of Gemmology* and *Gems&Jewellery* over a period of 25 years. A full obituary appears in the Spring 2020 issue of *Gems&Jewellery*, available on the Gem-A website to Members and Students: https://gem-a.com/news-publications/gems-jewellery.

Learning Opportunities

CONFERENCES AND SEMINARS

Jewelry Industry Summit
27 March 2020
Los Angeles, California, USA
www.jewelryindustrysummit.com/la-summit

Association for the Study of Jewelry and Related Arts' 15th Annual Conference
4 April 2020
New York, New York, USA
www.jewelryconference.com

10th National Opal Symposium
8–9 April 2020
Coober Pedy, Australia
www.opalsymposium.org

47th Rochester Mineralogical Symposium
23–26 April 2020
Rochester, New York, USA
www.rasny.org/minsymp

American Gem Society Conclave
27–29 April 2020
Denver, Colorado, USA
www.americangemsociety.org/mpage/conclave2020-home

Scottish Gemmological Association Conference
1–4 May 2020
Cumbernauld, Scotland
www.scottishgemmology.org/programme
Note: An excursion on 4 May will include a visit to the National Museums of Scotland Collection Centre.

6th Mediterranean Gemmological & Jewellery Conference
15–17 May 2020
Thessaloniki, Greece
https://gemconference.com

17th Annual Sinkankas Symposium—Agate & Chalcedony
16 May 2020
Carlsbad, California, USA
https://sinkankassymposium.net

34th Annual Santa Fe Symposium
17–20 May 2020
Albuquerque, New Mexico, USA
www.santafesymposium.org

49th Annual Society of North American Goldsmiths Conference
20–23 May 2020
Philadelphia, Pennsylvania, USA
www.snagmetalsmith.org/conferences/grit-to-gold-future-fifty-2020-snag-conference

Gemmological Association of Australia 74th Federal Conference
21–24 May 2020
Perth, Western Australia
www.gem.org.au/news_events

JCK Las Vegas
2–5 June 2020
Las Vegas, Nevada, USA
https://lasvegas.jckonline.com
Note: Includes a seminar programme

Swiss Gemmological Society Conference
7–9 June 2020
St Gallen, Switzerland
http://gemmologie.ch/en/current

19th Rendez-Vous Gemmologiques de Paris
8 June 2020
Paris, France
www.afgems-paris.com/rdv-gemmologique

Diamonds – Source to Use 2020
9–11 June 2020
Johannesburg, South Africa
www.saimm.co.za/saimm-events/upcoming-events/diamonds-source-to-use-2020

NAJ Summit
20–22 June 2020
Northamptonshire, East Midlands
www.naj.co.uk/summit
Note: Includes the IRV Valuers' Conference (20–22 June) and the JBN Retail Jewellers' Congress (22 June)

Sainte-Marie-aux-Mines Mineral & Gem Show
25–28 June 2020
Sainte-Marie-aux-Mines, France
www.sainte-marie-mineral.com
Note: Includes a seminar programme

9th International Conference Mineralogy and Museums
5–7 July 2020
Sofia, Bulgaria
www.bgminsoc.bg
Note: Gem minerals and archaeogemmology are among the topics that will be covered.

Dallas Mineral Collecting Symposium
20–23 August 2020
Dallas, Texas, USA
www.dallassymposium.org

Amberif 2020: 27th International Fair of Amber & Jewellery
26–29 August 2020
Gdańsk, Poland
http://amberif.amberexpo.pl
Note: Includes a seminar programme

3rd European Mineralogical Conference (emc2020)
6–10 September 2020
Krakow, Poland
https://emc2020.ptmin.eu
Session of interest: The Geology of Gem Deposits: A Session in Honour of Gaston Giuliani

International Jewellery London
13–15 September 2020
London
www.jewellerylondon.com
Note: Includes a seminar programme

31st International Conference on Diamond and Carbon Materials
13–17 September 2020
Palma, Mallorca, Spain
www.elsevier.com/events/conferences/international-conference-on-diamond-and-carbon-materials

Jewellery & Gem World Hong Kong
13–19 September 2020
https://exhibitions.jewellerynet.com/9jg/en-us/specialevents/specialevent
Note: Includes seminar programmes

Denver Gem & Mineral Show
18–20 September 2020
Denver, Colorado, USA
www.denvermineralshow.com
Note: Includes a seminar programme

13th Annual Portland Jewelry Symposium
27–28 September 2020
Portland, Oregon, USA
https://portlandjewelrysymposium.com

2020 American Society of Appraisers (ASA) International Conference
11–13 October 2020
Chicago, Illinois, USA
www.appraisers.org/Education/conferences/asa-international-conference

Japan Jewellery Fair 2020
14–16 October 2020
Tokyo, Japan
www.japanjewelleryfair.com/en
Note: Includes a seminar programme

Canadian Gemmological Association (CGA) Conference
16–18 October 2020
Vancouver, British Columbia, Canada
https://canadiangemmological.com/vancouver

Chicago Responsible Jewelry Conference
22–24 October 2020
Chicago, Illinois, USA
www.chiresponsiblejewelryconference.com

Munich Show: Mineralientage München
30 October–1 November 2020
Munich, Germany
https://munichshow.de/?lang=en
Note: Includes a seminar programme

OTHER EDUCATIONAL OPPORTUNITIES

Gem-A Workshops and Courses
Gem-A, London
https://gem-a.com/education

Lectures with Gem-A's Midlands Branch
Fellows Auctioneers, Augusta House, Birmingham
Email Louise Ludlam-Snook at
gemamidlands@gmail.com

- Peter Buckie—The Treasures Seen by an Expert Valuer
  27 March 20209
- Roy Starkey—Minerals of the English Midlands
  24 April 2020

Lectures with The Society of Jewellery Historians
Society of Antiquaries of London,
Burlington House, London
www.societyofjewelleryhistorians.ac.uk/current_lectures

- Carol Michaelson—Chinese Jade Jewellery and Ornaments from the Neolithic to the Present
  24 March 2020
- Ute Decker—TBA
  26 May 2020
- Kirstin Kennedy—TBA
  23 June 2020
- Prof. Gordon M. Walkden—The Rocks of Britain: Our Victorian Jewellery
  22 September 2020
- TBA—New Research
  27 October 2020
- Charlotte Gere—Colour in Victorian Jewellery
  24 November 2020

Gem-A East Africa Field Trip 2020
19–25 July 2020
https://gem-a.com/east-africa-field-trip-2020

mindat.org Euro Bus Tour 2020
28 June–6 July 2020
www.mindat.org/a/bustour

New Media

The Calligraphy Collection: Nicolai Medvedev, Intarsia Master Artist

By Elise Misiorowski, 2019. Kudos Publications, Newport Beach, California, USA, 34 pages, illus., ISBN 978-0464207122. USD280.00 hardcover.

The Calligraphy Collection is a short, 34-page volume that shows the genius of Nicolai Medvedev as a master intarsia artist. The 'Calligraphy Collection' is made up of eight gem boxes that took Medvedev nine years to complete. This collection represents a body of work that combines beauty and technical excellence.

This book is beautifully written by Elise Misiorowski in consultation with Mona Lee Nesseth. The text is clear and concise, and takes away nothing from the excellent photography of these eight glorious *objets d'art*. The book is illustrated by legendary photographers Erica and Harold Van Pelt, as well as James R. Thomas. The images beautifully document what it takes to be a master intarsia artist and fabricate by hand these wonderful works of art.

Misiorowski documents Medvedev's history from his birth in Ashgabat, Turkmenistan, through his studies at an art institute in Moscow, to his emigration in 1980 to the United States. Since then he has honed his talent, assembling gem materials into intricate and elegant designs on the surfaces of objects (commonly boxes).

Medvedev's gem intarsia has been exhibited in museums and galleries throughout the USA and collected by gem connoisseurs worldwide. Museums that own or have displayed his work include the Smithsonian Institution (Washington DC, USA), the Natural History Museum of Los Angeles County (California, USA), the Colorado School of Mines (Golden, Colorado, USA) and the Gemological Institute of America (Carlsbad, California), among many others.

The works of art in the 'Calligraphy Collection' feature the use of 14 different gem materials—including lapis lazuli, gold in quartz, turquoise, malachite, azurite, sugilite, maw-sit-sit and Australian opal—plus exotic woods. Each box has a name that describes the artist's intention: 'Scene and Unseen' (1996), 'Celebration Suite' (1997; two pieces), 'The Beginning' (1998), 'The Companion' (1998), 'Light of the World' (2000), 'Hope' (2003) and 'Unity' (2004). The top of each box features gem-intarsia Arabic letters in stylised calligraphy, the design of which complements the motif of each box and gives the collection its name.

Anyone who loves beauty and appreciates artists who work with gems should consider adding this limited-edition book to their library.

Bill Larson FGA
Pala International
Fallbrook, California, USA

Marchands de Perles: Redécouverte d'une Saga Commerciale entre le Golfe et la France à l'Aube du XXe Siècle/ Pearl Merchants: A Rediscovered Saga Between the Gulf & France at the Dawn of the 20th Century

By Guillaume Glorieux and Olivier Segura, 2019. L'École des Arts Joailliers/School of Jewelry Arts, Paris, France, and French Institute of the United Arab Emirates, Dubai, 224 pages, illus., no ISBN (in French, English and Arabic). EUR20.00 softcover.

This book is an excellent study of the commerce between the Persian (or Arabian) Gulf and French merchants. It was produced to accompany an exhibition that took place 28 March–13 April 2019 and was held during the second year of the 2018–2019 French-Emirati Cultural Dialogue in the Dubai Design District. The exhibition was organised

by the School of Jewelry Arts in partnership with the French Institute of the United Arab Emirates.

The book covers an era when Paris became the major player for pearl dealers, and is presented in three sections encompassing different languages. The first, in French, is the most detailed, with 93 pages of text and photographs. The second is a 42-page summary in English of the first section, without photographs. The third is similar to the first, in Arabic and with illustrations. The exhibition presented a chronological, thematic journey from the end of the 19th century to the present. The six chapters follow this design and, as translated in the English section, are:

1. Pearls of the Orient and the Luster of Pearls
2. After 1900, the Age of the Pioneers
3. The 1910s: The Explosion
4. PARIS, the Pearl Capital
5. The Dark Decade (1929–1939)
6. Between Resistance and Rebirth, the Pearl Trade of Yesterday and Today

At the end of the French section is a two-page colour map showing the Gulf region, followed by a chronological bibliography of sources and monographs.

Throughout the six chapters are many wonderful historical photographs, maps and jewellery renderings, in black and white and in colour. Often there is more than one photo or illustration/map on each page. The

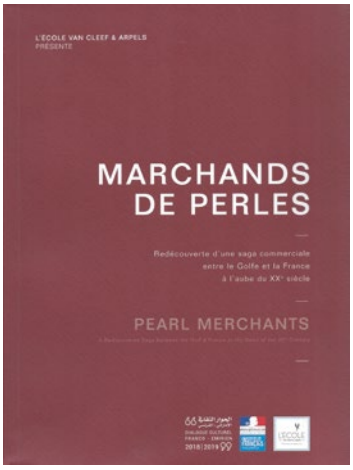

photographs tell the story nicely without needing English captions. The jewellery renderings show superb classics and are in colour.

I would recommend this book to anyone with even a passing interest in natural pearls. The authors' enthusiasm for these gems is well conveyed in the 'New Actors' paragraph of the final chapter of the book: 'Certain connoisseurs are always ready to spend considerable amounts to buy themselves a part of the great history of pearls, and of humanity; a fragment of dreams and passion; a small piece of emotion…these tears from heaven wept for the pleasure of mortals.'

Bill Larson FGA

Other Book Titles

COLOURED STONES

Rhodochrosit
By various authors, 2019. extraLapis No. 56, Christian Weise Verlag GmbH, Munich, Germany, 126 pages (in German). EUR19.80 softcover.

CULTURAL HERITAGE

The Contribution of Mineralogy to Cultural Heritage
Ed. by G. Artioli and R. Oberti, 2019. EMU Notes on Mineralogy Vol. 20, European Mineralogical Union and the Mineralogical Society of Great Britain & Ireland, xii + 448 pages, ISBN 978-0903056618, https://doi.org/10.1180/emu-notes.20. GBP40.00 (individuals) or GBP55.00 (institutions) softcover, or free chapter PDFs at www.minersoc.org/emu-notes-20.html.

Enigma dei Vasi Murrini/Enigma of Murrhine Ware
By Enrico Butini, 2019. Bibliotheca Archaeologica Vol. 59, «L'Erma» di Bretschneider, Rome, Italy, 144 pages, ISBN 978-8891318206 (in Italian and English). EUR90.00 softcover.

La Parure en Callaïs du Néolithique Européen [The European Neolithic Callaïs Ornaments]
Ed. by Guirec Querré, Serge Cassen and Emmanuelle Vigier, 2019. Archaeopress Publishing Ltd, Summertown, Oxford, 642 pages, ISBN 978-1789692808 (print) or ISBN 978-1789692815 (PDF) [papers in English and French]. GBP130.00 hardcover or free PDF at www.archaeopress.com/ArchaeopressShop/Public/download.asp?id={9306B133-D594-43FC-9D57-2076B7DAEC97}.

DIAMOND

Diamonds, 4th edn.
By Fred Ward and Charlotte Ward, 2019. Gem Book Publishers, Malibu, California, USA, 64 pages, ISBN 978-1887651189. USD19.95 softcover.

GEM AND MINERAL LOCALITIES

Cornwall
By various authors, 2019. extraLapis No. 57, Christian Weise Verlag GmbH, Munich, Germany, 132 pages (in German). EUR19.80 softcover.

Fluorite: Trésors de France – French Treasures
By Christophe Lucas, 2019. Les Éditions du Piat, Saint-Julien-du-Pinet, France, 232 pages, ISBN 978-2917198438 (in French and English). EUR40.00 hardcover.

Karakorum: Inferno di Rocce, Paradiso di Gemme e Cristalli [Karakorum (Pakistan): Hell of Rocks, Paradise of Gems and Crystals]
By Giuseppe Agozzino, 2020. LoGisma, Florence, Italy, 208 pages (in Italian). EUR40.00 hardcover.

Minerals and Gemstones of East Africa
By Bruce Cairncross, 2019. Penguin Random House South Africa/Struik Nature, Cape Town, South Africa, 160 pages, ISBN 978-1775845560 (print) or ISBN 978-1775846987 (ePub). ZAR250.00 softcover or USD7.99 Kindle edn.

Mont Saint-Hilaire: History, Geology, Mineralogy
By László Horváth, Robert A. Gault, Elsa Pfenninger-Horváth and Glenn Poirier, 2019. Canadian Mineralogist Special Publication 14, Mineralogical Association of Canada, Ottawa, Ontario, 372 pages, ISBN 978-0921294610. USD125.00 hardcover.

Spinel from Pamir—Kuh-i-Lal, Pamir, Badakhshan, Tajikistan
By Vladyslav Y. Yavorskyy, 2019. Yavorskyy Co. Ltd, Hong Kong, 236 pages, ISBN 978-1733486002. USD180.00 hardcover.

JEWELLERY HISTORY

A Arte de Coleccionar—Lisboa, a Europa e o Mundo na Época Moderna (1500-1800)/The Art of Collecting—Lisbon, Europe and the Early Modern World (1500-1800)
Ed. by Hugo Miguel Crespo, 2019. Pedro Aguiar-Branco, Lisbon, Portugal, 363 pages, ISBN 978-9899618053 (in Portuguese and English). Free PDF at www.pab.pt/_usr/downloads/Catalogo_Arpab_2019.pdf.

A History of the Tudors in 100 Objects
By John Matusiak, 2019. The History Press, Cheltenham, Gloucestershire, 352 pages, ISBN 978-0750991254. GBP14.99 softcover.

JEWELLERY AND *OBJETS D'ART*

The American Gem Art Collection of EF Watermelon Catalog
Ed. by Günther Neumeier, 2018. EF Watermelon, Old Lyme, Connecticut, USA, 76 pages, ISBN 978-0692058459. USD52.00 softcover.

The Collection of EF Watermelon—Masterworks of the American Gem Art Movement
Ed. by Günther Neumeier, 2018. EF Watermelon, Old Lyme, Connecticut, USA, 104 pages, ISBN 978-0692058442. USD52.00 hardcover.

Diamond Ring Buying Guide, 8th edn.
By Renee Newman, 2020. International Jewelry Publications, Los Angeles, California, USA, 168 pages, ISBN 978-0929975542. USD19.95 softcover.

A Vanity Affair: The Art of Necessaires
Ed. by Lyne Kaddoura, 2019. Rizzoli, New York, New York, USA, 320 pages, ISBN 978-8891817945. USD150.00 hardcover.

SOCIAL STUDIES

Botswana – A Modern Economic History: An African Diamond in the Rough
By Ellen Hillbom and Jutta Bolt, 2018. Palgrave Studies in Economic History, Palgrave Macmillan/Springer Nature, Cham, Switzerland, 235 pages, ISBN 978-3319731438 (hardcover), ISBN 978-3030103231 (softcover) or ISBN 978-3319731445 (eBook), https://doi.org/10.1007/978-3-319-73144-5. EUR119.59 hardcover, EUR119.59 softcover or EUR96.29 eBook.

SYNTHETICS AND SIMULANTS

The History of Synthetic Ruby
By James Evans, 2020. Lustre Gemmology Ltd, Sheffield, South Yorkshire, 60 pages, ISBN 978-1916165205. GBP18.00 softcover.

Literature of Interest

COLOURED STONES

American gems: New sources of inspiration for the European market. E. Thoreux, *InColor*, No. 45, 2020, 72–76, www.gemstone.org/incolor/45.*

Australian faceted fluorite specimen from the Natural History Museum, London. R.F. Hansen and L.J. Rennie, *Australian Gemmologist*, **27**(1), 2019, 12–17.

Bixbite [red beryl]: The rarest common gem in the world. M. Macrì, *Rivista Italiana di Gemmologia/ Italian Gemological Review*, No. 7, 2019, 47–55.

Blue gahnospinel crystals from Nigeria. J.-M. Arlabosse, *Gemmology Today*, December 2019, 5–8, www.worldgemfoundation.com/GTDEC2019DV.*

Characterization of amethysts from Sukamara, central Kalimantan, using laser-induced breakdown spectroscopy (LIBS). K.G. Suastika, H. Suyanto, Gunarjo, Sadiana and Darmaji, *Journal of the Physical Society of Indonesia*, **1**(1), 2019, 9–12, http://journal.fisika.or.id/jpsi/article/view/8/45.*

Color and local heritage in gemstone branding: A comparative study of blue zoisite (tanzanite) and color-change diaspore (Zultanite/Csarite). M. Altingoz, N.M. Smith, H.S. Duzgun, P.F. Syvrud and S.H. Ali, *Extractive Industries and Society*, **6**(4), 2019, 1030–1039, http://doi.org/10.1016/j.exis.2019.05.013.

Color varieties of gems – Where to set the boundary? M.S. Krzemnicki, L.E. Cartier, P. Lefèvre and W. Zhou, *InColor*, No. 45, 2020, 100–103, www.gemstone.org/incolor/45.*

Determination of demantoid garnet origin by chemical fingerprinting. C. Schwarzinger, *Monatshefte für Chemie - Chemical Monthly*, **150**(5), 2019, 907–912, https://doi.org/10.1007/s00706-019-02409-3.*

Fanciful fabulous fire agate. P. Rothengatter, *InColor*, No. 45, 2020, 70–71, www.gemstone.org/incolor/45.*

Fingerprinting Paranesti [Greece] rubies through oxygen isotopes. K. Wang, I. Graham, L. Martin, P. Voudouris, G. Giuliani, A. Lay, S. Harris and A. Fallick, *Minerals*, **9**(2), 2019, article 91 (14 pp.), http://doi.org/10.3390/min9020091.*

Flowers blooming on rocks; Cheongsong flowerstone of Korea. Y. Kim and J. Moon, *Journal of the Gemmological Association of Hong Kong*, **40**, 2019, 54–57, www.gahk.org/journal/GAHK_Journal_2019_v6.pdf.*

Gemmological characteristic and chemical composition of ruby from Guinea, Africa. J. Feng and M. Chen, *Journal of Gems & Gemmology*, **21**(3), 2019, 26–36 (in Chinese with English abstract).

Gemmological characteristic of grandidierite from Madagascar. N. Sun, G. Li, X. Li and B. Zhang, *Journal of Gems & Gemmology*, **21**(3), 2019, 37–41 (in Chinese with English abstract).

Gemological and spectral characteristic of sapphire from Australia. Y. Xu, J. Di and F. Fang, *Journal of Gems & Gemmology*, **21**(2), 2019, 24–33 (in Chinese with English abstract).

Gemstones of the garnet group – About mixed crystals and solid solution. H.A. Hänni, *Journal of the Gemmological Association of Hong Kong*, **40**, 2019, 36–42, www.gahk.org/journal/GAHK_Journal_2019_v6.pdf.*

Geographic origin determination of alexandrite. Z. Sun, A.C. Palke, J. Muyal, D. DeGhionno and S.F. McClure, *Gems & Gemology*, **55**(4), 2019, 660–681, http://doi.org/10.5741/GEMS.55.4.660.*

Geographic origin determination of blue sapphire. A.C. Palke, S. Saeseaw, N.D. Renfro, Z. Sun and S.F. McClure, *Gems & Gemology*, **55**(4), 2019, 536–579, http://doi.org/10.5741/GEMS.55.4.536.*

Geographic origin determination of emerald. S. Saeseaw, N.D. Renfro, A.C. Palke, Z. Sun and S.F. McClure, *Gems & Gemology*, **55**(4), 2019, 614–646, http://doi.org/10.5741/GEMS.55.4.614.*

Geographic origin determination of Paraíba tourmaline. Y. Katsurada, Z. Sun, C.M. Breeding and B.L. Dutrow, *Gems & Gemology*, **55**(4), 2019, 648–659, http://doi.org/10.5741/GEMS.55.4.648.*

Geographic origin determination of ruby. A.C. Palke, S. Saeseaw, N.D. Renfro, Z. Sun and S.F. McClure, *Gems & Gemology*, **55**(4), 2019, 580–612, http://doi.org/10.5741/GEMS.55.4.580.*

The geographic origin dilemma. S.F. McClure, T.M. Moses and J.E. Shigley, *Gems & Gemology*, **55**(4), 2019, 457–462, www.gia.edu/gems-gemology/winter-2019-geographic-origin-dilemma.*

Geology of corundum and emerald gem deposits: A review. G. Giuliani and L.A. Groat, *Gems & Gemology*, **55**(4), 2019, 464–489, http://doi.org/10.5741/GEMS.55.4.464.*

Masters of green: Chromium and vanadium. K. Feral, *Gemmology Today*, March 2019, 28–32, www.worldgemfoundation.com/GTMARCH2019DV.*

Masters of green: Chromium and vanadium (part 2). K. Feral, *Gemmology Today*, June 2019, 38–45, www.worldgemfoundation.com/GTJUNE2019DV.*

Mineral inclusions in ruby and sapphire from the Bo Welu gem deposit in Chanthaburi, Thailand. S. Promwongnan and C. Sutthirat, *Gems & Gemology*, **55**(3), 2019, 354–369, http://doi.org/10.5741/GEMS.55.3.354.*

Myanmar's fei cui raw materials market. R. Wang, *Journal of the Gemmological Association of Hong Kong*, **40**, 2019, 98–103, www.gahk.org/journal/GAHK_Journal_2019_v6.pdf.*

Our friends the inclusions. The detective at the party of inclusions. Sixth episode. L. Costantini and C. Russo, *Rivista Italiana di Gemmologia/Italian Gemological Review*, No. 8, 2019, 7–11.

Pastel pyrope: A new gem variety? K. Feral, *Gemmology Today*, December 2019, 38–42, www.worldgemfoundation.com/GTDEC2019DV.*

Pink and red gem spinels in marble and placers. G. Giuliani, A.E. Fallick, A.J. Boyce, V. Pardieu and P. Van Long, *InColor*, No. 43, 2019, 14–28, www.gemstone.org/incolor/43.*

Polycrystals of "Imperial" topaz from Minas Gerais State, Brazil. T. Gauzzi, G.Á. da Silva, R.S. Diniz and L.M. Graça, *Mineralogy and Petrology*, **113**(3), 2019, 273–283, http://doi.org/10.1007/s00710-019-00659-x.

The power of cobalt [spinel]. G. Dominy, *Gemmology Today*, June 2019, 34–37, www.worldgemfoundation.com/GTJUNE2019DV.*

Red beryl – A very rare and highly prized gem beryl. J. Holfert and J. Fuller, *InColor*, No. 45, 2020, 62–64, www.gemstone.org/incolor/45.*

Spinel inclusions: An exercise in aesthetics. E.B Hughes, J.I. Koivula, N. Renfro, W. Manorotkul and R.W. Hughes, *InColor*, No. 43, 2019, 66–73, www.gemstone.org/incolor/43.*

The story of Blue John. E.Z. Karlin, *Adornment*, **12**(1), 2019, 28–44.

Study on the infrared spectral characteristics of H_2O I-type emerald and the controlling factors. X. Qiao, Z. Zhou, P. Nong, M. Lai, Y. Li, K. Guo, Q. Zhong *et al.*, *Rock and Mineral Analysis*, **38**(2), 2019, 169–178 (in Chinese with English abstract).

A study of mineral inclusions in emeralds from Malipo, Yunnan Province. X. Jiang, X. Yu, B. Guo and C. Xu, *Acta Petrologica et Mineralogica*, **38**(2), 2019, 279–286 (in Chinese with English abstract).

Tantalizing turquoise. D. Schannep and C. Schannep, *InColor*, No. 45, 2020, 48–55, www.gemstone.org/incolor/45.*

Unique vanadium-rich emerald from Malipo, China. Y. Hu and R. Lu, *Gems & Gemology*, **55**(3), 2019, 338–352, http://doi.org/10.5741/GEMS.55.3.338.*

Use of meteorites in jewellery. C. Murdoch, *Australian Gemmologist*, **27**(1), 2019, 34–37.

Wearable wulfenite. M. Mauthner, *Rocks & Minerals*, **94**(1), 2019, 32–33, http://doi.org/10.1080/00357529.2019.1519670.

CULTURAL HERITAGE

Archaeological mineralogy and the dawn of gemmology: Prehistoric (7th – 5th millennium BC) gem minerals and gold from the Balkans (south-east Europe). R.I. Kostov, *Journal of Gems & Gemmology*, **21**(4), 2019, 25–35.

Early historic gemstone bead workshops at the Badmal Asurgarh and Bhutiapali in the middle Mahanadi Valley region, Odisha, India. P.K. Behera and S. Hussain, *Ancient Asia*, **10**, article 2 (16 pp.), 2019, http://doi.org/10.5334/aa.169.*

Gemmology in the service of archaeometry. M.P. Riccardi, L. Prosperi, S.C. Tarantino and M. Zema, In G. Artioli and R. Oberti, Eds., *The Contribution of Mineralogy to Cultural Heritage*. EMU Notes in Mineralogy, European Mineralogical Union and Mineralogical Society of Great Britain & Ireland, 2019, 345–366, https://doi.org/10.1180/emu-notes.20.9.*

Gems and man: A brief history. G. Rapp, in G. Artioli and R. Oberti, Eds., *The Contribution of Mineralogy to Cultural Heritage*. EMU Notes in Mineralogy, European Mineralogical Union and Mineralogical Society of Great Britain & Ireland, 2019, 323–344, http://doi.org/10.1180/EMU-notes.20.8.*

The importance of jade in the Mughal court. T. Schneider, *Gems&Jewellery*, **28**(3), 2019, 32–35.

Overlooked imports: Carnelian beads in the Korean Peninsula. L. Glover and J.M. Kenoyer, *Asian Perspectives*, **58**(1), 2019, 180–201, http://doi.org/10.1353/asi.2019.0009.

Poly-material ornaments: The Iron Age amber fibulae. N.L. Saldalamacchia, *Rivista Italiana di Gemmologia/ Italian Gemological Review*, No. 7, 2019, 65–68.

Precious gems silk routes. S. Martin, *Gems&Jewellery*, **28**(4), 2019, 24–27.

DIAMONDS

Automated FTIR mapping of boron distribution in diamond. D. Howell, A.T. Collins, L.C. Loudin, P.L. Diggle, U.F.S. D'Haenens-Johansson, K.V. Smit, A.N. Katrusha, J.E. Butler and F. Nestola, *Diamond and Related Materials*, **96**, 2019, 207–215, http://doi.org/10.1016/j.diamond.2019.02.029.

A comparative analysis of the luminescence spectra of diamonds. S.I. Zienko and D.S. Slabkovskii, *Optics and Spectroscopy*, **127**(3), 2019, 564–570, https://doi.org/10.1134/s0030400x19090273.

Deformation features of super-deep diamonds. A. Ragozin, D. Zedgenizov, V. Shatsky, K. Kuper and H. Kagi, *Minerals*, **10**(1), 2019, article 18 (14 pp.), https://doi.org/10.3390/min10010018.*

Inclusion extraction from diamond clarity images based on the analysis of diamond optical properties. W. Wang and L. Cai, *Optics Express*, **27**(19), 2019, 27242–27255, http://doi.org/10.1364/oe.27.027242.*

Natural-color Fancy white and Fancy black diamonds: Where color and clarity converge. S. Eaton-Magaña, T. Ardon, C.M. Breeding and J.E. Shigley, *Gems & Gemology*, **55**(3), 2019, 320–337, http://doi.org/10.5741/GEMS.55.3.320.*

The nature of the elongated form of diamond crystals from Urals [Russia] placers. E.A. Vasilev, I.V. Klepikov, A.V. Kozlov and A.V. Antonov, *Journal of Mining Institute*, **239**(5), 2019, 492–496, https://doi.org/10.31897/pmi.2019.5.492.*

Protogenetic garnet inclusions and the age of diamonds. F. Nestola, D.E. Jacob, M.G. Pamato, L. Pasqualetto, B. Oliveira, S. Greene, S. Perritt, I. Chinn *et al.*, *Geology*, **47**(5), 2019, 431–434, http://doi.org/10.1130/g45781.1.

FAIR TRADE

Formulating strategic interventions for the coloured gemstone industry in Namibia by utilising the logical framework approach. H.K. Musiyarira, M. Pillalamarry, D. Tesh and N. Nikowa, *Extractive Industries and Society*, **6**(4), 2019, 1017–1029, http://doi.org/10.1016/j.exis.2019.05.004.

Gemstones and sustainable development: Perspectives and trends in mining, processing and trade of precious stones. L.E. Cartier, *Extractive Industries and Society*, **6**(4), 2019, 1013–1016, http://doi.org/10.1016/j.exis.2019.09.005.

High-impact/low-budget capacity building. C. Lawson, *InColor*, No. 44, 2019, 52–57, www.gemstone.org/incolor/44.*

The journey towards responsibility. R.G. Sikri, *InColor*, No. 43, 2019, 86–92, www.gemstone.org/incolor/43.*

Rushing for gemstones and gold: Reflecting on experiences from the United States, Canada, New Zealand, Australia and Madagascar, 1848–present. R. Canavesio and V. Pardieu, *The Extractive Industries and Society*, **6**(4), 2019, 1055–1065, https://doi.org/10.1016/j.exis.2019.08.005.

Women sapphire traders in Madagascar: Challenges and opportunities for empowerment. L. Lawson and K. Lahiri-Dutt, *Extractive Industries and Society*, **6**(4), 2019, 1066–1074, https://doi.org/10.1016/j.exis.2019.07.009.

GEM LOCALITIES

Alexandrite of the Urals. E.V. Burlakov and A. Burlakov, *InColor*, No. 44, 2019, 22–34, www.gemstone.org/incolor/44.*

America's royal gem: Montana and Yogo sapphires. R.E. Kane, *InColor*, No. 45, 2020, 30–39, www.gemstone.org/incolor/45.*

Apache peridot - Born of fire from Mother Earth. C. Vargas, *InColor*, No. 45, 2020, 66–69, www.gemstone.org/incolor/45.*

The application of trace elements and Sr–Pb isotopes to dating and tracing ruby formation: The Aappaluttoq deposit, SW Greenland. M.Y. Krebs, D.G. Pearson, A.J. Fagan, Y. Bussweiler and C. Sarkar, *Chemical Geology*, **523**, 2019, 42–58, http://doi.org/10.1016/j.chemgeo.2019.05.035.

California gems: More than a century-old legacy. M. Mauthner, *InColor*, No. 45, 2020, 20–28, www.gemstone.org/incolor/45.*

Characteristic, development and utilization of nephrite from Luodian, Guizhou Province. Z. Zhong, Z. Liao, Z. Zhou, M. Lai, D. Cui and L. Li, *Journal of Gems & Gemmology*, **21**(1), 2019, 40–48 (in Chinese with English abstract).

Colored gemstones from Canada: An update. B.S. Wilson, *InColor*, No. 45, 2020, 78–85, www.gemstone.org/incolor/45.*

Development of small deposits and ASM in Africa. C. Simonet, *InColor*, No. 44, 2019, 47–51, www.gemstone.org/incolor/44.*

Enigmatic alluvial sapphires from the Orosmayo region, Jujuy Province, northwest Argentina: Insights into their origin from in situ oxygen isotopes. I.T. Graham, S.J. Harris, L. Martin, A. Lay and E. Zappettini, *Minerals*, **9**(7), 2019, article 390 (13 pp.), http://doi.org/10.3390/min9070390.*

Gem deposits in the U.S. state of Maine. J. Clanin and P. Pinette, *InColor*, No. 45, 2020, 40–45, www.gemstone.org/incolor/45.*

Gems of Italy [titanite to sulphur]. Various authors, *Rivista Italiana di Gemmologia/Italian Gemological Review*, No. 8, 2019, 20–27.

A golden frontier [gold-bearing quartz from Alaska, USA]. *Gems&Jewellery*, **29**(1), 2020, 30–31.

In search of cobalt blue spinel in Vietnam. P. Sokolov, K. Kuksa, O. Marakhovskaya and G.A. Gussiås, *InColor*, No. 43, 2019, 60–65, www.gemstone.org/incolor/43.*

A journey to Russia. D. Nini, *Gems&Jewellery*, **28**(4), 2019, 12–14.

Linking gemology and spectral geology: A case study of elbaites from Seridó pegmatite province, northeastern Brazil. T.A. Carrino, S. de Brito Barreto, P.J.A. de Oliveira, J.F. de Araújo Neto and A.M. de Lima Correia, *Brazilian Journal of Geology*, **49**(2), 2019, article e20180113 (15 pp.), http://doi.org/10.1590/2317-4889201920180113.*

Mineral association and graphite inclusions in nephrite jade from Liaoning, northeast China: Implications for metamorphic conditions and ore genesis. C. Zhang, X. Yu and T. Jiang, *Geoscience Frontiers*, **10**(2), 2019, 425-437, http://doi.org/10.1016/j.gsf.2018.02.009.*

Mineralogical and gemological characterization of emerald crystals from Paraná deposit, NE Brazil: A study of mineral chemistry, absorption and reflectance spectroscopy and thermal analysis. J.F. de Araújo Neto, S. de Brito Barreto, T.A. Carrino, A. Müller and L.C.M. de Lira Santos, *Brazilian Journal of Geology*, **49**(3), 2019, article e20190014 (15 pp.), http://doi.org/10.1590/2317-4889201920190014.*

New data on the genetic linkage of the beryl and chrysoberyl chromophores of the Ural's emerald mines with chromium-bearing spinels of the Bazhenov ophiolite complex. M.P. Popov, E.S. Sorokina, N.N. Kononkova, A.G. Nikolaev and S. Karampelas, *Doklady Earth Sciences*, **486**(2), 2019, 630–633, http://doi.org/10.1134/s1028334x1906031x.

One nation [USA], many gemstones. E.A. Gass, *Gems&Jewellery*, **29**(1), 2020, 14–21.

Oregon sunstone: A rare and beautiful American gemstone. A.P. Krivanek, *InColor*, No. 45, 2020, 56–61, www.gemstone.org/incolor/45.*

Origin of blue sapphire in newly discovered spinel–chlorite–muscovite rocks within meta-ultramafites of Ilmen Mountains, south Urals of Russia: Evidence from mineralogy, geochemistry, Rb-Sr and Sm-Nd isotopic data. E. Sorokina, M. Rassomakhin, S. Nikandrov, S. Karampelas, N. Kononkova, A. Nikolaev, M. Anosova, A. Somsikova *et al.*, *Minerals*, **9**(1), 2019, article 36 (23 pp.), http://doi.org/10.3390/min9010036.*

A review on gemstone potentials of Khorasan Razavi Province, northeast Iran; a special focus on turquoise gems. R. Ahmadirouhani, J. Taheri, M. Gholamzadeh, H. Azmi and M. Azadi, *Iranian Journal of Geoscience Museum*, **1**(1), 2019, 57–71.

The Russian emerald saga: The Mariinsky Priisk mine. A.C. Palke, F.J. Lawley, W. Vertriest, P. Wongrawang and Y. Katsurada, *InColor*, No. 44, 2019, 36–46, www.gemstone.org/incolor/44.*

Spinel from Tajikistan: The gem that made famous the word "ruby". V. Pardieu and T. Farkhodova, *InColor*, No. 43, 2019, 30–33, www.gemstone.org/incolor/43.*

The spinels of Mahenge, Tanzania. M. Kukharuk and C. Manna, *InColor*, No. 43, 2019, 54–58, www.gemstone.org/incolor/43.*

The spinels of Mogok: A brief overview. F. Barlocher, *InColor*, No. 43, 2019, 34–39, www.gemstone.org/incolor/43.*

Spinels from Sri Lanka. P. Lomthong, D. Schwarz, G. Zoyza [*sic*], C. Yanyu and Y. Liu, *InColor*, No. 43, 2019, 40–52, www.gemstone.org/incolor/43.*

INSTRUMENTATION AND TOOLS

3D imaging of gems and minerals by multiphoton microscopy. B. Cromey, R.J. Knox and K. Kieu, *Optical Materials Express*, **9**(2), 2019, 516–525, http://doi.org/10.1364/ome.9.000516.*

Advantages and disadvantages of Raman & Fourier transform infrared spectroscopy (FTIR) in the gemological field. A. Scarani and M. Åström, *AGTA Prism*, **2**, 2019, 18, 20, 22, 24, www.agtaeprism.com/pressroom/newsletters/prism2019vol2/mobile/index.html.*

Analysis of opals. The new opal master reference sets in LFG laboratory. A. Herreweghe and A. Delaunay, *Rivista Italiana di Gemmologia/Italian Gemological Review*, No. 8, 2019, 31–34.

Birefringence of gemstone materials and its application in identification. L. Yu, *Superhard Material Engineering*, **31**(3), 2019, 51–55 (in Chinese with English abstract).

ColorCodex™ – A new tool for the gemstone and jewelry industry. C.P. Smith, *InColor*, No. 45, 2020, 88–94, www.gemstone.org/incolor/45.*

Efficiently testing melee-sized colored stones: An analytical challenge. T. Hainschwang, *InColor*, No. 44, 2019, 58–62, www.gemstone.org/incolor/44.*

Identification of gemstones using portable sequentially shifted excitation Raman spectrometer and RRUFF online database: A proof of concept study. A. Culka and J. Jehlička, *European Physical Journal Plus*, **134**(4), 2019, article 130 (7 pp.), http://doi.org/10.1140/epjp/i2019-12596-y.

Identifying marks [Opsydia]. A. Rimmer, *Gems&Jewellery*, **28**(4), 2019, 28–29.

"LA-ICP-MS" spectrometry and its use in gemology. C. Schwarzinger and T. Engeli, *Rivista Italiana di Gemmologia/Italian Gemological Review*, No. 8, 2019, 50–52.

Laser inscription and marking of gemstones: An overview of options. L.E. Cartier, M.S. Krzemnicki, A. Rimmer, L. Fish, D. Myles, H.A.O. Wang and J.-P. Chalain, *InColor*, No. 43, 2019, 82–85, www.gemstone.org/incolor/43.*

Multidimensional luminescence microscope for imaging defect colour centres in diamond. D.C. Jones, S. Kumar, P.M.P. Lanigan, C.D. McGuinness, M.W. Dale, D.J. Twitchen, D. Fisher, P.M. Martineau *et al.*, *Methods and Applications in Fluorescence*, **8**(1), 2019, article 014004 (9 pp.), https://doi.org/10.1088/2050-6120/ab4eac.

QR code micro-certified gemstones: Femtosecond writing and Raman characterization in diamond, ruby and sapphire. A.J. Batista, P.G. Vianna, H.B. Ribeiro, C.J.S. de Matos and A.S.L. Gomes, *Scientific Reports*, **9**(1), 2019, article 8927 (7 pp.), http://doi.org/10.1038/s41598-019-45405-7.*

A review of analytical methods used in geographic origin determination of gemstones. L.A. Groat, G. Giuliani, J. Stone-Sundberg, Z. Sun, N.D. Renfro and A.C. Palke, *Gems & Gemology*, **55**(4), 2019, 512–535, http://doi.org/10.5741/GEMS.55.4.512.*

Screening for synthetic diamonds. A comparison of technologies. A. Scarani and M. Åström, *Rivista Italiana di Gemmologia/Italian Gemological Review*, No. 8, 2019, 61–65.

A study on near-infrared spectroscopy of different subgroup silicate gemstone minerals. X. Guo, H. Song, Q. Long and E. Zu, *Journal of Kunming University of Science and Technology (Natural Science)*, **44**(3), 2019, 22–25 (in Chinese with English abstract).

Testing times [Assure Program]. G. Dominy, *Gemmology Today*, December 2019, 18–34, www.worldgemfoundation.com/GTDEC2019DV.*

Through the looking glass – The giant loupe test. N. Zolotukhina, *Gemmology Today*, December 2019, 72–75, www.worldgemfoundation.com/GTDEC2019DV.*

Two decades of GIT's ruby and sapphire color standards. T. Leelawatanasuk, W. Atichat, V. Pisutha-Arnond, C. Sutthirat and J. Jakkawanvibul, *InColor*, No. 45, 2020, 96–98, www.gemstone.org/incolor/45.*

JEWELLERY HISTORY

Behind closed doors: A brief journey into the history of Christie's and jewellery. G. Piguet-Reisser, *Gems&Jewellery*, **29**(1), 2020, 42–45.

Cartier and the Mughal carved emeralds. C. Del Mare, *InColor*, No. 44, 2019, 72–77, www.gemstone.org/incolor/44.*

Gemstone conversations: Topaz. J. Benjamin, *Gems&Jewellery*, **28**(4), 2019, 40–41.

Gemstones in the era of the Taj Mahal and the Mughals. D.M. Dirlam, C.L. Rogers and R. Weldon, *Gems & Gemology*, **55**(3), 2019, 294–319, http://doi.org/10.5741/GEMS.55.3.294.*

Spinel: A gemstone for kings. M.-L. Cassius-Duranton, *InColor*, No. 43, 2019, 74–81, www.gemstone.org/incolor/43.*

MISCELLANEOUS

Field gemology: Building a research collection and understanding the development of gem deposits. W. Vertriest, A.C. Palke and N.D. Renfro, *Gems & Gemology*, **55**(4), 2019, 490–511, http://doi.org/10.5741/GEMS.55.4.490.*

Heavenly jewellery [space-inspired jewels]. E.Z. Karlin, *Gems&Jewellery*, **29**(1), 2020, 22–24.

Jeweller to the stars [Harry Winston]. *Gems&Jewellery*, **29**(1), 2020, 38–39.

José Manuel Rosas: The maestro of color. R. Galopim de Carvalho, *InColor*, No. 44, 2019, 78–81, www.gemstone.org/incolor/44.*

The "Nature's Creations in the Master Hands" exhibition [Vernadsky State Geological Museum, Russia]. V.V. Chernenko and L.S. Nazarov, *Mineralogical Almanac*, **24**(1), 2019, 41–47.

Small but mighty [Corgialenios Museum, Greece]. H. Serras-Herman, *Gems&Jewellery*, **28**(4), 2019, 20–22.

Women working in the Thai coloured gemstone industry: Insights from entrepreneurial ecosystems. L. Lawson, *The Extractive Industries and Society*, **6**(4), 2019, 1066–1074, https://doi.org/10.1016/j.exis.2019.08.002.

NEWS PRESS

Berlin's Stasi Museum looted days after Dresden jewelry heist. C. Otto and S. McKenzie, CNN, 2 December 2019, www.cnn.com/2019/12/02/europe/stasi-museum-berlin-theft-grm-intl/index.html.

Dresden Green Vault robbery: Fears historic jewels may be lost forever. BBC News, 26 November 2019, www.bbc.com/news/world-europe-50557436.*

Remains of a 2,000-year-old barbarian woman are found buried in North Caucasus with jewellery that was created in the Roman Empire – including glass beads and rare gems. W. Stewart, *Daily Mail*, 8 November 2019, www.dailymail.co.uk/sciencetech/article-7665209/Roman-jewellery-body-2-000-year-old-barbarian-woman-Caucasus.html.*

Scientist looks to resurrect Hong Kong's 'Pearl of the Orient' past. Phys.org, 6 June 2019, https://phys.org/news/2019-06-scientist-resurrect-hong-kong-pearl.html.*

World's oldest pearl discovered near Abu Dhabi. BBC News, 21 October 2019, www.bbc.com/news/world-middle-east-50125603.*

ORGANIC/BIOGENIC GEMS

Characteristics of hydrothermally treated beeswax amber. Y. Wang, Y. Li, F. Liu, F. Liu and Q. Chen, *Gems & Gemology*, **55**(3), 2019, 370–387, http://doi.org/10.5741/GEMS.55.3.370.*

Distinguishing extant elephants ivory from mammoth ivory using a short sequence of cytochrome b gene. J.N. Ngatia, T.M. Lan, Y. Ma, T.D. Dinh, Z. Wang, T.D. Dahmer and Y. Chun Xu, *Scientific Reports*, **9**(1), 2019, article 18863 (12 pp.), https://doi.org/10.1038/s41598-019-55094-x.*

Spectral characteristics of natural and heated blood-red ambers. R. Xiao, L. Wang, W. Chen and G. Shi, *Spectroscopy and Spectral Analysis*, **39**(4), 2019, 1053–1058 (in Chinese with English abstract).

PEARLS

Application of 3D scanning technique and colour measurement on pearl sorting. K. Cheng, Z. Li, L. Hao, L. Li, Z. Xiong and F. Ma, *Journal of Gems & Gemmology*, **21**(4), 2019, 36–44 (in Chinese with English abstract).

Chemical characteristics of freshwater and saltwater natural and cultured pearls from different bivalves. S. Karampelas, F. Mohamed, H. Abdulla, F. Almahmood, L. Flamarzi, S. Sangsawong and A. Alalawi, *Minerals*, **9**(6), 2019, article 357 (20 pp.), http://doi.org/10.3390/min9060357.*

Effects of mollusk size on growth and color of cultured half-pearls from Phuket, Thailand. K. Kanjanachatree, N. Limsathapornkul, A. Inthonjaroen and R.J. Ritchie, *Gems & Gemology*, **55**(3), 2019, 388–397, http://doi.org/10.5741/GEMS.55.3.388.*

Freshwater pearl culture. J. Li, X. Wu and Z. Bai, in J.F. Gui, Q. Tang, Z. Li, J. Liu and S.S. De Silva, Eds., *Aquaculture in China: Success Stories and Modern Trends*. John Wiley & Sons Ltd, New York, New York, USA, 2018, 185–196, https://doi.org/10.1002/9781119120759.ch3_1.

Identification of seawater cultured pearls. H. Zhu, T. Li, F. Yan, P. Wang, X. Zhao and Z. Huang, *Superhard Material Engineering*, **31**(1), 2019, 65–68 (in Chinese with English abstract).

Journey to the center of the pearl. Composition and structure. O. Segura, *Rivista Italiana di Gemmologia/Italian Gemological Review*, No. 8, 2019, 55–59.

Pearl fishery industry in Sri Lanka. J. Katupotha, *Windlanka*, **7**(1), 2019, 33–49.

A pledge to [American] pearls. R. Galopim de Carvalho, *Gems&Jewellery*, **29**(1), 2020, 32–33.

SOCIAL STUDIES

Central Asian crypto-Jews in the global emerald economy. B. Brazeal, *Extractive Industries and Society*, **6**(4), 2019, 1047–1054, http://doi.org/10.1016/j.exis.2019.03.014.

Semiotic distribution of responsibility: An ethnography of overburden in Colombia's emerald economy. V. Caraballo Acuña, *Extractive Industries and Society*, **6**(4), 2019, 1040–1046, http://doi.org/10.1016/j.exis.2019.03.018.

SYNTHETICS AND SIMULANTS

Effect of crystallization time on quality of synthetic jadeite under high pressure and high temperature. X. Zuozuo, C. Meihua and Z. Zuo, *Journal of Gems & Gemmology*, **21**(1), 2019, 31–39 (in Chinese with English abstract).

Identification characteristics of natural and synthetic amethyst by infrared and polarized Raman spectroscopy. W. Huang, X. Jin, R. Zuo, D. Zuo, G. Yang, P. Xue, X. Chen and J. Zhang, *Rock and Mineral Analysis*, **38**(4), 2019, 403–410 (in Chinese with English abstract).

Observation of surface microstructure of HPHT synthetic diamond crystals and genesis discussion. X. Wu, T. Lu, C. Yang, J. Zhang, S. Tang, H. Chen, Y. Zhang *et al.*, *Rock and Mineral Analysis*, **38**(4), 2019, 411–417 (in Chinese with English abstract).

Pressed gibbsite and calcite as a rhodochrosite imitation. H. Xu and X. Yu, *Gems & Gemology*, **55**(3), 2019, 406–415, http://doi.org/10.5741/GEMS.55.3.406.*

Research on laboratory testing features of chemical vapor deposition in overgrowth diamonds. S. Tang, J. Su, T. Lu, Y. Ma, J. Ke, Z. Song, J. Zhang, X. Zhang *et al.*, *Rock and Mineral Analysis*, **38**(1), 2019, 62–70 (in Chinese with English abstract).

Synthesis and characteristics of type Ib diamond doped with NiS as an additive. J.K. Wang, S.S. Li, N. Wang, H.J. Liu, T.C. Su, M.H. Hu, F. Han *et al.*, *Chinese Physics Letters*, **36**(4), 2019, article 046101 (6 pp.), https://doi.org/10.1088/0256-307x/36/4/046101.

Synthetic alexandrite, more magic than Rubik's cube. A. Malossi, *Rivista Italiana di Gemmologia/Italian Gemological Review*, No. 8, 2019, 37–49.

TREATMENTS

Filling material and characteristic of polymer-impregnated turquoise in Anhui Province. Y. Xu and M. Yang, *Journal of Gems & Gemmology*, **21**(1), 2019, 20–30 (in Chinese with English abstract).

Gemmological characteristic of electron irradiated amethyst. T. Shao, J. Zhang and A.H. Shen, *Journal of Gems & Gemmology*, **21**(5), 2019, 48–55 (in Chinese with English abstract).

Hydrogen-rich green diamond color-treated by multi-step processing. W. Huang, P. Ni, T. Shui and G. Shi, *Gems & Gemology*, **55**(3), 2019, 398–405, http://doi.org/10.5741/GEMS.55.3.398.*

The impact of electron beam irradiation in topaz quality enhancement. A. Maneewong, K. Pangza, T. Charoennam, N. Thamrongsiripak and N. Jangsawang, *Journal of Physics: Conference Series*, **1285**(1), 2019, article 012022 (8 pp.), http://doi.org/10.1088/1742-6596/1285/1/012022.*

Spectroscopic characteristic of orange red to purple colour-treated diamond from Lotus Colors, Inc. U.S.A. M. Qu and A.H. Shen, *Journal of Gems & Gemmology*, **21**(2), 2019, 17–23 (in Chinese with English abstract).

COMPILATIONS

***G&G* Micro-World.** 'Rain cloud' in alexandrite • Conichalcite in chalcedony • Emerald in rock crystal • Iolite-sunstone intergrowth and inclusions • Merelaniite in diopside • Pyrite in dravite from Mozambique • Dislocation chain in Oregon sunstone • Tourmaline in Russian alexandrite • Phenakite with tourmaline inclusion containing spiral growth • Metallic-looking bubble in quartz. *Gems & Gemology*, **55**(3), 2019, 426–433, www.gia.edu/gg-issue-search?ggissueid=1495292173965&articlesubtype=microworld.*

Gem News International. Blue gahnite from Nigeria • Emerald update with Arthur Groom • Deep blue aquamarine in Nigeria • Pearl in edible oyster from Pakistan • Sapphire with trapiche-pattern inclusions • Opal stability • Trapiche emerald from Pakistan • Uvarovite in prehnite from Philippines • Stellate inclusions in diamond • Artificial glass imitating blue amber • Black non-nacreous pearl imitations made from shell • Imitation play-of-color opal • Thorianite in heated blue sapphire • Recrystallization of baddeleyite in 'HPHT'-treated sapphire • 2019 GSA annual meeting • Gemstone portrait artist Angie Crabtree • Johnkoivulaite: A new gem mineral. *Gems & Gemology*, **55**(3), 2019, 434–455, www.gia.edu/gg-issue-search?ggissueid=1495292173965&articlesubtype=gni.*

Lab Notes. Faceted chiolite • Diamond octahedron with stellate cloud inclusion • Grossular crystals in demantoid • Resin imitation of ivory • Cobalt-coated sapphire • Possible natural abalone shell blister • Large synthetic star ruby and sapphire • Synthetic sapphire with unusual features • Faceted vlasovite. *Gems & Gemology*, **55**(3), 2019, 416–425, www.gia.edu/gg-issue-search?ggissueid=1495292173965&articlesubtype=labnotes.*

CONFERENCE PROCEEDINGS

1st Pearl Symposium. Manama, Bahrain, 14–15 November 2019, 36 pp., www.danat.bh/wp-content/uploads/2019/11/PEARL-SYMPOSIUM-V12.pdf.*

46th Rochester Mineralogical Symposium. Rochester, New York, USA, 11–14 April 2019, 42 pp., www.rasny.org/minsymp/Program%20Notes%20RMS%2046%20web.pdf.*

**Article freely available for download, as of press time*

Gem-A
THE GEMMOLOGICAL ASSOCIATION OF GREAT BRITAIN

Gem-A: **over 110 years of experience** in gemmology education

Our FGA and DGA Members are located around the world — join them by studying with Gem-A

STUDY IN ONE OF THREE WAYS

At Gem-A HQ London

Worldwide at one of our ATCs

Online with practical lab classes in your area

Find out more by contacting:
education@gem-a.com

Creating gemmologists since 1908

Gem-A, 21 Ely Place, London, EC1N 6TD, UK. T: +44 (0)20 7404 3334, W: www.gem-a.com. Registered charity no. 1109555.

PAUL WILD

EXCELLENCE IN
GEMSTONE INNOVATION

SAPPHIRE

A kingdom for this gemstone! Associated with royalty and romance,
the noble sapphire is one of the world's most coveted and treasured gemstones.

MINING • CUTTING • CREATION

PAUL WILD OHG • AUF DER LAY 2 • 55743 KIRSCHWEILER • GERMANY
T: +49.(0)67 81.93 43-0 • F: +49.(0)67 81.93 43-43 • E-MAIL: INFO@PAUL-WILD.DE • WWW.PAUL-WILD.DE

VISIT US AT

BASELWORLD

APRIL 30 – MAY 05, 2020 HALL 2.1 BOOTH B25